UNIVERSITY OF SOUTHAMPTON

The Electrostatics of Dispersed Systems

By

Ian Gerard Harpur BSc

Faculty of Engineering

Department of Electronics and Electrical Engineering

June 2002

A thesis submitted for the degree of **Master of Philosophy**

Abstract

Ian Gerard Harpur BSc

The Electrostatics of Dispersed Systems

Faculty of Engineering

Department of Electronics and Electrical Engineering

January 2002

A thesis submitted for the degree of **Master of Philosophy**

This thesis essentially records three theoretical and experimental studies into the behaviour of dispersed systems in intense electrostatic fields. The intent is to highlight common themes and key differences applicable to dispersions of solids in gases, liquids in gases and liquids in liquids. Electrostatic effects can be used to control the behaviour of such systems, to provide the energy to generate such systems or indeed to alter such systems so they lose their defining properties. This field of engineering, although specialised, has enormous commercial worth and all three studies were sponsored by companies interested in bringing novel processes to the marketplace. Thus, a high level of innovative work is covered within each study area. This studies are i) on a novel approach to electrostatically charge powder for use in powder coating applications, ii) into a device for nebulizing pharmaceutical material for direct inhalation by patients and iii) into the destabilisation of water in oil emulsions applicable to the oil industry.

On the face of it, such diverse aspects of technology appear irreconcilable under the banner of a thesis for a higher degree but there are a number of relating themes which are woven throughout which tie the thesis together. Principally, there is electrostatics and more formally, the electrostatics of dielectric material. Electrostatic stresses are effective at opposing the more familiar stresses of surface tension, aerodynamic drag or indeed gravity when they are present on bodies of high surface to volume ratio. All dispersed systems are characterised by the change in nature of the system across an interface. The interface defines the boundary of each phase of the system. If this interface has a very high radius of curvature, then the electrostatic stresses that can be set up there are often of the same order as the other defining forces of the system. The electrical properties of the phases of the system are the key to defining how successfully these stresses can be applied and to what happens to the system when they are applied. For example, in trying to atomize a liquid into a gas, the conductivity of the liquid defines the dynamics of the charge migration through the bulk to the surface from where the droplets are emitted. The dielectric strength of the surrounding gas controls the maximum electrostatic stress that can be maintained and hence the effective work done by the applied electrostatic field. In this case, gas ionization acts like a safety valve, channeling the charge carriers away from the liquid surface before they can disrupt it (alas!).

Contributions made to knowledge in this field include: i) experimental proof of the concept of inductively charging solid resinous powders for powder coating objects, a patent for which was granted to the author and collaborators, ii) a model which considerably aids technologists in predicting the critical parameters to control steady atomization of a liquid into a tightly defined size band, and iii) contributions to the experimental database for the droplet growth rate of the dispersed phase of a flowing water-in-oil emulsion exposed to an ac electrostatic field. The latter work helped build upon the University of Southampton's long line of research in this area and a recent patent was granted to the sponsoring companies who plan to develop commercial devices derived from the research.

Contents

List of Figures

List of Tables

Preface

All nature is but Art, unknown to thee;
All Chance, Direction, which thou canst not see;
All Discord, Harmony, not understood;
All partial Evil, universal Good.....

Alexander Pope from An Essay on Man

The experimental aspects of this research was undertaken in the Department of Electrical Engineering at the University of Southampton between January 1992 and September 1996. At that point, I left the employ of the University to re-enter the industrial world. My registration was put into suspension for three years whilst I set about establishing my engineering career. I subsequently re-registered in 1999 and some of the work within the final thesis has been informed by my experiences in that time working as an xerographic engineer for Xerox, at the corporation's European Technical Centre in Hertfordshire, UK. I had worked, following graduation as a Chemical Engineer in 1989, for over two years in the Research and Development Laboratories of Ricoh Company Ltd. of Japan's Toner Supply Division in Shizuoko, Japan. Although the work I undertook there is not included in this thesis, it was my experiences in electrophotographic toner which set me on my present path of research into the behaviour of dispersed media in electrostatic fields. In this thesis I hope to have given a good account of the science and to have fortified our understanding of the somewhat disparate fields of powder, liquid droplet and liquid emulsion systems and how electrostatic forces can be employed to engineer such systems to the benefit of mankind.

One could say, this thesis represents most of what I know as a specialist engineer, I hope the reader enjoys as the many aspects covered within it as much as I have in gaining the knowledge to record them.

Acknowledgements

- ✓ I would firstly like to record my deep appreciation for the support constantly tendered me by my loving wife, Wendy, whose encouragement and patience has sustained me to completion of this work.
- ✓ My heartfelt thanks goes to my supervisor, Professor A.G. Bailey for the opportunities and support he offered me during and after my time at the University of Southampton, I hope this work goes somewhat to repaying his belief in me.
- ✓ To Dr. Nick Wayth, with whom I worked for 18 months on the final study of this thesis. I cannot hear the marvelous voice of Kirstie McColl without recollecting the smell of gas oil!
- ✓ To Dr. Trevor Williams for support through all phases of this study and for being the oracle on electrostatic theory and practice.
- ✓ Mr. Reg Jones and Mr. Graham Hearn of the Wolfson Electrostatics Advisory Unit for being friends, colleagues and advisors (mostly on the best beer to drink at card evenings).
- ✓ To Dr. Adel Hashish with whom I collaborated on some of the material covered in the second study of this thesis.
- ✓ To Professor John Hughes for his guidance on the first study and for introducing Barbara Williams of eNexus Corporation to the University and the Wolfson Unit.
- ✓ To Dr. John Pritchard of Glaxo, who sponsored the work covered in study two of this thesis and to Dr. Olav Urdahl of Statoil who funded my position for the final study.
- ✓ To colleagues in the Electrostatics Research Group including Drs. Smallwood, Cartwright and Cheung.
- ✓ To Dr. Gareth Jones of the Department of Mathematics for sharing many lunchtime training runs.
- ✓ To former colleagues at Ricoh and at ***pbti***, including Mark Perry for helping me set my career on its current track.
- ✓ To Xerox Europe Limited for support over the last year or so of this work and to my colleagues at Xerox both in Europe and in the USA who daily do battle to tame one of the most difficult of applied sciences. I am proud to count myself within your ranks.
- ✓ To all my running friends and acquaintances near and far and especially to coach Tony Fern and former teammates in Southampton City AC, Southampton Running Club and Team Solent (not forgetting the great London Irish squad of the early 1990s!).
- ✓ And finally to my parents Gerard and Nuala Harpur who set me on way and supported me through to graduation with a Bachelor of Science degree.

Nomenclature

Symbol	**Definition**	*Unit*
γ	Surface tension	$N\,m^{-1}$
∇	Differential operator	-
∇^2	LaPlacian operator	-
ε_r	Relative permittivity	-
ε_0	Epsilon zero, permittivity of a vacuum (or air)	$F\,m^{-1}$
ζ	Electrokinetic or zeta potential	V
χ_e	Electric susceptibility	-
θ	Angular variable	*Radian*
κ	Complex permittivity	$S\,m^{-1}$
λ	Line charge density	$C\,m^{-1}$
μ	Charge mobility	$m^2\,V^{-1}\,s^{-1}$
μ	Dynamic coefficient of viscosity of liquid	$N\,s\,m^{-2}$
η	Kinematic viscosity of liquid (equivalent to μ/ρ_g)	$m^2\,s^{-1}$
η	The molecular dipole moment	*Debye*
η_c	Viscosity of the continuous phase	$m^2\,s^{-1}$
η_d	Viscosity of the dispersed phase	$m^2\,s^{-1}$
ν	Chemical valency	-
K	The electric double layer	
ρ	Volume charge density	$C\,m^{-3}$
ρ_g	Mass density	kgm^{-3}
σ	Conductivity	$S\,m^{-1}$
σ	Surface charge density	$C\,m^{-2}$
τ_η	Viscous relaxation time	s
τ_f	Flow advection time	s
τ_q	Charge relaxation time	s
ϕ	Volume fraction of the dispersed phase	
ω	Frequency	$Rad\,s^{-1}$
A_1	Constant	-
C	Capacitance	F
$\boldsymbol{D}$	Electric displacement	$C\,m^{-2}$
$d\tau$	Volume element	m^3
$D_{0.1}$	Particle diameter such that 10% of total volume is in particles of smaller diameter	m
$D_{0.5}$	As above but 50%. Where the mass density is independent of particle size, this is the mass median diameter as well as the volume median diameter (VMD).	m
$D_{0.9}$	As above but 90%.	m
d_{ci}	Diameter of the circumscribed circle	m
d_D	Diameter of the sphere with the same drag	m

d_{el}	Diameter of the sphere causing the same change in electrical resistance (Coulter counter)	m
d_{EN}	Diameter of the circumscribing sphere	m
d_{in}	Diameter of the inscribed circle	m
dl	Length element	m
d_p	Diameter of the circle with the same area	m
d_{pe}	Diameter of the circle with the same perimeter	m
D_{peak}	value of D corresponding to peak of particle size frequency curve.	m
dS	Surface element	m^2
D_S	Diameter of sphere with the same surface area	m
d_{Sca}	Diameter of sphere scattering light at the same intensity	m
d_{St}	Stoke's diameter	m
d_{SV}	Diameter of sphere with the same specific surface area	m
d_u	Diameter of the sphere with the same terminal velocity	m
d_V	Diameter of sphere with the same volume	m
E	Electric field	$V\ m^{-1}$
e	Electron, electronic charge	C
F_l	liquid volumetric flow rate	$m^3\ s^{-1}$
F_m	flow rate at middle of stability range	$m^3\ s^{-1}$
G_d	Potential energy of a dispersion of droplets	J
G_p	Potential energy of a parent droplet	J
(i, j, k)	Cartesian triad	-
J	Volume Current density	$C\ m^{-2}\ s^{-1}$ or $A\ m^{-2}$
k	Depth of moving liquid layer on a cone-jet surface	m
k	Boltzmann's constant	-
N	Total number of dispersed phase particles	-
n	the number density of counter ions in bulk solution	m^{-3}
p	Dipole moment	$C\ m$
P	Polarization	$C\ m^{-2}$
$P_{\frac{l}{2}}(\cos\theta)$	An associated Legendre function	
q	Point charge	C
Q	Total charge of a system	C
q_r	Rayleigh limit of charge for a liquid droplet to remain stable	C
$Q_r(x)$	A cumulative general particle size distribution of order, r	
$q_r(x)$	A frequency distribution akin to $Q_r(x)$	
r	Radius, radial distance	m
r	droplet radius	m
R	Linear measure of liquid volume	m
r_c	Cannula outside radius,	mm
r_j	Radius of a liquid jet	m
T	absolute temperature	K
U	Potential energy	J

u	Particle terminal velocity	$m\ s^{-1}$
U_E	Electric energy	J
V	Electric Potential	V
W	Work	W
W_e	Electrostatic Weber number	-
W_f	Work function	J
x	A measure of dispersity	
z_0	Distance of field point from electrode	m

Seeing Things

Close as I ever came to seeing things
The way the physicists say they really are
Was out on Sudbury Marsh one summer eve
When a silhouetted tree against the sun
Seemed at my sudden glance to be afire:
A black and boiling smoke made all its shape.

Binoculars resolved the enciphered sight
To make it clear the smoke was a cloud of gnats,
Their millions doing such a steady dance
As by the motion of the many made the one
Shape constant and kept it so in both the forms
I'd thought to see, the fire and the tree.

Strike through the mask? You find another mask,
Mirroring mirrors by analogy
Make visible. I watched till the greater smoke of night
engulfed the other, standing out
On the marsh amid a hundred hidden streams
Meandering down from Concord to the sea.

Howard Nemorov (b. 1920)

PART I FUNDAMENTALS OF ELECTROSTATICS AND DISPERSED SYSTEMS

CHAPTER 1

ELECTROSTATIC PHENOMENA

In this section a review of the principal laws, definitions and relationships of electrostatic phenomena is given. The interested reader is referred to the bibliography at the end of this chapter for a fuller and more in-depth introduction to the physics and mathematics of electrostatics. The approach taken is that familiar to electrical engineers; electrostatic phenomena are viewed as a subset of electromagnetic phenomena which are governed by Maxwell's equations. The S.I. MKS system of units is used throughout. The relevance of this section to this thesis is to show as clearly as possible the underlying physical models governing the behaviour of charge and its interaction with the more familiar energies acting on matter. Reference is made back to this section from various points in the main thesis.

1.1 Basic Physics of Electrostatic Phenomena

1.1.1 Point charge, q

When the volume containing q has linear dimensions negligible in comparison with distances from other charges or from observers, it can be treated as a single point charge q Coulombs.

1.1.2 Charge densities, ρ, σ, λ

These are appropriate when the linear dimensions of the volume containing the charge cannot be neglected, but the charge can be assumed to be spread continuously throughout a volume, over a surface or along a line.

The charge per unit volume at a point defines the *volume charge density* ρ with corresponding definitions for σ (surface) and λ (line). The total charge in a region is given by one of the following:

$$q = \int_{\tau} \rho \quad d\tau \tag{1.1}$$

$$q = \int_s \sigma \quad dS \tag{1.2}$$

$$q = \int_l \lambda \quad dl \tag{1.3}$$

Where τ refers to a volume integral, s refers to a surface integral and l a line integral.

1.1.3 Current density, J

The volume current density is a *flux* of charge i.e. a flow of charge in unit time normal to unit area. In vector form with **J** in the direction of flow and d**S** a vector area normal to the plane of the area then

$$I = \oint \mathbf{J} \cdot d\mathbf{S} \tag{1.4}$$

The units of **J** are Am^{-2}.

1.1.4 Forces and energies

Coulomb's Law: The force (Coulomb force) in Newtons between the stationary charged bodies carrying q_1, and q_2 Coulombs with dimensions negligible compared with their distance r meters apart is

$$\boldsymbol{F} = \frac{q_1 q_2}{4\pi\varepsilon_0 r^2}\hat{\boldsymbol{r}} \tag{1.5}$$

Where $\hat{\mathbf{r}}$ is a unit vector along r.

The following can be deduced from Coulomb's law: when two charges q_1, and q_2 change their distance apart from r' to r, the change in potential energy ∂U Joules is

$$\partial U = \frac{q_1 q_2}{4\pi\varepsilon_o}\left(\frac{1}{r} - \frac{1}{r'}\right) \tag{1.6}$$

As in Newtonian mechanics, the relationship between force and potential energy is that $\mathbf{F}_r = -\frac{\partial U}{\partial r}$ where $\mathbf{F}_r$ is the force on any charge in a general direction and $\frac{\partial U}{\partial r}$ is the rate of change of U with displacement in the same direction.

1.1.5 Definition of electric field strength, (E-field)

The electric field strength **E** at a point is precisely defined mathematically as

$$\mathbf{E} = \lim_{q \to 0} \frac{\mathbf{F}}{q_t} \tag{1.7}$$

where q_t is a test charge, the presence of which does not effect the sources of the electric force field. It is seen that the **E**-field is the force per unit charge at a point and so the SI unit for **E** is the Newton per Coulomb (N/C) but conventionally **E** is measured in the equivalent units of volt per meter (V/m).

From Coulomb's Law (Equation 1.5), the **E**-field due to a single point charge q at a distance r from it is:

$$\mathbf{E} = \frac{q}{4\pi\varepsilon_0 r^2}\hat{\mathbf{r}} \tag{1.8}$$

When the **E**-field at a point is due to a collection of point charges, then the principle of superposition gives

$$\mathbf{E} = \sum_i \frac{q_i}{4\pi\, r_i^2}\hat{\mathbf{r}}_i \tag{1.9}$$

1.1.6 Electric potential, V

Electric potential arises from the concept of potential difference between two points V_{AB}. For an electrostatic field, this is defined as the work done per unit positive test charge in taking charge from one point to another. Thus if the work is W_{AB} then

$$V_B - V_A = V_{AB} = \frac{W_{AB}}{q_t} \tag{1.10}$$

V forms a scalar field with a magnitude at every point in a region. V is given in terms of **E** by $\int -\mathbf{E} \cdot dr$ where the line integral extends from the zero to the field point at which V is required.

The potential energy of a charge q at a point where the potential is V is given by

$$U = qV \tag{1.11}$$

Thus the relation between **E** and V is the same as that between force **F** and potential energy U. **E** is the negative gradient of V or

$$\mathbf{E} = -\nabla V \tag{1.12}$$

Where ∇ (read nabla or 'del') is the differential operator. In Cartesian co-ordinates:

$$\nabla = \frac{d}{dx}\mathbf{i} + \frac{d}{dy}\mathbf{j} + \frac{d}{dz}\mathbf{k} \tag{1.13}$$

Where **(i, j, k)** is the fundamental orthogonal triad associated with Cartesian coordinates. Therefore, the vector function **E** is the gradient of a scalar function, V, and hence the **E**-field is **conservative.**

1.1.7 Electric dipole

A dipole consists of two equal and opposite charges $\pm q$ separated by a distance **l**.

The dipole moment is

$$\mathbf{p} = q\mathbf{l} \qquad \text{(Cm)} \tag{1.14}$$

An ideal dipole is one where **l** is negligible compared with the distance r of a field point. For such a dipole the potential at a field point having co-ordinates (r, θ) is:

(see Figure 1.1. (a))

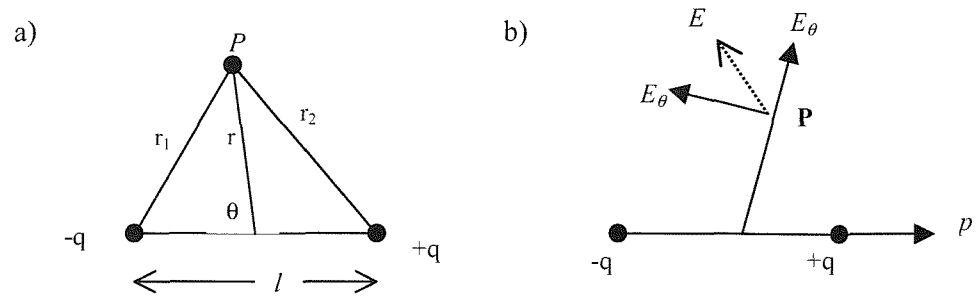

Figure 1.1: a) The potential at a field point due to a dipole. b) Components of the E-field at *P* due to an ideal dipole.

$$V = \frac{\boldsymbol{p}.\boldsymbol{r}}{4\pi\varepsilon_0 r^3} = \frac{p\cos\theta}{4\pi\varepsilon_0 r^2} \tag{1.15}$$

The components of the **E**-field are (See Figure 1.1 (b))

$$\boldsymbol{E}_r = \frac{2p\cos\theta}{4\pi\varepsilon_0 r^3} \quad ; \quad \boldsymbol{E}_\theta = \frac{p\sin\theta}{4\pi\varepsilon_0 r^3} \tag{1.16}$$

An ideal dipole situated in an **E**-field experiences a torque:

$$\mathbf{T} = \mathbf{p} \times \mathbf{E} \tag{1.17}$$

1.1.8 Gauss's Flux Theorem: Gauss's Law for E-field

Mathematically, the integral form of Gauss's theorem is written as

$$\oint \mathbf{E} \,.\, d\mathbf{S} = \sum_i \frac{q_i}{\varepsilon_0} \tag{1.18}$$

That is, the surface integral of the normal component of **E** over a closed surface equals the sum of the charges inside the closed volume divided by ε_0. **E** . d**S** is the **flux** of **E** over d**S** and is a scalar quantity.

1.1.9 Differential form of Gauss's Law

Gauss's law can be applied to a field point.

$$\nabla . \mathbf{E} = \frac{\rho}{\varepsilon_0} \tag{1.19}$$

1.1.10 Poisson's and Laplace's Equations

The differential form of Gauss's Law can be expressed in terms of V by substituting $\mathbf{E} = -\nabla V$ (Equation 1.12 into Equation 1.19).

$$\begin{aligned} \nabla . \nabla V &= -\frac{\rho}{\varepsilon_0} \\ = \nabla^2 V &= -\frac{\rho}{\varepsilon_0} \end{aligned} \tag{1.20}$$

This is Poisson's equation, and the operator ∇^2 (del squared) is called the Laplacian and is a scalar operator. In Cartesian co-ordinates

$$\nabla^2 V = \frac{\partial^2 V}{\partial x^2} + \frac{\partial^2 V}{\partial y^2} + \frac{\partial^2 V}{\partial z^2} \tag{1.21}$$

In cylindrical co-ordinates (r, θ, z)

$$\nabla^2 V = \frac{1}{r}\frac{\partial}{\partial r}\left(r\frac{\partial V}{\partial r}\right) + \frac{1}{r^2}\frac{\partial^2 V}{\partial \theta^2} + \frac{\partial^2 \theta}{\partial z^2} \tag{1.22}$$

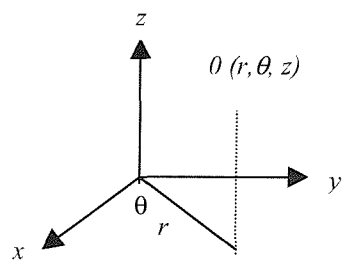

Figure 1.2: Cylindrical co-ordinates

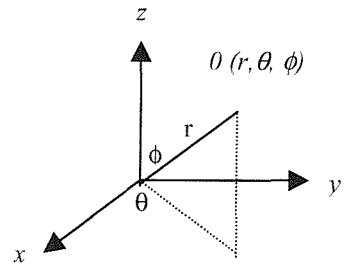

Figure 1.3: Spherical co-ordinates

In spherical co-ordinates (r, θ, ϕ)

$$\nabla^2 V = \frac{1}{r}\frac{\partial}{\partial r}\left(r\frac{\partial V}{\partial r}\right) + \frac{1}{r^2 \sin\theta}\frac{\partial}{\partial \theta^2}\left(\sin\theta\frac{\partial V}{\partial \theta}\right) + \frac{1}{r^2 \sin\theta}\frac{\partial^2 \theta}{\partial z^2} \tag{1.23}$$

At points where no charges exist, Poisson's equation becomes

$$\nabla^2 V = 0 \tag{1.24}$$

which is Laplace's equation.

Laplace's equation is a partial differential equation with an infinite number of solutions, each giving the variation of V as a function of position. The solution applicable to a particular problem is the one that obeys the boundary conditions for the problem. It can be shown that there is a unique solution to Laplace's or Poisson's equations with well defined boundary conditions. Once V has been determined, **E** is obtained from $E_x = -\frac{\partial V}{\partial x}$ etc. So solving Laplace's or Poisson's equation can be a very powerful and general method for solving electrostatic problems.

1.1.11 Circuital Law for E

The potential difference V between two points in an **E**-field is independent of the path and it changes sign when the path is reversed. If we take any two paths between points A and B in Figure 1.4 and label them I and II then it follows from the properties of V that the line integrals of **E** from A to B are the same by both paths so that

$$\int_{I\,A}^{B} \mathbf{E} \cdot ds = \int_{II\,A}^{B} \mathbf{E} \cdot ds \tag{1.25}$$

reversing path II we have

$$\int_{I\,A}^{B} \mathbf{E} \cdot ds + \int_{II\,B}^{A} \mathbf{E} \cdot ds = 0 \tag{1.26}$$

with the left hand side of Equation 1.26 now the line integral of E round a closed path so that

$$\oint \mathbf{E} \cdot ds = 0 \tag{1.27}$$

The left hand side is the circulation of **E.** The interpretation of equation (1.27) is that by moving a charge through a closed loop in an **E**-field, the nett work done on the system is zero

1.2 The Electrostatics of Dielectrics

No substance is a perfect insulator but there are many whose electric conductivity is small enough to be neglected as a first approximation. Such substances are known as dielectrics. The behaviour of dielectrics in electrostatic fields is governed mainly by polarization responses.

1.2.1 Permittivity

The relative permittivity ε_r of a substance is defined as

$$\frac{C_m}{C_0} = \varepsilon_r \tag{1.28}$$

Where C_0 is the capacitance of a capacitor in vacuo and C_m is that of the same capacitor with the dielectric medium filling the complete space in which an **E**-field exists.

1.2.2 Polarization, E-field and Susceptibility

When a dielectric is polarized, small movements of the positive and negative charges within it take place in opposite directions. Any element of the dielectric then becomes an electric

dipole and the polarization p at a point is defined as the electric dipole moment per unit volume at the point. Thus for a volume element $d\tau$, the dipole moment (see Equation 1.14) is

$$d\boldsymbol{p} = \boldsymbol{P}d\tau \tag{1.29}$$

The SI unit of **P** is Cm^{-2}.

1.2.2 Polarization, E-field and Susceptibility

If a piece of dielectric material is introduced into a region of steady externally maintained field strength $\mathbf{E}_0$, it will become polarized and its polarization charges produce extra fields outside the dielectric. If this additional field is $\mathbf{E}_p$, then the definition of the total **E**-field everywhere including the interior of the dielectric is

$$\mathbf{E} = \mathbf{E}_0 + \mathbf{E}_p \tag{1.30}$$

1.2.3 Electric susceptibility

If the **E**-field at a point in a dielectric as defined by Equation 1.30 is **E** and the polarization at the same point is **P**, the electric susceptibility χ_e, is defined as

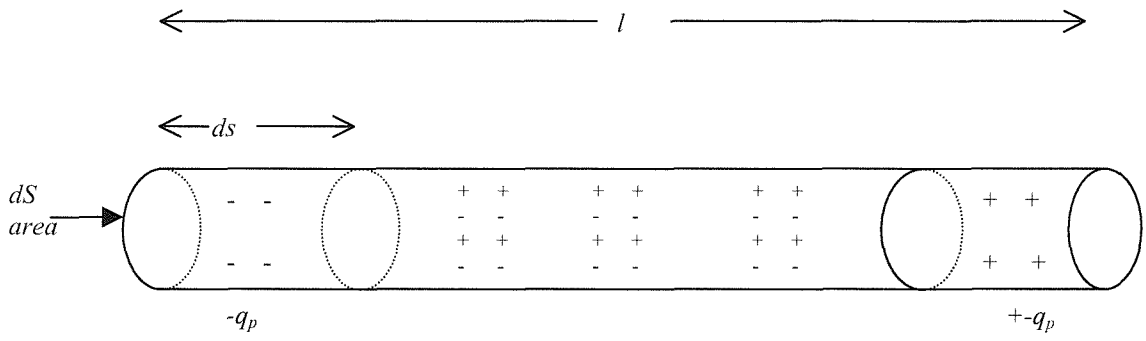

Figure 1.4: Relative displacement *ds* of uniform positive and negative charges results in induced polarization charges $+q_p$ and $-q_p$ at surfaces.

$$\boldsymbol{P} = \varepsilon_0 \chi_e \boldsymbol{E} \tag{1.31}$$

1.2.4 Gauss's Law for Dielectrics and D-field

Gauss's Law (Equation 1.18) must include both conduction charges q_c, (sometimes called free charges) and polarization charges q_p (sometimes called bound charges) on the right hand side.

$$\oint_S \mathbf{E} \cdot d\mathbf{S} = \sum \frac{q_c}{\varepsilon_0} + \sum \frac{q_p}{\varepsilon_0} \tag{1.32}$$

Now, the dipole moment $\mathbf{P}d\tau$ of Equation 1.29 can be written as $PdSd\mathbf{l}$ and this shows that the unbalanced part of the charge at each end of the element shown in Figure 1.5 is Pds (dipole moment $\mathbf{P} = q_p\mathbf{l}$). This amount of charge must have crossed any area dS when the polarization took place. For any area dS then

$$\sigma_p = \mathbf{P} \cdot d\mathbf{S} \tag{1.33}$$

and

$$q_p = -\oint \mathbf{P} \cdot d\mathbf{S} \tag{1.34}$$

Substituting Equation 1.34 into Equation 1.32 and re-arranging gives the form of Gauss's Law when dielectrics are present as:

$$\oint (\varepsilon_0 \mathbf{E} + \mathbf{P}) \cdot d\mathbf{S} = \sum q_c \tag{1.35}$$

The quantity ($\varepsilon_0\mathbf{E} + \mathbf{P}$) occurs once the E-field is as defined in Equation 1.30 and is the definition for the electric displacement **D**.

$$\mathbf{D} = \varepsilon_0 \mathbf{E} + \mathbf{P} \tag{1.36}$$

Its SI unit is Cm^{-2}.

Gauss's Law is then

$$\oint_S \mathbf{D} \cdot d\mathbf{S} = \sum q_c \tag{1.37}$$

The differential form of Equation 1.37 is

$$\nabla \cdot \mathbf{D} = \rho_c \tag{1.38}$$

and it is seen that while both conduction and polarization charges are sources of **E**-fields, the only sources of the **D**-field are conduction charges.

When no dielectrics are present $\mathbf{D} = \varepsilon_0 \mathbf{E}$

Substituting Equation (1.31) into Equation (1.37) gives the relationship between susceptibility and relative permittivity:

$$\mathbf{D} = \varepsilon_0 (1 + \chi_e) \mathbf{E} \tag{1.39}$$

By considering any system of conduction charges, **D** at any point is the same regardless of whether a dielectric material is present or not. In that case Equation (1.39) shows that **E** at any point will fall to $\frac{1}{(1+\chi_e)}$ of its vacuum value when a dielectric of susceptibility χ_e is introduced. However, when the vacuum round a capacitor carrying q_c conduction charges is completely filled with a dielectric material the capacitance increases by a factor ε_r according to Equation (1.28). If there are no connections to the plates, q_c remains constant and because $q_c = VC$, the voltage will fall by $\frac{1}{\varepsilon_r}$ of its vacuum value. The mean potential gradient and therefore the **E**-field will also fall by $\frac{1}{\varepsilon_r}$. Therefore

$$\varepsilon_r \equiv 1 + \chi_e \tag{1.40}$$

and

$$\mathbf{D} = \varepsilon_r \varepsilon_0 \mathbf{E} \tag{1.41}$$

and also

$$\mathbf{P} = \varepsilon_0 (\varepsilon_r - 1) \mathbf{E} \tag{1.42}$$

1.2.5 Electrostatic Energy, Stress and Force with Dielectrics

From Coulomb's Law the electric energy of a single charged conductor at potential V carrying charge q in a vacuum is

$$U_E = \frac{1}{2} qV \tag{1.43}$$

Consider Figure 1.6, a small element of the surface carries a charge dq and has energy $d\,U_E = \frac{1}{2} Vdqd$ associated with it . The tube of lines of force generated by dq intersecting with two typical equipotential surfaces differing in potential by dV are shown. If the electric field at the volume element is denoted by **E** then Gauss's Law applied to the volume bounded by the conducting surface having dq, dS and the sides of the tube gives

$$\mathbf{E} \,.\, dS = \frac{dq}{\varepsilon_0} \tag{1.44}$$

Thus

$$dU_E = \frac{1}{2} \varepsilon_0 \mathbf{E} \,.\, dSV \tag{1.45}$$

But $V = \int_{\infty}^{s'} -\mathbf{E} dr = \int_{s'}^{\infty} \mathbf{E} dr$ and because $dq = \varepsilon_0 \mathbf{E} dS$ applies to all the equipotentials cut by the tube

$$dU_E = \frac{1}{2} \varepsilon_0 dS \int_{s'}^{\infty} \mathbf{E} dr = \int_{s'}^{\infty} \frac{1}{2} \varepsilon_0 \mathbf{E}^2 dSdr \tag{1.46}$$

Integrating over the entire surface gives the total energy due to q and writing $dSdr$ as $d\tau$ we have

$$U_E = \int_{\tau} \frac{1}{2} \varepsilon_0 \mathbf{E}^2 \, d\tau \tag{1.47}$$

By differentiating both sides with respect to τ we have

$$\frac{dU_E}{d\tau} = \frac{1}{2} \varepsilon_0 \mathbf{E}^2 \tag{1.48}$$

and we have a convenient expression, in terms of the **E**-field, for the electrostatic stress (i.e. energy per unit volume or more conventionally force per unit area).This force is strictly exerted on the charges at the surface but because emission of charge may not always occur there must be a restoring non-electrostatic force exerted by the conductor on the charges. By Newton's 3rd law an equal and opposite force acts on the conductor itself so that:

Outward stress on the surface of a charged conductor in a vacuum (or air)

$$P_E = \frac{1}{2}\varepsilon_0 \mathbf{E}^2 = \frac{\sigma^2}{2\varepsilon_0} \tag{1.49}$$

The case with *dielectrics* present must be treated firstly by making some simplifying assumptions. Firstly ε_r must be single valued so that integrals have a unique magnitude. Secondly, a thermodynamical rather than a merely mechanical approach must be taken.

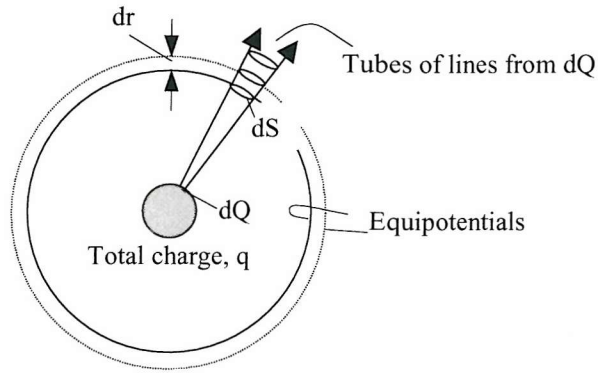

Figure 1.5: Calculation of the energy of a charged conductor in terms of E.

Instead of equating work done on a system W to the increase in mechanical energy U, the conditions should be specified more precisely. For example if the changes occur adiabatically (no heat transfer between the system and its surroundings) $dW = dU$, the increase in internal energy. For a reversible isothermal change, $dW = dF$, the increase in Helmholtz free energy. Because ε_r varies with temperature and it is advisable to avoid this complication, it is assumed that all processes are carried out reversibly and isothermally (at constant temperature). Strictly speaking, therefore, $dW = dF$ but the symbol U_E will be retained here as the energy is electrical in nature.

Thirdly and finally, stresses in a dielectric caused by polarization will usually strain the material (electrostriction) and bring about changes in **E**. The assumption is made that the dielectrics discussed in this thesis are incompressible.

Referring again to Figure 1.6 and applying the generalized form of Gauss's Law (Equation 1.37) to the volume bounded by *dq, dS* and the lines of force gives

$DdS = dq$ so that

$$dU_E = \frac{1}{2}\mathbf{D}dSV \tag{1.50}$$

The relation dq = DdS applies to all equipotential surfaces cut by the tube and thus

$$dU_E = \frac{1}{2}\mathbf{D}S\int_{S'}^{\infty}\mathbf{E}dr \tag{1.51}$$

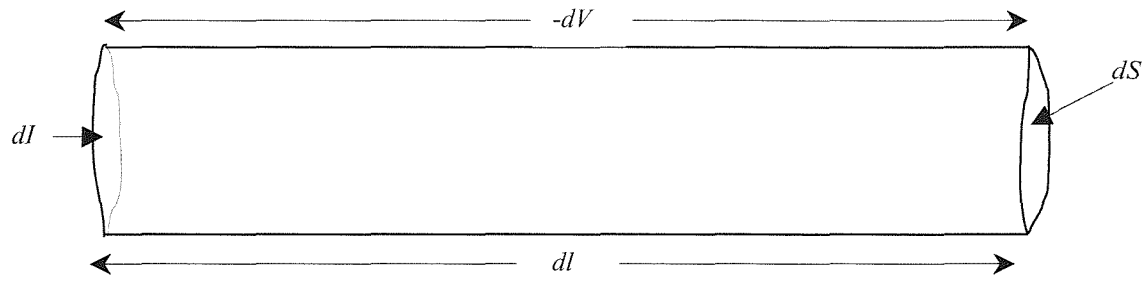

Figure 1.6: An element of a current carrying material

and the free energy is

$$U_E = \int_\tau \frac{1}{2}\boldsymbol{D}.\boldsymbol{E}\,d\tau \tag{1.52}$$

$$= \int_\tau \frac{1}{2}\varepsilon_r\varepsilon_0\,\boldsymbol{E}^2\,d\tau \tag{1.53}$$

By similar arguments as before, the force on the surface of a charged conductor in contact with a fluid dielectric is

$$P_E = \frac{1}{2}\mathbf{D}.\mathbf{E} = \frac{\sigma_c}{2\varepsilon_r\varepsilon_0} \tag{1.54}$$

1.3 The Continuity Equation in Electrostatics: Charge Conservation

1.3.1 Ohm's Law at a Point

The expression of Ohm's Law as $V = IR$, where V is the potential dropped across a constant resistance R when a current I flows through it, applies for example between two points along the length of a conducting wire or cable. A more general form that twill apply at any single point within a material can be derived as follows. Consider a cylindrical element of a material of conductivity κ carrying a current I (Figure 1.7). The voltage across the element is $-dV$ (negative in the direction of I).

$$-dV = R\,dI = \frac{dl}{\kappa dA}\,dI \tag{1.55}$$

rearranging gives:

$$-\kappa\frac{dV}{dl} = \frac{dI}{dA} \tag{1.56}$$

In the limit as dl and dA approach zero Equation (1.56) can be written

$$\mathbf{J} = \kappa\,\mathbf{E} \tag{1.57}$$

The above is strictly a definition of κ at a point. For an ohmic conductor κ is independent of $\mathbf{J}$ and $\mathbf{E}$.

1.3.2 Current Densities in terms of Moving Charges

The volume current density was defined in Section 1.1.3. A similar definition can be used for *surface density* $\mathbf{J}_s$ which is a useful quantity in the case where current flows in thin surface layers or in sheets. It is defined as the current per unit width perpendicular to the flow (see Figure 1.8).

$$dI = \mathbf{J}_s\,db\perp \tag{1.58}$$

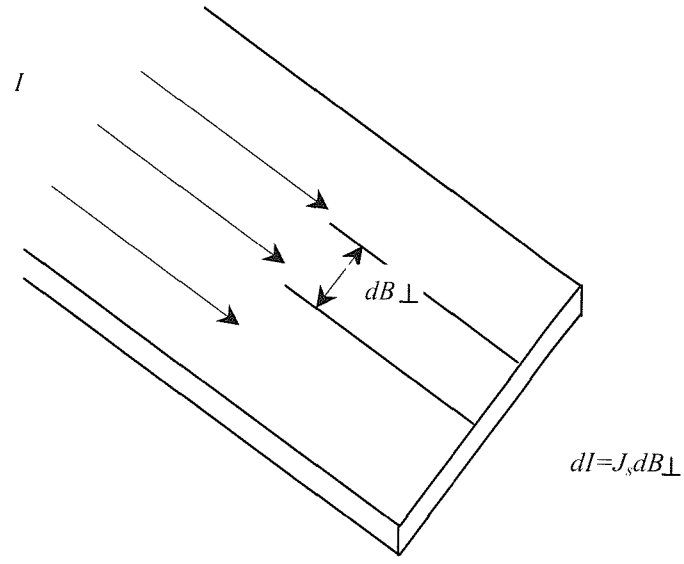

Figure 1.7: Surface current density J, is the current per unit length perpendicular to the flow.

The current densities **J** and $\mathbf{J}_s$ usually refer to macroscopic systems. Where elementary charges are carrying the current, an average value for **J** or $\mathbf{J}_s$ over a great many charges can be used to model the situation. Thus if charges of volume density thus if charges of volume density ρ are moving with velocity **v** (also an average) then

$$\mathbf{J} = \rho\mathbf{v} \tag{1.59}$$

Similarly, it can be shown that

$$\mathbf{J}_s = \sigma\mathbf{v} \tag{1.60}$$

If ρ is written as nq, where n is the number of charge carriers of charge q, then $\mathbf{J} = nq\mathbf{v}$ is a very general expression giving any current density in terms of its constituent moving charges. For example, if there are i different species present, the total current density can be found be summing over all the species.

$$\mathbf{J} = \sum_i \mathrm{n}_i q_i \mathbf{v}_i \tag{1.61}$$

1.3.3 Charge Mobility

Examination of Equations (1.57) and (1.61) reveals two independent expressions for **J**, the volume current charge density. Equation (1.57) applies only to conductors whereas Equation (1.60) applies to all conduction processes. Therefore in a conducting material

$$\kappa \boldsymbol{E} = \sum_i n_i q_i \boldsymbol{v}_i \text{vv} \tag{1.62}$$

The quantity $\frac{\mathbf{v}_i}{\mathbf{E}}$ the drift velocity per unit electric field, is defined as the *mobility* of the carrier, μ.

$$\mu \equiv \frac{\mathbf{v}_i}{\mathbf{E}} \tag{1.63}$$

Thus, the conductivity, κ, can be expressed as

$$\kappa = \sum_i n_i q_i \mu_i \tag{1.64}$$

1.3.4 Charge Continuity

Consider Equation (1.59). A volume of space of bounding surface S can be imagined to contain ρ charges per unit volume. The total charge enclosed is thus $q = \rho d\tau$, where $d\tau$ is the volume. If these charges move, then the charge q inside S will change in such a way that the total outward current over S *is* $-\frac{dq}{dt}$. The total outward current can also be written as $\oint \mathbf{J} \cdot d\mathbf{S}$ (Equation 1.4) thus

$$\oint \mathbf{J} \cdot d\mathbf{S} = \frac{dq}{dt} \tag{1.65}$$

The above can be applied to a single point in a similar way to Gauss's Law (Sections 1.1.8,1.1.9)

$$\nabla \cdot \boldsymbol{J} = \frac{d\rho}{dt} \tag{1.66}$$

Many of these expressions are used in the following chapters.

CHAPTER 2

DISPERSED SYSTEMS

2.1 Principles of Dispersed Systems

In this section, an introduction is given to the science of dispersed systems. Many materials exist in the form of a disperse system, for example powders, pastes, slurries, emulsions and aerosols. The studies of this thesis deal with three of those systems so it is appropriate that the basis of the general behaviour of disperse media be set out prior to discussing the electrostatic interactions of three such systems.

2.2 Definitions

2.2.1 Disperse System

A *disperse system*, in its simplest definition, consists of two distinct and separate phases. The thermodynamic definition of a *phase* is a homogenous region of matter, which need not be continuous. Examples of discontinuous phases are a gas dispersed as bubbles in a liquid, a liquid dispersed as droplets in another liquid with which it is immiscible and a crystalline or amorphous solid dispersed in either a gas or a liquid. In each case, a dispersed phase is distributed throughout a continuous phase. The complete system is described as a dispersed system- an abrupt change in properties always occurs at the boundary between phases. The continuous phase is called the dispersion medium whereas the discontinuous phase is called the *dispersed medium*. The elements of the dispersed medium are called *particles*.
Disperse systems are often thermodynamically unstable, because any free energy associated with the large interfacial area between the dispersed phase and the continuous phase can decrease by aggregation or coalescence of the dispersed phase.
A definition as broad as that given above naturally encompasses a huge variety of systems. Classification of disperse systems is done on the bases of

i) the nature of each phase (gas, liquid, solid)

ii) the 'size' of the particles of the dispersed phase

iii) the mechanism (if any) by which the dispersed phase is stabilized.

Figure 2.1 shows a schematic classification of disperse systems, which is subdivided first according to the phases and then particle size.

2.2.2 Particle size

The use of the term *particle size* generally implies that the user has answered two questions to his own satisfaction.

1) What is meant by *particle*? and

2) What is meant by *particle size*?

Both terms are usually highly ambiguous unless they are carefully defined.

A particle has earlier been defined as an element of the dispersed medium. It can therefore be a solid, a liquid or a gas. In its most general sense, the word 'particle' refers to any object having definite physical boundaries in all directions, without any limit with respect to size. For the purposes of this thesis, the definition of particle will be limited by size, however. The reason for this is not one of convenience but rather arises due to the coupling of electrostatic forces with the other physiochemical forces acting or capable of acting on the particles. As will be detailed later, solid powders of relative density close to unity can be manipulated in air by electrostatic forces if the particle size is in the range of approximately 2 μm to 5 mm. Aerosol droplets will deposit within the lung most efficiently if their size is about 6 μm and water droplets dispersed in oil can be separated by cyclonic devices if their size exceeds about 30 μm. Therefore, for engineering purposes, the particles referred to here will lie in the range 1 μm to 1 mm.

The terms *size, radius* and *diameter* also need careful definition. The word *diameter* was originally defined for circles, discs and spheres but it is useful also to define the term for irregularly shaped particles. Diameters of individual irregular particles may be defined in terms of the geometry of the particle. To extend this definition so it has meaning to a population of particles, large numbers of particles must be measured and the results averaged. The term statistical diameter is then used to describe this measure.

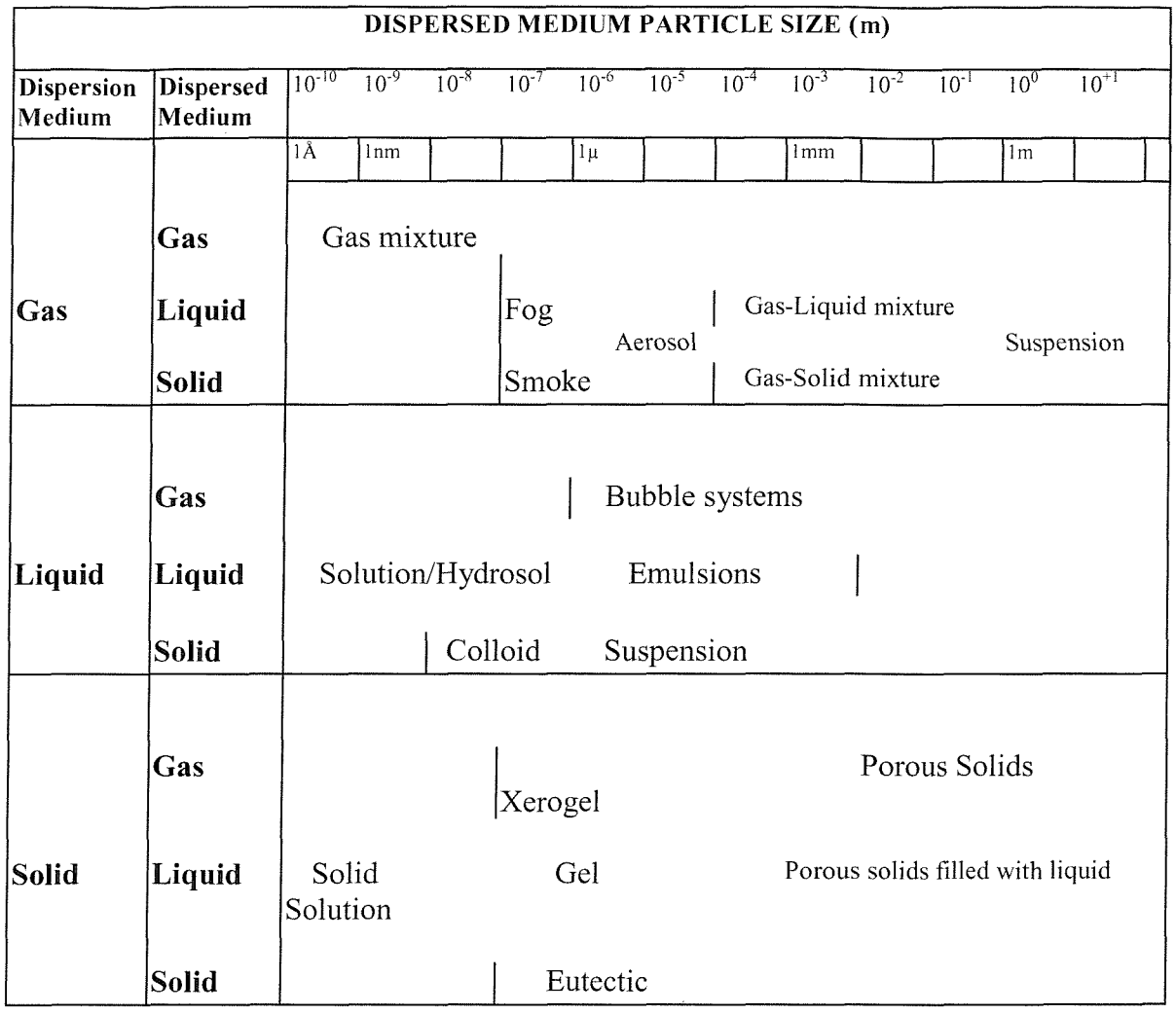

Figure 2.1: Schematic classification of disperse systems (After Rumpf, 1990)

Generally, the nature of the disperse phase has to be represented by one or more numerical values and associated units (Rumpf, 1990). As the disperse phase consists of a population of particles, it is necessary to describe it in terms of a distribution function. The particles must be classified according to some property having a measurable physical magnitude - an example of which is the statistical diameter described above. Such measures of dispersity, which can be directly or indirectly linked to the particle 'size', are termed fineness parameters.

Many fineness parameters can be expressed in terms of equivalent diameters (Table 2.1). These are the dimensions of a particle of defined geometrical shape that has the same property as the property of interest of the particle (or population of particles) under investigation.

GEOMETRIC EQUIVALENT DIAMETERS	SYMBOL
Diameter of sphere with the same volume	d_V
Diameter of sphere with the same surface area	d_S
Diameter of sphere with the same specific surface area	d_{SV}
Diameter of the circumscribing sphere	d_{EN}
GEOMETRIC EQUIVALENT FROM THE PROJECTION OF THE PARTICLE*	
Diameter of the circle with the same area	d_p
Diameter of the circle with the same perimeter	d_{pe}
Diameter of the inscribed circle	d_{in}
Diameter of the circumscribed circle	d_{ci}
HYDRODYNAMIC EQUIVALENT DIAMETERS	
Diameter of the sphere with the same drag	d_D
Diameter of the sphere with the same terminal velocity	d_u
Stoke's diameter	d_{St}
OTHER EQUIVALENT DIAMETERS	
Diameter of sphere scattering light at the same intensity	d_{Sca}
Diameter of the sphere causing the same change in electrical resistance (Coulter counter)	d_{el}

*Projection will depend on particle orientation i.e. either a stable alignment or a random alignment.

Table 2.1: Important Equivalent Diameters (After Rumpf, 1990 and Lefebvre, 1989)

2.2.3 Particle size distribution

Let x be any measure of dispersity, e.g. d_V, d_{St} etc. The population of particles being measured is distributed according to some function of x, call it $Q_r(x)$. It is most common and appropriate that x is a linear dimension such as many of the equivalent diameters discussed earlier. The numerical value of this dimension can, in principle, lie anywhere between zero and infinity. In practice, however, there is always a minimum value x_{min} and a maximum

value x_{max}. The distribution function $Q_r(x)$ indicates which proportion of the total population lies between x_{min} and x_{max}. Thus (see Figure 2.2)

$$0 < Q_r(x) < 1 \tag{2.1}$$

$$Q_r(x_{min}) = 0 \quad and \quad Q_r(x_{max}) = 1 \tag{2.2}$$

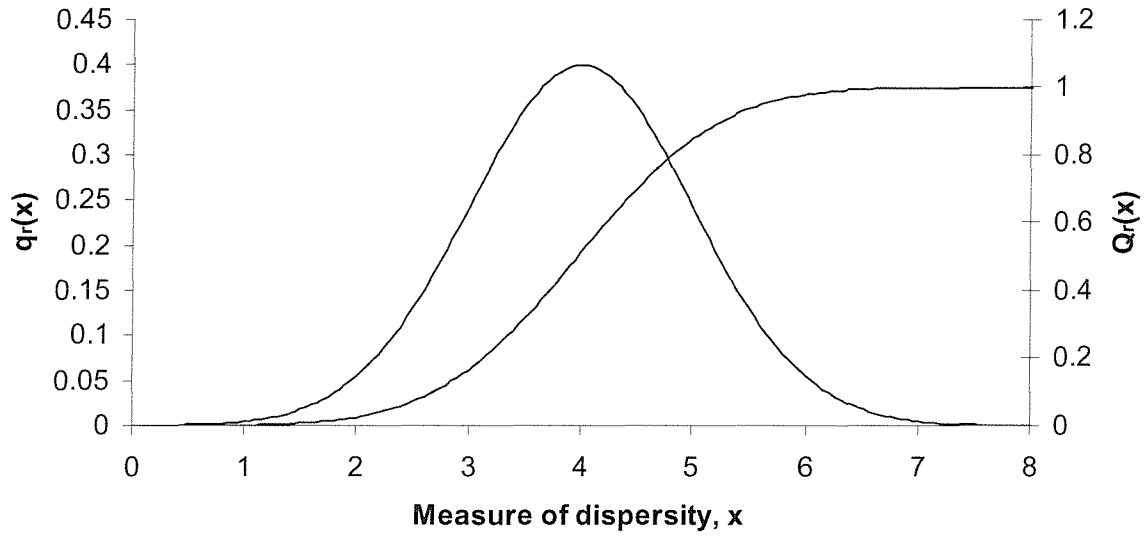

Figure 2.2: Graphical representation of particle assemblies: $q_r(x)$ is a density distribution while $Q_r(x)$ is a cumulative function distribrution with x a measure of dispersity.

By introducing $Q_r(x)$ the question as to how the population is to be measured is left open. It can, for example, be measured by number, by surface area, by mass etc. Defining the distribution by surface area is perhaps most appropriate when discussing dispersed systems interaction with electrostatic fields. The subscript r is used to designate the kind of measure being made. If the particles are being counted, then the population is measured by number and $Q_0(x)$is written, by length $Q_1(x)$, by surface area $Q_2(x)$ and by volume $Q_3(x)$ (see Figure 2.3). For measurement by mass $Q_3(x)$ is used also so long as the particle mass density is independent of particle size.

With all the particle assemblies dealt with in this thesis the number of particles is so large that the distribution function $Q_r(x)$ can be regarded as continuous and it can be differentiated as follows:

$$q_r(x) = \frac{dQ_r(x)}{dx} \tag{2.3}$$

where $q_r(x)$ is the density distribution function corresponding to the cumulative distribution function $Q_r(x)$. In the case of $Q_0(x)$, $q_0(x)$ is the frequency distribution (that is the ordinate gives the number of particles that have dimension x).

Conversely, the cumulative distribution function can be obtained from the population density by integration:

$$Q_r(x) = \int_{x_{min}}^{x} q_r(x)\, dx \tag{2.4}$$

2.2.4 Moments, mean diameters and representative diameters of particle assemblies.

For calculations involving distributions, condensed expressions called moments are used for certain integrals. Each moment is defined on the basis that certain quantities are proportional to particle size raised to a power, such as surface area ($\propto x^2$) or volume ($\propto x^3$).

In general, the k-th complete moment of the Q_r distribution is defined as:

$$M_{k,r} = \int_{x_{min}}^{x_{max}} x^k q_r(x)\, dx \tag{2.5}$$

Means are calculated from moments. For example, if d_V is measured for x and $Q_r(x) = Q_0(d_V)$, then a mean diameter (called the length mean diameter or the numerical mean diameter) is

$$D_{10} = \frac{M_{1,0}}{Q_0(d_{max})} = \frac{\int_{d_{V_{min}}}^{d_{V_{max}}} d_V\, q_0(d_V)\, dd_V}{\int_{d_{V_{min}}}^{d_{V_{max}}} q_0(d_v)\, dd_V} \tag{2.6}$$

Other mean diameters of interest include the surface mean

$$D_{20} = \left[\frac{M_{2,0}}{Q_0(d_{V_{max}})}\right]^{\frac{1}{2}} = \left[\frac{\int_{d_{V_{min}}}^{d_{V_{max}}} d_V{}^2\, q_0(d_V)\, dd_V}{\int_{d_{V_{min}}}^{d_{V_{max}}} q_0(d_V)\, dd_V}\right]^{\frac{1}{2}} \tag{2.7}$$

Volume mean

$$D_{30} = \left[\frac{M_{3,0}}{Q_0(d_{V_{max}})}\right]^{\frac{1}{3}} = \left[\frac{\int_{d_{V_{min}}}^{d_{V_{max}}} d_V{}^3 q_0(d_V)\, dd_V}{\int_{d_{V_{min}}}^{d_{V_{max}}} q_0(d_V)\, dd_V}\right]^{\frac{1}{3}} \tag{2.8}$$

In general, mean diameters are given by the expression (Lefebvre, 1989) as

$$(D_{kr})^{k-r} = \left[\frac{M_{k,r}}{Q_r}\right] = \left[\frac{\int_{x_{min}}^{x_{max}} x^k q_r(x)\, dx}{\int_{x_{min}}^{x_{max}} x^r q_r(x)\, dx}\right] \tag{2.9}$$

where k and r take on the values corresponding to the effect being investigated and the sum k + r is called the order of the mean diameter. Where a discrete distribution has been measured, Equation 2.9 can be written as

$$D_{kr} = \left[\frac{\sum Q_{ri} x_i^{\,k}}{\sum Q_{ri} x_i^{\,r}}\right]^{\frac{1}{k-r}} \tag{2.10}$$

where i denotes the size band considered, Q_{ri} is the number of particles in size band i and x_i is the middle dispersity parameter of size band i. Thus D_{30} is the diameter of a particle whose volume, if multiplied by the number of particles, equals the total volume of the sample and D_{32} (the Sauter mean diameter) is the diameter of the particle whose ratio of volume to surface area is the same as that of the entire sample. These and other important mean diameters are listed in Table 2.2 along with the field of application most commonly associated with them.

Instead of using a mean diameter as a fineness parameter describing a particle assembly, a representative diameter may be used. Either a mean or a representative diameter together with a measure of the spread about that diameter can then be used to represent concisely the particle assembly.

a	b	a+b order	Symbol	Name of mean diameter	Application
1	0	1	D10	Length	Comparisons
2	0	2	D20	Surface length	Surface area controlling
3	0	3	D30	Volume	Volume controlling, e.g., hydrology
2	1	3	D21	Surface area-length	Absorption
3	1	4	D31	Volume-length	Evaporation, molecular diffusion
3	2	5	D32	Sauter (SMD)	Mass transfer, reaction
4	3	7	D43	De Brouckere or Herdan	Combustion, equilibrium

Table 2.2: Mean diameters and their applications. (After Lefebvre, 1989)

There are many possible choices of representative diameters including the following:

$D_{0.1}$ = particle diameter such that 10% of total volume is in particles of smaller diameter

$D_{0.5}$ = as above but 50%. Where the mass density is independent of particle size, this is the mass median diameter as well as the volume median diameter (VMD).

$D_{0.9}$ = as above but 90%.

D_{peak} = value of D corresponding to peak of particle size frequency curve.

2.2.5 Mathematical Distribution Functions

Many workers have sought to replace experimentally determined and graphically represented distribution functions with mathematical expressions whose parameters can be obtained from a limited number of particle size measurements. Suitable mathematical expressions would have the following attributes (Lefebvre, 1989):

1. Provide a satisfactory fit to the particle size data.

2. Allow extrapolation to particle sizes outside the range of the measured values.

3. Permit easy calculation of mean and representative particle diameters and other parameters of interest.

4. Provide a means of consolidating large amounts of data.
5. Ideally, furnish some insight into the basic mechanisms involved in comminution, agglomeration, coalescence etc.

Where a deterministic model for a process leading to a particle assembly has not or cannot be formulated, a number of functions have been proposed, based on either probability or purely empirical considerations, that allow the mathematical representation of measured particle size distributions (Cadle, 1965).

Among those in general use are normal, log-normal, Nukiyama-Tanasawa, Rosin-Rammler and upper-limit distributions. Since there are many and varied processes leading to particle assemblies, many of which are far from being understood at the fundamental level, no single distribution can represent all particle size data. Details of these distributions and the area in which they are more successfully applied can be found in most texts on dispersed systems.

PART II

STUDY ONE: THE CHALLENGE OF CHARGING SOLID PARTICLES BY INDUCTION CHARGING

CHAPTER 3

INTRODUCTION TO POWDER COATING

3.1. Forces on Small Discrete Bodies

The electrostatic body force, or Coulomb force, on a body that is charged to q coulombs in an electric field of local magnitude $\boldsymbol{E}$ volts per meter was introduced in Chapter 1, equation (1.7). Rewriting that equation to give a direct expression for force gives:

$$\boldsymbol{F}_e = q\boldsymbol{E} \tag{3.1}$$

With dielectric media, the charge which the body can hold and the local field strength is limited by the break-down strength of the surrounding gas. Consider a spherical particle suspended in air at ambient conditions carrying a uniform surface charge density of σ Cm^{-2}. The electric field strength $\boldsymbol{E}$, at the particle surface is given by Gauss's law (equation (1.41) as:

$$\boldsymbol{E}_s = \frac{\boldsymbol{D}}{\varepsilon_r \varepsilon_0} = \frac{\sigma}{\varepsilon_0} \tag{3.2}$$

where ε_0 is the permittivity of a vacuum (8.85 x 10^{-12} Fm^{-1}) and ε_r is approximately 1. When the electric field at the particle/air interface is high enough to cause electric breakdown of the air, electron avalanches occur, generating a large number of ion pairs (Alston, 1968). Some of these ions combine with ions on the particle surface and thus discharge a portion of the particle charge. The corona inception field strength of air at ambient conditions has been measured by Peek to be approximately $3MVm^{-1}$ (Peek, 1929). Taking this value, the maximum surface charge density on the particle is $2.64 \times 10^{-5}\ Cm^{-2}$ from Equation 3.2, and this value may be considered as the maximum limit for the surface charge density for larger particles ($\geq 50\mu m$ diameter). For smaller particles, considerably denser levels of charge can be maintained (Hamamoto and Nakajima, 1992). Thus the maximum charge on a small body is proportional to its surface area to the power of at least one or, equivalently, to D_{32}^{2-n}. The function describing how the maximum charge-to-mass ratio changes as D_{32} changes therefore

has a term $D_{32}^{2-n} / D_{32}^{3}$ or a term in D_{32}^{-1-n} where D_{32} is the Sauter mean diameter of the particle and $n \leq 0.5$ (Hamamoto and Nakajima, 1992). Here, n is assumed = 0.

One can easily calculate a cross-over diameter at which point the electrostatic force begins to dominate the gravitational force. The gravitational force on a sphere (e.g. a liquid droplet in equilibrium with its surroundings) of diameter d and density ρ_g is

$$\boldsymbol{F}_g = \frac{\pi}{6} d^3 \rho_g g \tag{3.3}$$

whereas the electrostatic force is

$$\boldsymbol{F}_e = q_{max} \boldsymbol{E}_{max} \tag{3.4}$$

$$\boldsymbol{F}_e = 2.64 \times 10^{-5} \times \pi d^2 \times 3 \times 10^6 \tag{3.5}$$

The two forces are equal when $d = 48\ mm$ with $\rho_g = 1000\ kgm^{-3}$. In practice, it is not possible to maintain a stable electric field close to the breakdown strength of 3 MVm^{-1} and the practical upper limit of the applied field is about $5 \times 10^5\ Vm^{-1}$ (Cross, 1987). Thus, the cross-over diameter will be around $5mm$ or even less. This ties in with practical experience and observation. Phenomena which work to counter the maintenance of a strong electrostatic force bring the total charge below the theoretical q_{max} level.

To utilise electrostatic forces to manipulate small charged particles or droplets aerodynamic drag forces must be overcome in addition to gravitational forces. Drag forces oppose the relative motion between the particle and the surrounding gas. If the drag force is assumed to obey Stoke's law then equating the electrostatic force on the particle to the drag force gives:

$$3\pi\mu d\boldsymbol{u} = 2.64 \times \pi d^2 \boldsymbol{E} \tag{3.6}$$

where μ is the dynamic viscosity of air, 1.8×10^{-5} Nsm^{-2}, $\boldsymbol{u}$ is the particle's terminal settling velocity and d its aerodynamic diameter (SMD) then

$$\boldsymbol{u} = \frac{1}{2}\boldsymbol{E}d \tag{3.7}$$

For the above quoted field strength of 5 x 10^5 Vm^{-1}, a particle of diameter 2 μm charged to a surface charge density of 2.64 x 10^{-5} Crn^{-2}, will achieve a terminal velocity of approximately 0.5 ms^{-1}. For engineering purposes, it can therefore be seen that the range of particle diameters where the electrostatic forces may be greater than gravitational forces and overcome sufficiently aerodynamic drag forces is between about 2 μm and 5 mm.

One such area of engineering endeavour is the use of electrostatic forces to deposit dry powder paints onto surfaces to which they adhere, also by electrostatic forces. The powder is then thermally fused and the surface *finished* in the parlance of the industry.

3.2 Powder Coating Fundamentals

3.2.1 History

Fluidized-bed coating processes were developed in the mid-1950's, the first patent being granted in Germany in 1955 (Gremmer). The first basic US patent was issued to the same company in 1958 and exclusive rights licensed in North America to The Polymer Corporation of Pennsylvania. Acceptance of the technology was slow due to conservative attitudes and the inevitable scale-up problems and associated costs attendant on any technological break-through.

In the fluidized-bed process, the coating powder is placed in a container with a porous plate as its base. Air is passed through the porous plate causing the powder voidage to increase and eventually fluidize. The part to be coated, usually metallic, is heated in an oven to a temperature above the melting point of the powder and dipped into the bed. Particles then collide and fuse to the surface of the hot metal to form a coating. In electro-fluidized beds, charging of the fluidized powder by ionized air enhances collision probability with the workpiece and decreases substrate residence time while improving the finish quality. It is possible to apply coatings ranging in thickness from circa 250 to 2500 μm with this process. It is difficult to obtain coatings of less than 250 μm and therefore fluidized-bed applied coatings are generally referred to as thick-film coatings, differentiating them from most conventional thin-film coatings of the time that were applied from solution at thicknesses of 25 - 75 μm.
In the early 1960's, the electrostatic powder-spray-coating equipment became available, firstly in France then worldwide. The process was viewed as a natural development of electrostatic painting with many of the basic components of both systems being similar. This and the advantages of switching to dry powder finishing detailed below made it possible for prototype application devices to be developed and made available very rapidly, (Bright et al, 1970).

3.2.2 The Case for Powder Coating

The case for powder coating has strengthened in the years since its introduction. The criteria for judging the performance of powder coating over other finishing techniques are:

i) Economic

ii) Environmental impact

iii) Finish quality

iv) Corrosion resistance/longevity

v) Safety and health factors

3.2.2.1 Economic Advantages

Powder coating is one of the least expensive finishing methods available today (Moore, 1993). While material and equipment costs are similar to liquid finishing systems, the savings achieved in energy, labour, production, waste disposal and meeting environmental regulations makes the true cost of powder coating less than liquid finishing.

Powder coating systems reduce energy consumption because there are no solvents to be evaporated. This reduces the need for air heating and fresh air make-up. No solvents mean that air and water pollution problems are virtually eliminated, reducing capital expenditure on anti-pollution equipment and the expense of dealing with regulatory agencies. The cost of disposal of sludge and other by-products is also reduced.

Lower unit costs are achieved with powder because of the absence of a 'flash-off' time, closer packing of parts to be finished on conveyors and a lower reject rate. Greater automation is often achievable with powder coating installations and with lower clean-up times and a better working environment, labour costs can be kept down.

3.2.2.2 Environmental Advantages

In the US, more than any other factor, the Clean Air Act of 1970 propelled powder coating processes to the forefront as a method to reduce air pollution by eliminating volatile organic compounds (VOC's). The impetus was maintained with the passing of the Clean Air Act Amendments in 1977 (see e.g. Plastics World, 1980), and 1990.

During the fusion or curing of a coating powder, some volatile organic compounds are liberated but, with the exception of the caprolactum used as a blocking agent in the polyurethane coatings, most are only in trace quantities. For example, of the volatile materials emitted during the bake cycle of an epoxy, polyester-epoxy hybrid and a polyester-TGIC powder (TGIC is triglycidyl isocyanurate, a curing and antisintering agent), up to 99% was found to be absorbed moisture or condensed product (Mayer and Kordes, 1977).

The powder coating system itself is also of benefit to the environment as less oven air is exhausted to the outside, first pass transfer efficiency is high and powder coatings are usually

collected and recycled. Furthermore, disposal methods, when necessary, are the same as for non-hazardous wastes in most cases. (Powder Coating Handbook, 1994).

3.2.2.3 Finish Quality Advantages

Powder coatings provide several important advantages in quality compared with conventional liquid finishes.

a)**Consistent Results:** Powders are supplied ready to use without additional pre-mixing, stirring, solvent addition or viscosity adjustments. Besides the obvious savings in labour, this implies that finish quality variations are minimized.

b) **Film Thickness** A major quality advantage with powder coated parts is the ability to achieve an optimum film thickness in a single pass operation without problems of drips, sags or runs. Thick or thin films can be applied in a controlled and repeatable manner depending on the end use of the part. The current range in thickness most successfully achieved with sprayed powder coatings is between 25 μm to 375 μm.

c)**Edge Coverage** Powders can be formulated to provide a wide range of melt viscosities and can be applied over a wide range of film thickness (see above). Therefore, powder can provide better edge coverage protection than can be achieved in single-coat liquid application.

d) **Corrosion Resistance and Longevity** While the importance of the role which proper substrate pretreatment plays in achieving optimum corrosion resistance cannot be overemphasized, the combination of good pretreatment and powder coatings can provide outstanding corrosion resistance. Corrosion resistance and the longevity of the protection and appearance are linked to the ability of the powder coating process to consistently deliver high film builds and good edge coverage. Equally important are the facts that powders provide high crosslink density, good resistance to hydrolysis, low resistance and oxidising agent diffusion rates and films free from residual solvents.

The testing of the long term performance of powder films is covered in detail in the ASTM Standard (1979).

3.3 A New Challenge for Powder Coatings

Before moving on to discuss in detail why and how powder can deliver the advantages outlined in section 3.2, it is tantalizing to close this chapter with perhaps the biggest challenge

that powder coating as a technology has ever been faced with automotive finishing. The following chapter will detail why electrostatic phenomena are an integral part of that challenge and how the work described later aims to meet it.

3.3.1 Automotive Finishing and the Low Emissions Consortium

Powder coatings have been used for a long time in automotive "under hood" applications. Coil springs, brake housings and even engine blocks are powder coated, often with black epoxy powder coatings for corrosion resistance. Decorative applications include oil filters, some exterior trim and styled aluminium hubs (Moses, 1993).

In the US, automobile manufacturers have experimented with powder coatings on a more ambitious scale. General Motors and Ford evaluated powder as an exterior full body colour topcoat in the 1970's. Pilot plant facilities were installed in assembly plants, with poor results, liquid based technology out-performing powder (Moses, 1993).

In the interim, several factors have caused automobile manufacturers to re-examine powder technology for assembly operations. The overriding factor has been environmental legislation and in 1993 the "big three" automobile manufacturers - Ford, General Motors and Chrysler - joined forces to form the United States Council for Automotive Research Low Emission Paint Consortium (LEC). Their aim is to conduct research and development programmes in paint related technologies to reduce or eliminate solvent emissions from automotive paint systems. Such a move is regarded as "revolutionary" and is a testimony to the difficulties that need to be overcome (Koop, 1993). Car manufacturers in Europe are also involved in development of powder systems (Ref: AUDI/VW, Mercedes Benz), and powder technology heads the programme of the LEC at present.

The clear-coat that is the final layer on a finished automobile is the immediate target of all automobile manufacturers. To keep equipment costs down, plants must be retrofitted with powder equipment and use of the current ovens for curing maintained. To limit material costs, a coating that can be applied in thin films with high first-pass transfer efficiency (FPTE) and recyclability is required. Furthermore, automation with robotic systems capable of keeping pace with current production line speeds is a must. The clearcoat has to be compatible with the vehicle's basecoat and provide a world-class finish with five-year durability. The powder must be stable and handle well and the finish must be capable of being repaired in the field.

The paint consortium gives itself twelve years to test its long-term ambitions to develop a low-emissions paint system, a further indication of how big a job developing the powder technology represents.

CHAPTER 4

ELECTROSTATIC PROCESSES IN POWDER COATING

Bailey (1998) reviews the science and technology of electrostatic powder spraying and provides an excellent synopsis of the state of this technology from in theory and practice. This chapter was prepared by the author before Bailey's review and serves as a foundation for Chapter 5.

In the previous chapter, the qualitative aspects of powder coating were introduced and the advantages of the method outlined. In this chapter the electrostatic processes governing the behaviour of a powder coating operation are quantitatively discussed.

The discussion will examine how electrostatic charging of the individual powder particles is achieved in practice, how the combined electrostatic and aerodynamic forces bring about deposition on the workpiece, how self-limiting of layer thickness occurs and examines the adhesion forces holding the particles to the workpiece prior to thermal fusion. The limitations inherent in each step will be examined as well as the effect of a powder diameter and electrical properties.

Finally, a new approach, induction charging, is introduced which has many advantages to offer in taking the technology into the future.

4.1 Powder Particulate Charging: General

In dealing with the engineering of powder particulates and powder particulate bulks or clouds, it is almost inevitable that generalization of the properties of a single ideal particle is extended to represent the bulk of all the particles. Although based on sound engineering practice, such a smoothing or averaging approach will always have limits especially when dealing with phenomena which are dependent on particle shape and surface area to volume (or mass) ratio. As electrostatic charging of a particle is a surface area phenomenon, considerable care must be taken when assumptions are made as to the particles dimensional characteristics. For reasons of simplicity and practicality, a spherical representation of the particle is usually made with the linear average dimension of the bulk cloud based on either a representative diameter such as the $D_{0.5,}$ (the diameter of a particle below which half the volume of the bulk is made

up of smaller particles), a modal diameter (e.g. the most commonly occurring diameter in the bulk) or a diameter figured by some averaging process over the entire bulk, or a representative sample thereof.

In powder coating, where the electrostatic force is used to control the motion of a particle to the workpiece and its adhesion to it prior to curing, modelling of the powder cloud is by the volume or mass median diameter (mmd) so that the representative diameter is one which assumes that the particles in a cloud of powder coating powder can be replaced by the same volume (or mass) of monodispersed spherical particles of diameter d.

With the preceding comments in mind one can now examine the physics of the charging processes.

4.1.1 How Much Charge?

If one takes the case of an isolated particle of typical mmd of 50 μm having a mass density of 1200 kgm^{-3} and further assumes that the only electrostatic field acting on it is that due to its self-field arising from the charges it is carrying and that it is carried to a workpiece by aerodynamic forces, the charges it needs to allow deposition and adhesion to the earthed workpiece can be calculated. The mass of the particle is:

$$\rho_m \frac{\pi}{6} d^3 = 1200 \frac{\pi}{6} \left(50 x 10^{-6}\right)^3 \tag{4.1}$$

$$= 7.85 \text{ x } 10^{-11} \text{ kg}$$

The gravitational force is therefore:

$$mg = 7.7 x 10^{-10} \ N \tag{4.2}$$

If one assumes that the total adhesion force is due to the electrostatic image force given by:

$$\frac{|q|^2}{4\pi\varepsilon_0 \langle r \rangle^2} \tag{4.3}$$

with $\langle r \rangle = d$, we can calculate the minimum value of $|q|$ as

$$|q| = \left(4\pi\varepsilon_0 x\ 7.7 x 10^{-10}\ d\right)^{0.5} = 1.46\ x\ 10^{-14}\ C \tag{4.4}$$

Or

$$1.86\ x\ 10^{-4}\ Ckg^{-1}$$

Expressing this charge as a surface charge density on our representative particle gives:

$$\sigma = \frac{q}{\pi d^2} = 1.85\ x\ 10^{-6}\ Cm^{-2} \tag{4.5}$$

Now, a typical throughput of powder from a gun is $2\ x\ 10^{-3}\ kgs^{-1}$. This is equivalent to a surface area flow rate of:

$$\dot{N} = \frac{2\ x\ 10^{-3}}{\frac{\pi}{6}\rho\left(50\ x\ 10^{-6}\right)^3} = 25.5\ x\ 10^{-6}\ \ s^{-1} \tag{4.6}$$

$$\dot{A} = \dot{N}\ x\ \frac{\pi}{4}\left(50\ x\ 10^{-6}\right)^2 = 0.05\ m^2 s^{-1} \tag{4.7}$$

This amounts to a required current 9.25 x 10^{-8} A to be transferred to the particles' surface as reliably and as uniformly as possible throughout the entire powder cloud. Two methods, or a combination thereof, are currently used for this task, they are corona charging and triboelectric charging.

4.2 Corona Charging: Theory and Practice

The term *corona discharge* generally refers to the ensemble of phenomena that occur in a gaseous medium in the vicinity of conductors of small radius of curvature, subjected to intensive, but not disruptive, electric fields (Goldman and Goldman, 1975). The book by Loeb (1965) and the chapter in Gaseous Electronics written by Goldman and Goldman (1975) cover in detail these phenomena. The use of corona discharge to charge powder particles in powder coating applications is discussed from a theoretical and practical point of view by a number of authors including Singh (1981), Moyle and Hughes (1983) and in the book by Hughes (1984).

The basic principle is illustrated in Figure 4.1. Powder from the hopper is fed to a spray gun. A corona discharge is generated either within the gun (Hughes, 1986) or more commonly at the exit to the gun, producing a spare charge of ionized air molecules.

Powder particles pass through this region where they become charged by collision with the ions. The charging efficiency is dependent on a number of factors:

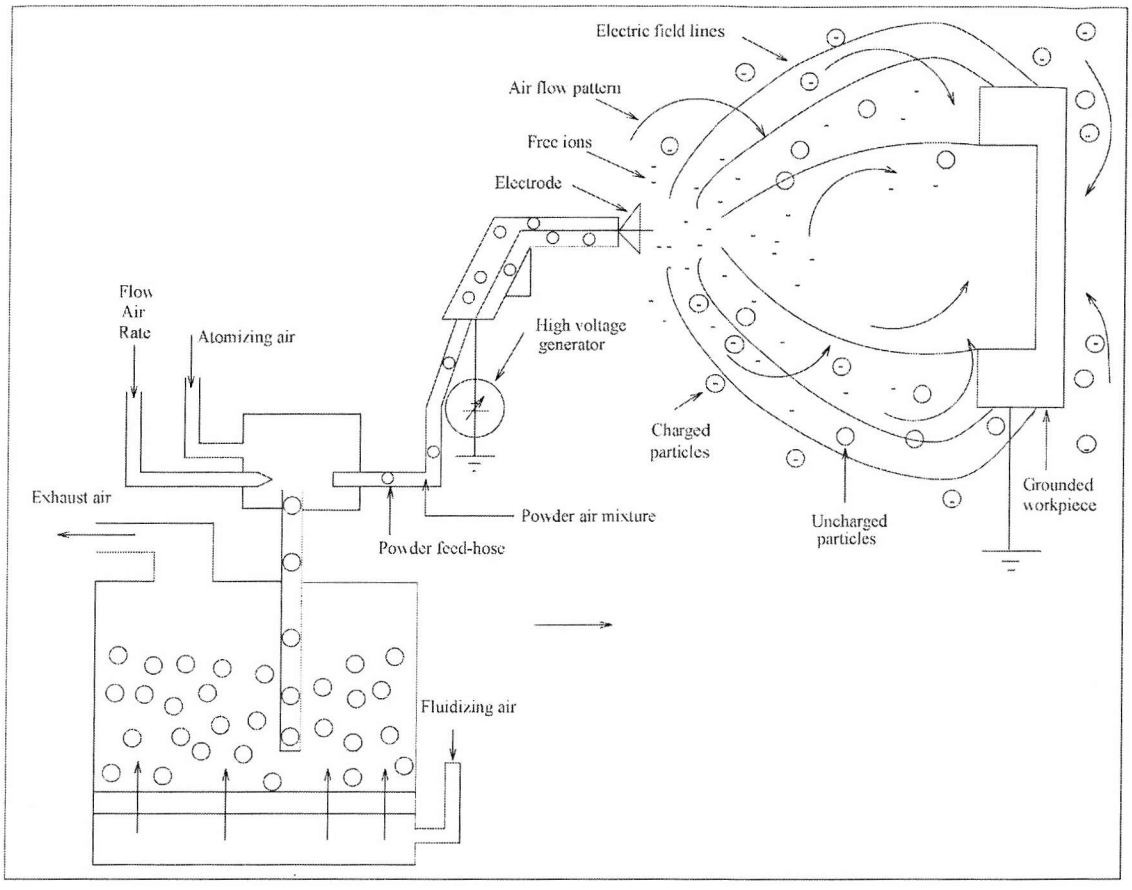

Figure 4.1: Principle of corona charging powder coating gun

a) The time spent by the particle in the ionized region.
b) The degree of powder dispersion to aid uniform charging.
c) The surface charge limit which has been shown by Pauthemier (1932) to be

$$q = \pi \varepsilon_0 d^2 \boldsymbol{E} K_\varepsilon \tag{4.8}$$

Where K_ε , is a constant depending on the particle's dielectric constant:

$$K_\varepsilon = 1 + \frac{2(\varepsilon_p - 1)}{(\varepsilon_p + 2)} \tag{4.9}$$

and $\boldsymbol{E}$ is the local electric field in the region of the particle due to the superpositioning of space charge and applied field (i.e. field between point and workpiece).

It is evident that corona charging efficiency is dependent not only on the characteristics of the particles but on the local field strength and the time and distance the particles are in the space charge region, which is influenced by the air and powder flow rates.

d) It has also been suggested that the powder surface chemistry plays a role in the charging efficiency (Singh, 1981).

A series of experimental studies on the corona charging of insulating powders in a conventional powder coating gun have established the following facts:

a) Even under optimised conditions, corona charging is an inefficient process, with less than 1% of the available free ions ending up on the powder particles (Moyle and Hughes, 1984).
b) Accurate measurements of the charge-to-mass ratio have shown that individual particles are very unlikely to be charged to the Pauthemier Limit (which is difficult to calculate as the local field strength is dependent upon many factors). Ratios of between 2 to 7 $x\ 10^{-4}\ C\ kg^{-1}$ been measured for powders of approximately 60 μm in diameter (Moyle and Hughes, 1983) just above the minimum necessary for electrostatic adhesion.
c) The free ion component of the current emitted from a corona spray gun affects the deposition efficiency, the critical coating thickness and the film appearance. The critical coating thickness phenomenon is explained by Hardy (1974) by applying electrostatic theory with experimental measurements to describe the electrostatic stress which builds up in a deposited layer of powder. In his model, Hardy only considered the parameters of bound particle charge and packing density. He predicted at what surface coverage the electrostatic stress develops to the extent where dielectric breakdown of the air in the voids between particles occurs. This surface coverage was then labelled the critical coating thickness. The thickness thus obtained depends on the particle average charge, average diameter, density, bulk density and the dielectric constant of the material. For an epoxy powder of average diameter *24 μm* carrying an average charge of $4.17\ x\ 10^{-4}\ C\ kg^{-1}$ with density *1530* kgm^{-3} and bulk density *590* kgm^{-3} with relative dielectric constant 5.5, the critical thickness was found to be approximately 240 μm. (Figured from Hardy's data).

The figure of 240 μm overestimates the critical thickness because consideration is not given to the presence of a high concentration of ions within or on the surface of a layer deposited from a conventional powder gun. The accumulation of excess ions adds to the surface

potential, making it higher than that due solely to the bound charge on the particles. Bassett et al. (1975) analysed the influence of voltage and polarity on coating thickness, with measurements of ion flux before and after coating and clearly showed that critical coating thickness is highly dependent on ion current. Singh et al (1979) observed the discharges as soon as the first monolayer of powder was deposited on a workpiece with both negative and positive corona charged powder (equivalent to 25 - 30 μm). The film grew to a thickness of between 190 - 200 μm before any discharges were observed for tribo charged powder, more in line with Hardy's calculations.

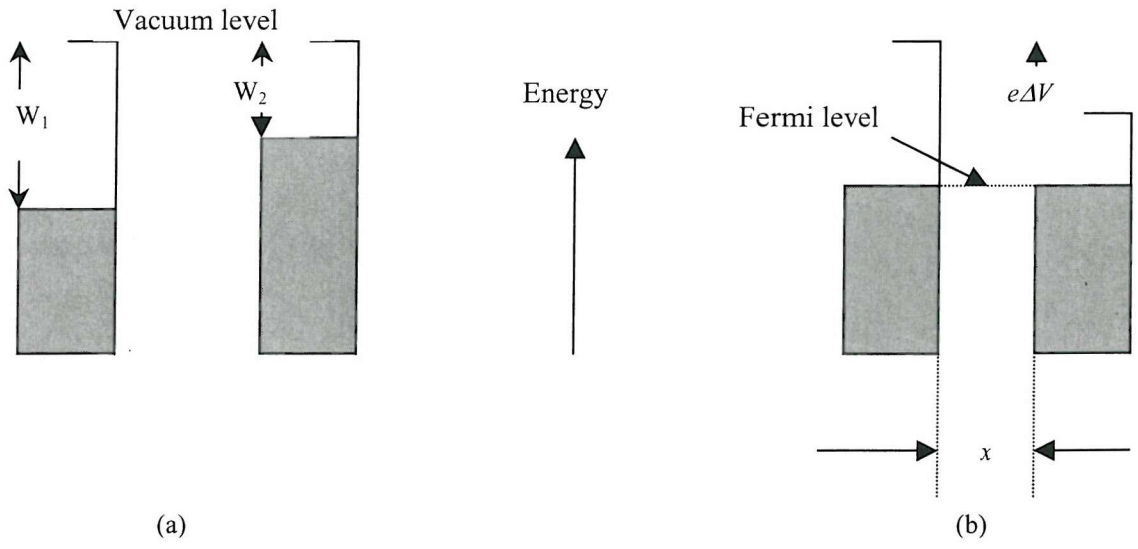

Figure 4.2: Energy-level diagrams for two different metals: (a) before contact and (b) after contact.

4.3 Triboelectric Charging: Theory

Frictional or tribo charging is one of the earliest aspects of electrical phenomena to be observed, yet our understanding of it is far from complete. This is due partly, no doubt, to the fact that contact charging is essentially a surface effect, suffering from the usual complications of high concentrations of impurities and structural defects which tend to be more prevalent at surfaces.

The phenomenon itself is most frequently explained using a contact potential difference model in which contact with an insulator is treated in the same way as contact with a metal. When two metals are brought together there is a contact potential difference between them by virtue of electron drift from the metal having the higher surface energy states to the lower energy states of the other metal. A dynamic equilibrium state is reached where the total energy of the surface states is a minimum (Davies, 1969).

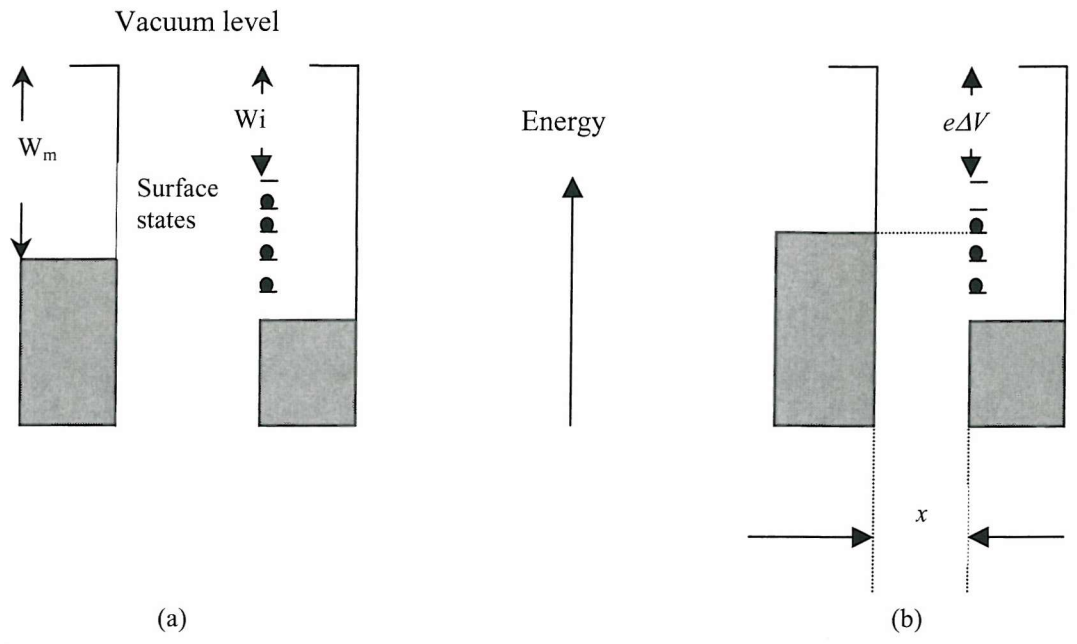

Figure 4.3: Energy-level diagrams for a metal and an insulator: (a) before contact and (b) after contact.

This results in a net charge transfer and associated potential difference as shown in Figure 4.2. Insulating materials have no "free" energy for which a mean energy can be defined but there are a large number of surface and impurity states in which relatively loosely bound electrons are localised at a position on the surface (Harper, 1967).

These tend to have a wide range of energies and are localised at a particular position on the surface. A hopping-type process may allow some electronic mobility between such sites. Bauser et al (1971) considered the energy level scheme for a simple model of metal-insulator contact charging involving only surface states on the insulator and assuming that the energy density of surface states per unit area D_s is uniform.

In the particular case shown in Figure 4.3, the Fermi level (for a metal this corresponds to the topmost filled electronic energy state) the work function is the depth of the Fermi energy level below the vacuum level (for metals $W_f \cong 4 - 5\ eV$) in the metal W_m is lower in energy than the

limit W_i (surface Fermi level) to which the surface states on the insulator are filled. Upon contact there will be an immediate flow of electrons from the insulator surface states to the metal, the charge transferred per unit area of contact being given by:

$$\sigma_S = eD_S \Delta W_i \tag{4.10}$$

Where ΔW_i is the shift $(W_i' - W_i)$ to the new surface Fermi level W_i' caused by the surface charge. Denoting the consequent contact potential difference developed between the metal and insulator surfaces by ΔV, gives:

$$W_m - e\Delta V = W_i + \Delta W_i \tag{4.11}$$

But the capacitance per unit area between them for a separation x is:

$$C_A = \frac{\varepsilon_0}{x} \tag{4.12}$$

So that:

$$\Delta V = \frac{\sigma_S}{C_A} = \frac{\sigma_S x}{\varepsilon_0} \tag{4.13}$$

Combining equations 4.10 to 4.13

$$\sigma_S = \frac{eD_S\ (W_m - W_i)}{1 + \dfrac{e^2 D_S x}{\varepsilon_0}} \tag{4.14}$$

It can be assumed that the density of surface states on a molecular solid such as a polymer is low $(\leq 1 \times 10^{16}\ \ eV^{-1}m^{-2}$ or less) therefore

$$\frac{e^2 D_S x}{\varepsilon_0} \leq 1 \tag{4.15}$$

And equation (4.14) simplifies to

$$\sigma_S = eD_S\ (W_m - W_i) \tag{4.16}$$

The above equation predicts that the surface density imparted by metal contact to the insulator surface is directly proportional to the work function of the metal.

Furthermore, the charge is not sensitive to any critical separation at which electric contact is lost.

Davies (1969) studied the charging of polymers by contact with metals of varying work functions and showed for a series of polymers that the charge density did in fact depend on an essentially linear fashion on the work function. These results provide convincing evidence that contact charging of this type is an electronic process and that Equation 4.16 is valid.

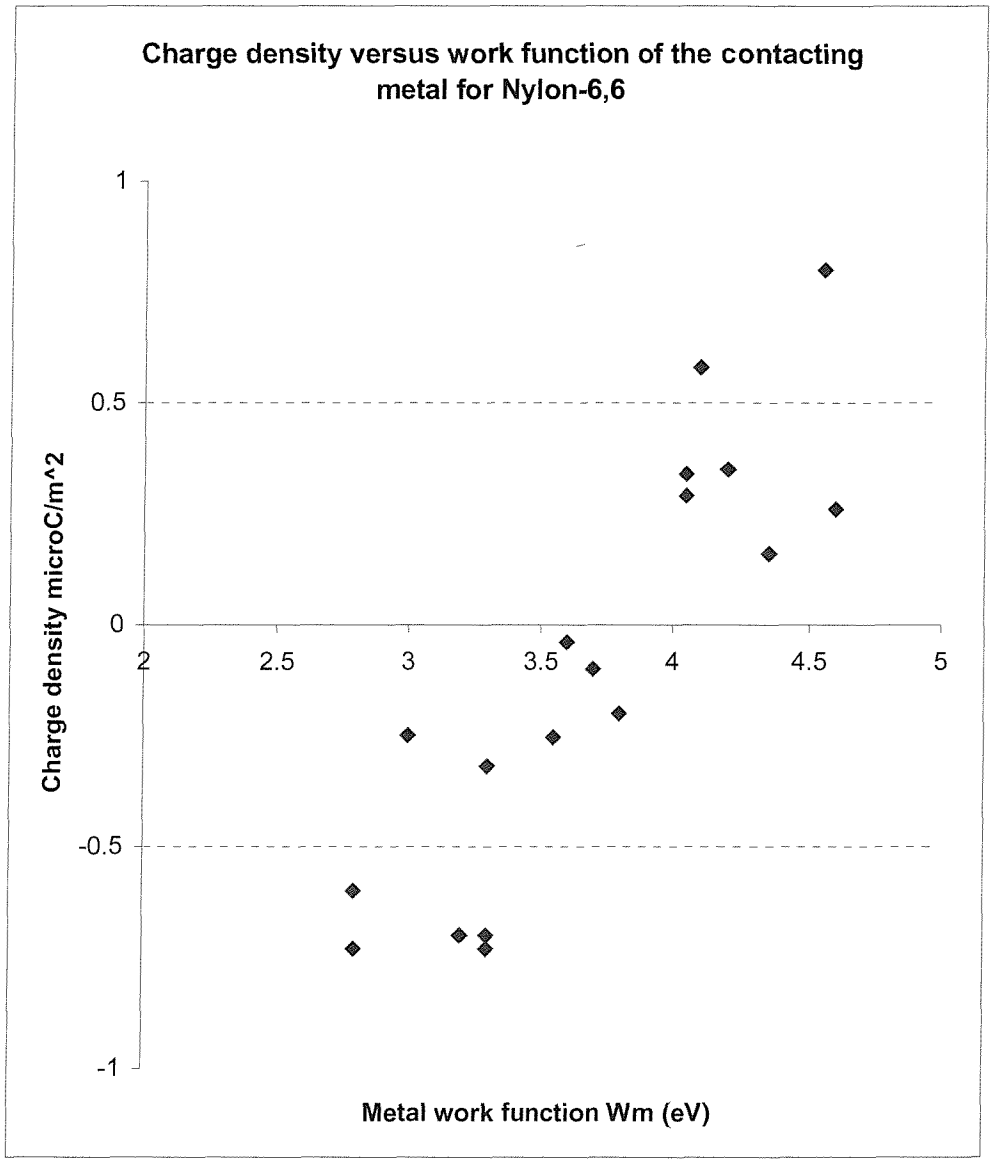

Figure 4.4: Plot of charge density against work function of the contacting metal for Nylon-6,6. From Davies (1969).

Table 4.1: Calculated density of surface states

Polymer	Work Function, W_i (eV)	Surface state density, D_s ($eV^{-1}\ m^{-2} \times 10^{-16}$)
Polyvinylchloride (PVC)	4.85	1.34
Polyimide (PI)	4.36	1.89
Polycarbonate (PC)	4.26	1.80
PTFE	4.26	0.85
Polyethylene terephthalate (PET)	4.25	1.29
Polystyrene (PS)	4.22	0.69
Nylon-6,6	4.08	0.76

Contact charging via surface states is also consistent with the observation that charging is a fairly rapid process in most cases. An effective work function for each polymer surface can be determined by finding the intercept on the work function axis. The results from Davies are given in Table 4.1, which includes the calculated density of surface states (from the slope of the lines). See for example Figure 4.4.

From the table of polymer work functions it can be predicted in what direction charge transfer will take place when contact is made between any two of these polymers. By extending the surface-state model to insulator-insulator contacts, it may be shown that the density of charge transferred upon contact is given by:

$$\sigma_S = \frac{e(W_1 - W_2)}{\frac{1}{D_{S1}} + \frac{1}{D_{S2}}} \qquad (4.17)$$

Where W_1, W_2 and D_{S1}, D_{S2} are the surface work functions and surface state densities of insulators 1 and 2. When $W_1 < W_2$, insulator 1 will acquire a positive charge. In a second series of experiments Davies (1970) confirmed this deduction and the results are given in Table 4.2. Included are theoretical values calculated using the data from Table 4.1 in equation (4.17). In all cases, the correct sign of charging is predicted but quantitatively the agreement is at best reasonable.

The above theoretical examination of the phenomenon of triboelectric charging in fact lags far behind experimental and empirical engineering in its use. The single most profitable invention of all time (pre-digital age) is in fact heavily reliant on utilising triboelectric charging of dispersed powders. Chester Carlsson's invention of photocopying had to wait until experiments yielded a powder that could be reliably charged to a given level to act as a toner to develop the latent image on the photoreceptor. See Anderson for a recent advances in reconciling the theory of dielectric material tribocharging to experimental results (Anderson, 1997, a and b)

In powder coating, tribocharging has established itself as a reliable and viable alternative to corona for some powders and application systems (Kleber, 1993).

	PI	PTFE	PS	Nylon-6,6
PVC	+0.20 (0.61) -0.19	+0.80 (0.73) -0.49	+0.13 (0.46) -0.12	+0.05 (0.60) -0.19
	PI	+0.0 (0.15) -0.21	+0.11 (0.0.07) -0.02	+0.27 (0.61) -0.93
		PTFE	+0.14 (0.03) -0.16	+0.17 (0.15) -0.48
			PTFE	+? (0.08) -0.?

Experimental values taken from Davies (1970)

Table 4.2: Charge densities (μCm^{-2}) transferred in polymer-polymer contacts theoretical values are given in parentheses

4.4 Practical Tribocharging

In the previous section some of the theory of how polymeric surfaces become charged by tribo-electrification was discussed without mention of how tribocharging is realised in practice.

In triboelectric powder coating devices (Figure 4.5) the powder flows through a channel, usually annular, made of dielectric material and situated immediately prior to the spray head. Charging occurs during contact and separation of the particles with the dielectric of the

channel. In the previous section, it was shown how the electronic work function and the density of surface states governed the polarity and magnitude of acquired charge on separation. In Table 4.4 the structures and electrical properties of selected polymer materials common in powder coatings are compared. The polymers are listed in a triboelectric series and as is common with this phenomenon, the order does not follow strictly that expected from the respective work functions as shown in Table 4.3. The main reason for this, as mentioned in section 2.3, is the influence that minor impurities can have. This opens up the possibility of admixing small quantities of specific impurities into the bulk powder to influence the chargeability.

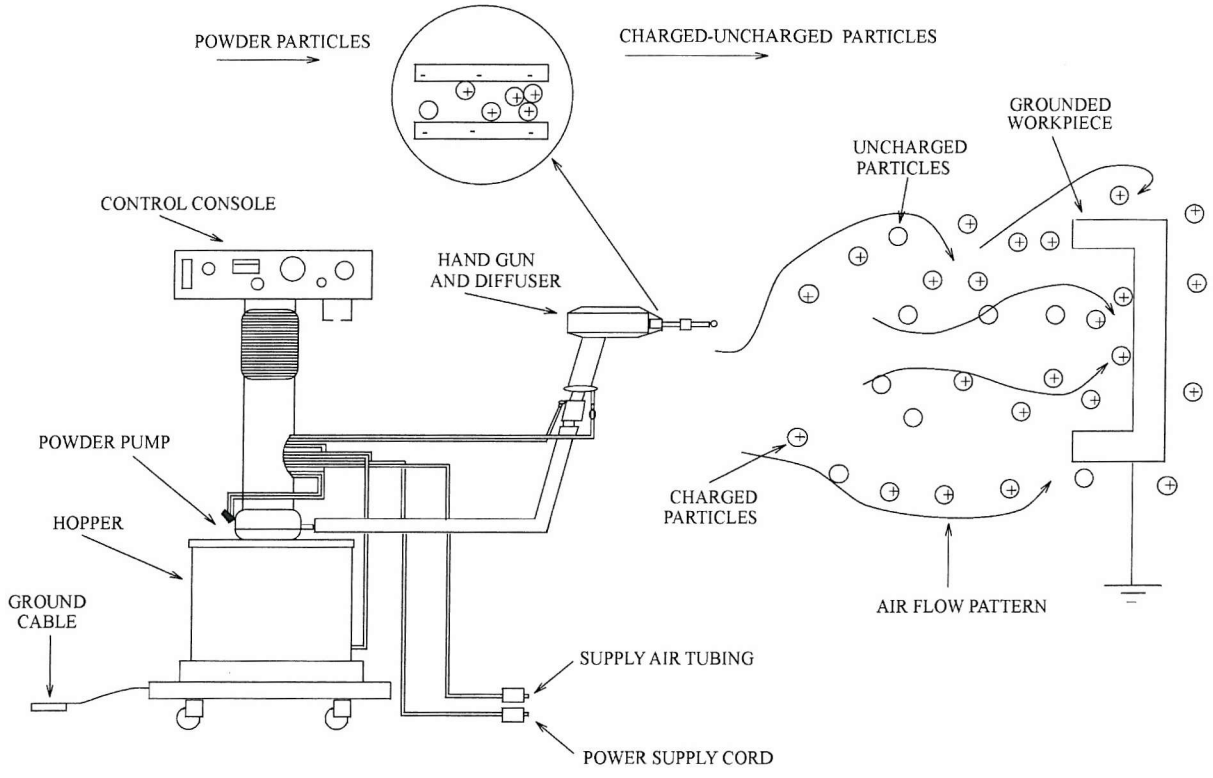

Figure 4.5: Principle of tribo charging powder gun

The addition of amines or other salt compounds is used to this end and imparts a positive tribochargeability to, for example, polyester powders in contact with PTFE. (Bauch, 1992). To couple triboelectric guns with high voltage corona guns, which almost invariably charge negatively, additives that impart a negative tribochargeability are required. Such additives are well known in xerography (see for example Kamiyama et al, 1997) but partly due to high cost have yet to make an appearance in powder coating.

Tribocharging of powder coatings is now a viable method with manufacturers of powder tailoring certain powders for use in triboguns and compares and contrasts their performance versus corona guns under a variety of headings; his conclusions are summarised in Table 4.4. A typical tribogun is shown in Figure 4.6. The charge partner used for charging the modified powder is invariably PTFE. This is not solely due to its position in the triboelectric series but because of its anti-adhesion properties, which prevent powder build up within the gun. The negative charge that builds up on the PTFE surface is conducted to earth via an array of grounding strips situated within the gun. Monitoring of this current effectively monitors the charge on the powder since free ion formation is negligible in well-designed guns (Cross and Cetronia, 1977).

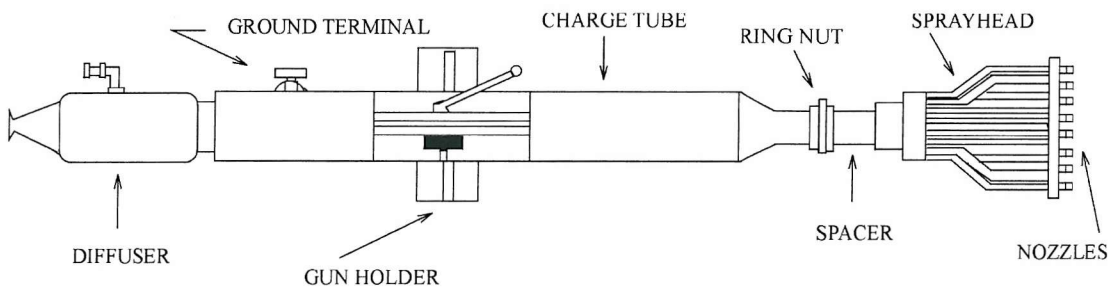

Figure 4.6: Automatic tribogun (Tribomatic gun with adjustable spray head)

4.5 Induction Charging of Powder Coating An Alternative

The idea of charging powder coating particles by induction charging was first mooted by Prof J.F. Hughes of the Department of Electrical Engineering in a number of articles which appeared in the technical press in the early-mid 1980's (Hughes, 1982, 1984, 1985) and at an International Symposium in Electrostatics in Southampton in 1984.

The strengths and weaknesses of corona and tribo charging systems have been summarised in Table 4.4 and from that, it is obvious that neither are ideal solutions to the charging and deposition requirements.

CHARGING	MATERIAL	REPEAT GROUP	FUNCTIONAL GROUP(S)
STRONGLY POSITIVE	Polyamide	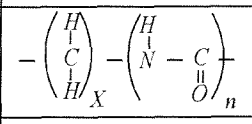	-NH- Amine -C=O Carbonyl
	Polyurethane	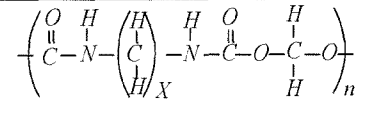	-NH- Amine -O- Ether -C=O Carbonyl
	Epoxy Resin	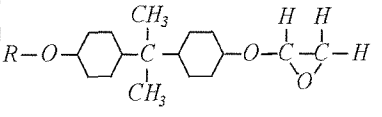	Epoxy -O- Ether -NH- Amine
	Epoxy Polyester	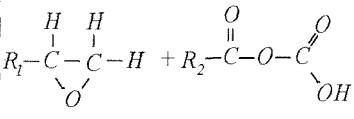	Epoxy Ester, Carboxyl
	Polyester	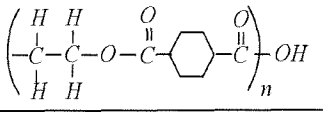	Ether, Carboxyl
WEAKLY POSITIVE	+TGIC	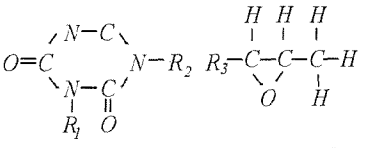	Epoxy Carbonyl
	PMMA	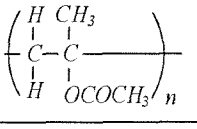	Acryl
0	Polystyrene	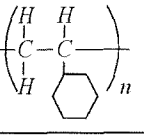	Phenyl
WEAKLY NEGATIVE	Polyethylene	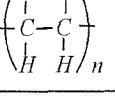	Methyl
	PVC	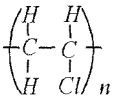	Chlorine Methyl
STRONGLY NEGATIVE	PTFE	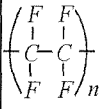	Fluorine

Table 4.3: Polymer materials and their properties

Characteristic	Corona Gun (C)	Tribo Gun (T)	Relative Strength (C or T)
Capital cost	HV generator, cables, insulation	High capacity air compressor (+30%)	No HV generator, safer, less technical - T
Charging mechanism	Ionic attachment	Tribocharging	Smaller no. of free ions, less back ionization, higher charge efficiency - T
Workpiece current	Ion current and charged particles ratio > 10:1	Charged particles only (usually)	Advantage for thicker build/coat - T
Powder flow rate	Up to 30 $kghr^{-1}$	15 to 20 $kghr^{-1}$ for comparable dimensions	Maximise flow per unit - C
Coated area/gun	50 to 100 m^2hr^{-1}	On the order of 20-30% lower	For 2-D objects - C For profiled objects with closer packing - T
Wrap around	External E field enhancement	Space charge and image forces only	Better wrap around - C
Penetration	External field reduces penetration	Reduction of spacing between gun and piece is possible without side-effects	High penetration cavity coating - T
Edge effects	External field enhances deposition at edges	Less enhanced deposition	Layer thickness more uniform - T
Final finish	Can induce alignment of non-spherical particles	Overlapping in powder layer	Good structure - C Less porosity, better protection - T
Gun to workpiece distance	Minimum distance of 15 to 25cm	Normally 8 to 20cm can work at closer distances	Flexibility - T
Workpiece-workpiece distance	High spacing due to external field	Good packing density	Higher space utilization - C
Manual touch-up	Usually required in automated plants	Better penetration so less often required	Superior automation capability - T
Powder type	Theoretically little influence between types of similar size distribution	Highly dependent, may need modification.	Wide choice of powders

Table 4.4: Comparison between corona and tribolelectric guns.

The following is from the 1984 article by the then Dr J.F. Hughes:

" A particle charging mechanism which has not yet been fully exploited, at least in powder coating technology, is induction or influence charging. This technique is used widely and very successfully for toner charging in electro-copying machines. The

technique is potentially very attractive in that it combines the advantages of both corona and tribo charging, while at the same time eliminating the disadvantages of these two methods. In other words, it retains the controllability of corona charging and may be operated at relatively low voltage, while eliminating the unpredictable nature of tribo charge exchange phenomena. Induction charging may only be effected, however, with materials that are sufficiently conducting to support either volume or surface charge transportation. In most electrostatic powder coating applications this will not be possible due to the inherently high volume resistivity of the powder...

... It is interesting to note how induction charging has been successfully adopted for electro-photographic toner handling, where electrostatic requirements are very similar to those in powder coating. At the powder charging station, the powder should be relatively conducting for charging to occur. After charging, however, and for the remainder of the particle's duty cycle, the volume resistivity should be as high as possible in order to ensure adequate adhesion to the substrate. The substrate in electrocopiers is the photoconducting Imaging drum, while in powder coating the article to be coated will be the station at which high resistivity is desirable. On considering these characteristics, it is obvious that a contradiction in requirements exists between high and low resistivity. This has been successfully overcome by careful formulation of toner particles in such a way that electric field dependent resistivity characteristics are displayed. At the high electric field station, which is at the development stage, the resistivity will be relatively low. At all other stations, which will be subjected to low, electric field, the resistivity remains high."

Dr Hughes pointed out that no powder manufacturer could offer a powder with such extraordinary characteristics but the merits of the approach and the fact that induction charging of powders does find successful application in electrophotography certainly warranted investigation. The next chapter details this investigation.

CHAPTER 5

AN INVESTIGATION INTO POWDER CHARGING BY INDUCTION

5.1 Toner Charging Methods in Electrophotography

Induction charging is successfully used in electrophotographic devices to charge specially formulated toner. This section describes basic toner properties and discusses instances where the toner formulation has a bulk resistivity that is dependent on local values of certain parameters including electric field strength.

5.1.1 Basic Toner Properties

There are two main methods of toner charging used in conventional electrophotography and they are contact electrification (frictional charging, triboelectrification) and conduction charging. Both methods find slightly different applications with the triboelectric method being used in dual component developers e.g. magnetic brush development to give high speed and high-resolution copiers which are not constrained by size consideration. Charging toners by conduction finds application in the smaller, more compact, desk-top copiers.

The charging principles are quite different but they both have one thing in common: the toner is designed under the following constraints:

- The toner size must be quite fine for high image resolution. Lately, finer and finer toners are being manufactured; some having an average VMD as low as 7.5μm, but on average toner is in the range of 10-15μm (Ott and Mizes, 1994, Kamiyama et al, 1997).

- Toner must be highly coloured. An obvious requirement for imaging purposes, traditionally carbon black has been used but lately colour copier technology has developed a range of dyes to produce the yellow, cyan and magenta toners of these machines. (Macholdt and Sieber, 1988).

- The thermal behaviour of toner must be such that it is capable of being softened at reasonable temperatures (i.e. those reached on passing a sheet of paper quickly through the machines fuser roller) and must have a melt viscosity low enough to allow it to flow into the paper and affix to it. Thermal degradation must be negligible.

The electrostatic behaviour of the toner must be such that the following conditions are met:

- The toner has a reasonably high resistivity (circa 10^{12} Ωm).
- Is capable of becoming charged (by whatever method) to a level which is repeatable and falls within design limits (usually 15-30 μCg^{-1})
- Bi-polar charging and unequal uni-polar charging of individual particles be avoided as this causes background development and poor image resolution.

These constraints are met by a variety of designs and more and more sophisticated techniques are constantly being developed.

5.1.2 Field Dependent Resistivity

One system of interest is a particular type of monocomponent development, where magnetic toner particles are used without carrier beads being necessary
and where the magnetic property of the toner gives rise to a type of field dependent resistivity. This system and the toner used in it is described in UK Patents 1,527,291, 1,539,080 (Feb 1976) and 2,021,794 A&B (1979) all assigned to Hitachi Metals Ltd, Tokyo, Japan, and also in US Patent 4,121,931 assigned to 3M, Minnesota, USA.

Both companies describe a method of producing a toner which they claim comes within the constraints listed in Section 5.1.1 above and has the peculiar property of displaying a type of field dependent resistivity. This latter property, allows the toner particles to be "injected" with charge emanating from an electrode in a high electric field and once removed from the high field area to retain that charge in the manner of a highly resistive powder. The 3M Patent describes the mechanism thus:

> *"The process of this invention embodies the discovery that one-component -developer of magnetically attractable toner particles, which are very insulating while stationery in a relatively high electric field, when brought into relatively rapid repetitive*

electrical contact with the conductive surface of an electric field producing member of such a relatively high electric field by means of rapid, turbulent, physical mixing of the toner particles exhibit charge transport properties that are equivalent to toner having several orders of magnitude higher conductivity.

It is further speculated that:

"Electric charge of a predetermined polarity is injected onto the toner particles when they are brought into contact repetitively with a conductive surface from which a high electric field emanates. Since the toner particles are insulating, the injected charge is bound on a site on the toner particles, that is, the injected charge cannot rapidly move either laterally along the surface or through the bulk of the toner particles. However, in the presence of an electric field, some electrical charge can be transferred or re-injected from one toner particle to another when a charge-containing site on one particle contacts a site on the other toner. Therefore, electrical charge is transported and distributed throughout the toner particles in the high electric field region in proportion to the degree of physical mixing action experienced by the toner particles."

According to Hitachi in Patent GB 2021794A

"The smaller the resistivity of magnetic toner in the developing stage, (the stage in the photocopying process when the toner is transferred from the development area onto the latent image on the photoconductive drum) the better the image obtained, whereas the higher the resistivity of magnetic toner in the transfer stage, the larger the transfer efficiency.

(Transfer refers to transferring the toner from the photoconductive drum to the copy paper)

"In order to meet such contradictory requirements, different measures have been proposed for example by employing anisotropically magnetic particles. These particles have electric resistivity reduced at the time of development because magnetic particles are aligned in the developing stage and the magnetic attractive force increases the contact pressure among the toner particles to reduce the contact resistance."

A typical recipe of such a toner is

Thermoplastic Resin[1]	**32%**	**wt**
Magnetic Powder[2]	**65%**	**wt**
Carbon Black[3]	**3%**	**wt**

The quantities of each ingredient are a compromise between too little magnetic force if lower levels of magnetic powder are used and insufficient binding if lower levels of resin are used. Carbon black is necessary, according to Hitachi, to reduce so-called *edge-effects* (enhancement of image density at edges compared with central portions of a solid area of a copied or electrophotographically printed document)

5.1.3 Conclusions on Field Dependent Resistivity of Toner

The processes leading to field dependency described in Section 5.1.2, although intriguing, are not practically extendable to powder coating formulations. The high concentration of magnetic material in the toner blend means that, in the immortal words of Henry Ford, one can have any colour so long as it's black! No other examples of field dependency have been uncovered. Strictly speaking, the toners described in Section 5.1.2 do not display an electric field dependency but a mechanically driven dependency on the basis of the 3M descriptions and a magnetic field driven dependency on the basis of the Hitachi descriptions.

In the broadest sense, then, *situation dependent* resistivity is an achievable aim, one which perhaps could be developed independently of magnetic additives. However, it was disappointment that technology transfer from electrophotography could not be implemented. Therefore an alternative route was chosen - a compromise resistivity. If the powder has a resistivity low enough to allow charging to proceed in a short time yet high enough to allow adhesion forces due to Coulombic attraction to remain active until fusing of powder takes place, then in concept induction charging could be implemented. This "window" approach was therefore taken.

[1] e.g. polyethylene wax, epoxy resin, acryl resin etc
[2] e.g. magnetite, Fe_3O_4, alpha-ferric oxide Fe_2O_3
[3] carbon black can further control the resistivity of the resultant toner

5.2 Compromise Resistivity

5.2.1 Charging and Discharging - First Order Rate Processes

Induction or conduction charging of a particle relies essentially on the flow of charge over the surface or through the bulk of the material. The terms induction and conduction are used interchangeably because they depend on the same mechanism. Strictly, induction occurs when the particles are located on the inactive electrode in an idealized dual electrode defining field and charge is induced onto the surface of the particles by the field emanating from the active electrode; with conduction charging the reverse case applies. That is to say, with conduction charging, the particles are in inherent contact with the "hot" or "live" electrode. Here, the charge acquired by a single particle over a particular interval of time in an electric field is examined and also the rate of discharge of the particle once it has left the field and deposited on an earthed plane in a zero field region.

A particle located at an electrode in an electric field of magnitude $\boldsymbol{E}\ Vm^{-1}$ will become charged according to the following expression:

$$q = q_{eq}\left[1 - e^{-\frac{t}{\tau}}\right] \tag{5.1}$$

Where q is the charge acquired by the particle at time t, q_{eq} is the final equilibrium charge of the particle and τ is a time constant dependent on the particle's electrical properties and the particle-electrode contact resistance.

In theory the final equilibrium charge can only be calculated for particles of regular shape such as a sphere (Lebedev and Skal'skaya,1962),

$$q'_{eq} = \varepsilon_0 \frac{\pi}{6} \boldsymbol{E} d^2 \tag{5.2}$$

Where q'_{eq} is the final equilibrium charge for a sphere of diameter d. Cho (1964) has presented experimental results which show good agreement with Equation 5.2 and it will be used to give an approximation for particles of non-spherical geometry.

For particles of low conductivity, the particle-electrode contact resistance can safely be ignored so that the charge transfer time constant τ can be expressed by the well-known formula (see for example Balachandran, 1985).

$$\tau = \frac{\varepsilon_0 \varepsilon_r}{\kappa} \tag{5.3}$$

Where ε_r is the relative permittivity of the particle and κ its conductivity. The ε_r of materials used in powder coating lies in the range 2.3-6 (Bauch, 1992), with 3 being a typical value. Thus, the most important factor influencing the rates of charging of different materials is the conductivity of the particles of the material. Substituting $t = \tau$ into Equation 5.1 gives the approximate time required for the particle to reach 63% of its final equilibrium value. For practical purposes, charging times of seconds are required i.e. for τ to be $\leq 10s$. For a typical powder coating powder $\varepsilon_r = 3$ then, the conductivity κ, needs to be $\geq 2.6 \times 10^{-12} Sm^{-1}$ or ($\omega \leq 3.8 \times 10^{11} \Omega m$ where ω is the resistivity).

In section 4.1.1, a charge of $1.46 \times 10^{-14} C$ was shown to be necessary for adhesion of a spherical $50\mu m$ particle of density $1200kgm^{-1}$ to the workpiece. According to Equation 5.2, the final equilibrium charge for such a particle in an electric field of $1 V/m$ is

$$q'_{eq} = 1.16 \times 10^{-20} C \tag{5.4}$$

If a charge level on this particle of $1.46 \times 10^{-14} C$ is to be reached in *one* time constant then from equation (5.1) q'_{eq} needs to be

$$q'_{eq} = \frac{1.57 \times 10^{-14} C}{1 - e^{-1}} = 2.5 \times 10^{-14} C \tag{5.5}$$

And the field strength at the electrode from equation (5.4) needs to be

$$E_{ind} = \frac{2.5 \times 10^{-14} C}{1.16 \times 10^{-20} CV^{-1}m} = 2.15 \times 10^{6} Vm^{-1} \tag{5.6}$$

This is considerably lower than in corona charging situations where fields in excess of $3 \times 10^{6} Vm^{-1}$ are required.

Once charged, the particle can be transferred by aerodynamic forces towards the earthed conductive substrate. Coulombic attraction between the particle and its image charge will ensure deposition onto the substrate. Again ignoring the contact resistance between the particle and the conductor, the charge will immediately flow from the particle at a rate proportional to the charge on the particle at any instant (i.e. a first order rate process and assuming contact resistance is negligible with respect to the particle resistance). The rate equation can be easily shown as:

$$q = q_0 e^{-\frac{t}{\tau}} \tag{5.7}$$

where q is the charge at time t and q_0 is the initial charge at the time the particle alights on the workpiece i.e., here $q_0 = 1.57 \times 10^{-14} C$ and with τ as before being $\leq 10s$, the charge will decay to 37% of q_0 in 10s or shorter.

The key point which arises from this analysis is this: if the charge can be induced effectively onto the particles via induction and the particles can be carried to an earthed workpiece via aerodynamic or electrostatic forces or a combination thereof, can adhesion be guaranteed over a sufficient period to make the technique viable? It is important to realize that the adhesion question only arises when the workpiece is a better conductor than the particle *and* the particles adhere to the workpiece chiefly due to electrostatic image forces. This is of course the case for the majority of powder coating applications (Bailey, 1998). Other applications can be envisaged e.g.

- The workpiece is a conductor that has been previously coated with a thin dielectric coating (e.g. has been painted or coated with a "first-coat").
- Is a conductor that has been preheated so the powder becomes "tacky" or fused on alighting onto the workpiece.
- Is an insulator that has been pre-charged to an opposite polarity to the inductively charged powder. The charge is thus bound to the workpiece rather than the powder as in the traditional case.

The experimental investigations set out next were aimed at investigating the "window" question nonetheless.

5.3 Experimental Investigation into Induction Charging of modified powders

For this study, six commercially available resinous powders of three different chemical types were selected for investigation. Initial characterization of some of the physical and electrical properties of the powders was undertaken. Work then commenced to find suitable additives and processes so that the surface and/or bulk resistivity of the powders could be lowered into a range suitable for the "window" approach. This section concludes with Chapter 6, which deals with the methodology of modification to basic polymers to alter the charge relaxation time of the resultant powder. The modification work was undertaken by a company, eNexus Corporation, which sponsored this work.

5.3.1 Properties of base powders

These powders were selected as between them they represent a large portion of the total market and potential applications and are typical of the chemical types on the market. The following table presents results of characterization work undertaken after receipt of the powders. As can be seen, the results are typical of commercially produced powders for application using corona gun techniques.

5.3.2 Properties of modified powders

With the intention of producing powders having shorter charge relaxation times, a series of experiments were carried out using three separate techniques. All involved the addition of an additive to the powder either during initial processing or as a surface additive blended into the powder in a post-processing step.

Trade name	Manufacturer	Chemical type	Chief application
Evlast 5500/5C102	Evtech (Kodak)	Acrylic/Polyurethane	General surface finish and protection
Scotchkote 213	3M	Epoxy	Corrosion protection
Scotchkote 134	3M	Epoxy	Corrosion protection
Evlast 3000/3U103	Evtech (Kodak)	Polyester/Epoxy	General surface finish and protection
Evlast 1000/1C01	Evtech (Kodak)	Polyester/Polyurethane (clear)	General surface finish and protection
Evlast 1000/1W104	Evtech (Kodak)	Polyester/Polyurethane (white pigment)	General surface finish and protection

Table 5.1 Base Powders Basic Information

The three additives can broadly be termed as

1) Conductor
2) Ionomer
3) Anti-static agent (ASA)

The idea behind incorporating a conductor into the powder bulk is apparently simple. If sufficient number of finely dispersed conducting particles can be incorporated into each powder particle, then alteration of the bulk resistivity should follow. Chapter 6 discusses in detail the practical applications of such additives.

Trade name	**Key**	**Particle size $D_{4,3}$ µm**	**Bulk resistivity 20% RH /Ωm**	**Bulk resistivity 60% RH /Ωm**	**Ratio 20% RH: 60% RH**	**Charge relaxation time[+] /Hour**
Evlast 5500/5C102	AC Acrylic	38.1	$1x10^{17}$	$1x10^{16}$	10	56.5
Scotchkote 213	BE Base Epoxy	51.2	$3x10^{14}$	$1x10^{14}$	3	0.6
Scotchkote 134	EP Epoxy Potable	46.7	$4x10^{14}$	$1x10^{14}$	4	0.6
Evlast 3000/3W103	HW Hybrid White	36.5	$1.5x10^{15}$	$1x10^{15}$	1.5	5.7
Evlast 1000/1C01	PC Polyester Clear	25.9	$1x10^{16}$	$1x10^{16}$	1	56.5
Evlast 1000/1W104	PW Polyester White	56.7	$1.5x10^{15}$	$1x10^{15}$	1.5	5.7

[+] Assumes ε_r =2. Specific gravity of all powders 1.1 - 1.2. Size data from measurements using a Malvern Particle Sizer.

Table 5.2 Physical and electrical data of base powders

An ionomer is so called because it is in effect an "ionic polymer" with partial crosslinking due to ionic bonds rather than the more prevalent polymeric bonds (which are covalent in nature). These materials have been researched due to their influence on the electrostatic properties of resins in which they are incorporated, mainly due to their ability to influence the tribocharging properties of toners, for example (Diaz, 1989).

Addition of an anti-static agent or additive to the bulk or surface of the polymeric powders was predicted to be effective in reducing the resistivity and the charge relaxation time. Anti-

static agents are effectively complex salts which dissociate in the presence of moisture. Thus, free ionic charge carriers become available for charge transport in a layer close to the surface, the quantity of which is strongly related to the ambient humidity in which the polymer is conditioned.

The three additives were blended into the resins in the extrusion process. This ensured they were well mixed through the bulk but also that they were subject to the full thermal and mechanical stresses associated with production of the standard powders. Additives levels of between 1 to 4% by weight were used and one kilogram of each was supplied for testing and analysis. Powders were labelled using the key shown in Table 5.2 to indicate the parent polymer with an A, C or I indicating the type of additive used and finally a numeral giving the weight percent of the additive. For example, the powder from the trial to manufacture a powder from the Scotchkote 134 epoxy resin with the silver conductive particles at 4% was given the code EPC4.

Before characterization, it was necessary to screen some of the modified powders to remove an oversize fraction that appeared due to the need to salvage the maximum quantity from each trial. Results could then be compared with the unmodified base powders. In Table 5.3, these powders are indicated by italics being used in the particle size column. The other powders had size distributions similar to the unmodified parent.

All modified powders (there was 32 in all) were conditioned at 20% relative humidity and resistivity measurements taken Those powders which showed a decreased resistivity over the base powders (10 in total) were then conditioned at 60% RH and the resistivity was again measured. Again, Table 5.3 shows the results.

5.4 Discussion of Modification Trial Results

5.4.1 Effect of Modifiers

5.4.1.1 Conductor

The effect on the resistivity of the powders of both the conductor and the ionomer additives in the quantities added is negligible. At a concentration of 1% for example, the average change in resistivity due to the conductor is less than one order of magnitude. In some cases, the observed deviation from the base resin value is within the experimental error.

Trade name	Key	Particle size $D_{4,3}$ µm	Bulk resistivity 20% RH /Ωm	Bulk resistivity 60% RH /Ωm	Ratio 20% RH: 60% RH	Charge relaxation time[+] 20% RH /second
Evlast 5500/5C102 with antistat	ACA2 Acrylic	38.1	$8.1x10^{13}$	$3.3x10^{13}$	2.4	1650
Evlast 5500/5C102 with ionomer	ACI3 Acrylic	*73*	$9.4x10^{14}$	$1x10^{15}$	1	19100
Scotchkote 213 with antistat	BEA2 Base Epoxy	51.2	$1.87x10^{10}$	$1x10^{4}$	$1.9x10^{6}$	0.381
Scotchkote 213 with antistat	BEA3 Base Epoxy	51.2	$1.23x10^{9}$	$3x10^{6}$	410	0.025
Scotchkote 213 with conductor	BEC1 Base Epoxy	*56.7*	$1x10^{15}$	$2.4x10^{14}$	~4	20350
Scotchkote 134 with antistat	EPA2 Epoxy Potable	*55.2*	$4.8x10^{8}$	$5x10^{6}$	100	0.01
Evlast 3000/3W103 with antistat	HWA3 Hybrid White	36.5	$1.2x10^{15}$	$1.2x10^{13}$	100	24400
Evlast 1000/1C01 with conductor	PCC3 Polyester Clear	25.9	$1x10^{15}$	$1x10^{15}$	1	20350
Evlast 1000/1C01 with antistat	PCA2 Polyester Clear	*71.3*	$1.3x10^{15}$	$1x10^{15}$	<1	26500
Evlast 1000/1W104	PWA2 Polyester White	29.5	$1.2x10^{11}$	$2x10^{6}$	6000	2.44

[+] Assumes ε_r =2. Specific gravity of all powders 1.1 - 1.2. Size data from measurements using a Malvern Particle Sizer.

Table 5.3 Physical and electrical data of selected modified powders

Further, no significant changes were observed at higher concentrations and an increase in humidity did not produce any increase in the conductor's influence. The same observations hold for the ionomer.

The reason behind the failure of the conductor to modify the powders' resistivity can be explained by simple geometry allied with a number of assumptions. Insufficient quantity was added and the surface morphology of the additive was insufficiently complex to bring about significant changes in the base polymers conductive pathways. It is interesting to note that, although silver has significant advantages over other metal or non-metal additives in terms of its intrinsic resistivity, its density at $10.5 \times 10^3\ kgm^{-3}$ means that significant weight percentage must be added to achieve similar volumetric or surface loading, structure being similar.
For further details of the theory and practice of conducting additives, the reader is referred to Chapter 6.

5.4.1.2 Ionomer

The situation with the powders modified with the ionomer is more difficult to theorise but the results were very disappointing. Studies on the electrical properties of these materials appear to be confined to their triboelectrical properties and not on how they behave in an electric field (Diaz et al, 1981, Diaz, 1989). Diaz et al (1981) describe how the charge transferred in contact charging appears to be due to ion transfer if the ions are present on the powder surface. The quantity of charge transferred appears to depend on the surface concentration of the transferring ion and also on the aggregation state of the ion, i.e. the cation-anion interaction. The degree of charge build-up on the powder containing the ionomer appears merely to be due to the physical transfer of material from the powder to the charge partner. As this material forms one half of an ion pair, charge is simultaneously transferred. Thus, the mechanism is not strictly one of triboelectrification, where electrons migrate from one material to another so that the electric potential of the transferred charge goes to reduce differences in electron work functions of the two materials.

5.4.1.3 Anti-Stat Agent

The effect of addition of the anti-stat Cyostat LS on the resistivity of the base resins varied from no clear effect to a very significant reduction depending on the resin type. Of the six resin types tested, three show no significant modification. These are

(i) The clear acrylic/polyurethane sample Evlast 5500/5ClO2.

(ii) The hybrid of polyester and epoxy sample Evlast 3000/3WI03.

(iii) The clear polyester sample Evlast 1000/lClOl.

The remaining three samples showed a strong response which increased with increasing humidity.

Chapter 6 has detailed evidence of variation in efficacy of anti-stats due to base polymer differences.
Besides this reason, a simple answer as to the variability in the responses is that the melt/mix and powderisation process destroyed the anti-stat. However, both PWA2 and PWA3 were processed by melt/mix powderisation and show a clear reduction in resistivity.
The other simple possibility is that the processing conditions (especially the temperature of the melt/mix process) were more severe for the samples ACA2, HWA2, HWA3 and PCA2, PCA3 so destroying the anti-stat, which decomposes at 235 ^{0}C. One thing is clear, however, and that is the fact that all the powders that were simply dry blended with the anti-stat showed a significant reduction in resistivity, so perhaps the resin's properties are not as vital as would be expected when examining the melt/mix results.

5.4.2 Scanning Electron Micrograph

Having examined preliminary results from the resistivity tests, the following interesting question was posed:

Why, given the similarity in the base polymer and the level and type of dopant present and also in the type of processing used, do the results of resistivity for the samples PCA2 and PWA2 differ so much? The binder resin in both cases is manufactured by Evtech (a Kodak company) in their "Evlast" Polyester/Epoxy Powder Coatings, 1000 series. PCA2 has a clear polyester as binder resin and has a resistivity of 10^{15} Ωm at 20% RH. PWA2 has the same polyester as binder resin but also contains a white pigment of titanium dioxide. It too has a resistivity of the order of 10^{15} Ωm so the basis of the differences in the resistivities of the modified samples PCA2 and PWA2 does not *appear* to lie in the materials of the binder resin or other additives such as pigments. (This may not be so clear-cut. The possibility of some interaction between the anti-stat additive and for example the pigment should not be ruled out).

To try to identify the true basis for the difference in the resistivity of these two samples, samples were prepared for Scanning Electron Microscopy on the Department of Geology's JEOL JSM-6400 microscope, which has coupled to it a TRACOR NORTHERN X-RAY analyser capable of qualitative and quantitative identification of the elements in the periodic table capable of x-ray excitation.

Micrographs at 300 times magnification show the particles lying in the size range of a few micrometers to about 100 micrometers confirming the Malvern data that gave PCA2 a volumetric average diameter of 71.3 μm. Particles have an angular appearance consistent with resinous particles produced by comminution in a jet mill or similar device. The only visual difference between the PWA2 sample and the PCA2 sample is that the former has many more sub-micron particles attached to the surface of the larger particles. These sub-micron particles are the white pigment TiO_2, blended into the powders before comminution to colour the powder.

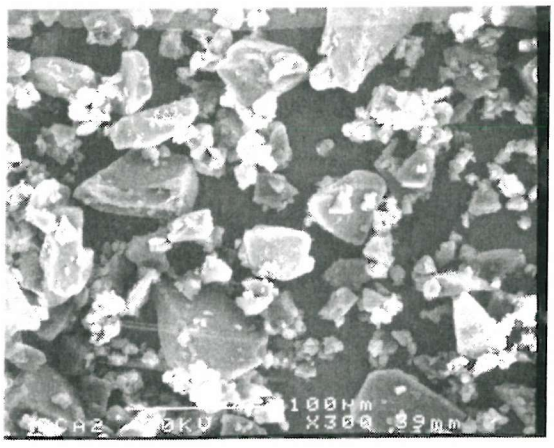

Figure 5.1 SEM Image of PCA2 powder

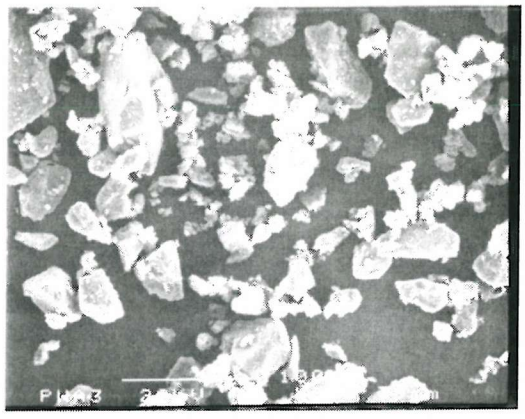

Figure 5.2 SEM of PWA3 Powder

An x-ray analysis of samples PCA2 and PWA2 was then undertaken to attempt to identify differences in the surface compositions of the powders which might explain the observed difference in resistivity. A scan across the complete sample of PWA2 showed a high surface concentration of sulphur could be identified. A spot analysis (across an area of approximately 1 μm) produced two clear peaks corresponding to titanium and sulphur. A third, smaller, peak at the level corresponding to oxygen was also observed. The molecular formula of the anti-static agent Cyastat is

$$[C_{11}H_{23}COHCH_2CH_2NCH_3(CH_3)_2]^+ [CH_3SO_4]^-$$

The sulphur atom in the methysulphate anion can be used to trace the presence of the agent and thus the conclusion is that the spot analysis confirmed the presence of the agent on the surface of the PWA2 sample.

The result of x-ray analysis on the PCA2 sample was different, however. No sulphur could be found on the surface although a titanium peak was observed. TiO_2 doubles as a flow-enhancing agent and may have been added to the powder to improve its flowability, thus giving a peak under x-ray analysis. The absence of a peak for sulphur suggests one of three possibilities:

(i) No anti-stat was added to the powder.

(ii) During the melt/mix operation the temperature exceeded the decomposition temperature of the anti-stat agent (235 ^{0}C).

(iii) Anti-stat was added but is completely miscible with the base polyester resin and thus is distributed throughout the bulk and not just on the surface where its effect on the particles resistivity is greatest.

In this latter point, it differs from the PWA2 sample and the reason may be due to the presence in a relatively large proportion of pigment, TiO_2. The powder, PWA2, can be viewed as a three phase solid mixture with components being the base resin, the pigment and the anti-stat. The miscibility of the anti-stat in the resin/pigment binary may be low causing it to migrate to sites close to the surface. If this is the case the possibility exists that a procedure of solubility parameter matching could be used to tailor various anti-stat agents to the other materials of the powder so that maximum phase separation occurs, with the result of an increase in the concentration of anti-stat agent at the surface.

5.5 Conclusion on Powder Modification

Following testing of the formulated powders the following conclusions can be made.

(i) Neither the conductor or ionomer additives at the levels tested alter the composite powders resistivity by a significant level.

(ii) The anti-stat additive is effective in modifying the resistivity of 50% of the samples tested. The reason why it is not 100% successful is unclear but may be due to the positioning of the additive within the composite powder, or the processing conditions varying.

(iii) The effect of the anti-stat agent increased with higher humidity in those samples in which it was successful.

(iv) The most important conclusion is that it has been shown that modification of the electrical properties of commercial powder is possible by a simple process using a material which is highly effective at low concentrations. With further research it should be possible to optimise a range of powders for commercial exploitation with induction charging and to further tailor their electrostatic properties without any negative effect to the other vital properties of the powder.

5.6 Apparatus for coating substrates with inductively charged resinous particles – US Patent 5,518,546

A patent, co-written by the author, was successfully filed in the United States under number US 5,518,546, which describes an apparatus for coating substrates with inductively charged resinous powder particles. The abstract from the patent is shown in Appendix 1 of this thesis. The patent itself contains details of experiments to prove the concept. Key extracts from the patent are reproduced here. The patent was drafted by the author and the published patent is largely unaltered from that draft. All experiments documented in the patent were carried out by the author. The design and manufacture of the prototype apparatus was undertaken by the author with assistance of members of the Wolfson Electrostatic Unit, most notably Mr. Graham Hearn who is named as co-inventor.

5.6.1 Claims

5.6.1.1 An apparatus for coating a substrate with electrically charged resinous powder particles which subsequently form on said substrate a uniform, continuous coating, said apparatus, comprising in combination:

(a) an electrically insulating fluidized bed for inductively charging resinous powder particles,

(b) high voltage means disposed in one portion of the fluidized bed and connected to a variable high voltage power supply,

(c) grounded electrode means disposed in another portion of the fluidized bed, whereby an electrical field is created between the high voltage and grounded electrode means to inductively charge the particles,

(d) fluidizing air means in communication with said fluidized bed for introducing air into the, fluidized bed thereby establishing in the presence of the resinous powder particles, an electrostatically charged powder cloud within the fluidized bed,

(e) conveying means connected to the fluidized bed for transporting electrically charged powder particles from the fluidized bed, and

(f) dispensing means affixed to the conveying means for directing the electrically charged particles onto the substrate.

5.6.1.2. The apparatus of claim 5.6.1.1 wherein the high voltage means provides up to 60 kV.

5.6.1.3. The apparatus of claim 5.6.1.1 which provides the resinous powder particles upon ejection with a resistivity of from about 10^{9} to about 10^{13} ohmmeters at a relative humidity of 20 percent.

5.6.1.4. The apparatus of claim 5.6.1.1, wherein said dispensing means comprises in combination, a spray gun having:

(a) a barrel through which particles are conveyed to a substrate and means for holding the gun,

(b) an electrostatically induction charging zone at one end of the barrel, the zone comprised of two spaced electrodes between which charged particles are passed to an exterior, one of the electrodes being a high voltage electrode, and the other a grounded electrode,

(c) a high voltage resistor means embedded in the gun barrel and connected to a high voltage source,

(d) means for connecting the grounded electrode to an exterior grounding source, and

(e) means for introducing fluidized powder particles into the other end of the barrel.

5.6.1.5. The apparatus of claim 5.6.1.4 wherein the high voltage means provides up to 60 kv.

5.6.1.6. The apparatus of claim 5.6.1.4 wherein the resinous powder particles upon ejection have a resistivity of from about 10^9 to about 10^9 ohmmeters at a relative humidity of 20 percent.

5.6.1.7. A process for forming a durable coating of a resin on a substrate which comprises applying to said substrate electrostatically charged powdered resin particles utilizing an apparatus comprising in combination an electrically insulating fluidized bed for inductively charging resinous powder particles, high voltage means disposed in one portion of the fluidized bed and connected to a variable high voltage power supply, grounded electrode means disposed in another portion of the fluidized bed whereby an electrical field is created between the high voltage and grounded electrode means to inductively charge the particles, fluidizing air means in communication with said fluidized bed for introducing air into the fluidized bed thereby establishing in the presence of the resinous powder particles, an electrostatically charged powder cloud within the fluidized bed, conveying means connected to the fluidized bed for transporting electrically charged powder particles from the fluidized bed, and dispensing means affixed to the conveying means for directing the electrically charged particles onto the substrate and fusing said resin to said substrate before the charge on the said particle is dissipated.

5.6.2 Preferred Embodiment

Figure 5.3 is a reproduction of Figure 6 from US Patent 5,518,546 and is directed to the inventive concept of the invention and shows the preferred representation of the basic design for a powder induction charging apparatus. It shows a fluidized bed type electrostatic charger and powder applicator. Powder is fed continuously to an electrically insulated bed or zone (10) from powder reservoir (not shown) through port (12). The whole bed can sit on a vibrating table (14) which helps loosen the powder in the bed. Fluidizing air (16) is fed to beneath the air distributor plate (18) and transport air enters the bed near the top in a radial direction from (20) positioned directly opposite exit port (22) to nozzle (24) which directs the powder to the substrate (26). An electric field is set up across the bed, the electrodes being a

high voltage electrode (28) supplied by an extra high tension source (30). The lower electrode is formed by the upper layers of the fluidized powder, in contact with a sintered grounded grid (32). Charge is induced on the powder as it enters the bed and once carried upwards and out of the bed by the fluidizing and transport air, this charge is locked on the powder until it reaches the workpiece. An electric field created between the high voltage nozzle of the applicator and the grounded workpiece assists in the transport and deposition of the charged powder.

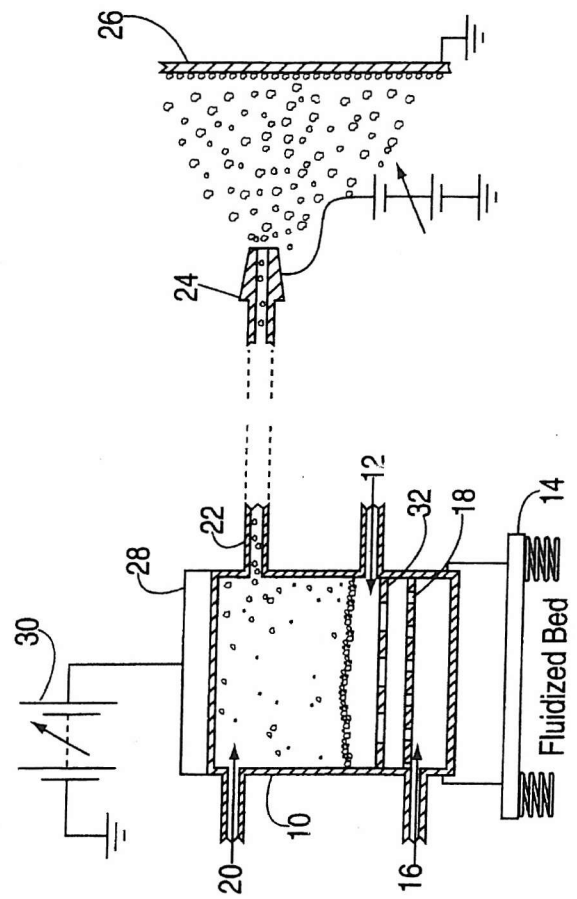

FIG. 6

Figure 5.3 a schematic diagram depicting the apparatus which utilizes the inductive/conductive principle employed in the invention.

5.6.3 Experimental Demonstration

Evlast 1000/1W104, a commercially supplied white polyester resin powder manufactured by EVTECH Co. of North Carolina, U.S.A., was used in this test example.
The resistivity of the powder at 20% relative humidity was determined to be 1.5×10^{15} ohmmeters. The resistivity was measured using a powder resistivity measurement cell developed by Wolfson Electrostatics, University of Southampton, UK.

One kilogram of this powder was mixed with 2% by weight of Cyostat LS agent. The mixture was melted, extruded, cooled and ground to a fine powder. The resulting powder was further sieved and the portion passing 150 μm used in this test example.

The resistivity of the test powder at 20% relative humidity was determined to be 1×10^{11} ohmmeters. The volume average diameter of the test powder was determined to be 40 μm .

A feed of 4×10^{-3} kg min^{-1} of the test powder was supplied to an apparatus similar to that shown in Figure 5.3. Once a sufficient reservoir of powder was present in the bed, the fluidizing air and transport air supplies were opened and adjusted so that steady state conditions were reached, that is, exactly as much powder left the bed through the nozzle as entered in the feed. Once these conditions had been reached, a voltage of 20 kV was applied to the upper electrode. The gap between the upper electrode and the grounded plate was 0.10 m, thus a minimum electric field of 200 kV m^{-1} was set up across the bed.

A conductive target plate (test workpiece) of approximately 1×10^{-2} m^2 was placed 0.30 m directly in front of the nozzle. The target plate was grounded via an electrometer which was set to measure the amount of charge flowing to the plate.

Powder was collected on the plate for 20 seconds, beginning 5 seconds after the voltage was applied. In this time 1.1×10^{-3} kg of powder was collected on the plate, to which 9.4×10^{-8} Coulombs of charge had flown. This indicates that a charge of almost 1×10^{-4} Coulombs per kilogram was applied to the powder by induction charging. Such specific charge levels are sufficient for good powder adhesion (see section 4.1.1). All of the powders adhered to the plate for at least 2 minutes after the spraying had ceased, sufficient for workpiece transport to a curing oven for permanent fixing.

CHAPTER 6

A PRACTICAL REVIEW OF METHODS FOR MODIFYING THE ELECTROSTATIC CHARGE RELAXATION TIME OF POLYMERS

Introduction

This review is based on information supplied by various speciality polymer producers as well as other industrial sources. It is less scientifically thorough as other parts of this thesis, but serves well to round off Part II. The material for this review was gathered from sources within Xerox and thanks goes to Graham Lewis of Xerox Europe Technical Centre for providing much of the information. The intent is to indicate to interested readers avenues where practical industrial solutions to some of the challenges inherent in induction charging commercially available polymer powders may be found. The most important application of the techniques reviewed here is in the so-called "static dissipative" and "anti-static" branches of the polymer industry, whether for packaging material or material suitable for shielding electromagnetic fields. There is ample scope for these techniques to crossover to developments in powder coating using induction charging.

6.1 Additives and Fillers - Basic Overview

The static control industry as applied to polymers is a mature and active one (Rapra, 1993). Additives, fillers and special chemical preparation processes are all widely used to modify or

control the electrostatic properties of polymeric materials such as those used in the powder coating industry (GE Plastics, 1995).

Table 6.1 summarises the main types of fillers and additives used to produce electrostatically "controlled" polymers, the typical dosage levels and indications as to the relative cost of each type of treatment per kg of polymer.

6.2 Antistatic agents

The main advantages of antistatic agents include:

- Relatively low cost.
- Transparency and colourability.
- Significant alteration of the base polymer's physical characteristics is rare.
- Some antistatic agents also have antiblocking properties; this eliminates mutual adhesion of films or thermoformed parts, especially important for polyester films. Such antistatic - antiblocking agents are perfectly transparent because of their chemical nature, and therefore do not affect the optical properties of finished products, very important in powder coating applications.

Disadvantages include:

- Due to their mode of action, most require the presence of moisture to function properly and are therefore their efficacy is related to ambient humidity. The antistatic surface layer becomes ineffective if the ambient air is relatively dry, which occurs frequently when rooms are heated or air-conditioned.
- Thermal stability: most antistatic additives (for example, those based on esters of fatty acids) decompose or evaporate at temperatures below 180 ^{o}C, which is below the processing range of many plastics.
- The overall efficacy of internal antistatic additives can be influenced by such factors as the reactivity of the polymer and the presence of other additives e.g. pigments, fillers, initiators and residual monomers.
- Of key import here is that currently available successful antistatic agents have been derived after extensive experimentation and are specifically formulated for each polymer and end use requirement - as yet there is no "universal" antistatic agent commercially available. This situation is akin to additives used to boost the tribocharging properties of powders used with tribo-guns as outlined in Chapter 4.
- Some chemical antistats have been reported to contribute to corrosion of metals within electronic components and to stress cracking of polycarbonate. Tertiary amine types in

particular are regarded as unsuitable for antistatic film packaging of PC circuit boards due to their reactivity and corrosive nature. Non-migratory or "non-blooming" antistats have been developed to try to combat this problem, such as neoalkoxy titanates and zirconates [e.g. Ken-Stat from Kenrich Petrochemicals]. It has been reported that these do not appear to have achieved widespread commercial success due to their limited thermal stability.

Additive or Filler	Comment	Dosage/% by wt	Incremental cost £/kg (1995)
Chemical antistatic agents	Examples include • Armostat from Akzo • Zelec from Du Pont • Hostastat from Hoechst (note: cleared for use in food packaging by FDA)	0.05-8.0	2.0-3.0
Carbon black	• Low Conductivity • Standard Conductivity • Enhanced Conductivity (Best known suppliers are Akzo and Degussa)	20-40 15-35 5-15	1.4-2.0 2.0-3.0 6.0-11.5
Carbon fibres		5-20	28-38
Stainless steel fibres		3-7	45-60
Nickel-coated graphite fibres		5-10	32-42
Inherently dissipative polymer (IDPs)		10-20	N/A

Table 6.1 Additives and Fillers used for Electrostatic Control

- The main disadvantage of external antistats is that they can easily be removed by wiping or washing and in some cases they have been observed to encourage growth of fungus and bacteria.
- Many external antistatic agents are based on quaternary ammonium salts, which have only limited food contact approval.

6.2 Conductive Fillers

The main advantages of conductive fillers include:

- Provision of a permanent, highly dissipative solid.

- Efficacy at relatively low loadings.
- Provision of some degree of reinforcement, which could be an important property for a coated layer.

Disadvantages include:

- The high cost of some metal fillers.
- The lack of colourability (in the case of carbon black).
- Difficulty in consistently reaching the dissipative range (less important for the "window" approach where the target is 10^{10}-10^{12} Ohm m).
- So-called "hot spots" of conductivity which may lead to arcing or other ***E***-field problems.
- Physical properties of the base polymer, such as impact strength and flow behaviour, are affected to some degree. Contamination introduced by carbon blacks, such as water, metals, ash, and sulphur, may be detrimental to the polymer stability. Surface finish of the final product may be affected and ease of processing is often reduced.
- Handling problems caused by dust, especially in the case of carbon black.
- Conductive carbon blacks are more compatible with non-polar polymers, which can lead to dispersion problems.
- Conductivity of the compound does not rise in direct proportion to the amount of filler. Thus, a small change in filler concentration has a large effect on conductivity and control over filler loadings and filler distribution is critical.

6.2.1 Chemical antistatic agents - technical review

The most widely used method of making polymers antistatic is the use of chemical antistatic agents. These materials, which can be applied topically (e.g. as post processing surface additives blended into bulk powder) or as migrating additives within the plastic, dissipate the charge on the surface of the polymer products by reducing surface resistivity.

The primary compounds used as antistatic agents are as follows:

- Fatty acid esters.
- Amine derivatives e.g. tallow amine, stearyl amine and cocoamine.
- Quaternary ammonium salts.
- Phosphate esters.
- Polyethylene glycol esters

6.2.2 Classification of antistatic agents

Antistatic agents are usually surfactant-type molecules (see Chapter 10), with a strongly polar hydrophilic head and a long chain hydrophobic tail. They function by promoting the loss of electrostatic charge through mechanisms such as surface conduction or transfer to atmospheric water vapour. Chemical antistats can be classified in general terms according to their mode of application: **internal** and **external.**

6.2.2.1 Classification by mode of application

Internal antistatic agents are compounded into the polymer matrix either before or during the extrusion or moulding process. Incorporation in this manner allows for a reservoir of antistatic agent within the polymer matrix and ensures lengthy antistatic protection.

The incompatible, immiscible antistat then migrates or "blooms" to the polymer/air interface from the interior of the plastic product. At the interface, the antistat molecule orients itself such that the hydrophilic, polar head sits on the polymer surface with the hydrophobic, usually aliphatic "tail" anchored into the matrix of the polymer. The hydrophilic end of the molecule then absorbs water molecules at the surface. A thin, highly conductive film of water develops and effectively dissipates the static charge.

Some of the fundamental requirements that have to be met by such products are:

- Compatibility with relevant polymer matrix materials across the entire range of expected processing conditions.
- A balanced affinity for relevant polymers.
- Compatibility with other additives.
- No adverse effect on other required physical or chemical properties.
- Thermal stability.
- Sufficient polarity to increase surface conductivity and hygroscopicity to effective levels.
- For "food contact" plastics there is an additional requirement: that the additive has the required indirect food contact clearances.

Should the internal antistat molecules - despite being anchored in the polymer matrix - be washed off, the equilibrium situation will soon regenerate the original antistatic protection. This process can be repeated frequently, although for some materials this regenerative process is much weaker.

External antistatic agents are applied via dilute (0.1% to 2.0%) solvent mixtures onto the surface of the final polymer article, usually by spraying, wet coating or dipping. The solvent, which may be water, lower alcohols, hydrocarbons etc, is then evaporated and a molecular layer of antistat is left on the surface of the polymer article. Finely dispersed solid external additives can be surface-added to a powdered polymer in a dry blending operation.

These types of products are effective because they are hygroscopic. They contribute to the formation of a thin, invisible water film on the surface of the plastic, decreasing the surface resistivity for ion conductivity. A second mechanism for charge transfer, which happens simultaneously, involves a continuous exchange of (evaporating) water molecules between the plastic surface and the surrounding atmosphere.

Since the surface resistance of these antistatic agents is not dependent on migration or on air humidity, the manufacturing and storage conditions of finished products are much less critical than is the case with internal additives. Moreover, in contrast to internal antistats external products become effective immediately after they are applied.

The first external antistatic agents used in the 1960s were simple surfactants such as detergents, which quickly lost their activity. However, products now on the market can meet almost all antistatic requirements by the proper choice of type and amount of the substance. Their adhesion to the surface of the plastic can be so good that they remain effective for several years. This level of adhesion is gained by the use of surface treatment, such as corona, low-pressure plasma or flame treatments. In these processes free radicals are formed which react with the antistatic agents.

Within certain limitations, external antistats offer a number of advantages, some of them unmatched by other modes of treatment:

- Due to their ability to readily dissolve in cheap or reclaimable liquid carriers, application can be both simple and reliable.
- Quantities used depend on surface area rather than volume of material. Typical requirements range from 25 to 75 $mg\ m^{-2}$.

- Efficacy extends over a broad range of base polymers
- They are not subjected to the plastics processing conditions which may, for instance, include temperatures that would degrade internal antistats.
- Re-application can be carried out if circumstances demand subsequent treatment.

6.2.2.2 Classification by Ion Type

Since internal antistats are usually also surfactants, they can also be categorised as **cationic, anionic,** and **nonionic** compounds, depending on their ionisation characteristics in solution.

Cationic antistats are usually long-chain alkyl quaternary ammonium, phosphonium or sulphonium salts, with e.g. chloride counter ions. Surface activity of these materials is related to the presence of water or oil soluble cations. Quaternary ammonium salts are the most widely used products in this class.

Anionic antistats are usually alkali salts of alkyl sulphonic, phosphonic, dithiocarbamic or carboxylic acids; of these, sodium alkylsulphonates have gained the widest acceptance. Ionisation occurs in solution and they behave as electrolytes with their surface activity related to anion formation.

Nonionic antistats represent by far the biggest group of chemical antistats. They usually belong to the classes of ethoxylated fatty amines, fatty acid esters or ethanolamides, polyethylene glycol-esters or ethers, and mono- and diglycerides. They are often supplied in liquid form or as waxes with a low softening point. Non-ionic surfactants do not ionise in solution but owe their surface activity to polar groups within the molecule such as hydroxyl or ether linkages.

6.2.2.3 Mode of action of antistatic agents

It is generally assumed that interfacially active molecules accumulate on the surface of the polymer and are oriented with the hydrophobic part containing the paraffin chain extending into the plastic and the hydrophilic part pointing outwards where it is able to adsorb water on the surface. In consequence of their interfacially active character, antistatic agents decrease the phase boundary angle between water and plastic, thus allowing water to be uniformly distributed on the surface. A water film, whose thickness depends on the atmospheric

humidity, forms on the plastics' surface, thus increasing the conductivity by means of an ion conduction process. This also explains why the surface conductivity and hence the antistatic action progressively decrease with decreasing atmospheric humidity.

More recently, it has been postulated that charge exchange, in addition to the ion conduction mechanism, is effected through a constant exchange of water between the surface and the environment. This would be in accord with the mechanism of air ionization. In contrast to this, however, the antistatic agent on the surface acts as a contact point for the charge exchange.

In addition, charge transfer can be accomplished by a proton shift. Antistatic agents bearing -*OH* or -NH_2 groups are able to associate in chain form via hydrogen bonding, and display antistatic activity even at low atmospheric humidity, unlike compounds, which are able to form only intramolecular hydrogen bonds.

Many antistatic agents also show hygroscopic properties, thereby intensifying the attraction of water to the surface. At constant atmospheric humidity, a hygroscopic compound combines more water at the surface and so increases the antistatic effectiveness.

Controlled compatibility between the antistatic agent and the polymer is desirable so that the agent migrates to the surface at comparable rates with its removal from the surface by handling and washing. Insufficient compatibility would result in excessive migration and excess antistatic agent on the surface of the product, with consequent problems for any post moulding printing or adhesion processes. Conversely, excessive compatibility would lead to very low concentrations of agent on the surface and therefore poor antistatic properties.

6.2.2.4 Performance of antistatic agents

Internal antistatic agents are normally compounded into the polymer matrix in its molten state, usually with a compounding extruder, together with other additives or pigments. When the matrix solidifies, the (slightly) immiscible antistat molecules start migrating to the surface area until an equilibrium position is reached.

The rate at which this happens depends not only on antistat compatibility (or miscibility) and concentration, but also on process-related parameters such as temperature, type of moulding process, shear, draw ratio, cooling rate, and on such factors as polymer type, density and crystallinity. The antistatic performance of injection-moulded parts, for example, depends on

the mould temperature. Lower mould temperatures generally lead to increased migration and thereby improved antistatic performance. For example, in injection moulded low-density polyethylene panels antistatic protection is reached almost immediately after moulding, whereas it takes several hours for the same effect to be achieved in high-density polyethylene, and 10 to 20 days for polypropylene under similar conditions (Rapra, 1993)
When dosed in recommended concentrations, both internal and external antistats can lower the surface resistivity from about 10^{14} - 10^{16} to about 10^{9} ohms/square. To safeguard against explosions in a hazardous environment, surface resistivities should not exceed 10^{6} ohm/square; obviously, this level cannot be reached by the use of chemical antistats. Any further decrease is only obtainable by increasing the volume conductivity by, for example, conductive carbon blacks.

6.2.2.5 Usage levels of antistatic agents

The selection of an antistatic agent, most critically an internal one, can be quite difficult and in most cases is derived via experimentation and end use requirements. The effectiveness of any one system depends on concentration. The threshold concentration level above which reproducible antistatic behaviour is obtained is influenced by the type of polymer and specific grade; the processing conditions; the presence of other additives and the level of relative humidity.

For example, the differences between various polyethylene and polypropylene grades in density, crystallinity and molecular structure mean that the optimum structure for every given antistatic agent has to be arrived at by variation in the chain length of the alkyl radical and in the number of hydroxyl or polyether groups, so as to ensure that it will perform effectively in the intended application. For instance, typical agents for polypropylene are less effective in low-density polyethylene, and vice versa.

Some general guidelines for application concentrations of antistatic agents are given in Table 6.2. The table lists typical concentrations for the major polymers; for certain processing techniques, however, the necessary amounts are likely to be greater than these. Addition rates can vary from 0.05% to 8% and in some cases may be as high as 10%.

- Untreated inorganic fillers and pigments like titanium dioxide can adsorb antistatic molecules onto their surface, and hence lower their efficiency. This is usually compensated for by increasing the dosage level.

- Certain agents tend to degrade specific polymers: for example fatty acid based amines are known to react with chlorine in PVC.
- Excess antistatic agent in a formulation can lead to tacky, smeared films on the surfaces of finished products. Not only do such films detract from the visual appearance of the product, they are also an obstruction to subsequent printing, adhesive or lettering processes.

Polymer	Antistatic Agent (% by wt)
LDPE	0.05-0.1
HDPE	0.2-0.3
PP	0.5
Rigid PVC	0.5-1.5 (depending on stabilizer system)
PS, crystal	2.0-4.0
PS, impact resistant	1.5-2.5

Table 6.2 Importance of polymer type on dosage level

Other factors have to be taken into account i.e.

- High antistatic agent concentrations may cause interference in moulding since most of these products are viscous liquids and are apt to act as lubricants in the moulding material and hinder Its flow into the extruder. This difficulty can be overcome by the inclusion of a small amount of a filler which will increase the friction e.g. SiO_2.
- The fact that some antistatic agents have a melting point close to room temperature can sometimes cause handling problems, and their incorporation into the polymer matrix can lead to mixing and dispersing problems e.g. screw slippage.
- Many antistatic agents exhibit relatively low heat stability which hinders their use in certain engineering polymers which require high processing temperatures.
- Since many antistatic agents are hygroscopic, compounded materials based on polymers which are not normally classed as hygroscopic may require drying prior to processing.

6.2.2.6 Areas of application for chemical antistatic agents

6.2.2.6.1 Application by Polymer type

Polyolefins

By far the largest quantities of internal antistatic agents go into polyethylene and polypropylene for applications in film, sheet, injection-moulded articles, and containers, especially packaging.

Styrenics

Recent years have seen the growing use of antistatic agents in styrenic polymers (polystyrene, impact-resistant polystyrene). In contrast to polyolefins, higher loadings of up to 4% antistatic agent are necessary in these substrates for a good level of activity due to their relatively high compatibility with the most common antistatic agents; consequently the cost factor limits their use to specialty products such as video cassettes, instrument housings etc.

PVC

PVC requires special consideration since the requirement of rigid and flexible materials are quite different. In rigid PVC, the quaternary ammonium compounds are generally recommended. The potential antagonism with heat stabilisers must however be considered. In flexible PVC, ethoxylated alcohol and alkoxylated fatty acid esters are preferred. As might be expected the type and concentration of the plasticiser has a significant effect on antistatic performance.

Engineering plastics

In engineering plastics, such as PET, PMMA, polycarbonate and polyacrylates, internal antistatic agents have not found widespread use for two main reasons. Firstly, their thermal stability is usually insufficient to survive the high processing temperatures used for engineering plastics. Secondly, some of these materials have important intrinsic properties e.g. transparency in polymethacrylates and polycarbonates, which could be affected by the use of antistatic additives.

6.2.2.6.2 Application by type of antistatic agent

Cationics

Cationic antistatic agents work best in polar substrates e.g. PVC and styrenic polymers. Their application is however restricted by their adverse influence on the thermal stability of some polymers. They often have to be used at concentrations 5 to 10 times greater than those of nonionic compounds in order to achieve comparable antistatic action. Dosage levels for cationics in rigid PVC and polyolefins are typically 1 to 2%. The most common class of cationic antistatic agent, quaternary ammonium salts, has not been FDA-accepted.

Anionics

Anionics are also mainly used in PVC and styrenic-based materials; their behaviour in polyolefins is comparable to cationic antistats.

Nonionics

The low polarity of nonionic antistatic agents makes them ideal internal antistatic agents for polyethylene and polypropylene, with which they are highly compatible. Typical dosage levels for nonionic internal antistats range from 0.05 (low density polyethylene) to 2.5 (polystyrene) wt %; high density polyethylene and polypropylene need levels somewhere in between. Crystal polystyrene is the most difficult to make antistatic and may need higher levels.

Ethoxylated amines are widely used in PE, PP, ABS and other styrenics. Several types are available that differ in alkyl chain length and level of non-saturation. These characteristics determine their melting point, volatility and their migration speed. Ethoxylated amines are very effective even at low levels of relative humidity, and remain active over prolonged periods. Furthermore, these products have generally been approved for use in food contact applications.

Highly purified glycerol monostearate is widely used, especially in polypropylene. This additive shows a very quick build-up of antistatic performance and is approved for food contact applications. Glycerol monostearate gives only a temporary antistatic effect, and is

therefore often combined with ethoxylated amines in order to obtain short and long term antistatic action.

Fatty alkanol amides are used in polyethylene and polypropylene. These additives offer quick and prolonged antistatic action in most applications. Amide-based antistats produced from lauric and coco fatty acid are widely used in electronics packaging. Some types are approved for food contact use.

Sodium alkyl sulphonates are used in PVC, styrenics and in engineering plastics. They offer outstanding heat stability and are therefore the preferred choice for high temperature processing and most are approved for food contact use.

6.2.2.7 External antistatic agents

As far as external antistats are concerned, the main areas of application are in textiles, flooring and packaging for products such as cosmetics. The article is sprayed or wetted with a solution of the antistatic agent, or dipped into the solution, and then dried. One example is in the finishing of PVC floor coverings, where surface-active agents are added to the rinsing water at the cleaning stage. Dry blending can be utilised when the target polymer has been powderised and a sufficiently small particle size of the additive is available.

Along with the higher cost of this plant- and labour-intensive method, a big drawback of external application is the inadequate stability of the antistatic effect. On the one hand, the action is extinguished once the surface is cleaned with the aid of moisture, since there is no internal agent that can migrate to the surface to replace the loss, and on the other, the effect often wears off due to migration of the agent into the interior of the product.

6.3 Static Fillers

Fillers that alter the electrostatic nature of the polymer can be incorporated into polymers but are not generally considered ionic in character. These additives are listed in Table 6.1. The main polymers used in with these fillers include nylon (carpets and business machine parts), polyethylene (flexible packaging products), polypropylene, ABS (business machine housings), PVC (flooring) and others such as polyimide, polyester and phenolics.

6.3.1 Classification and mode of action of conductive fillers

The major conductive fillers and fibres used have not changed in recent years but there have been improvements in their performance, the result of newer grades featuring better compatibility or higher conductivity. There are also some relatively new specialty fillers that employ substrate metallisation to improve performance; typical substrates include micro-spheres and mica.
The additives used may take the form of fillers or reinforcing fibres, which are conductive in the mass or at their periphery. They vary greatly in size and shape and their effect on conductivity can be described using the following characteristics.

6.3.1.1. Critical loading

The conductivity of a filled material does not increase linearly with the percentage of the conductive additive used. At low concentrations, there is no effect. Above a certain level a reduction in resistivity occurs, the magnitude of which increases exponentially with concentration. This level is defined as the critical load rate or percolation threshold. It is influenced by the nature of the resin and other additive related parameters such as aspect ratio and particle size distribution.

6.3.1.2 Aspect ratio

Aspect ratio is the ratio of length to diameter of the filler particle. The higher the aspect ratio, the more contact between particles and hence higher conductivity. In the case of carbon black for example, for a given volume, a large number of small particles is better than a small number of large particles due to the increased surface area provided for electrical conductivity. In addition, irregular shaped particles are better than particles with a sphericity close to unity.

It is possible to control the degree of electrical resistivity of a compound by varying the percentage or type of conductive additive used. For example, static dissipative compounds with surface resistivities of 10^5 to 10^9 ohms/square are frequently used for products that come into direct contact with electronic components. They must not be so conductive that a

discharge through the part is too fast and damages the part or shorts out the device leads by contact with the conductive materials. Correspondingly, there must be sufficient conductivity to control the build-up and dissipation of static charges. This is a similar scenario to the "window" approach to spraying of powders by inductively charging the polymeric particles. Too conductive and adhesion decays too swiftly, too insulating and charging cannot occur in a practical time frame.

The various filler types differ in efficacy and are therefore used at different loading levels to deliver the same degree of conductivity. It has been reported that an application which would require about 15 % by weight of carbon fibres, for example, would require only 5 - 6 % of stainless steel fibres and about 6 - 8% of nickel-coated graphite.(Rapra, 1993).

6.3.2 Carbon black

Carbon black is the most popular method of making thermoplastics conductive - probably accounting for the production of over 90% of conductive and static dissipative compounds. It is inexpensive, widely available and easy to process, providing permanent conductivity. There are myriad grades of carbon black on the market, each with its own special profile of characteristics. Usage levels are generally between 15 and 30%. At these levels, it is of course highly improbable that the use of carbon black as a modifying agent would find a wide-spread use for powder coating. Due to its widespread use, there is a large base of technical understanding surrounding its use in alternate applications and this is worth reviewing discussing other types of fillers.

6.3.2.1 Varieties of Carbon Black

There are several different types of carbon black: furnace black offers the best economic solution for most applications. More than 98% of the industrial carbon blacks produced throughout the world, approximately 6 million tonnes per year are furnace blacks. Acetylene blacks are particularly important for conductive applications. They are very pure, with no sulphur content; therefore, they offer the least potential for corrosion, such as in electrical contacts. Specialty blacks, with high surface area, provide the best conductivity at low loadings (3 to 5 wt %). They are also high in purity and low in sulphur content.
In recent years, several so-called "super-conductive" blacks, such as *Ketjenblack EC* from Akzo, have been made available for use as conductive filler's. They can be as much as six to eight times as efficient as standard acetylene-based and other furnace blacks, due to their

greater surface area (finer particle size) and higher structure. They also provide better physical properties in the finished product, but at a higher cost since they are significantly more expensive than standard grades of carbon black. Temperature has less of an effect on their conductivity, which has enabled their use in engineering resins.

Typical prices for commercially available carbon blacks are:

Type	Price (£/kg 1995)
Low conductivity	1.4 - 2.0
Standard high conductivity	2.0 - 3.0
Ultra high conductivity	6.0 - 11.5

6.3.2.2 Mode of action of Carbon Black

Various theories have been proposed as to the mechanism of electrical conduction in polymers filled with carbon black powders. These include:

- The formation of a continuous chain of the carbon black particles with electronic movement occurring along this continuous chain due to inter-particle contact (conduction path theory)
- In addition to the above, conduction can occur due to the ability of electrons to "jump" across gaps that exist between carbon black particles within a polymer matrix (tunnel effect theory).

Research studies have indicated that the phenomenon of electrical conduction does occur in the absence of a continuous chain and is determined by the size of the gap (inter particle distance).

Four particular properties influence the ability of carbon black to provide conductivity in plastic compounds:

1. Small particle size, allowing more particles per unit volume, so reducing inter-particle distances.
2. High structure i.e. clusters of particles that are multi-branched. These increase inter-aggregate contact and improve electrical conductivity.
3. High porosity, yielding more particles per unit weight than solid particles, which results in smaller distances between them.
4. Low volatile content, ensuring that a minimal quantity of chemi-sorbed oxygen is present to reduce the conduction of the material.

In general, the addition of carbon black has predictable effects on the physical properties of the polymer. It increases conductivity, flexural modulus, tensile strength, hardness, viscosity and heat distortion temperatures. However, impact strength, elongation and melt flow index are decreased. Adverse effects on mechanical properties can however be overcome by combining carbon black with impact modifiers, glass fibres or mineral fillers. Colour, of course is another matter!

Resin type influences the degree of conductivity in a carbon black filled composite. Highly crystalline resins tend to impart slightly higher conductivity than less crystalline resins at a given carbon black loading. Conductivity reduces when the composite is cross-linked as a result of lower density and less crystallinity.

Very often the desired properties of the composite cannot be achieved at the required conductivity level without modification of the base resin, and sometimes complex formulations are needed to give a balanced set of properties.

Carbon black structure is measured by dibutyl phthalate (DBP) absorption. The greater the absorption, the greater the structure and the higher the conductivity. The same relationship applies to surface area, calculated by nitrogen absorption. Surface chemistry is another factor; chemi-sorbed oxygen on the surface (volatile content) reduces conductivity.

One criticism levelled at carbon black fillers is that they exhibit a "step" effect. Conductivity of compounds increases slowly as the level of filler increases, up to a particular point at which there is a dramatic increase. Trying to obtain conductivities within this transition zone is not easy, but can be achieved by mixing standard carbon black with super-conductive grades.

6.3.3 Other Conductive Fillers

Incorporation of conductive metal fillers or metal-coated fibres into a thermoplastic is an effective means of achieving electrostatic dissipation; however, this method is often limited by cost. Metal fillers generally require high volume loadings resulting in rather brittle compounds. They can be difficult to process and to achieve the required dispersion. They are also relatively heavy, which may be a disadvantage for some products. The most widely used conductive fillers in this class are carbon or graphite fibres, stainless steel and uncoated or nickel-coated graphite. Other fillers (used more frequently for EMI shielding applications) include aluminium coated glass fibres, aluminium flakes and silver coated glass spheres.

6.3.3.1 Carbon Fibres (graphite Fibres)

Carbon fibres produce the same conductivity as carbon powder at about one-third to one-half lower loadings and do not have the particle-shedding tendencies of many powder compounds. Carbon fibres offer the maximum reinforcement of any fibre; because of their exceptional stiffness, parts manufactured from them have high structural strength. Shrinkage and warpage can be a problem however.

Carbon fibres are widely used in engineering thermoplastics in place of glass fibres to give the same (or better) mechanical performance, whilst adding conductivity. PAN (polyacrylonitrile) and mesophase pitch are the two basic types of carbon fibres, depending on the starting material used in their manufacture. Compounds are available using milled, chopped or continuous forms. The performance range of these compounds in regard to strength, conductivity, dimensional stability and appearance is tailored for optimum performance by varying the type, form and loading level. To reduce material costs, carbon powder can be blended with the fibre to obtain various levels of conductive properties.

6.3.3.2 Stainless Steel Fibres

Stainless steel fibres have become a major factor in ESD applications and are probably the most efficient of all conductive fillers. Although stainless fibres cost about 40% more than carbon fibre, equivalent performance can be obtained at about half the loading. They have a high aspect ratio (200 to 300) and so readily form conductive networks in the compound. Usage levels are around 5 to 7% by weight for ESD purposes.

A significant advantage over carbon fibres is flexibility. This minimises fibre breakage during processing, which translates into more predictable electrical properties in the moulded part and economises on loading requirements. Mechanical properties of finished parts are good and abrasion of metal surfaces during processing is low.

A further advantage is that stainless steel compounds can be pigmented or easily painted, which has led to their widespread use for appearance parts. Electronics plants are also turning to stainless steel compounds for trays and containers to enable them to colour code parts. They thus offer excellent prospects for powder coating applications.

6.3.3.3 Nickel-coated graphite

Introduced in the mid-1980s by AMERICAN CYANAMID Co, nickel-coated graphite (NCG) fibres are highly conductive - about 50 times as conductive as uncoated graphite. They combine the high electrical and thermal conductivity of metals with the exceptionally high strength-to-weight ratio of carbon fibre reinforcement. Their structure consists of a thin, continuous sheath of electroplated metal about 0.4 μm in thickness surrounding a 7 μm diameter carbon fibre core. Nickel offers corrosion resistance and cost advantages over other metals, whilst its thermal and electrical conductivities are excellent.

Generally, NCG fibres act like standard graphite; stiffness benefits and shrinkage are similar. As with other fibres, processing conditions should be designed to minimise fibre breakage. One problem is the relatively poor aesthetics of moulded parts produced.

NCG fibres are more commonly used where it is necessary to have maximum conductivity and EMI shielding performance with some degree of reinforcement, and cost is a secondary consideration. Levels of 3 to 5% are usually sufficient for static dissipation purposes.

6.3.3.4 Alternate Fillers

Several types of conductive fillers employ the strategy of metallisation on a lightweight substrate as an alternative to solid metal powders.

Silver has been chosen as the metallising element for several substrates. It is a highly conductive metal that does not require an oxidation-preventive coating. Metallised "microballoons" are used mainly in thermosets; unfortunately, their thin walls will not survive thermoplastic processing methods. For such applications, metallised hollow "microspheres" (which are smaller but have much thicker walls) are used. These methods are more cost effective than silver powders, but are still too expensive for ESD applications and they are used mainly for EMI shielding compounds, sometimes in combination with a conductive fibre. The same, alas, must be said of applications in the majority of powder coating markets, but future developments may make improve cost effectiveness. One of the modifiers selected for the proof of concept stage of the charging by induction experiment described in Chapter 5 was to add small quantities of silver.

6.3.3.5 Processing Considerations

The majority of static dissipative compounds are produced by extrusion compounding using twin-screw extruders. One of the most important aspects of processing is to maintain the high aspect ratio of the fibres. For instance, nickel coated graphite fibres suffer significant aspect ratio degradation during twin screw extrusion compounding.

In the case of carbon black filled compounds, excessive mixing can destroy the structure of the black and hence reduce conductivity. The use of carbon black does however permit the use of processing techniques such as blow moulding or vacuum forming, which are difficult or impossible with the use of conductive fibres.

Optimum processing conditions vary with the type and form of conductive material and the base resin. Among the fibre systems, stainless steel based compounds are easiest to mould because of the relatively low loadings used and their ability to resist fracture compared to uncoated and nickel coated graphite. Carbon powder systems require similar processing conditions to those for the base resin, but require higher injection pressures because of their higher stiffness.

6.4 Static control by the use of intrinsically conductive polymers and alloys

A third method of producing static control polymers is by the use of intrinsically conductive polymers (ICPS) such as polyaniline, polyacetylene, polypyrrole and polythiophene. In general, these materials are polymeric charge-transfer complexes in which conductivity arises from the mobility of ions or electrons along the polymer backbone. Although these materials have the potential to replace metals and composites in a number of applications, only a few, high-value, low-volume applications have been commercially exploited to date, mostly in the area of high-energy batteries. However, these materials are now finding applications in static control.

Researchers working on intrinsically conductive polymers have found that as conductivity increases, the material becomes less soluble, brittle and infusible. Long-term thermal and environmental stability has also been found to be a problem. The high cost of these materials, together with their poor mechanical performance and/or difficult processing, has led to their

use either as coatings or as additives in other polymers creating products which can be used for static dissipation and electrostatic shielding purposes.

6.4.1 Conductive Polymer products on the market

This section provides some information on the main suppliers of antistatic agents, conductive fillers and static control polymers and their activities in terms of product developments.

6.4.1.1 Antistatic agents

ICI have probably the largest product range on the market. The *Atmer* series of antistatic agents is available for many applications, and products are available in concentrated and masterbatch form.

Among amine-free products is HOECHST *Hostastat System E 6952,* a laurylamide concentrate in linear low density polyethylene, for used in extruded and moulded parts. According to Hoechst, the product, which has recommended use levels of up to 2.5%, is not corrosive and is thus better suited to contact with polycarbonate components than the ethoxylated amines typically in use.

Hoechst have also introduced an aliphatic sulphonate antistatic agent in a 100% active pellet form, trade named *Hostastat HS* 1, which can be used in PS, ABS, PVC and styrenic alloys.

Another amine-free formulation is PPG POLYMER PRODUCTS' *Durastat AS-6004* concentrate and *Durastat AS-6050,* an amine antistat used in bi-axially oriented PP films. In food packaging, *Durastat AS-5814* concentrate for use in HDPE materials requiring FDA approval is said not to impart a greasy feel to injection moulded products. Use levels of 7% of the concentrate have provided surface resistivity in the 10^{10} ohms/square range, according to the company.

AKZO CHEMIE are marketing a variety of *Annostat* antistats based on ethoxylated amines, glycerol monostearates and sodium alkyl sulphonates. Products are also available in concentrate form under the trade name *Nourymix.*

One of the improved amine-based antistats offered by suppliers is CABOT PLASTICS' XP material, which incorporates an ethoxylated amine into an LDPE carrier. The masterbatch,

which can be used in LDPE, LLDPE, HDPE, and ethylene-vinyl acetate at a recommended level of 2 - 3%, is said not to interfere with the physical properties of the polymers.

In addressing the "non-permanent" antistatic issue KENRICH PETROCHEMICALS INC. has been working on a series of non-blooming internal antistats under the trade name Ken-Stat that reportedly do not require humidity to function. The products are neoalkoxy titanates and zirconates, which form soluble complexes within the polymer - their non-migratory nature is attributed to their orientation in alternating bipolar charge layers. However, the products have been found to exhibit only limited thermal stability and have to date achieved only limited commercial success.

DOW has developed *Stature II,* an additive targeted at polyurethane packaging foams for electronics packaging applications, for example. The additive is thermally stable, which is important when foaming polyurethanes with high peak exotherms. According to DOW, foams produced using the additive are non-corrosive and are static-dissipating almost independently of ambient humidity. Apparently, because the product is bonded to the foam, it becomes part of the entire matrix. Therefore, it cannot migrate to the surface where it could be removed by contact or evaporation, hence providing a long service life.

Other suppliers of antistatic agents include HARCROS CHEMICALS and in the US, CHEMAX and Du PONT.

6.4.1.2 Conductive fillers

AKZO, CABOT and DEGUSSA are the main suppliers of carbon black. For some time, the "superconductive" blacks category was dominated by AKZO, with their Ketjenblack products. Superconductive grades are now also available from CABOT and DEGUSSA.

Nickel-coated graphite fibres are available from AMERICAN CYANAMID, which provides the fibres in both continuous form and in a pelletised dry blend.

Stainless steel fibre is produced by BEKAERT. The basic fibre diameter is from 6.5 to 8μm.

DU PONT supply *Zelec ECP Electroconductive Powders* based on doped metal oxides, which are said to offer several benefits over carbon black - white, transparent or Coloured products are easily achievable, with surface resistivities in the 10^3 to 10^{12} ohms/square range. The

products can be used in films, foams, static dissipative packaging, fluoropolymer coatings and antistatic fibres. The products are manufactured by coating a thin layer of antimony-doped tin oxide onto the surface of less expensive, inert powders.

Nickel-coated mica has been developed by SUZORITE MICA PRODUCTS (Boucherville, Quebec) in conjunction with SHERRIFF GORDON MINES in Canada. The platelet form of mica flakes contributes reinforcing value as well as aiding in the formation of conductive paths. Typical loadings for ESD applications are in the range 10 to 15 % wt.

LNP ENGINEERING PLASTICS supply numerous *Stat-Kon* grades containing either carbon black or metal fibres. Latest products include Stat-Kon PDX-S, an injection mouldable and extrudable conductive nylon 12 made with stainless steel fibres. Inherent corrosion resistance is claimed to make it suitable for such automotive fuel applications as fuel filters, connectors and lines.

PerrnaStat 600 ABS compounds from RTP are said to contain an "electronically altered" polymer additive that provides surface resistivity of 10^{10} to 10^{11} ohms/square. Static decay rate meets Mil Spec B-81705C specifications, which makes them suitable for applications that include packaging for electronics. RTP says flexural strength is about 20% less than that of unmodified ABS, while impact strength is slightly improved. Compounds are available in unreinforced and flame retardant grades.

Other suppliers include DSM with their *Faradex* range (ABS/polycarbonate and ABS/polyvinyl chloride with stainless steel fibres), CABOT PLASTICS, BASF *(Ultramid 85* nylon 6 and *Ultramid* A3WC4, containing carbon black and carbon fibres respectively), BIP CHEMICALS (Beetle polyester moulding compounds) and HOECHST.

AMERICHEM of dispersions of various fillers which are available in polyvinyl chloride, polyethylene, polypropylene, polystyrene, ABS, SAN, TPE, polyacrylonitrile, nylon, acetal, ionomer, polyesters, TPO, polycarbonate, various weatherable polymers, TPR, and most other thermoplastic resins, alloys, and compounds.

6.4.1.3 Intrinsically Conductive Polymers and alloys

This is a fast developing area of polymer technology. The interested reader is referred to a review paper by R. Rosner, 3M Corporation entitled "**Conductive Materials for ESD**

Applications: An Overview" presented at the Electrostatic Discharge Society's annual conference at Annaheim, CA in September 2000.

PART III

STUDY TWO: GENERATION OF DISPERSED MEDIA BY ELECTROSTATIC FORCES – LIQUID ATOMIZATION

CHAPTER 7

A REVIEW OF THE LITERATURE RELATING TO ELECTROSTATIC SPRAYING OF LIQUIDS

7.1 Foreword

The aim of this work was to gain understanding of aerosol generation of semi-insulative liquids using electrostatic forces to supply the dispersion energy. The work was sponsored by Glaxo Pharmaceuticals and the area of application was envisaged as a liquid pharmaceutical atomizing device similar to pressurised inhalers.

A full background introduction to the area of electrostatic spraying is given. Electrostatic spraying relies upon the resistance to flow of inherent electrical charge carriers except where free charge is injected into the liquid before dispersion. Liquids may be dispersed into ions, sub-micron drops carrying high specific charge or larger charged drops. Applications for electrostatic spray systems include paint spraying, electrostatic printing, fuel atomization in combustion systems, electrostatic emulsification, ion sources for spacecraft propulsion, microscopy, sputtering and micromachining, thin-film coating, the production of ultra-fine powders and many others of considerable scientific and industrial importance. A comprehensive list of references is cited. A far-reaching book on the topic by Professor A.G. Bailey was published in 1988.

Here, an introduction is first given to the early studies into the phenomenon in a largely qualitative review with some key principles. Progress to more recent developments and an outline of important advances and current investigative fronts then follows.

The experimental work that is later described in Chapter 8 is founded on this review.

7.2 Introduction

The earliest studies of electrostatic spraying of liquids were performed with thin glass capillaries containing liquid at zero or very low hydrostatic pressures. Bose (1670) recorded

the disruption of such a liquid surface into a spray of charged droplets when subjected to an intense electrostatic field. With no electrostatic field the dripping rate from a downward pointing capillary depends solely upon the balance between the downward gravitational force driven by the mass flow rate in the tube and the restoring force of surface tension. When a sufficient mass of liquid gathers at the capillary outlet so that the downward gravitational force overcomes the upward surface tension force a drop will detach. The mass of which can be determined if the liquid surface tension and density and the capillary diameter are known.

This dripping rate is increased if an electrostatic field is present as the liquid emerging has charge induced on its surface and this generates an outward stress. The downward component of the force due to this stress adds to the gravitational force so that progressively smaller drop detach from the tube as the tube's electrostatic potential, and hence electrostatic field, is increased.

7.2.1 Early Experimental Investigations

Zeleny (1914, 1917, 1935) was the first to publish an experimental study on the subject earlier this century. These publications serve equally as an introduction to the subject and a rich source of key discoveries pointing the way to subsequent research by others in the field. In his first published study, Zeleny (1914) observed the behaviour of a hemispherical liquid surface at the tip of a glass capillary under various conditions of applied voltage and surrounding gaseous medium. For the experimental case of water in the capillary emerging into air at atmospheric pressure the following train of events were observed.
Having adjusted the hydrostatic pressure in the capillary to produce a hemispherical surface, the voltage on the capillary was increased. The surface of the liquid was observed to deform from the hemispherical profile and the hydrostatic pressure was adjusted downward until the original profile was again obtained. This procedure was continued until at a certain voltage the surface of the drop suddenly snapped back into a more flat position and a current was observed to flow in a Galvanometer connected to an earthed counter electrode situated 2 *cm* beneath the capillary tip. The pressure was again adjusted to produce the original surface profile and the procedure repeated. This time a discharge did not occur until a higher voltage was reached than previously. Zeleny explained this latter point as being due to contaminants being expelled in the first discharge. Contaminants at a liquid/gas interface can be expected to reduce the interfacial tension beneath that for the pure liquid case (see Chapter 10).
On continued increase in the applied voltage, periodic oscillations of the surface were observed and synchronous current was observed in the galvanometer. The oscillations

increased in frequency until at a particular voltage, the outline of the meniscus suddenly became still and a steady current was recorded. Zeleny observed that at this stage the luminosity was confined to a very thin portion of the liquid surface, whereas in the intermittent stage a faint light was observed extending, in the form of a brush, towards the counter-electrode.

Zeleny went on to describe the behaviour of water and alcohol surfaces emerging from thin capillaries into various media including carbon dioxide and gases at different pressures. His observations are summarised below.

With a water-in-air system at pressures below 60 cm of mercury (0.8 bar), the intermittent stage of current was not obtained. In addition, he observed that the voltage could be lowered beneath the onset value of measured current while current was still maintained, thus showing hysteresis. For a water surface in carbon dioxide at atmospheric pressure the initial behaviour with increasing voltage is similar to the behaviour in air but the change from the blurred meniscus did not give rise to a distinct hemispherical surface but to a steady cone shape with a line extending from the apex into the surrounding gas. At lower liquid pressures, the cone was observed to flatten out and at higher voltages the surface became very agitated. The potential at which the current ceases from a water surface in carbon dioxide was found to be almost identical with that at which the current ceases from a point of the same dimensions in air. This voltage was found to be constant right down to approximately one third of an atmosphere but the conical meniscus was not observed at pressures lower than atmospheric.

The behaviour of an alcohol surface in both air and carbon dioxide was found to be similar to a water surface in carbon dioxide. The amplitude of surface oscillations and the current reaching the counter electrode were smaller than the equivalent water cases due, it was surmised, to alcohol's lower surface tension. Meniscus profiles with alcohol were unaffected by pressure down to the measured minimum of 12 *cm* mercury in air and 25 *cm* mercury in carbon dioxide. The potential at which current ceased was found to be the same in both carbon dioxide and hydrogen at all pressures at about 0.6 that at which discharge stopped in air.

Zeleny (1914) recorded in sketches the form of the menisci he observed and in a later paper (1917), photographs of ethanol surfaces undergoing electrically induced disruption. Conditions and equipment were similar to those discussed in his first paper and voltages of 5000 - 6000 *V* and liquid heads of 3 - 4 *cm* were used. The effect of electric field shielding by emitted drops is clearly shown with an emitted train of drops following a zig-zag pattern due to being emitted alternately from one side then the other of the vertical axis. The photographs also show alcohol assuming a conical meniscus at the end of the capillary with a single ligament emerging from the apex. Measurement of the diameter of this ligament from

photographs put it at approximately 4 x 10^{-6} *m*. This form was obtainable only at certain conditions of potential and hydrostatic pressure. The disintegration of the ligament into droplets occurred a short distance beneath the cone apex but attempts to observe the droplets were futile due to their minute size and the resolution of the optical equipment available. Zeleny remarked on the fact that the spray of droplets appeared coloured by both transmitted and reflected light and that the colours persisted when the eye was within about 45^0 of the direction of the light. The colours depended not only on the angle of sight but they differed depending upon the portion of the spray which was observed, indicating that different droplet sizes were grouped according to position in the spray. This phenomenon was later clearly demonstrated by Gomez and Tang (1991) using phase doppler anemometry and digital imaging techniques to investigate an electrostatically generated spray of heptane doped with anti-static agent.

Zeleny (1917) commented that the outside portion of the spray, which he observed to be more or less conical in volume, was presumably made up of the set of comparatively small drops that form between the main drops whenever any liquid jet breaks up into drops. He was obviously drawing on the work of Lord Rayleigh (1878) whose famous analysis of jet break-up was published some years earlier.

Zeleny (1914) also used glycerine in one of his experiments because its viscosity is so much greater than alcohol. He noted that when the conditions were arranged for a single thread coming from a steady surface its length was some 15 *cm* before disintegration into drops. This jet broke into larger and smaller drops, the larger drops forming a conical volume shrouded by the smaller drops which formed an outer boundary described by a paraboloid of revolution about the vertical axis. The potential in this case was 7000 *V*, the diameter of the ligament was 7 μm, and the average size of the larger and smaller droplets was estimated at 10 μm and 2.5 μm respectively.

Zeleny (1917) tested the hypothesis that all the current flowing from the capillary in the conical form of discharge was carried by the liquid droplets and not by ionic carriers. By noting the effect a blast of air, directed at right angles to the electric field between the point and the plate, would have upon the current received by the plate, he intended to differentiate between the two distinct charge carriers. It was found that the air flow had considerable effect on the charge carriers, contrary to what Zeleny erroneously expected with ionic carriers of high mobility. It was thus concluded that with an alcohol surface emitting current, solely small charged droplets were carrying this current.

In a further paper, Zeleny (1935) showed that it is only under certain conditions that solely droplets of the liquid carry the whole discharge current from an alcohol drop and under more restricted conditions the same may be true for a water surface.
Zeleny reviewed developments by Macky (1930), Nolan (1926) and Wilson and Taylor (1925) on the stability of hemispherical soap bubbles resting on earthed liquids and of uncharged water drops falling through uniform electric fields. He then refined his experimental technique to determine charge carriers in order to bring into accord their work with his and to clarify the difference between self-sustaining glow discharges (corona discharges) from liquid surfaces and discharges due to surface instability (Zeleny, 1935).
Zeleny then posed the question whether at atmospheric pressure a gaseous discharge always accompanies the disruption of a liquid surface made unstable by a high electric field. It should be noted that such an unstable surface can lead to the enhancement of the electric field by the deformation arising from the instability.
Zeleny refined his earlier (1917) experiments of preventing charge carriers from reaching the earth plate beneath the charge emitting capillary or metal point by directing an air stream parallel to the plate. He showed that the mobilities of the charge carriers, whether ionic or drops of liquid, were similar and that it was possible for drops of alcohol of the estimated size (circa 1 - 10 μm) to carry the sort of charges need for them to be of a comparative mobility with air ions. He also pointed out drop mobility will increase with evaporation. Therefore blowing experiments alone could not determine whether the charges were carried mainly by gas ions or solely by liquid droplets. Zeleny's next step was to measure the current flowing to the earthed plate with increasing and decreasing potential and marking where luminosity (attendant on gaseous discharge) appeared or disappeared as the case was. Figure 7.1 shows the results for two separate capillaries containing ethanol.
The break at point C on both curves is best explained by considering the curve at potentials below c as being the discharge current due solely to charged liquid droplets and above c as being due to both charged liquid droplets and a self-sustained discharge through the gas.

So Zeleny answered his question, it is possible to have a discharge from a liquid meniscus under electrostatic stress whereby all the discharge current is carried by droplets of the liquid charged by conduction from the high potential at the capillary.

7.2.2 Mathematical Treatment of Liquid Surface Instabilities

Zeleny's mathematical treatment of the phenomena leading to the disruption of liquid surfaces is based upon extensions to Rayleigh's analysis of the stability of a charged droplet in the

absence of an applied electric field (Rayleigh, 1882). The conditions necessary for a charged surface to become unstable are exemplified by considering the energy balance equation for a spherical drop.

$$\frac{2\gamma}{r} - P - \frac{\sigma^2}{2\varepsilon_0} = 0 \tag{7.1}$$

Where γ is the interfacial or surface tension,r is the radius of the drop, P is the pressure internal to the drop and σ is the surface charge density.

The equilibrium of the surface becomes unstable (and the internal pressure becomes zero) when a small outward displacement of a portion of the surface increases the outward force due to the surface charge density σ, because of the increased curvature produced, more than it does the restoring force arising from surface tension. At this point, it can be easily shown that the absolute charge limit on the droplet is given by

$$q_r = 8\pi\left(\varepsilon_0\ \gamma\ r^3\right)^{\frac{1}{2}} \tag{7.2}$$

Where γ is the interfacial or surface tension, r is the radius of the drop, P is the pressure internal to the drop and σ is the surface charge density. (Note: SI units used throughout).

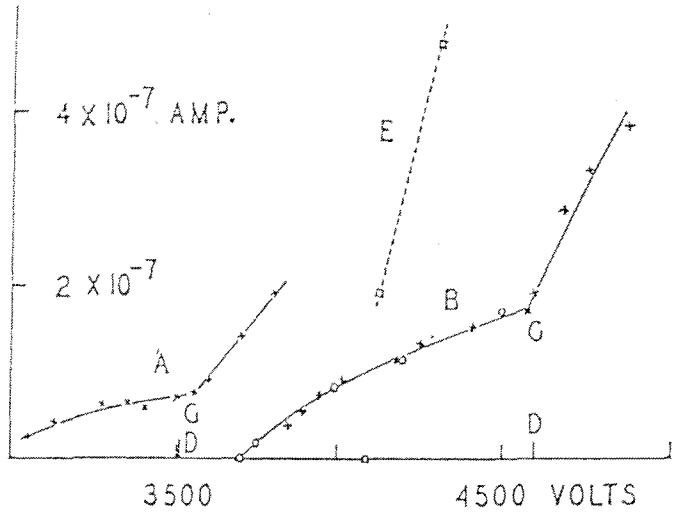

Variation with voltage of current from an alcohol point. Curve *A*. Radius of point, 0.28 mm. Distance to plate, 1.03 cm. Curve *B*. Radius of point, 0.46 mm. Distance to plate, 1.50 cm. Curve *E*. Metal point of radius, 0.20 mm. Distance to plate, 1.50 cm. Luminous effects were first observed at voltage *D*.

Figure 7.1 Zeleny's plot of current from an alcohol tip versus applied voltage

To apply the results of Lord Rayleigh to a liquid surface at the end of a capillary at high potential it is necessary to know the shape of the surface as well as the charge distribution on it, both before and after the displacement in question.
Working with these arguments, Zeleny derived the following equation predicting the onset of instability

$$V^2 = cr\gamma \tag{7.2a}$$

Where γ is the interfacial or surface tension as before, r is the radius of the drop, and V is the potential applied to the capillary from which the droplet protrudes.

The work of various researchers has built upon the above, most notably Taylor (1964) and Rosenkilde (1969), in analyzing the stability of a droplet (for theoretical arguments, usually considered isolated and uncharged) in an applied electric field.
According to Rosenkilde, an uncharged droplet in an applied electric field assumes an approximately prolate ellipsoidal shape. At the point of instability the ratio, r_1/r_2 of the lengths of the semi-major and semi-minor axes, has a value of 1.838 (c.f. Taylor, 1964) and the following relation holds:

$$\frac{r\varepsilon_0 E_0^{\,2}}{\gamma} = 0.2045 \tag{7.3}$$

Where E_0 is the applied electric field strength.

The dimensionless terms shown in equations (7.2) and (7.3) are essentially the same and are related to the electrostatic Weber number defined below

$$W_e = \frac{d\varepsilon_0 E_0^{\,2}}{\gamma} \tag{7.4}$$

Where d is a characteristic dimension of a particle or droplet, typically replaced by the diameter of a sphere having the same volume.

Rosenkilde's value for the maximum value of the electrostatic Weber number for a droplet is then seen to be $W_e = 0.409$.

Sir Geoffrey Taylor (1964) reviewed Zeleny's stability criterion (equation 7.2) for a drop held at the end of a cannula. He proved that the assumption that pressure inside the bound droplet would equal the external pressure at the point of instability was not the case. He then revisited Rayleigh's analysis with the intent of developing a model for thinking about the mechanics of the development of the liquid jets associated with one form of electrical instability observed by Zeleny and others.

If the transition from stability to instability is synchronous with the transition from a conical meniscus to a "cone-jet", then, by understanding the equilibrium equations necessary for a stable electrified cone to exist, one can hypothesize about the formation and subsequent break up of the meniscus into droplets in this mode.

For the case of a conducting liquid emerging from a cannula at potential V_0, a conical meniscus can be maintained under the influences of an electric field and surface tension if the electric field is such that the outward stress on the liquid surface due to it balances at every position both the magnitude and direction of the inward stress due to surface tension.

$$\frac{\gamma}{r\tan\alpha} = \frac{1}{2}\varepsilon_0 E_\theta^2 \tag{7.5}$$

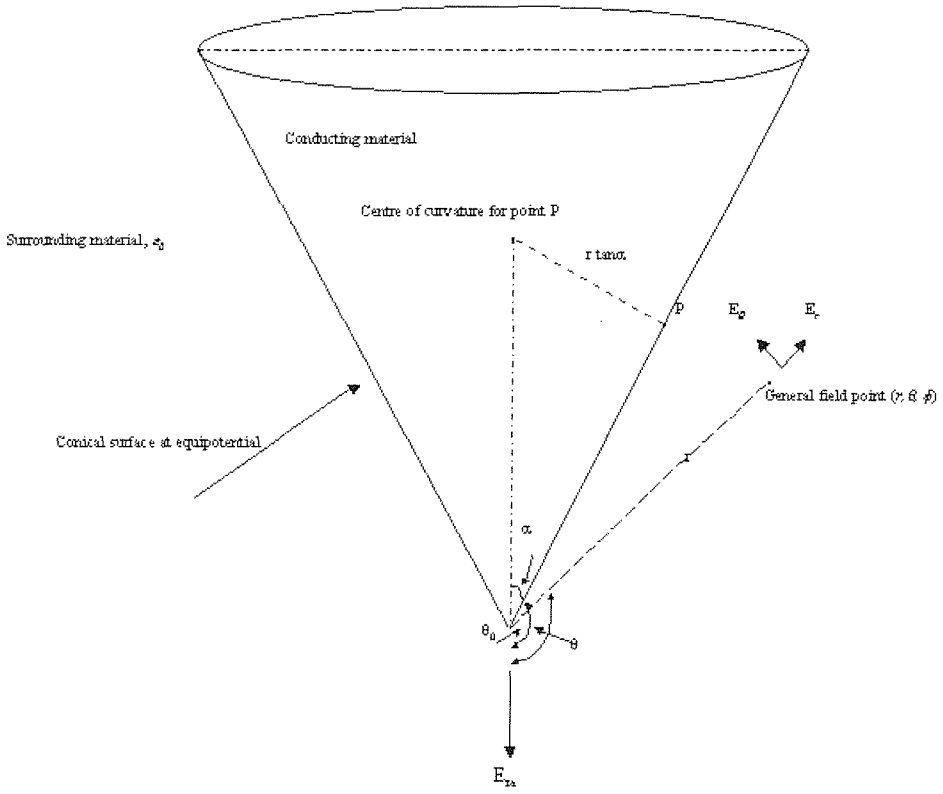

Figure 7.2: The electrified Taylor Cone of semi-vertical angle 49.3°

The stress at a point on the surface such as P, due to surface tension, is inversely proportional to its distance *r* from the vertex. If this is to be balanced by electrostatic stress, the electric field normal to the cone must therefore be inversely proportional to the square root of this

distance. Such a field is possible if its potential is specified in terms of the conical function $P_{\frac{1}{2}}(\cos\theta)$ (which is a special case of an associated Legendre function) as follows:

$$V = V_0 + Ar^{\frac{1}{2}} P_{\frac{1}{2}}(\cos\theta) \tag{7.6}$$

Where V_0 is the potential applied to the cannula, which in turn fixes the potential on the surface of the cone. It corresponds to $P_{\frac{1}{2}}(\cos\theta) = 0$.

Now $P_{\frac{1}{2}}(\cos\theta)$ is finite in the range $0 \leq \theta \leq \pi$ and has only one zero which occurs at an angle $\theta = \theta_0 = 130.7099^{o}$. This implies that the only cone which can be held stable under the two opposing forces has a semi-vertical angle of $\alpha = 49.2011^{\circ} \cong 49.3^{\circ}$.

Taylor (1964) tested the usefulness of his analysis by using specially constructed apparatus to produce the potential field described by equation (7.6). Two conducting surfaces were fabricated, one a frustrum of semi-vertical angle 49.3° with a truncated vertex so that its upper edge was a horizontal circle which could form the lower edge of a conical liquid surface and the other, upper, electrode having a profile specified by $r = r_0 [P_{\frac{1}{2}}(\cos\theta)]^{\frac{1}{2}}$. Although the acceleration of the liquid filament which was forced from the apex of the cone (and the subsequent alteration of the electric field) caused oscillations to occur, the form of the entire surface at the peak of its oscillation was indeed very close to 49.3°. The applied voltages required to produce conical surfaces for a variety of liquids were found to be slightly larger than predicted, due perhaps to imperfect insulation of the electrodes.

The assumptions and special experimental arrangements made by Taylor in this work have been often scrutinized and on occasion, unfairly criticized. Taylor proved that the cone observed could indeed be mathematically modelled. His motivation, as alluded to earlier, was to provide a sound basis for thinking about the mechanism that leads up to the formation of the change in meniscus profile at the apex of a drop near the Rayleigh limit. In some cases, this instability culminates in the formation of a stable jet of liquid at the apex of a near conical interface - the so-called cone-jet mode of electrostatic atomization of liquids.

Considering equation (7.6), the transverse and radial electric fields can be established as follows:

$$E_\theta = -\frac{1}{r}\frac{\partial V}{\partial \theta} = -Ar^{-\frac{1}{2}}\frac{d}{d\theta}P_{\frac{1}{2}}(\cos\theta) \tag{7.7}$$

According to Taylor, $\frac{d}{d\theta}P_{\frac{1}{2}}(\cos\theta)$ = -0.974 when $\theta = \theta_O$ and so equation (7.7) becomes:

$$E_{\theta_0} = \frac{-0.974A}{r^{\frac{1}{2}}} \tag{7.8}$$

Recalling equations (7.5):

$$\frac{\gamma}{r\tan\alpha} = \frac{1}{2}\varepsilon_0 E_{\theta_O}^2 \tag{7.5}$$

And combining it with equation (7.8)

$$\frac{\gamma}{\tan\alpha} = \frac{1}{2}\varepsilon_0 (0.974A)^2 \tag{7.9}$$

Substitution of $\alpha = 49.3^\circ$ and solving for A gives:

$$A = 1.347\left(\frac{\gamma}{\varepsilon_0}\right)^{\frac{1}{2}} \tag{7.10}$$

Thus the magnitude of the field normal to the surface is:

$$E_{\theta O} = 1.312\left(\frac{\gamma}{\varepsilon_0 r}\right)^{\frac{1}{2}} \tag{7.11}$$

By taking, for example, the surface tension of water as 72 mNm^{-1} and assuming it is exiting from a cannula of 0.3 *mm* diameter (typical of experimental observations), calculation of the normal field at the top of the meniscus (where $r=0.3/2 \sin 49.3^o$) gives: $E_{\theta_0} = 8.41\ MVm^{-1}$.

A reasonable estimate for V_0 for this situation is E_{θ_0} *x 0.3mm/2* = 1261 V.

The radial electric field can be found from equation (7.6) as follows;

$$E_r = -\frac{\partial V}{\partial r} = \frac{-AP_{\frac{1}{2}}(\cos\theta)}{2r^{\frac{1}{2}}} \tag{7.12}$$

Substituting for A from equation (7.12) gives

$$E_r = -\frac{\partial V}{\partial r} = -0.6734\, P_{\frac{1}{2}}(\cos\theta)\left(\frac{\gamma}{\varepsilon_0\, r}\right)^{\frac{1}{2}} \tag{7.13}$$

The value of $P_{\frac{1}{2}}(\cos\theta)$ at $\theta = 0$ is 1, so the electric field along the axis of the cone into the surrounding medium is given by:

$$E_r = -0.6734\left(\frac{\gamma}{\varepsilon_0 r}\right)^{\frac{1}{2}} \tag{7.14}$$

From equation (7.14) above, the electric field at the vertex takes an infinite value. This is where the liquid jet issues from and explains why, even with specially constructed electrodes, a perfectly still meniscus of a true conical shape oscillates.

Again, using the properties of water and the cannula size as before, the electric field say one cannula radius along the vertex is 4.96 MVm^{-1}. Even at interfaces between a highly curved surface and air, these sorts of fields are highly likely to cause air breakdowm.

7.2.3 Later Experimental Investigations in Droplet Formation under Applied Fields

Important work was carried out by Vonnegut and Neubauer (1952) using similar apparatus to Zeleny. That is, a simple glass tube drawn to a capillary of outside diameter a few tenths of a mm filled with a liquid which was connected to a source of variable high d.c. voltage by a wire placed in the tube.

With water as the liquid in the tube, before voltage was applied, drops formed at the rate of a few per minute. The drops broke away from the capillary at sizes of approximately 1 mm in diameter. On raising the potential to 500 V, droplets of the order of 100 μm were produced at the rate of about 100 per second. These droplets were highly charged. Generation of fine streams of droplets using a high voltage source of 60-hertz a.c. was also recorded and it was shown that the stream carried no net charge but individual droplets were charged half to one polarity and half to the opposite polarity. The authors suggested that the use of a.c. or pulsed d.c. could be used to accurately control the frequency of drop formation.

Perhaps the most significant results were obtained with liquids of intermediate conductivity such as distilled water, lubricating oil and alcohol. When a positive potential falling within a narrow range was applied, the electrostatic dispersion was so efficient that an extremely fine smoke of droplets was produced. When the smoke was illuminated with a beam of parallel

white light it displayed the phenomenon of "higher order Tyndall spectra" with the light being scattered into the colours of the spectrum, the colour viewed depending on the angle of observation. This indicates that the droplets were of the order of 1 μm in size and were uniform in size i.e. monodispersed. The magnitude of an applied electric field that can be sustained in air varies with polarity and is higher for positive potentials. This is due to the mobility differences between positively charged particles (ions) and negatively charged particles (electrons). Thus, the magnitude of the applied field at positive potentials is higher and can be sustained at a level necessary for this mode of electrospraying.
Vonnegut and Neubauer, unlike Zeleny, made no mention of gaseous discharges being attendant on the electrostatic dispersions they observed; neither did they record the form of the liquid meniscus commenting merely that it was convex. Vonnegut and Neubauer are generally attributed with putting forward the idea that the energy of a system of drops, consisting principally of surface and electrical energy, tends to be minimised during spraying. It is an important idea and has been developed by subsequent workers including Ryce (1964) and Pfeifer and Hendricks (1967). It was, however, Zeleny who first indicated this approach in a footnote to his 1935 paper.

To assess the minimum energy concept, consider the following. Having predicted that a droplet will become unstable and disrupt when it possesses at least the Rayleigh charge limit as given in Equation (7.1), then if N equi-size droplets result from the break up of a larger droplet of volume V carrying charge Q by whatever process that leads to atomization and that each daughter droplet is of radius r and carries charge q the total potential energy of the system G_d (assume no droplet-droplet interactions) is

$$G_d = N4\pi r^2\gamma + \frac{Nq^2}{8\pi\varepsilon_0 r} \tag{7.15}$$

The first term is associated with the free surface energy of the system and the second the energy associated with stored charge; effectively N times $\frac{1}{2}CV^2$ *where C is the capacitance of an isolated droplet and V the surface potential of the droplet.*

By applying charge and volume conservation to the system i.e. $Q=Nq$ *and* $V=\frac{4N\pi r^3}{3}$ gives

$$G_d = \frac{3V\gamma}{r} + \frac{Q^2r^2}{6\pi\varepsilon_0 V} \tag{7.16}$$

The principle of the minimum energy hypothesis, then, implies that the above quantity will most likely tend to a minimum. By differentiating the above expression with respect to r and equating to zero, the radius at which the energy is minimised can be shown to be

$$r = 3\left(\frac{V^2}{Q^2}\right)^{\frac{1}{3}}(\varepsilon_0\gamma)^{\frac{1}{3}} \tag{7.17}$$

Furthermore

$$r^3 = 9\left(\frac{V}{Q}\right)^2 \varepsilon_0\gamma \tag{7.18}$$

$$r^3 = 9\left(\frac{4\pi r^3}{3q}\right)^2 \varepsilon_0\gamma \tag{7.19}$$

$$q = 4\pi\left(\varepsilon_0\gamma\, r^3\right)^{\frac{1}{2}} \tag{7.20}$$

Which is half the Rayleigh limit charge as given in Equation (7.1)

This is the most utilised outcome of the minimum energy concept. Of further note is an analysis building on the above, to calculate the range of daughter droplets that will result from the break up of a droplet carrying the Rayleigh limit of charge. Such an analysis was performed by Pfeifer and Hendricks (1967) as follows.

From equation (7.1), the Rayleigh charge limit gives the relation between Q and V

$$\frac{Q}{V} = \frac{6(\varepsilon_0\gamma)^{\frac{1}{2}}}{R^{\frac{3}{2}}} \tag{7.21}$$

Where R is the radius of the parent drop. Thus

$$R = \left(\frac{36\varepsilon_0\gamma V^2}{Q^2}\right)^{\frac{1}{3}} \tag{7.22}$$

The energy, G_p, of the parent drop from equation (7.5) is

$$G_p = 4\pi R^2\gamma + \frac{Q^2}{8\pi\varepsilon_0 R} \tag{7.23}$$

As Q is the Rayleigh charge limit, substitution for it leads to

$$G_p = 12\pi R^2\gamma \tag{7.24}$$

The energy of the daughter droplets, G_d, is

$$G_d = N4\pi r^2\gamma + \frac{Nq^2}{8\pi\varepsilon_0 r} \tag{7.25}$$

Further algebraic manipulation and substitution leads to an expression for the ratio of G_d/G_p as

$$\frac{G_d}{G_p} = \frac{N^{\frac{1}{3}}}{3} + \frac{2}{3N^{\frac{2}{3}}} \tag{7.26}$$

Figure 7.3 Normalised energy of daughter droplets to parent droplet (After Pfeifer and Hendricks (1967)

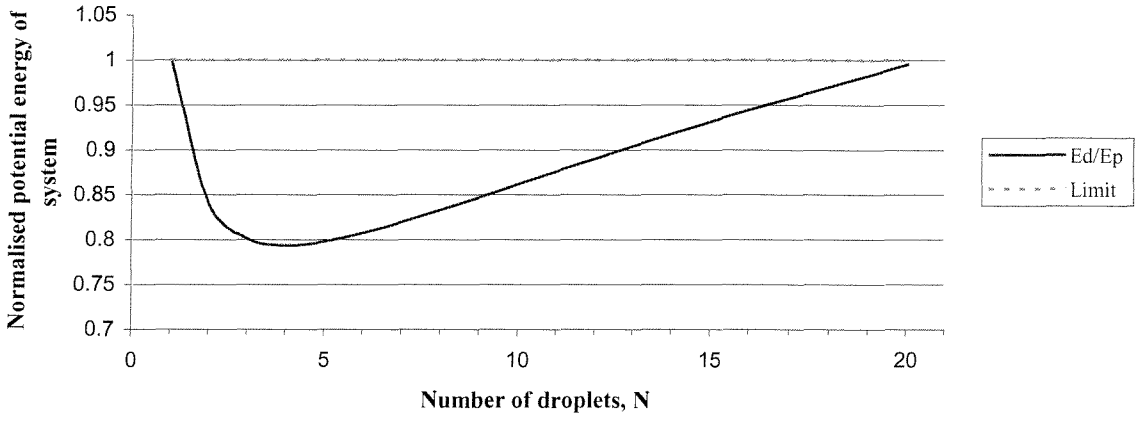

From the plot, we can see that the maximum number of droplets formed will be 20 and the number of droplets equivalent to the most probable radius is 4.
Pfeifer and Hendricks compared these predictions with experimental results for disintegration of various liquids following break up due to Rayleigh instability. There results for Octoil (γ= 31mNm^{-1}) and shown in Figure 7.4.

Figure 7.4 would appear to show that there us a strong tendency for a large droplet to break up into smaller droplets such that the resulting total energy is minimised. The energy lost by the system in doing this will obviously flow to the surroundings mostly in the form of heat.

7.2.4 Monodispersity

Two recent papers have shed light on the mechanism for the monodisperse spraying that Vonnegut and Neubauer observed. In the first, Joffre and Cloupeau (1986) discuss the regulating effect that charge emission can have on the form of the meniscus emitting the

charge. Zeleny (1914) observed that one stable mode of meniscus when he was spraying ethanol was a cone shape, from the apex of which there extended a ligament or liquid jet. The break-up of this jet, though generated by the action of electrostatic stress and carrying on electrostatic charge, is now known to be almost independent of charge (Schneider et al, 1967, Neukermans, 1973) and should proceed in a manner accurately described by Rayleigh (1878) giving a pattern of large drops with small single satellite drops between them. As the droplets all carry a charge of the same polarity, the Coulombic repulsion far from the intense field at the apex should give rise to a symmetric conical cloud of droplets in which the outer shroud contains the small satellite drops and the inner the larger drops as observed by Gomez and Tang (1991).

Figure 7.4 Droplet number density versus radius for octoil (After Pfeifer and Hendricks, 1967))

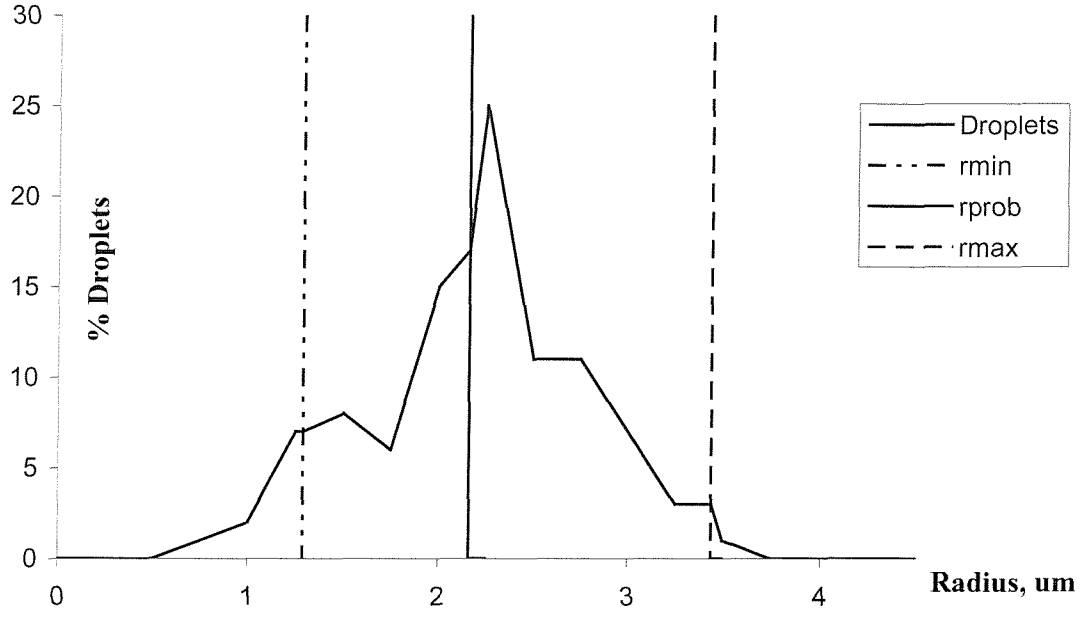

Thus, current evidence suggests that the break-up of a ligament extending from a conical meniscus, which may be a stable form of liquid meniscus beyond the strict electrode geometry described by Taylor (1964) due to space charge effects, will give rise to a duo-dispersed cloud of droplets.

A logical deduction, though unproven to the author's knowledge, is that true monodispersity can occur if, under extremely critical conditions of liquid flow rate, field strength and geometry and liquid properties, each satellite droplet coalesces with the larger droplet formed immediately ahead of it. The smaller droplet will have a higher mobility and close to the apex,

will be traveling faster than the main droplet. Under balanced conditions, collisions at the jet break-up frequency can be envisaged leading to cloud of monodispersed droplets.

7.2.5 Liquid Dispersion Criteria

Drozin (1955) studied the electrostatic dispersibility of a number of liquids and developed a number of quantitative guidelines on the likelihood of electrostatic generation of aerosols based on liquid properties such as surface tension, conductivity and dipole moment. Drozin also noted the dependence of atomization on the shape, radius, wall thickness and symmetry of the capillary, and the effect of placing a grounded electrode at various distances from the high voltage capillary.

In his quantitative study, Drozin used the same capillary, of diameter 0.06 *mm*, placed 10 *cm* from a grounded plate with C.P. grade liquids. His table of results is reproduced here. Neglecting hydrostatic pressure (due to the fineness of the capillary) and vapour pressure (see section 10.4), the electrostatic tension, exerted by a liquid on a non-polarizable boundary is given by (Panofsky and Phillips, or Abraham and Becker)

$$p = \frac{1}{8\pi}(\varepsilon - 1)\left[E^2 + (\varepsilon - 1)E_N^2\right] + \frac{1}{8\pi}E^2\frac{d(\varepsilon - 1)}{d\rho}\rho \qquad (7.5)$$

Where E is the electric field strength, E_N its normal component, ε is the electric permittivity of the liquid ($\varepsilon = \varepsilon_r\varepsilon_0$) and ρ the density of the liquid.

The first term represents the force perpendicular to the surface of the insulator where the latter forms a boundary with a non-polarizable medium (e.g. air $\varepsilon_r = 1$). This force tends to pull the insulator into the air. The second term represents electrostriction. The following assumptions are made in the derivation:

1) The liquid is an insulator. Drozin quotes a figure of $10^{-3}\ S\ m^{-1}$ as being an experimental limit (empirically measured).
2) The dielectric constant on the boundary between liquid and air changes continuously in the surface layer (which is assumed to have the dimensions of the dipole length).
3) The drop at the end of the capillary is an ideal hemisphere, then the tangential component E_T of the field strength is negligible and $E \cong E_N$.

Drozin estimated $E_N = V/r_c$ where V is the potential on the capillary and r_c is a radius of curvature of the meniscus and used two equations expressing ε as a function of ρ, one

Onsager's for non-polar liquids and the other Henriquez' for liquids with greater polarities (see e.g. Frohlich, 1958).

	Fluid	σ	γ	ε_r	$\eta . 10^{11}$	$Cf(\varepsilon)$
1	Water	$1x10^{-4}$	73	81	1.84	257
2	Glycerin	$6x10^{-6}$	65	56.2	2.66	110.5
3	Methyl alcohol	$2x10^{-5}$	22	31.2	1.68	35.6
4	Acetone	$6x10^{-6}$	24	21.5	2.80	16.75
5	Ethyl nitride	$5x10^{-5}$	-	19.7	2.91	13.4
6	Acetic acid	$1x10^{-5}$	24	6.3	1.73	1.0
7	Chloroform	$2x10^{-6}$	27	5.1	1.10	0.36
8	Ether	$4x10^{-11}$	16	4.4	1.15	0.35
9	Xylol	$1x10^{-13}$	27	2.4	0.36	0.11
10	Toluene	$1x10^{-12}$	27	2.34	0.37	0.11
11	Benzene	$1x10^{-16}$	29	2.24	0.08	0.11
12	Carbon tetrachloride	$4x10^{-16}$	26	2.25	0.00	0.09
13	Melted microcrystalline wax	From $1x10^{-12}$ to $1x10^{-14}$	-	2-2.5	-	0.08-0.05

Where σ is conductivity S m^{-1}, γ is surface tension in N m^{-1}, ε_r is relative dielectric constant [-] and η is the molecular dipole moment.

Table 7.1 Drozin's dispersion criteria

$$p = \frac{1}{8\pi} E_N^2 \left[\varepsilon(\varepsilon - 1) - \frac{d(\varepsilon - 1)}{d\rho} \rho \right] \tag{7.6}$$

$$p = cf(\varepsilon)\, E_N^2$$

Table 7.1 shows the results of applying both equations to give the value of $cf(\varepsilon)$. Drozin used $cf(\varepsilon)$ as a criteria to predict whether a particular liquid could be electrostatically dispersed saying that if this parameter calculated for a given liquid using Henriquez's equation of state is ≥ 1 the liquid can be dispersed.

This approach needs to be extended and clarified so that the effect of significant conductivity on the bulk force is included and the term $cf(\varepsilon)$ is included in the equilibrium equation more

explicitly. Nonetheless, in a qualitative sense it is the first attempt to tie the liquid properties to the dispersion energy.

Drozin put forward an explanation of the formation mechanism for the fine atomization he observed. At the critical potential for the onset of fine atomization, the electric forces of repulsion exceed the surface tension forces and the main filament stretching out from the capillary breaks down into a multitude of symmetrically arranged fine filaments, which become unstable and immediately disintegrate into very fine charged drops. It is this mechanism, and the attendant instability criteria giving rise to break-up, that has attracted most attention from this work and gained credence since it was first proposed (see for example Joffre et al (1982).

7.2.6 Experimental evidence for the minimum energy hypothesis

Charles D. Hendricks Jr. (1962) examined the velocity and charge of octoil droplets produced at the point of a hollow stainless steel needle maintained at high (12-13 kV) potential. His interests were to overcome some of the difficulties inhibiting development of a space-craft propulsion system utilising a beam of ions as the working fluid. Broad distributions were found for droplet radii and charge-to-mass ratio. Droplets carrying an absolute charge of less than 10^{-15} C could not be detected. A plot on log-log scale showed that the curve of maximum q/m ratio as a function of radius is a straight line of slope $-\frac{3}{2}$. Less than 0.3 % of data points lay above this line (equivalent to the Rayleigh limit) and the average charge/radius was 50% of this limit.

7.2.7 Classifying the phenomenon of electrostatic atomization

In a review paper, Kozhenkov and Fuks (1976) analyzed the development of the science of producing highly dispersed monodispersed aerosols of similar charge up to that date. They group processes covered by the term "electrostatic atomization of a liquid" into three groups.

(1) Electrostatic atomization with large flow rates of liquids (up to circa 0.20 m^3hr^{-1}) fed under pressure to multi-nozzled spraying apparatus and operating at potentials up to 100 kV and above. This process causes the formation of coarsely polydispersed charged aerosols and finds industrial application in electrostatic painting and crop spraying.

(2) Electrostatic atomization with extremely low liquid flow rates (circa 10^{-9} - 10^{-3} m^3 hr^{-1}) fed under steady-state conditions usually to a single capillary tube sprayer in a vacuum

maintained at potentials of approximately 10 - 15 kV. Most of the research work in this regime was undertaken on molten metals and the analyses of workers in the field such as Krohn (1961, 1974) and Clampitt et al (1972, 1974) help establish the importance of the Taylor cone in understanding the mechanism of dispersal of the metal into sprayed drops or ions. The production of monodisperse aerosols by this method of electrostatic spraying was first reported by Sample and Bollini (1975). Pure dielectrics can be atomized to highly dispersed aerosols in this regime if charge is injected into the liquid (Kelly, 1984). Industrial applications include microelectronics manufacture, thin film coating, production of ultra-fine powders and for colloid thrusters for spacecraft propulsion.

(3) Electrostatic atomization under ambient conditions with small liquid flows (10^{-8}- 10^{-4} m^3 hr^{-1}) with relatively low voltages on the liquid (3-10 kV). Under certain conditions of liquid flow rate and applied potential, this process yields a monodisperse aerosol from liquids of many types over a wide range of droplet sizes (0.1 - 1000μm). Aerosol droplets generated in this process carry charges which can be predicted by the minimum energy theory (Zeleny, 1935 and Vonnegut and Neubauer, 1952) or the minimum entropy theory (Kelly, 1976). Kozhenkov and Fuks state that it is this third regime of electrostatic spraying that the term "*electrohydrodynamic atomization of a liquid*" is mainly applied.

This term first appeared in a paper by Pfeifer and Hendricks (1967) in which the energy minimisation theory is used to predict the charge level on sprayed droplets. Data obtained from spraying of octoil, Wood's metal and glycerine substantiate the model which is based on the premise that an unstable liquid mass disrupts into equally sized and charged particles so that the energy tends toward the minimum value. Although the mechanism of liquid break-up is immaterial to the theory, it is interesting to note that the model predicts specific charges on the droplets which are exactly half the Rayleigh limit for instability (Ryce, 1964) (and see section 7.2.2). Pfeifer and Hendricks (1967) explain this as an emerging droplet connected to the high voltage capillary has charge accumulating on its forward portion so that this portion becomes unstable according to Rayleigh's criterion. Thus upon separation from the capillary, the droplet tends to possess roughly half the Rayleigh limiting charge.

The reviewers correctly point out that the problem of the mechanism by which aerosol droplets - and particularly monodispersed aerosol droplets - are formed is basic to the understanding of the atomization process.

The problem of obtaining a satisfactory physical model for the break-up mechanism is complicated by the fact that there are a number of distinct modes of operation depending on the voltage applied to a particular system. These range from (Bailey, 1988) field enhanced dripping through intermittent spraying/dripping to continuous spraying from a single jet to finally a 'brush' effect or multi-ligament spraying as described by Hendricks (1962).

7.3 Expressions for the field strength and parametric studies

DeShon and Carson (1968) investigated the pulsed mode of liquid spraying by assuming the liquid tip was in the form of a prolate spheroid.
Using an expression (Eyring et al, 1928) for the electric field developed for a metallic point-to-plane geometry:

$$E_0 = \frac{2V}{r_c \ln\left(\frac{4z_0}{r_c}\right)} \tag{7.27}$$

and substituting a value for the liquid surface curvature in place of the metallic point, they compared the value of the field thus calculated with the field calculated from the equilibrium equation for the liquid surface at various values of electric potential and capillary to plate spacing. Using glycerine, they found that for the type of spraying considered (pulsing mode) the same trends were observed for both expressions but that, on average, the field predicted from the analytical expression for point-to-plane geometry was 20% less than that calculated from the equilibrium consideration. DeShon and Carson (1968) attributed the error to the expression for the electric field since it was developed for metal points in the shape of a hyperboloid of revolution. It is interesting to note that by assuming the liquid tip remains in the shape of a prolate spheroid and that there is no effect from the internal pressure, the break-up mechanism is governed by Rayleigh instability corresponding to n = 2, as investigated and disproved by Taylor (1964) in the particular cases described by Zeleny (1917).
If indeed the analytical equation is in error by circa 20% then the pulsing mode of spraying which occurs at low potentials is very well modelled by the Rayleigh instability criterion adopted for droplets at the end of a capillary. At higher voltages, however, this analysis

breaks down and a different model is required to describe the mechanism of break-up in the region beyond the pulsing mode.

Kozhenkov and Fuks (1976) recognised this absence of an exact theory for the atomization of a liquid in the steady meniscus mode or multi-ligament mode but reject the Taylor cone model as representation of only a particular case of atomization and of being too simplistic by ignoring a variety of process parameters and liquid properties. It is interesting to note how modern developments have since confirmed the Taylor cone model (Smith, 1986, Cloupeau and Brunet-Foch, 1989, Hayati et al 1989a and Meesters, 1992) in many cases of highly dispersed monodispersed spraying systems and also how much controversy it has caused Chung et al, 1987 and Kingham and Bell, 1984).

The reviewers further claim that the formation of a monodisperse cloud of droplets of size r = 5-20 μm of various liquids (dibutyl phtalate, ethanol and a 50% solution of the two) results from the emission of single droplets from a liquid apex or from the tip of a small liquid cylinder and not by the stretching, out and rupture of a liquid filament. For this, they claim an analogy with the formation mechanism of a monodisperse aerosol by spinning disc atomization with a small supply of liquid. The charge on the particles was also found to be close to the equilibrium charge calculated from the minimum energy theory.

Despite concentrating their review on electrohydrodynamic systems producing monodisperse aerosols, the reviewers appear to have overlooked two key papers published in 1971 by Jones and Thong (1971) and Thong and Weinberg (1971). In the former, the electrical dispersion of a jet of kerosene, doped with an anti-static agent (ASA-3, Shell) to increase its conductivity, is discussed. Generation of monodispersed droplets was particularly desirable to simplify the study of their behaviour in an electric field. Droplets produced in this manner were used in combustion systems are described in the latter paper.

Both vertical and horizontal sprays were studied and the apparatus included a flow system capable of providing a steady measurable flowrate to variously sized stainless steel capillaries. A micro-ammeter was included in the earth circuit to the counter electrode which allowed charge to mass measurements to be made for the droplets. For vertically downward spraying, this counter electrode was a brass gauze of 50 mesh 17.8 cm in diameter 5.6 cm from the capillary tip. The internal and external diameter of the capillaries used was 0.191 mm, 0.404 mm for flow rates less than 0.25 $cm^3\ min^{-1}$ (1.5 x $10^{-5} m^3 hr^{-1}$) and 0.211 mm, 0.44 mm for flow rates in the range 0.1 to 0.4 $cm^3\ min^{-1}$ (0.6 x $10^{-5} m^3 hr^{-1}$). Jones and Thong (1971) found that for a given flowrate between 0.1 and 0.4 $cm^3\ min^{-1}$ monodisperse sprays could be obtained within a narrow voltage range of 3.60 to 4.15 kV (the voltage being measured at the capillary by an electrostatic voltmeter). Schlieren photographs of the sprays show a jet of liquid being emitted from the capillary which subsequently breaks up into droplets.

Within the range of voltage for which monodisperse sprays were formed, the droplet size increased with flow rate. Droplets of between 40 μm to 70μm were produced, depending on the flowrate, from a capillary of 0.191 mm i.d., 0.404 mm o.d. at 4.15 kV, the flowrate varying between approximately 0.14 cm^3 min^{-1} to 0. 24 cm^3 min^{-1}.

Similar results were observed for horizontal sprays and it was observed that the ratio of the diameter of the jet of kerosene emerging from the capillary (dj) to that of the droplets (dp) was dp/dj = 1.89 throughout the experiments. This value is in close agreement with the theory of the stability of an electrified liquid jet which gives dp/dj = 1.89. This result is from Lord Rayleigh's work on the stability of non-viscous liquid jets under laminar flow conditions (1882). Rayleigh's analysis was extended by Schneider et al (1967) to examine the effect of electric charge on the jet (later corrected by Neukermans (1973) who showed that there should be little change in the break-up rate even when the jet is highly charged).
Jones and Thong obtained an expression for the electric field configuration between the capillary and the earthed electrode by approximating the capillary as a semi-infinite line of charge. At the capillary tip of radius r_c, the magnitude of the electric field is expressed as

$$E_0 = \sqrt{2}\,\frac{V}{r_c \ln\left(\frac{4z_0}{r_c}\right)} \tag{7.28}$$

Smith (1986) rewrote the expression for the field strength at the capillary point as

$$E_0 = \frac{1}{A_1}\,\frac{V}{r_c \ln\left(\frac{4z_0}{r_c}\right)} \tag{7.29}$$

treating A, as an empirical constant, which he determined to be 0.667 the value of which should be best found from experiment. Regardless of the analytical expression for E_0, Jones and Thong showed that monodisperse spraying is onset at the applied voltage for a particular electrode geometry.

In their work, DeShon and Carson (1968)suggest that with A_1 at 0.5, the above equation underestimates the electric field at the tip of the jet by a factor of about 20%. In examining their procedure, it is more likely that the form of the tip of the liquid jet departs from the

prolate spheroid shape assumed by them just before the expulsion of a droplet. As Smith (1986) points out, in the pulsating mode the liquid will possess a momentum due to the action of the electrical stress on it so that the flowrate predicted from the Poiselle equation will be momentarily exceeded thus contravening one of Deshon's and Carson's assumptions. The shape of the surface may tend to become cuspidal in this event and the actual value of the liquid surface curvature increases beyond that predicted giving rise to a higher electric field. The potential drop along the liquid will also increase accordingly, lowering the field near the apex below the value required to maintain cuspidal geometry. The meniscus then relaxes back to its original position and the action continues.

By concentrating on the conditions which lead to a steady meniscus being formed, Smith (1986) attempted to characterise the EHD atomization process in terms of the fluid delivery system and the liquid properties. Prime interest was focused on the effect of liquid conductivity and Smith explained the extrusion of liquid from the conical meniscus as being due to a radial electric field component.

EHD mode onset was described as following the following mechanism: when the potential on the meniscus is raised to a value above the critical value for instability, the meniscus tends toward zero radius of curvature on the axis (see e.g. Taylor (1964) and Miksis (1981)). This gives rise to high field strengths in this region and charge is emitted by some mechanism. There is therefore necessarily a conduction current to compensate for loss of charge and the fluid cone presents a resistance to this current depending on the conductivity of the liquid that forms its. Thus, a radial electric field is created which gives rise to surface stress in the radial direction and causes liquid near the surface to move toward the apex.

By using tracer particles of lycopodium, Hayati et al (1989) were able to take streak photographs of a stable jet. The motion of the liquid in an EHD jet could thus be observed and it was shown that there is an axi-symmetric circulation of the liquid in the conical base of the jet. The origin of this motion was explained as being due to interfacial electric shear stresses at the surface of the cone set up by the simultaneous presence of surface charge and tangential electric field due to the semi-insulating nature of the fluid. If a highly conducting fluid is used, these convection currents are not noted and a stable jet will not form. A finite element method was used to calculate the potential distribution in the cone and jet and it was shown that the shear force acting on the cone was between approximately 5 to 10 times smaller than the normal force. The normal force was found to be fairly constant and independent of applied voltage whereas the shear force tended to reduce with increase in voltage. This confirmed experimental evidence which showed that the jet length tends to decrease as voltage increases and may divide into multiple jets if the tangential force is sufficiently reduced.

Smith (1986), in a qualitative model, expressed the flowrate of the jet as

$$F = \frac{4\pi\varepsilon_0 \sin\theta_0 \cos\theta_0 \; k}{(1-\cos\theta_0)} \frac{\gamma}{\rho_g \sigma} \tag{7.30}$$

θ_0 is the cone half-angle

k is the depth of liquid assumed to move on the cone surface (to approximate viscous flow)

γ is the liquid surface tension

ρ_g is the liquid mass density

σ is the liquid conductivity

Smith also gave an expression relating the steady state current flowing through to the sprayed droplets in terms of liquid properties as

$$I \propto \frac{\gamma^{\frac{3}{2}}}{\rho_g \; \sigma \; r_j^{\frac{1}{2}}} \tag{7.31}$$

where r_j is the radius of the liquid jet or filament which in turn is proportional to the inverse of conductivity.

Smith carried out a large number of experiments to study the effects of variations in flow system parameters and liquid property values. His findings are summarised here.

The most appropriate expression for the electric field at the tip of the capillary was

$$E_0 = 1.5 \frac{V}{r_c \ln\left(\frac{4z_0}{r_c}\right)} \tag{7.32}$$

where

E_0 is the field strength at the capillary

V_0 is the voltage applied to the capillary

r_c is the outside radius of the capillary

z_0 is the separation to the planar counter electrode.

The onset of the EHD mode was found to occur at approximately equal values of field strength.

Smith found that liquids of surface tension greater than 0.05N m^{-1} could not be atomized in the EHD mode due to ionisation of the air occurring at field strengths lower than that necessary to overcome the surface tension forces of these liquids. From results on liquids of various values of surface tension, it was found that the square of the onset potential of the EHD mode was proportional to the surface tension. If the surrounding gas was one of higher breakdown strength than air the EHD mode was reached even with liquids of high surface tension.

According to equation (7.31), the current measured should be proportional to $\gamma^{1.5}$. Indeed, Smith noted that the current drawn by water containing a surfactant to reduce its surface tension into the range $0.04 < \gamma < 0.05$ N m^{-1} was greater than that for liquids of lower surface tension but that this effect seemed to be swamped by the dependence of current on liquid conductivity. The effect of surface tension on liquid flowrate was not investigated.

The effect of increased conductivity on the EHD mode was examined by the addition to a given liquid of an ionic substance so that the other properties of the liquid were held essentially constant and any differences in behaviour could be attributed solely to changes in conductivity.

Drozin (1955) quoted a range of conductivity of $10^{-11} < \sigma < 10^{-3}$ S m^{-1} outside of which fine atomization could not occur. This range has been quoted since but the existence of the upper limit never explained. Smith claimed that there is in fact no upper limit for a liquid to atomize in the EHD mode. As conductivity increased, he observed the aerosol droplet size decreased and at a value of 0.1 Sm^{-1}, the size had decreased to a point where the light-scattering was too low for Tyndall spectra to be observed. A conical meniscus was maintained, which gave rise to droplet emission, at all values of conductivity, and the current at onset of the EHD mode was weak but an increasing function of conductivity. Flowrate at EHD mode onset was a strongly decreasing function of conductivity, but the rate of fall-off decreased at higher conductivities. The radius of the filament at the end of the conical meniscus also decreased with increase in conductivity but conductivity had no significant effect upon the onset potential of the EHD mode.

Although it was difficult to isolate the effect of variation of viscosity from other important liquid properties, increased viscosity was seen to cause a significant increase in aerosol droplet size.

Cloupeau and Brunet-Foch (1989) re-termed Smith's EHD mode as the "cone-jet" mode as they felt this compound word simply denotes the meniscus profile without prejudging as to the stability of the jet or the mechanism with which it is established. They back up Smith's claim that this mode can be effectively observed in air at atmosphere pressure with liquid of conductivity as high as 0.1 S m^{-1} when the liquid has a low surface tension, but point out that there is no proof showing the absence of an upper limit to the conductivity.
Smith's findings on surface tension were disputed, however, and the authors state that liquids having surface tension as high as 0.073 N m^{-1} can be shown to take up the EHD mode at atmospheric pressure. A decrease in both flowrate and jet diameter with increasing conductivity was noticed in agreement with Smith.

These parametric studies guided the author in planning the experimental investigation and model set out in the Chapter 8. Chapter 8 closely follows the paper "A design method for the electrostatic atomization of liquid aerosols" by Ian G. Harpur, Adrian G. Bailey and Adel H. Hashish and published in Journal of Aerosol Science, Vol 27, No. 7, pp 987-996, 1996.

CHAPTER 8

A DESIGN METHOD FOR THE ELECTROSTATIC ATOMIZATION OF LIQUID AEROSOLS

Abstract A design method based on analysing and matching the physical time constants of the electrostatic atomization process in the cone-jet mode is presented. An algorithm is developed whereby the liquid properties are used as a basis for recommending a cannula diameter and a liquid flow rate such that a stable spray will result once appropriate electric field conditions are established. The algorithm also predicts the droplet diameter about which the aerosol is distributed. Experimental results are presented which confirm the design methodology. This chapter closely follows the paper "A design method for the electrostatic atomization of liquid aerosols" by Ian G. Harpur, Adrian G. Bailey and Adel H. Hashish and published in Journal of Aerosol Science, Vol 27, No. 7, pp 987-996, 1996. The experimental results are the author's work and the design method is based upon research carried out by the author.

8.1. Introduction

The first practical design data for a device to generate aerosol droplets electrostatically are described by Meesters *et al.* (1992). The device described, however, is designed to produce micron-sized drops and has a complicated electrode arrangement. Prior to or since then little or no attention has been paid to this topic despite the wide and varied number of applications to which aerosols generated in this manner can be used. These applications are far ranging and include drug delivery to the lungs (Hashish *et al.*, 1994), advanced manufacturing processes (Rulison and Flagan, 1992), applying thin films to surfaces (Zomeren *et al.*, 1994), as well as many others of basic and applied scientific interest.

The basic electrospraying device consists of a vertical cannula, usually of a conducting material, open to the atmosphere. Liquid to be atomized flows through the cannula, usually at a rate such that at zero applied electric field, the liquid drips from the end of the cannula at a critical drop weight which mainly depends on the liquid surface tension and density and on

the cannula outside diameter. A potential difference applied between the cannula and a counter electrode establishes an electric field which is dependent upon the applied voltage and the geometry of the cannula and counter electrode.

Perhaps, the simplest and certainly the most investigated geometry is where the counter electrode is a planar conductor held at earth potential and placed at a known distance from the cannula, normal to the cannula centre-line (Grace and Marijnissen, 1994). This geometry will be assumed here.

8.1.1 Cone-jet mode of electrostatic atomization

Many modes of operation whereby liquid atomization occurs are possible with the device described above. These modes are described by Bailey (1988) and Cloupeau and Prunet-Foch (1994), and are complicated functions of the applied voltage, the liquid flow rate, the cannula diameter and, most critically, the liquid's physical properties. The most studied mode is that which has been termed the "cone-jet" mode, and is one mode of operation under which the production of a regular spray pattern of charged, effectively monodispersed droplets is possible (Vonnegut and Neubauer, 1952; Fernandez de la Mora *et al.*, 1990). Monodispersity is, however, rather exceptional even in the cone-jet mode of electrostatic atomization and where it does occur small variations in the value of one of many parameters influencing the system leads to wider size distributions grouped around an average droplet size which may or may not be equal to the monodisperse diameter (Cloupeau and Prunet-Foch, 1989). Monodispersity is defined here as $\alpha < 0.1$, where α is the relative standard deviation in droplet radii about the mean value.

8.2 Aims of this Chapter

The aims of this chapter are centred on designing an electrostatic atomizing system that operates within the cone-jet mode. The design approach is such that either:

(i) Based on known, fixed, liquid properties as the input variables, the output gives the range of flow rate at which cone-jet atomization occurs and the average droplet radius which results when one particular flow rate is used and tentatively recommends an optimum cannula radius for stable operation, or

(ii) Based on the requirement to produce droplets of a given average radius, the output specifies required liquid properties and predicts a range of flow rates for stable spraying.

It is then a matter of establishing a sufficient electric field to bring about cone-jet atomization by applying voltage directly to the cannula which is situated a suitable distance from an earth plane. Grace and Marijnissen (1994) discuss the behaviour of the system in potential space.

8.3 Theoretical and empirical fundamentals

The cumulative research of many workers has allowed the following observations to be made (see Chapter 7):

(i) Production of monodisperse droplets occurs from the break-up of an electrically accelerated jet which extends from the apex of a conically-shaped meniscus. The conical shape is a resultant of the balance of the electrostatic, surface tension and hydrostatic forces acting on the liquid (Hayati *et al.,* 1989; Taylor, 1964).
(ii) Cone-jet formation is possible for liquids spanning an enormous range in electrical conductivity (Grace and Marijnissen, 1994).
(iii) The fastest growing disturbance on the jet, in the varicose mode, occurs at a wavelength which is relatively unaffected by the charge on the jet below a certain critical charge (Bailey, 1981; Melchor and Taylor, 1969; Mutoh *et al.,* 1979; Neukermans, 1973; Schneider *et al.,*1967; Taylor and Van Dyke, 1969) and may lead to uniformly sized drops. Above this level of charge break up is controlled by the growth of a laterally propagating wave which has the tendency to produce a polydispersed spray (Bailey, 1981; Taylor and Van Dyke, 1969) or alternatively the rim emission or multi-jet mode is onset whereby several spray sites are distributed at equal spacings around the rim of the cannula (Meesters, 1992). The rim mode is usually observed with liquids of low surface tension and at high field values, especially with low flow rates. The size distribution of the droplets is a complex function of the liquid's physical and electrical properties and the system parameters.

8.4 Characterising the system using time constants

The spraying system is characterized by the physical and electrical properties of the liquid - most importantly the electrical conductivity (σ), the relative permittivity (ε_r), the kinematic

viscosity (η) and the surface tension (γ) and by the parameters of the spraying system in the volumetric flow rate (F) and the cannula diameter (r_c). The output that we wish to design for is the droplet radius (r).

Pfeifer (1973) has characterized the spray system by considering three time constants: the dielectric or charge relaxation time, the viscous relaxation time and the flow characteristic time.

The **charge relaxation time**, τ_q, gives a measure of the time required for charge in a volume of liquid to exponentially decay to an equilibrium level.

The **viscous relaxation time** indicates the time it takes for a flowing liquid volume to relax so that velocity gradients are no longer temporally dependent. It is calculated as R^2/η, where R is a linear measure of the liquid volume. The viscous relaxation time of a liquid droplet of radius r is thus r^2/η and is labelled τ_η.

The **flow characteristic time** (or flow advection time), τ_f, is defined here as the time required for sufficient liquid to flow into the system to produce a defined volume, e.g., the conical meniscus or a liquid droplet.

The single most important parameter is the charge relaxation time of the liquid. As Pfeifer (1973) has stated, spray regimes based on the relative magnitudes of the charge relaxation time and the other key characteristic times can be identified from empirical evidence. By varying the parameters that determine the characteristic times, we can cause the system to operate within a particular regime and at desired values of one or more of the parameters (e.g. droplet radius and liquid flowrate). It is this principle that forms the basis of the design approach used here.

8.4.1 Regime 1, $\tau_q >> \tau_\eta$

With poorly conducting liquids, where $\sigma < 10^{-11}$ Sm^{-1} and τ_q is of the order of seconds, (e.g. long chain hydrocarbons, toluene, benzene, liquid hydrogen, etc.) dispersion into droplets is relatively difficult and indeed spraying due to charge conduction mechanisms may not occur at all. Direct charge injection into the liquid can alter τ_q, so that spraying becomes possible, with τ_q now being determined by the mobility of the injected charge.

8.4.2 Regime 2, $\tau_q \approx \tau_\eta$

In this case, dispersion into droplets is possible with conduction mechanisms providing the charge carriers. The forces dominating droplet formation depend strongly on the flow characteristic times. In the case where $\tau_q << \tau_f$, the formation of fine droplets occurs much as

in Regime 3 described below and the formation mechanism is strongly dependent on electrostatic forces. In the case where $\tau_q >> \tau_f$, the droplet size increases until the droplet formation mechanism is dominated by gravitational and surface tension effects. For $\tau_q \approx \tau_\eta$ a stable cone-jet is formed at a sufficiently high cannula potential. Droplet formation is by varicose instability break-up of the jet as recently reported by Tang and Gomez (1994).

8.4.3 Regime 3, $\tau_q << \tau_\eta$

As established by Smith (1986), very fine dispersions can occur for highly conducting fluids. Spraying occurs from one or more definite locales on the surface of the meniscus depending on the applied voltage, the flowrate and the surface tension of the liquid. For $\tau_q << \tau_f$, the cannula becomes "starved" of liquid and the meniscus retreats into the cannula, which may result in the rim mode of spraying. As flow rate increases, a Taylor cone-like meniscus forms and droplet ejection appears to occur from the cone apex (Fernandez de la Mora, 1992). Further increase in flow rate sees the development of a jet of liquid protruding from the cone apex but in this regime, the stability of the cone-jet formation cannot be guaranteed due to the short charge relaxation time of the liquid.

In considering the above regimes, it is important to consider the influence that the cannula radius has on determining the balance of forces acting on the stressed meniscus. In fact, Pfeifer's regimes are based on the time characteristics of the meniscus rather than the droplet but in the following section an approach is outlined whereby a cannula radius for a particular set of input parameters is recommended. This approach is justified by the argument that the cannula radius promotes spray stability, and the above regimes are considered in light of this radius (Hayati et al, 1989).
Empirical evidence suggests that for dispersion into fine droplets

$$\tau_q \approx \tau_\eta \quad \text{and} \quad \frac{\tau_q}{10} \leq \tau_f \leq 10\tau_q .$$

8.5 Determining the cannula radius

Based on the experimentally determined current and cone-jet profile, Hayati *et al.* (1989) were able to determine the electrical forces acting during a stable cone-jet atomization. The result of that work of import here is the observed, experimentally calculated, ratio of electrical normal force to electrical shear force at the cone surface. This ratio was determined for different flow rates and applied cannula potentials to lie in the range of 4-10 for a stable jet

produced from a cannula of radius 0.9 mm with liquid conductivity of 1.4×10^{-6} S m^{-1}. Similar results were obtained for liquids of different conductivities but it is not stated over what range the liquid conductivity was varied. The value of this ratio is a function of the area of the cone surface, which is in turn determined by the radius of the cannula for any given cone angle.

To generalize these findings so as to develop a method for recommending a particular cannula radius which will enable a given liquid to spray in the cone-jet mode a number of assumptions must be made to scale the experimental data from the original study. Thus, a scaling law for the liquid atomization current and the cone-jet profile must be found. The normal electric field at the conical surface must also be assumed. By making some assumptions for these parameters, a graph has been produced of cannula radius versus charge relaxation time for high and low viscosity liquids (see Fig. 8.1). The low viscosity curve is for liquids of *ca* 1 mPa s; the high viscosity case is for liquids of two orders of magnitude greater viscosity. It is not recommended to extrapolate the curves outside the charge relaxation times shown but the general trend does show that for very conducting liquids of low viscosity very tiny cannulas need to be used at vanishingly small liquid flow rates, in agreement with results reported for spraying water for example.

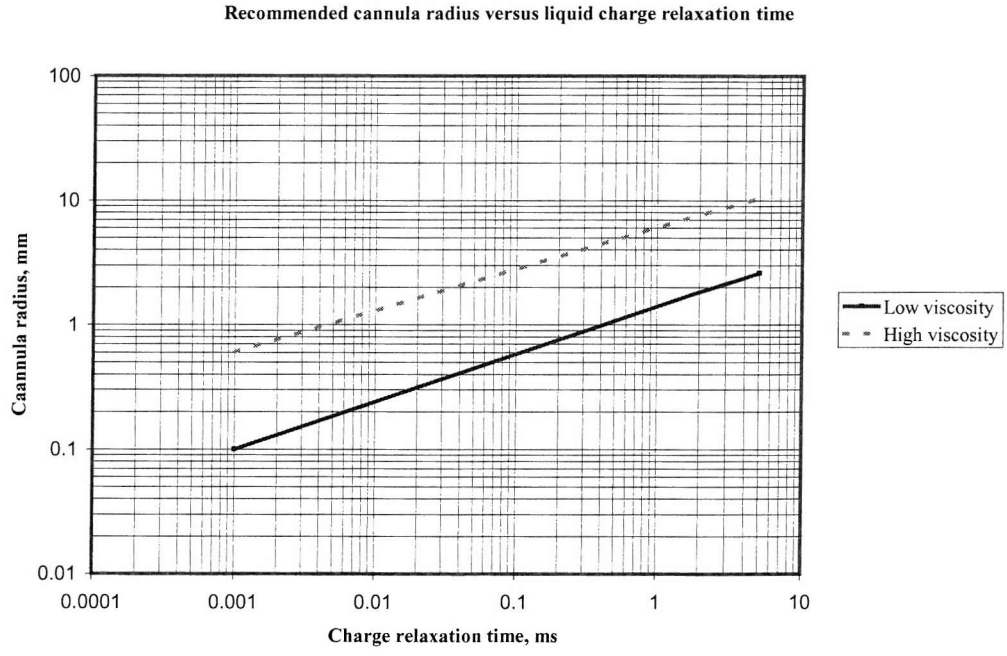

Figure 8.1 Cannula radius for spraying in stable cone-jet mode.

8.6 The design algorithm

The assumptions made to produce Figure 8.1 are that each droplet of radius deduced from the algorithm outlined below will carry a charge close to half the Rayleigh limit at the mid-range flow rate (see Section 6.2.3). By continuity, this fixes the current flowing in the conical region. We fix a cone half-angle of 40^0 (see Section 6.2.2, on the Taylor cone which has semi-vertex angle 49.3^0, after the onset of the cone-jet mode, this angle is reduced) and, following the Hayati *et al.* findings, a constant 3 MVm^{-1} for the normal electric field on the cone surface is assumed. Figure 8.1 is only intended as a guideline in selecting a cannula radius. There are other factors influencing the stability of the cone-jet from a particular cannula including liquid surface tension, viscosity, flow rate and applied voltage. Nonetheless, by combining the ideas outlined in Section 8.4, an algorithm can be assembled which takes the liquid properties as its input variables and outputs a droplet radius and range of flow rates which can be achieved when working with a cannula of a radius based on the considerations outlined in Section 8.5.

The appendix at the end of this Chapter lists the equations to use. The charge relaxation time is determined from equation (7.Al) and r, the droplet radius formed at the liquid volumetric flow rate F_m, determined from equation (7.A3). F_m is in turn determined from equation (7.A5). Finally, the range of stable flow rates is found from equation (7.A6).

8.7 Results

8.7.l. Comparison of predictions with published results on cone-jet atomization

Although we are concerned with producing a method whereby a laboratory-scale electrostatic atomization device can be designed with specified performance, the logic contained in the method can be tested against published results to assess the validity of the approach. There is a variety of results in the literature relating to the size of droplets produced at particular liquid flow rates but only a few give full details of the electrical and physical properties or have used liquids in a reasonably pure state whereby literature values for these properties can be confidently used.

Despite this, some suitable results do exist and the most intriguing of these doubtlessly pertain to cases where the production of droplets from the jet break up is reported to be

monodisperse. Cloupeau and Prunet-Foch (1989) used laser photometry to measure a spray of water doped with 0.5 % surfactant and found about 99.8 % of the volume of liquid sprayed was contained in droplets of diameter 0.94 to 1.1 μm. The flow rate was 1×10^{-3} m^3 s^{-1}. The properties of the water were reported as $\sigma = 1.5 \times 10^{-3}$ Sm^{-1}, $\eta = 1 \times 10^{-6}$ $m^2 s^{-1}$, the surface tension was unreported even though a surfactant had been used. Although not stated explicitly, it is likely that the smallest of the cannulas discussed in the paper was used for this atomization. This had an outside diameter of 0.12 mm. Predictions from time constant matching are for the droplet diameter to be approximately 1.4 μm and for F to lie between 3×10^{-13} $m^3 s^{-1}$ and 3×10^{-11} $m^3 s^{-1}$. The predicted diameter for the droplets is thus about 30% greater than the top of the measured range and the flow rate is within the predicted range. Tang and Gomez (1994) and Gomez (1993) have produced extensive results on the atomization of heptane doped with an anti-static additive to decrease its charge relaxation time. The liquid properties were quoted as $\sigma = 1.15 \times 10^{-6}$ Sm^{-1}, $\gamma = 18.1 \times 10^{-3}$ Nm^{-1}, $\varepsilon_r = 1.83$ and $\mu = 0.61 \times 10^{-3}$ Pa s. The density of heptane is approximately 700 kg m-3 so that $\eta = 8.71 \times 10^{-7}$ $m^2 s^{-1}$. With these figures, a spray droplet diameter of 7.0 μm is predicted at a flow rate within the range 1.28×10^{-12} to 1.28×10^{-10} $m^3 s^{-1}$. Gomez (1993) reports a monodisperse diameter of 4.7 μm at a flow rate of 7×10^{-11} $m^3 s^{-1}$ from a cannula of 0.45 mm outside diameter. The predicted diameter is approximately 1.5 times larger than the experimentally measured droplet diameter. The deviation can perhaps be assigned to the behaviour of the anti-static additive (Stadis 450, Du Pont). Its performance under non-steady-state conditions is known to be different from its static performance (private communication with distributor in U.K.), which would alter the conductivity of the liquid. The flow rate is again within the range expected.

8.7.2 Experimental technique

Figure 8.2 shows the experimental arrangement used to generate data to test the design approach. Liquid flow was produced using a motorized dispensing system comprising a low voltage motor, 3000:1 ratio gear head, micrometer drive and syringe. With this arrangement it was possible to produce very low flow rates and measure the volume of liquid dispensed. From calibration data, the percentage error in flow rate was estimated to be within $\pm$ 5%. A high-tension supply (Brandenburg Alpha Series II) was used to establish a high potential on the cannula with an aluminium plate of dimensions 20 x 15 cm earthed through an electrometer (Keithley Model 602, not shown) serving as the counter electrode. The electrometer current during steady spraying provided a means of monitoring the charge level on the droplets.

Each droplet size measurement was taken between six and eight times using a Malvern Laser Particle Sizer (model 2600). A stereo microscope with a 4 : 1 objective magnification and a 10 : 1 eyepiece magnification and light source provided means of viewing the cannula and cone-jet during spraying.

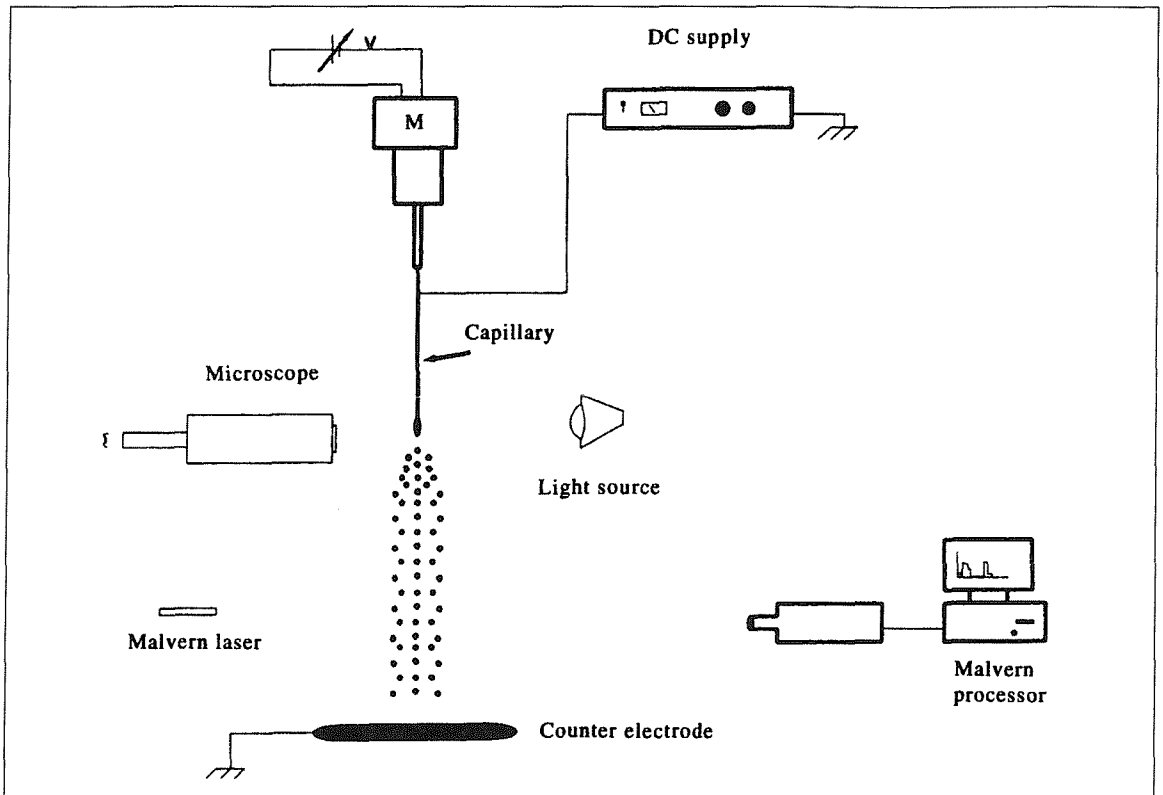

Figure 8.2 The Experimental arrangement for atomizing liquids and measuring droplet size

Off-line measurements of liquid properties were performed at 25^0 C. Surface tension was measured to $\pm$ 0.2% using a torsion balance (type OS supplied by White Electrical Instrument Co. Ltd). Liquid viscosity was determined using the Ostwald method in which the time taken for a fixed volume of liquid to fall through a cannula under a variable pressure head was measured. The time, t_1 is a function of the kinematic viscosity of the liquid and the dimensions of the viscometer. The kinematic viscosity of the liquid was obtained relative to that of a reference liquid such as distilled water (q_2, t_2) so that

$$\eta_1 = \eta_2 t_1 / t_2$$

Based on repeated measurements, the error in this measurement was determined to be $\pm$ 4%. For liquids of higher viscosity (greater than about 10 mPa s), a viscometer supplied by Viscometers Ltd, U.K. (type LV-8) was used, with associated accuracy of $\pm$ 5%. Liquid density was measured at 25^0 C using a 10 ml flask weighed to 4 decimal places (to $\pm$ 1 %).

The electrical conductivities of the more conducting liquids were determined using a conductivity cell having two platinum electrodes and an ac bridge operated at 1 kHz. The bridge had an accuracy of $\pm$ 2% over the range encountered. The cell constant is given to two significant figures and so does not effect the overall accuracy of the method. For liquids of lower conductivity, an instrument supplied by Wolfson Electrostatics Advisory Unit, University of Southampton, was used. The instrument was calibrated in units of conductivity and had a dynamic range of 10^{-2} to 10^{-12} S m^{-1}, though in our work we restricted its use to liquids of conductivity 10^{-6} S m^{-1} and lower. Within this range the accuracy is about $\pm$ 5 %. Literature values of permittivity were used.

8.7.3. Experimental results

Test example one. Spray tests were conducted with ethyl acetate having the following properties: conductivity 1.3 x 10^{-7} S m^{-1}, kinematic viscosity 5.3 x 10^{-7} m^2 s^{-1} relative dielectric constant 6 and surface tension 27 mN m^{-1}. Thus, τ_q = 0.4 ms.
With these values as input variables to the algorithm, a droplet diameter of 30 μm is predicted assuming that the viscous relaxation time matches the charge relaxation time. At an appropriate field strength, the flow rate about which the establishment of a cone-jet should be possible from a cannula of diameter 0.65 mm is 3.4 x 10^{-11} m^3 s^{-1}. A flow rate in the range of 0.1-10 times this value can be chosen to give stable cone-jet operation.
Ethyl acetate was fed to a cannula of 0.55 mm outside diameter at a flow rate of 3.3 x 10^{-11} m^3 s^{-1}. The counter electrode was set at 40 mm from the end of the cannula. At a cannula voltage of + 4.1 kV, a stable spray resulted. The droplets produced were measured using the Malvern laser system and the volume mean diameter (D4,3) was determined to be 27 μm. The histogram in Fig. 8.3 shows the volume of the spray contained in each band of width 1 μm for band size in the range of 17-36 gm. 99.4% of the spray was contained in this diameter range and the standard deviation was 9 μm. The relative standard deviation is therefore 0.33, not meeting the monodispersity criteria but the expected diameter is within one standard deviation of the measured average diameter. The fine scale of the abscissa used in Fig. 3 emphasises the difference between the predicted and experimental data.
Test example two. Benzyl alcohol was used in a further series of tests. The sample used had the following properties: conductivity 1.05 x 10^{-5} S m^{-1}, kinematic viscosity 5.2 x 10^{-6} m^2 s^{-1}, density 1061 kg m^{-3} and surface tension 0.042 Nm^{-1}. The relative permittivity of benzyl alcohol is listed in International Critical Tables as 13.

Proceeding as before we find τ_q, = 1.1 x 10^{-5} s. From the simulation results, the droplet diameter we expect from cone-jet atomization is 15 μm at a flow rate in the range 1.64 x 10^{-9} - 1.64 x 10^{-11} m^3 s^{-1} from a cannula of outside diameter 0.3 mm. Figure 4 shows the result of the size measurements made on a spray of this liquid fed to a cannula of diameter 0.3 mm at a flow rate of 3.5 x 10^{-10} m^3 s^{-1}.

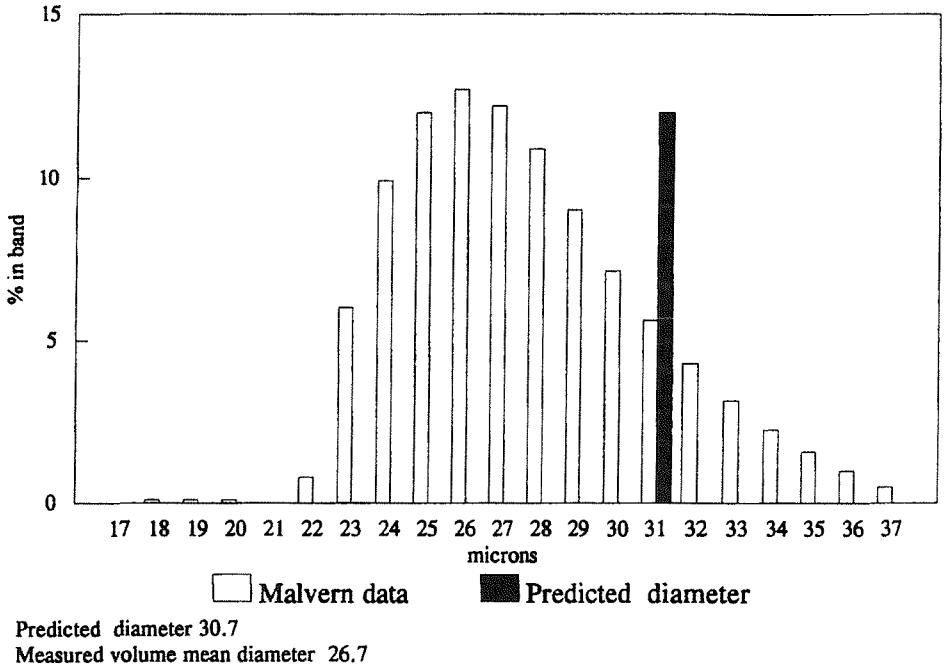

Figure 8.3 The droplet size distribution for electrostatically sprayed ethyl acetate

The counter electrode was situated 30 mm below the tip of the cannula and a voltage of 4.4 kV was applied to the cannula. As can be seen, a practically mono-disperse spray resulted. The volume mean diameter was 14.8 μm with a standard deviation of 1.4 μm.

Test example three. To assess the effect of viscosity on spraying, tests were conducted with glycerol. A slight trace of hydrochloric acid was added to pure glycerol to increase its conductivity to 9.3 x 10^{-5} S m^{-1}. It was fed at a flow rate of 7.8 x 10^{-9} m^3 s^{-1} through a cannula of outside diameter 1.1 mm which was situated 70 mm from the earthed plate. At a voltage of 5.9 kV, measurement of the resulting stable spray produced the data shown in Fig. 8.5. As can be seen a broad distribution having a long "tail" towards large droplet sizes resulted.

The measured values of 3.1 x 10^{-4} m^2 s^{-1} for viscosity, 0.063 N m for surface tension combined with the above value of the conductivity when used as before, predict a diameter of 39 μm for a flow rate to be in the range 2.78 x 10^{-9} m^3 s^{-1} - 2.78 x 10^{-7} m^3 s^{-1}. The recommended cannula diameter is 0.7 mm but the cone-jet was stable at the larger diameter of 1.1 mm.

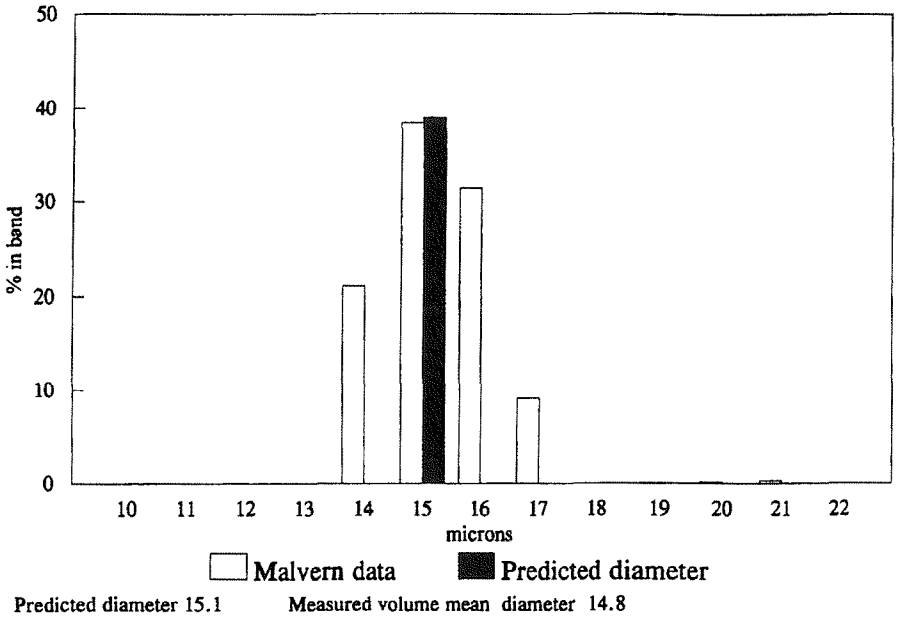

Figure 8.4 The droplet size distribution of electrostatically sprayed benzyl alcohol

The results of the size measurements show a polydisperse spray of droplets grouped around a volume mean diameter of 45.3 μm, 1.15 times the expected diameter, with a standard deviation of 13.8 μm, $\alpha = 0.3$. The expected diameter and measured average diameter lie within one standard deviation. The greater spread in the data is a result perhaps of a true lack of stability in the cone-jet because of the larger cannula size used.

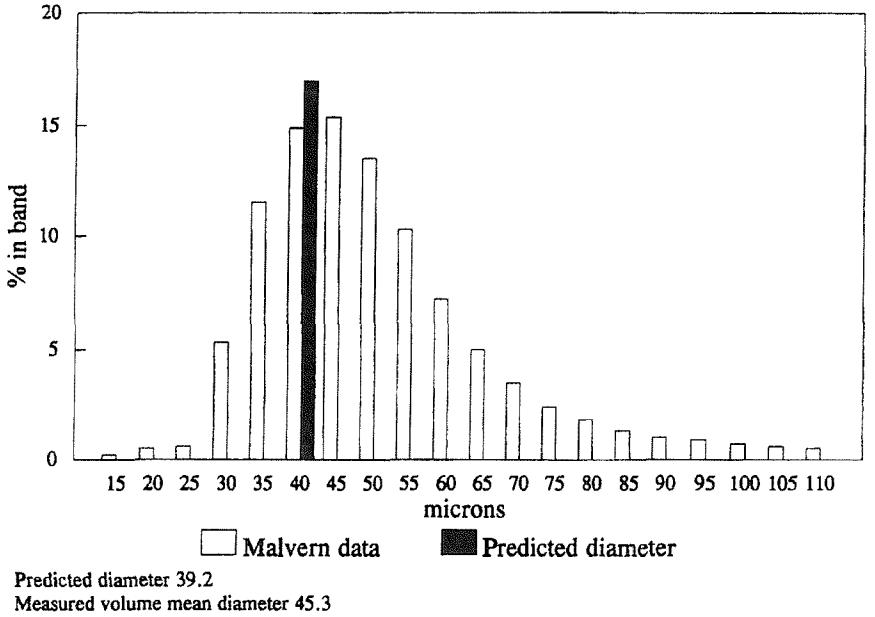

Figure 8.4 The droplet size distribution of electrostatically sprayed glycerol doped with HCl.

8.8 Conclusions

In this chapter, a design method allowing the key parameters to be set and the expected droplet size to be predicted for an electrostatic atomization device operating in the stable cone-jet mode is presented. Analysis of the hydrodynamic and electrostatic forces is simplified by contracting the terms into characteristic times describing the liquid and flow system which are then matched to ensure stable behaviour of the spray system. Stability is only ensured if the cannula, at the end of which the liquid meniscus is acted on by the electrostatic field, is of a diameter such that the electric field penetration into the meniscus, which ultimately leads to reduction of the flow into a thin jet, is sufficient. A particular diameter is recommended which guides this selection.

Results which confirm the design methodology are presented which indicate that, based on the electrical and physical properties of the liquid of interest, a straightforward device can be designed which will ensure, within one standard deviation, that the liquid can be atomized into droplets of a predicted diameter over a pre-determined range of flow rates purely by electrostatic forces. Alternately, the liquid properties can be pre-selected to ensure droplets of a particular diameter will result from a stable electrostatic atomizer.

The method described here of designing an electrospraying system to give a particular predictable output is unique in this field of science. The approach is entirely based on the author's research and is validated experimentally and by comparison with published data. It represents a contribution to knowledge in this area as it will allow others to design electrospraying systems with greater certainty.

Appendix to Chapter 8: List of equations

The charge relaxation time is calculated from

$$\tau = \frac{\varepsilon_0 \varepsilon_r}{\sigma} \tag{8.A1}$$

The radii of droplets most likely to form are those for which the viscous relaxation time:

$$\tau_\eta = \frac{r^2}{\eta} \tag{8.A2}$$

is of the same order as the electric relaxation time. Thus,

$$r = (\tau_q \eta)^{0.5} \tag{8.A3}$$

Formation of droplets which are most likely to be of this size will occur when the flow characteristic time:

$$\tau_f = \frac{\frac{4}{3}\pi r^3}{F} \tag{8.A4}$$

is also of the same order as the charge relaxation time. The flow rate at the middle of a stable range of flow rates is thus,

$$F_m = \frac{\frac{4}{3}\pi r^3}{\tau_q} \tag{8.A5}$$

and the flow rate lies within:

$$\frac{F_m}{10} \le F \le 10 F_m \tag{8.A6}$$

PART IV

STUDY THREE: ELECTROSTATIC COALESCENCE FOR DEWATERING WATER-IN-OIL EMULSIONS

CHAPTER 9

ELECTROSTATIC DESTABILISATION OF EMULSIONS

9.1 Abstract

In this Chapter, the background to the final study of this thesis is set out. Firstly, the rationale behind the research is given along with some history of work in the University of Southampton involving collaboration between the Mechanical and Electrical Engineering Departments. The process of breaking or separating oil from and w/o emulsion is known as "dewatering" in the crude oil industry. The chapter concludes with a literature review of research is this area effectively providing the background to the experimental results and analyses of Chapters 11 and 12. The key novelty associated with this area of research is the study of electrostatically induced coalescence of a water-in-oil emulsion in a state of laminar or turbulent flow.

9.2 Water-in-crude oil emulsions

9.2.1 A brief history of petroleum and dewatering

In ancient times, the oil used to burn in lamps for illumination was derived from plant and animal sources. Through the long eons of geological time, the oil-rich tiny animals that live in the shallow seas of the earth have sometimes, in dying, escaped being eaten but mingled with the mud on the floor of the sea and were buried under subsequent sedimentary layers. After slow chemical change, the oil was converted to a complex mixture of hydrocarbons and is now properly called petroleum (from the Latin, *petra* meaning stone and *oleum* oil). Such is its importance to humanity over the last number of generations that the simple word *oil* has come to mean nothing else to the general populace. It is reported that the great Russian

chemist, Dmitri Ivanovich Mendeleyev, when told of the vast array of chemicals within crude oil, was horrified to think it should be burned for fuel!

Oil is sometimes found on the surface of the earth, particularly in the oil-rich Middle East. It was the *pitch* that Noah was instructed to smear on his ark inside and out to keep it waterproof. In the same way, when Moses was set afloat as a baby in his "ark of bulrushes", it too was daubed with pitch to keep it afloat. Lighter fractions of the oil (*naphta*) were sometimes collected and used in lamps or for flames used in connection with religious rites (Asimov, p427).

In the 1850s, the demand for oil for illumination increased due to the growing populations in towns and cities, a key shift in demographics brought about by the Industrial Revolution. The chief sources at the time were whale oil, coal oil (obtained by heating coal in the absence of air) and *kerosene.* Kerosene is produced by heating shale, a soft waxy material that was found, most famously, in western Pennsylvania, USA. An American railway conductor, Edwin Laurentine Drake, decided to try something new. He knew that people sunk wells for water and even deeper wells to get brine for salt extraction. Sometimes, an inflammable oily liquid came up with the brine and there were reports that this oil had been used in China and Burma two millennia previously as a source of fuel to evaporate off the water and leave the salt behind. Drake decided to try to dig a well to find this oil, seeing the opportunity to market it for either fuel or medicinal purposes. On 28 August 1859, he dug a 69-foot well near Titusville in western Pennsylvania and "struck oil".

Thus, we see that water, oil and salt are intrinsically related. The oil wells of Pennsylvania were quickly used up but much larger fields were of course discovered in Texas and California early in the twentieth century, then still larger ones in the Middle East in the middle of the twentieth century.

The co-production of formation water or as a water-in-oil emulsion from oil wells in California in the early part of last century was an enormous obstacle to commercial exploitation of the reservoirs. Dr. Frederick G. Cottrell in a stroke of insight from working on the precipitation of solids from flue gases using intense electrostatic fields, proposed that the emulsion could be broken by the application of an intense electrostatic field across it. The first commercial electrostatic treater was installed in 1909 at the Lucille Oil Company at Coalinga, California. In 1911, pioneering patents (US 987114/5/6/7) on the subject were granted. (Williams, p2 Chapter 1).

Williams (1989), describes how the theoretical and industrial aspects of the technique were developed for example in 1935 the technique was extended to facilitate the removal of sediment and corrosion-causing inorganic contaminants from crude (desalting) and also the extensions in 1950 to remove organic impurities from petroleum distillates.

9.2.2 Recent history of dewatering and the stimulus for this research

The early electrostatic "treaters" were little more than large settling tanks within which electrodes were variously placed to effect a reasonable strong constant electric field across the w/o emulsion (Cottrell, F.G. and Speed, J. B., 1911, US Patent 987115). The separated phases were allowed to settle under gravity. Little has changed in the commercial world since then apart from designs to improve the internal flow and electric fields. Thus, a large inventory is held up, as residence times are necessarily large. Capital cost is also large and as one of the phases is inflammable, from a hazard and operability analysis point of view, in such large volume, represents a safety risk that should be minimised. In the case where treatment occurs offshore, such large vessels (of the order of 10^2 m^3) often serve the purpose of primary gaseous phase separators but nonetheless are inefficient in the use of expensive space. These vessels are relatively inflexible when it comes to accepting inputs of varying water-cut (Gramme, Per Eivind, Developments in Production Separation Systems, London, 4/5 March 1993).

When a new oil reservoir is discovered, it usually possesses the natural pressure to move the oil to the production wells by expansion of volatile components (Ling et al, 1981). This phase of oil recovery is called the primary phase. When the natural pressure decreases, it is necessary to increase the pressure by injection of water. This secondary oil recovery phase or water-flooding phase is stopped when the production costs become significant to the value of the produced oil, however water content, or "water cut" as it is termed, can commonly reach 80% by volume before production ceases and indeed higher cuts can still be economical (Wayth, p1). In fact, the value of the produced oil is often determined by the efficiency with which the oil can be separated from the water. The total recovery of the oil by the primary and secondary phases of production is usually less than 40% of the original oil in place in the reservoir. The remaining oil is the target for enhanced or tertiary recovery. There are several techniques for tertiary recovery and they include: surfactant-polymer flooding, CO_2 flooding, caustic solution flooding, steam injection and thermal combustion. As can be imagined, the use of secondary and tertiary recovery methods often results in the production of mixtures having very high water cut, increasing the need for efficient de-watering technology.

In a keynote address on Developments in Production Separation Systems (London, 1993), Per Eivind Gramme (Norsk Hydro Research Centre), laid down the challenges ahead for sustained recovery of oil for the future. Although seven years old, the points raised are still relevant today and most relate to the problems associated with water. With few exceptions,

production separation systems have been based on gravity separation with limited successful deployment of cyclonic separators. Hence, there is still a great dependency on production chemicals such as demulsifiers and anti-foaming agents to attain the necessary separation. The challenges facing oil production for the future were summarised as

- to maximise utilisation of existing infrastructure
- to design solutions that enable longer transport of well streams from the well to the production site or vessel
- to be able to process and separate water at cooler temperatures
- to implement more flexible process solutions to petroleum transport and handling (to react to changing oil/water conditions)
- to deploy lightweight process solutions
- to deal with the production and processing of higher water cuts
- to lower chemical use
- to react positively to tighter environmental regulations.

9.2.2.1 Efficient and early removal of water - environmental and economic imperative

The rheology of oil/water systems (to be discussed later) is often a major problem associated with the transport of the well stream through long pipelines. As water cut increases to the point of inversion (of a w/o emulsion) the viscosity increases which can result in a limit to the production from lower pressure wells and lowers the efficiency of heat exchangers used to preheat the well-stream prior to separation.
Hydrates can precipitate out during shutdowns causing scaling on process equipment internals and the use of hydrate inhibitors, which is costly due to the large volume of water to be treated, has side effects such as increasing aromatic and phenolic content of the eventually separated water. The rate of process equipment and pipeline corrosion is strongly dependent on the water content and its associated salinity. Salinity can also poison refinery catalysts and a premium on low salinity crudes is now common (Grover ,1996, Wayth, 1999).
Dewatering on its own is often insufficient to adequately desalinate the crude and additional washing with fresh water (or sea water for extremely saline oil) is required with subsequent additional dewatering.
Further imperatives for reducing the water downstream of the production vessel are the marginal increase in cost of transporting the produced stream due to the volume of water within it to be transported and because of the higher viscosity of a w/o emulsion alluded to earlier.

9.2.2.2 Compact Rapid Throughflow Equipment can meet the Challenge

There are of course myriad practical problems associated with the maximization of recovery of oil from a complex three phase flow such as interfacial detection for standard separators, control of continuous phase peak flows (slugs) and dealing with the time varying properties of the flow. Nonetheless, the development of lightweight rapid throughflow equipment is a seriously viable approach to this goal (Loken et al Statoil report).
As part of this multi-disciplined development, a compact electrostatic coalescence device, which can rapidly aid the separation of turbulently flowing w/o emulsions, is a highly desirable technological breakthrough.

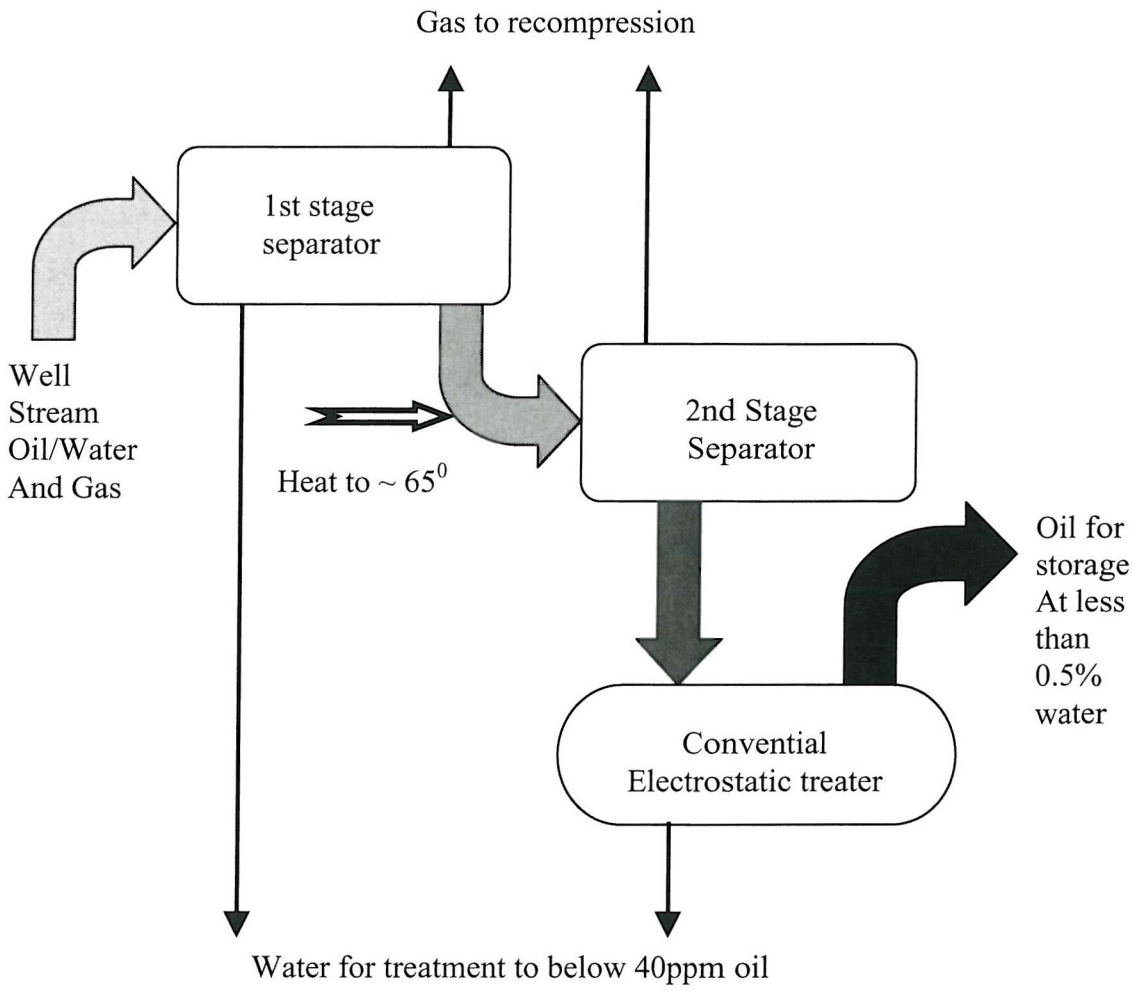

Figure 9.1 Conventional Oil Separation Process Scheme based on Loken and Gramme (1996)

Figure 9.1 shows a typical layout for process equipment with all the disadvantages referred to above. A future process for treating well stream oil could involve combinations of degassers, a rapid throughflow compact electrocoalescer as well as various hydrocyclonic devices (as shown in Figure 9.2).

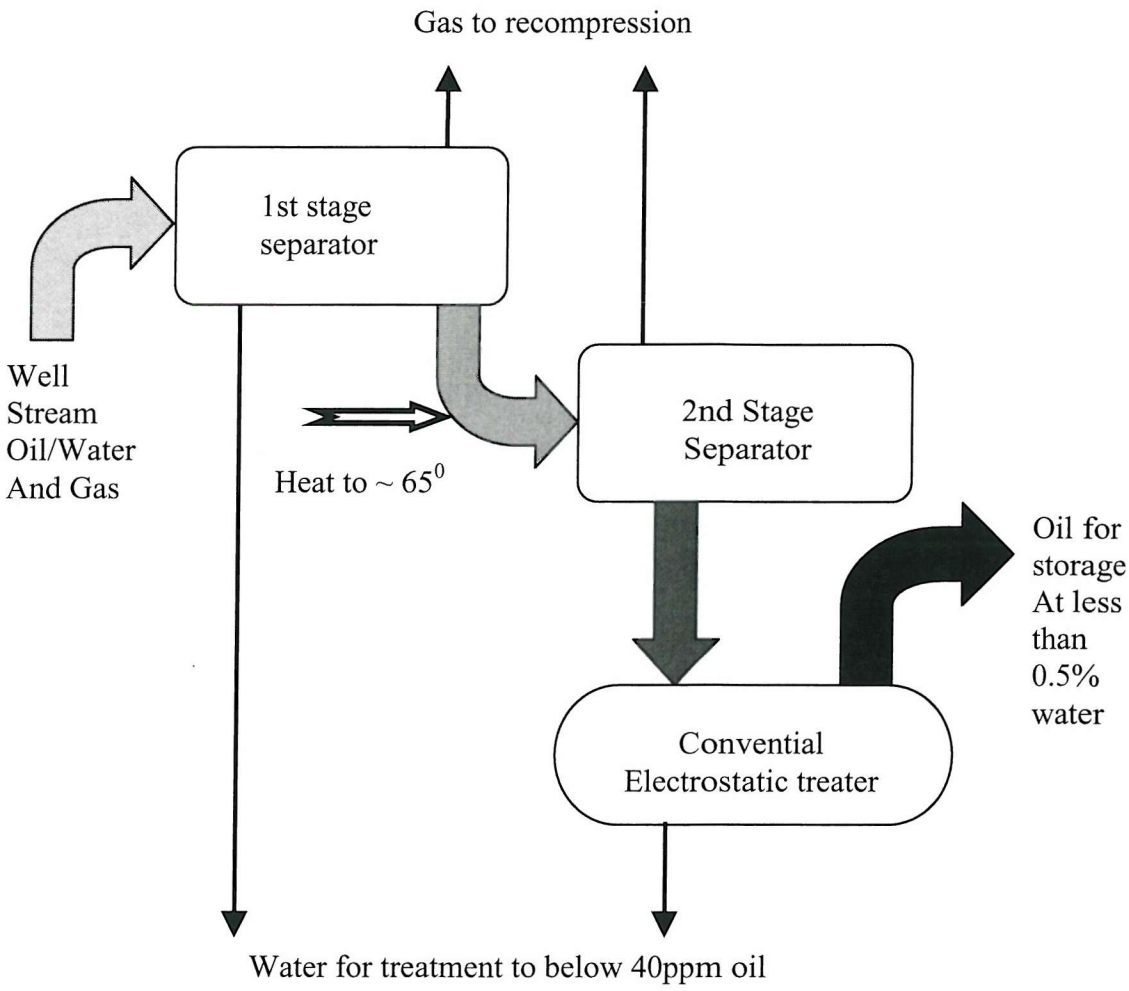

Figure 9.2 Future Oil Separation Process Scheme based on Loken (1996) and Cowie (1995)

The flexibility of such a set-up, coupled with the low inventory compared to the conventional approach as well as the capability to lower treatment chemical amounts make it an attractive proposition. This study, which was co-sponsored by Statoil and BP, concentrated on taking the work to develop a compact electrocoalescer forward.

9.3 Research at Southampton University

Wayth (1999) gives a review of the research carried out in the last three decades in the Engineering Faculty at Southampton into separation devices for dewatering and deoiling emulsions, chiefly for application within the oil industry. The author was fortunate to benefit from this background and worked with Wayth in extending the understanding on rapid throughflow coalescence.
The Department of Mechanical Engineering has been strongly involved in the development of the first deoiling hydrocyclone and continues to be active in this field and in developments of dewatering cyclonic devices. The Department of Electrical Engineering has been active over many years in the research and design of the technology of electrostatic treaters. Funded work jointly undertaken between the departments commenced in 1989 and concentrated on the early development of a compact, rapid throughflow electrostatic treater for w/o emulsions. The intent was to develop sufficient understanding of the technological elements of cyclonic and electrostatic devices for treating w/o emulsions. The guiding vision was to deploy this knowledge to aid the commercial development of an integrated rapid treatment process applicable to the oil industry.

A brief synopsis is given here but for a fuller review please refer to the cited references.

9.3.1 Early Southampton Investigations into Electrostatic Dehydration

Williams and Bailey, working under sponsorship from Plenty Bescon Ltd. and the Department of Energy utilised a number of advanced experimental techniques including turbidimetry and a **Malvern Laser Diffraction Particle and Droplet Sizer** in studies of the performance of conventional electrostatic treaters.
Emulsion resolution times (1983) and changes in water droplet distribution (1984) under the application of an electric field were reported on.

9.3.2 Treatment of Water Offshore (TWO) Phase 1

The TWO programme was managed by the Institute of Offshore Engineering, part of Heriot-Watt University, under the sponsorship from the Marine Technology Directorate (MTD) along with support from various offshore operators including Statoil, Elf and Chevron. During the period covering April 1989 to October 1990, the departments of Mechanical and Electrical Engineering became a joint partner to the TWO initiative effectively marrying the deoiling (Thew, 1986 and Colman, 1981) and more latterly dewatering (Sinker, 1995) hydrocyclonic know-how of the former department with the electrostatic treatment know-how of the latter.

Although Phase 1 of the TWO programme was primarily a paper based study on the merits of sequential layouts of electrostatic treaters and hydrocyclones for dewatering, it was during this period that concept for a *compact electrostatic coalescer* (termed a ***CEC*** by Wayth) devices was first investigated at the University. A short investigation was undertaken as a proof-of-concept type study. This utilised a non-optimal electrocoalescer and hydrocyclone sequence (Williams, 1991).

9.3.3 Treatment of Water Offshore (TWO) Phase 2

Between November 1990 and July 1993, a decent sized laboratory rig was designed and constructed. Of modular construction and rectangular cross-section, the rig was designed to allow investigations to be carried out on the effects of an applied electric field on a flowing w/o emulsion. The duct consisted of eight acrylic modules of rectangular cross section of internal dimensions 100 x 20 mm. Seven of these sections had insulated electrodes capable of being independently excited or grounded, depending on the experimenters intent. Acrylic material was chosen for two reasons: its transparency and because of its availability within the department. Despite its known mechanical deficiencies of its material of construction, the rig allowed for studies under laminar or turbulent flow conditions. A variety of inlet droplet sizes were possible by varying the pressure drop across an inlet ball valve and experiments with different water cuts could easily be undertaken.

To simulate water in crude oil emulsions, kerosene as the oil phase had been used in the Phase 1 studies and its use was initially continued here. Unfortunately, kerosene can be synthesized readily by certain bacteria and even with the subsequent use of a biocide to control contamination, latter studies were conducted using gas oil (Williams et al, 1992).

9.3.4 Direct Sponsored work for Statoil

From circa September 1993 to March 1994, work continued using the rectangular duct as the chief experimental vehicle. This work was directly sponsored by Statoil who directed that higher water cuts of up to 30% should be investigated. The intent here was to simulate the stability of the crude oil emulsions found in the Norwegian Statfjord wells and a chemical surfactant was used to stabilise the water-in-gas oil experimental emulsion so its stability modelled the crude. In addition, the rig was modified to allow air injection into the emulsion flow to study the effect of a co-flowing gaseous phase on water droplet coalescence. To further model real crude oil emulsion systems and help assure laboratory findings could be extended with confidence to real systems, experiments where salt was added to the aqueous phase were also carried out (Williams et al, 1994, Urdahl, 1995).

9.3.5 Recent Work

From April 1995 until April 1999, work was carried forward within the University. A further research contract was signed with Statoil for which funding for a full-time research assistant was provided, a role the author filled until October 1996. A doctoral student, Wayth, also began work at this juncture under a BP Exploration sponsored CASE studentship and the author and Wayth largely worked together in gathering the experimental data presented in Chapter 11. Tests were proposed at higher flow rates (up to 100 l min^{-1}) than had been previously studied (Williams et al, 1995, present results at 60 l min^{-1}).

The objective of the work was to investigate the critical parameters governing water droplet growth in a flowing w/o emulsion in order that design and development work on a commercial CEC could be taken forward. To these ends, Kvaerner Process Systems Inc. (KPSI) were appointed as an enterprise partner to develop and build commercial versions of the hardware which could be deployed at oil processing sites. The results presented in Chapter 12 cover extensive experimental work carried out by the author working with Wayth using the rectangular experimental duct. Investigations into the rate of water droplet growth were carried out by studying this growth as a function of emulsion flowrate, water cut, water salinity, emulsion temperature, emulsion stability and initial inlet water droplet size distribution.

A patent, US6136174, entitled "Compact electrostatic coalescer" was recently granted to Kvaerner Process Systems, Alberta, Canada and Den Norske Stats Olejeselskap A.S., Thondheim, Norway sponsors of this work along with Statoil. Inventors named include Berry, Mulvey, Bailey, Thew, Williams, Wayth and Urdahl.

CHAPTER 10

EMULSION SCIENCE

10.1 Introduction to Emulsion Science

As emulsions are the most complicated of the dispersed systems investigated in this thesis, the aim of this chapter is to review the science and technology of emulsions in general and water in oil emulsions in particular before advancing to the results and analysis presented in Chapter 11.

The chapter begins with an overview of the physics of the liquid condensed phase before moving on to discuss two and three phase mixtures of liquids. The rheological, electrical and other key properties of emulsions are introduced so the reader may develop a keener incite into the discussions of results presented in Chapter 11.

10.2 The Importance of the Interface

An emulsion was introduced in Chapter 2, Table 2.1 as a type of liquid-liquid dispersed system in which the dispersed phase has particle size of approximately $1x10^{-7}$ to $1x10^{-4}$ m. Emulsions are a subset of what is known as colloidal dispersions. Colloidal science represents a "grey area" between continuum fluid mechanics and kinetic theory and marks a boundary where body or particle sizes become comparable with molecular sizes (Panton, 1996). The essential character common to all colloidal dispersions is, not surprisingly, the large surface to volume ratio for the particles involved. At the interface between the dispersed phase and the dispersion medium, characteristic surface properties such as adsorption and electric double layer effects play a prominent role in determining the physical properties of the dispersed system as a whole (Shaw, 1975). For this reason, surface chemistry is closely linked with colloid and emulsion science.

In theoretical analysis of the dynamics of emulsion systems, it is often the case that the driving forces are modelled from molecular concepts and the restoring viscous forces are assumed to obey the laws of continuum mechanics (Panton, 1996).

10.2.1 Van der Waals forces

As two of the phases defining an emulsion are liquids, it is informative to review some properties of liquids. The existence of the liquid state at or below ambient temperature is attributable to the so-called van der Waals binding force (Pryde, 1966). This force is an amalgam of forces due to various mechanisms that cause net attraction between molecules. If one considers the case of the mutual potential energy that exists between two molecules, three distinct contributions need to be considered.

10.2.1.1 The polar contribution

If the molecules are polar, there will be a potential energy due to the interaction of their permanent dipoles. This is termed the electrostatic energy; ϕ_s and can be expressed as shown in equations (1.14) to (1.16) or their equivalent expressions in E.S.U. units:

$$V = \frac{\mu_p}{r^2} \quad and \quad E_r = \frac{2\cos\theta\,\mu_p}{r^3} \tag{10.1}$$

For example, consider the situation 3 Å from an HCl molecule, regarded as an ideal dipole of moment 1.08 x 10^{-18} e.s.u. cm. The potential is

$$V = \frac{1.08\,x\,10^{-18}}{\left(3\,x\,10^{-8}\right)^2} = 1.2\,x\,10^{-3}\ e.s.u.$$

and the field on the dipolar axis is $8.0\,x\,10^{4}\ e.s.u.cm^{-1}$. There are approximately 300 volts in 1 e.s.u., hence the potential is then 0.36 V and the electric field 0.24 MVm^{-1}.

10.2.1.2 The induction contribution

Secondly, there will be a contribution due to the interaction of the dipole induced in each molecule with the permanent dipole of the other. This is termed the induction energy; ϕ_i. Consider for example an argon atom, which has polarisability of α = 1.6 x 10^{-24} cm^3 placed in the field of the HCl molecule. An induced dipole of moment $\mu_i = \alpha E = 1.3\,x\,10^{-19}\ e.s.u.\ cm$ results.

10.2.1.3 The dispersion contribution

Finally, there is a third contribution, the origin of which is not immediately apparent. This attractive force is known as the London or dispersion energy; ϕ_d, and explains the cohesion of non-polar substances. Theoretically, ϕ_d can be derived from quantum theory but simply is usually thought of as the net effect of instantaneous "ripples" in the electronic distribution about one of the molecules which takes the distribution away from being spherically symmetrical[4]. This effect leads to an instantaneous dipole being present which in turn induces a dipole in the other molecule. An attractive force between the two results, similar to the induced dipole present when one or other of the molecules is polar.

10.2.1.4 The combined contribution

To a good approximation, the three contributions can be treated separately and added to give the total energy. That is

$$\phi(r) = \phi_s + \phi_i + \phi_d \qquad (10.2)$$

Where $\phi(r)$ is the total potential energy of the pair of molecules expressed as a function of r, the distance between them.

Table 10.1 shows the relative magnitudes of the contributions to the van der Waals energy, all of which vary as the inverse sixth power of the distance between the molecules. To calculate them, the dipole moments and polarisability of the molecules is first found from measurements of the refractive indices and dielectric constants of the molecules in the gaseous phase (London, 1930).
It is always the case that the induction contribution is small and that the dispersion effect is large and dominant when the dipole moment is less than about one Debye unit.
The phenomena of surface and interfacial tension are readily explained in terms of these forces. The molecules that are located within the bulk of the liquid are, on average, subjected to equal forces of attraction in all directions. Molecules located, for example, at a liquid-gas interface experience unbalanced attractive forces resulting in a net inward pull. As many molecules as possible will leave the surface for the interior of the liquid and the surface will,

[4] One of most elegant analogies for picturing the motion of electrons about an atom or molecule is captured in the poem by Howard Nemorov entitled "Seeing Things" in which he describes the motion of a swarm of gnats circling a tree on the horizon at sunset. The poem is copied in full in the Preface.

therefore, tend to contract spontaneously. For this reason, droplets of liquid and bubbles of gas tend to attain a spherical shape. It is important to note that the surface at equilibrium is not in a quiescent state but rather in a state of great turbulence on the molecular scale due to the flux of material entering and leaving the fluid via the surface. The average residence time of a molecule at the surface of water is circa 10^{-6} s (Pryde, 1966).

Molecule	**Permanent Dipole Moment** (10^{18} *e.s.u. x cm (Debye units)*)[5]	**Polarisability** ($\alpha x\ 10^{24}\ cm^3$)	**Electrostatic** ($r^6\phi_s x\ 10^{60}$ *erg* cm^6)	**Induction** ($r^6\phi_i x\ 10^{60}$ *erg* cm^6)	**Dispersion** ($r^6\phi_d x\ 10^{60}$ *erg* cm^6)
CO (carbon monoxide)	0.12	1.99	0.0034	0.057	67.5
NH_3 (ammonia)	1.5	2.21	84	10	93
H_20 (water)	1.84	1.48	190	10	47

Table 10.1 The relative contributions to the van der Waals force

10.3 The Interfacial Tension

The *surface tension,* γ_0 of a liquid-air interface and the *interfacial tension,* γ_i between two liquids (and the more fundamental quantities, the *surface free energy* or *interfacial free energy* α_0, α_i) define the most important parameters in the physics and chemistry of surfaces and interfaces. The surface tension has been much used in Chapters 7 and 8 but here is given a more in-depth theoretical treatment to ensure sufficient weight can be applied to the analyses of Chapter 11.

The surface tension γ_0 is often defined as the force acting at right-angles to any line of unit length on the liquid surface. However, this definition is a little misleading especially for liquid surfaces, as there is no tangential force as such on the surface of a pure liquid. It is more satisfactory to define the surface tension and the surface free energy as the work required to increase the area of a surface isothermally and reversibly by unit amount (Shaw, 1975). The

[5] One Debye is the permanent electric dipole when two equal and opposite charges of magnitude equivalent to the electronic charge are a distance of one Ångstrom apart. The elementary or electronic charge is $4.8x10^{-10}$ e.s.u. and one e.s.u. is one coulomb divided by one-tenth the speed of light in cms^{-1} i.e. there are approximately $3x10^9$ e.s.u. units (known as franklins!) in a coulomb.
An Ångstrom is 10^{-10} m.

same considerations apply to the interface between two immiscible liquids i.e. there is an imbalance of intermolecular forces, but of lesser magnitude. The interfacial energy between two *pure, immiscible* liquids usually lies between the individual surface energies of the two liquids in question.[6]

In considering predictions for water against oil interfacial tension, Fowkes (1962) proposed the following. Since the surface tension of water has large contribution from both electrostatic and dispersion force effects within the molecule as per Table 8.1 plus that from hydrogen bonding (whereby preferential alignment of the water molecules increases the intermolecular attraction), the tension could be split into these two elements ($\gamma_w = \gamma_w^h + \gamma_w^v$). With water in contact with a saturated hydrocarbon, for example, there is no hydrogen bonding in the surface tension and $\gamma_w = \gamma_w^v$ i.e. the interfacial tension is due mainly to the van der Waals forces. Fowkes used this argument to modify a thermodynamically derived equation of Girifalco and Good (1957) to produce the following expression:

$$\gamma_{wo} = \gamma_w + \gamma_o - 2\left(\gamma_w^v \gamma_o\right)^{\frac{1}{2}} \tag{10.3}$$

Where γ_{wo} is the interfacial tension between the water and oil, and γ_w^v is approximately 21.8 mNm^{-1} at 20^0 C.

Liquid	γ_o	γ_i	γ_i *(from Eq. (10.2))*
Water	72.75	-	
n-Hexane	18.4	51.1	50.09
n-Octane	21.8	50.8	50.9
n-Octanol	27.5	8.5	51.3
Gas oil*	37	16	52.9+
Tellus R5*	37	17	52.9+

Table 10.2 Surface tension and interfacial tension against water for liquids at 20^0 C

* Values from Wayth (1999) see Chapter 11.

\+ The deviations are most likely due to two causes, there are polar (e.g. -OH) or aromatic molecules in the oil or additives such as anti-oxidants etc. show some amphiphilic behaviour.

This equation has met with success in predicting the pure liquid interfacial tensions for water against non-polar oil systems (see Table 10.2) and for predicting the interfacial tensions of

[6] Solubility of a liquid can be similarly described in terms of the same molecular forces.

systems containing emulsifying agents. The equation fails when the oil has polar or aromatic groups present and is perhaps most useful as an indication that these groups are present.

10.4 The Dynamics at the Interface - the Interface as a Barrier

The exact value of the surface or interfacial tension in a dynamic system is a function of the flow on both sides of the surface, the curvature of the surface and the thermodynamic state of the system (temperature and composition). The following simplified equation relates the surface tension γ_0 to the flow properties on either side:

$$(p - \tau_{nn})_a - (p - \tau_{nn})_b = \gamma_i \left(\frac{1}{R_1} + \frac{1}{R_2} \right) \tag{10.4}$$

Where p is the pressure, τ_{nn} is the normal viscous stress and R_1 and R_2 are the principle radii of curvature of the surface. The subscripts a and b refer to the concave side (usually the liquid phase) of the surface and the convex side (usually the vapour phase) respectively.

A more familiar formula (see also equation (7.1) is where there is no flow and the surface is spherical

$$p_a - p_b = \frac{2\gamma_0}{R} \tag{10.5}$$

This equation implies that the vapour pressure over a small droplet or over a convex meniscus is greater than over a plane surface. The transfer of liquid from a plane surface to a droplet requires the expenditure of energy since the area, and hence the surface free energy, of the droplet will increase.
By assuming ideal gas behaviour for the vapour phase, it can easily be shown that

$$RT \ln \left(\frac{p_r}{p_0} \right) = \frac{2\gamma_0 M}{\rho r} = \frac{2\gamma_0 V_m}{r} \tag{10.6}$$

Where R is the universal gas constant, T the temperature, p_r the vapor pressure above the droplet of radius r, p_o the vapour pressure above a plane surface, M the molar mass, ρ the mass density of the liquid and V_m the molar volume.

This expression is known as the Kelvin equation and has been verified experimentally. For example, for water droplets (assuming γ_0 to be constant)

r	$\frac{p_r}{p_0}$
10^{-7}	1.01
10^{-8}	1.1
10^{-9}	3.0

Table 10.3 The vapour pressure increase above a highly curved surface of water at constant temperature.

The effect of curvature on vapour pressure and more importantly, in the case of emulsion science, on solubility provides an explanation for the ability of vapours and solutions to saturate. If condensation has to take place via droplets containing only a few molecules, the high vapour pressures involved will present an energy barrier to the process.

10.5 Variation of surface tension with temperature

The variation of surface tension with temperature is one whereby the tension usually reduces with temperature although certain molten metals form an exception. As temperature increases, the kinetic energy of the molecules in both the liquid and vapour phase increase until at the critical temperature, they are equal and the surface tension disappears. A satisfactory empirical equation for how the surface tension varies with temperature is due to Ramsey and Shields (1893):

$$\gamma = \frac{k\,(T_c - T - 6)}{\left(\frac{M\,x}{\rho}\right)^{\frac{2}{3}}} \qquad (10.7)$$

Where T_c is the critical temperature of the liquid, T the temperature, M the molar mass, ρ the mass density of the liquid and x the degree of molecular association.

10.6 Measurement of Surface and Interfacial Tension

There are a number of methods for the measurement of surface and interfacial tension, mostly for the static case. The one used in the studies of Chapter 11 is perhaps the most well known and practical, namely the (du Nuoy) ring method. In this, the force required to detach a ring from a surface or interface is measured either by suspending the ring from the arm of a balance or by using a torsion wire arrangement. The detachment force is related to the tension by the expression:

$$\gamma = \frac{\beta F}{4 \pi R} \tag{10.8}$$

Where F is the force to detach the ring, R the mean radius of the ring and β is a correction factor.

A platinum ring is used for most interfacial work with water if it is the denser liquid. It is essential that the ring be perfectly flat, so that the complex surface shape at detachment can be corrected for and clean, to prevent errors due to wetting. The correction factor is usually incorporated in a commercial piece of equipment's calibration, with instructions for additional corrections based on the density of the fluids used.

10.7 Solubility and amphiphilic behaviour - the key to emulsion behaviour and stability

As mentioned above, the solubility behaviour of molecules can be understood by consideration of the molecular forces in a similar manner to those discussed in section 10.2. In the emulsions considered here, one of the phases is aqueous and the other is (in the widest sense of the term) an oil. If the oil is the dispersed phase (as defined in Chapter 3), the emulsion is termed an *oil- in- water* (o/w) emulsion; if the aqueous medium is the dispersed phase, the emulsion is termed a *water-in-oil* (w/o) emulsion.
In emulsion science, w/o emulsions are considered "inverted" due to the fact they are less common. However, as Wayth (1999, Chapter 2, p19) points out, in the oil industry, o/w emulsions are termed "inverted".
Rarely are stable emulsions truly of only two phases but rather a third or even a fourth phase is found necessary to stabilise the system. Where the third phase is an *amphiphilic* material and present in substantial concentration in comparison to the oil and water phases, the system is termed a *macroemulsion*. Macroemulsions are mentioned in this chapter but their behaviour in an electric field was not studied.

10.7.1 Identification of basic type of emulsion

There are several methods by which the emulsion type may be identified (Williams, 1989 Chapter 3 p 40).

1. Generally, an o/w emulsion has a creamy texture and a w/o emulsion feels greasy.
2. The emulsion mixes readily with a liquid which is miscible with its dispersion medium.
3. The emulsion is readily coloured by dyes which are soluble in the dispersion medium.
4. o/w emulsions have much higher electrical conductivity than w/o emulsions.

Factor number 4 is the key to destabilisation of emulsions using applied electrostatic fields.

10.7.2 Emulsifying agents and emulsion stability

The stability of an emulsion is one of the most important of its physical parameters. A definition of stability is, nonetheless, difficult since it is largely a subjective concept. The term stability can be used with reference to three essentially different physical phenomena.

1. Creaming or sedimentation, where the density difference between the two phases causes a net mass transfer and separation of the phases under the action of gravitational or centrifugal forces. Should the droplets of the dispersed phase not coalesce by the time they reach the top or bottom of the emulsion, creaming (or stratified layers) results. The emulsion may be restored by gentle shaking or inversion (in a gravitational sense).
2. Flocculation, whereby natural (Brownian motion, differential sedimentation) or imposed (fluid mixing, electrophoretic or dielectrophoretic migrations) droplet collisions cause the droplets to adhere to each other without coalescence into a larger distinct droplet.
3. Coalescence, whereby the dispersion medium gradually becomes distributed over fewer distinct particles and the average size of each becomes larger. Eventually, the dispersion medium can become a continuous phase separated from the dispersion medium by a single interface. The time taken for such complete phase separation can be anything from the order of seconds to years.
4. Phase inversion is the manifestation of emulsion instability. This process is where the dispersion medium and the dispersed medium reverse their rôles. An emulsion still

results but one usually having different bulk electrical and rheological properties to the original. Phase inversion is dealt with in detail later.

If an emulsion is formed by homogenizing from two pure liquid components, phase separation will generally be rapid, especially if the dispersed medium is present in high concentration. To prepare reasonably stable emulsions, a third component must be present. This third agent, known as an *emulsifying agent* or *emulsifier* can be broadly classified as:

- Surface-active agents (surfactants).
- Naturally occurring materials.[7]
- Finely divided solids.

10.7.3 The nature of surfactants

As mentioned previously, the solubility of a liquid can be described in terms of molecular forces. Early workers realised the importance of electrostatic interactions (Hildebrand, 1916; Langmuir, 1917) the very fact that solvents are described as polar or non-polar, clearly illustrates this.

Solvents such as water, which is highly polar, and oil (a paraffinic hydrocarbon) represent liquids whose solubilising properties are extremely different. In fact, solvents cover a complete spectrum, the majority of which have properties intermediate between these two extremes. To understand emulsion stability in the presence of surfactants, it is key to have a model for the solubility behaviour of two-phase or more complicated three and higher phase mixtures.

Some materials will not dissolve in any solvent, while others dissolve or only sparingly dissolve in solvents of one type. However, some materials such as short-chain fatty acids and alcohols readily dissolve in both oil and water, the hydrocarbon part of the molecule being responsible for its solubility in oil, while the polar -COOH or -OH group has sufficient affinity for water to drag a short length, non-polar hydrocarbon chain into aqueous solution with it. Such molecules are usually depicted as having a polar "head" and a hydrocarbon "tail".

Due to the presence of both a hydrophobic and a hydrophilic part, such molecules may be considered amphiphilic. If they become located at an oil/air, oil/water or water/air interface the respective hydrophilic or lipophilic parts can escape from the phase in which they are not compatible to form an orientated mono-molecular layer (monolayer), which is an energetically more favourable situation than complete solution in either phase. This

adsorption, termed surface-activity, is a dynamic phenomenon since at equilibrium there will be a balance between the tendency for absorption at the interface and that for mixing due to thermal motion.

Since individual amphiphilic monomers in very dilute aqueous solutions tend to migrate to the surface or interface, with a concomitant decrease of the surface tension of the air/water interface or the interfacial tension at the water/oil interface, amphiphiles are also called surface-active agents or surfactants. The decrease in the surface tension arises because of the balance between the normal tendency of a surface to contract and this adsorption, which favours an expansion of the surface. If p is the surface pressure of an adsorbed layer of surfactant, and γ_0 the surface tension of pure water, the surface tension of the solution will be lowered to a value:

$$\gamma = \gamma_0 - p \tag{10.9}$$

Certain molecules, for example some electrolytes and sugars, show small increases in surface tension due to negative adsorption. Here, because the solute-solvent attractive forces are greater than the solvent-solvent attractive forces, the solute molecules tend to migrate away from the surface into the bulk of the liquid.

It is reasonable to assume that increasing the hydrocarbon chain length of a surfactant, the greater will be the tendency for surfactant molecules to adsorb at the air-water surface and lower the surface tension. Indeed, for very dilute solutions this is the case (Traube, 1891), and a rough generalisation, known as Traube's rule, is that for a particular homologous series of surfactants the concentration required for an equal lowering of surface tension in dilute solution decreases by a factor of about three mNm^{-1} for each additional CH2 group.

Similarly, it might be expected that increasing the surfactant concentration of the bulk solution may result in linear decreases of the surface tension. Although this may hold for very dilute solutions, as the concentration of the bulk increases, progressively the effect ceases to hold. This is firstly because the surface area is finite, therefore molecules will eventually occupy the total interfacial area and secondly solute-solute interactions progressively become more important, such interactions interfering both with the surface packing and in the bulk before maximal adsorption is achieved.

10.7.4 Aggregation and Micellization

Molecular aggregation is a common phenomenon by which molecules may achieve a lower energy state than individual monomers; for example, acetic acid in the vapour phase consists

[7] Which often are critical to the behaviour of water-in-crude oil emulsions.

of dimers[8]. Surfactant monomers in solution may also aggregate, especially at concentrations above which they can no longer escape to an interface and this provides an alternative mechanism by which unfavourable interactions are minimised. If the Krafft point is exceeded (i.e. the temperature which provides the surfactant with sufficient solubility), and the concentration is greater than a critical concentration called the critical micelle concentration (c.m.c.) aggregation results in the formation of micelles.

The term '*micelle*' was first used by McBain (1913) for a highly associated particle of colloidal material which could explain the abrupt changes in several physical properties, such as osmotic pressure, turbidity, electrical conductance and surface tension in aqueous solutions of highly surface-active materials. McBain proposed that the hydrocarbon chains oriented towards the interior of the micelle, leaving the hydrophilic groups in contact with the aqueous medium. More recently, Hartley (1977) proposed a spherical shape for micelles and laid the foundations for the present view.

Today the word micelle in physical chemistry is solely reserved for an aggregate of amphiphilic molecules (Tanford, 1980) and unlike earlier workers (McBain, 1950; Debye, 1949) no emphasis is placed on attraction of the 'liquid-like' surfactant hydrocarbon chains for each other. Essentially, a micelle can be looked upon as a monolayer curved upon itself (Mittal and Murkerjee, 1977). Therefore, in a non-polar solvent, the opposite topology to normal 'oil-in-water' (o/w) type micelles is possible. Here the head-groups are directed towards the centre and the tails are on the outside, and these 'water-in-oil' (w/o) type structures are termed reverse micelles, see Figure 10.1 for representations of the rich polymorphism of micelles in emulsions.

In dilute amphiphilic solutions, micelles are regarded as approximately spherical, however, the shape and size will fluctuate since these are dependent on the dynamic equilibrium of the system. Typical values for the radius of o/w micelles are between 30 - 50 Å containing of the order 50 - 100 molecules, while the size of w/o micelles can quite easily range between 10 - 100 Å, perhaps even larger since the core may incorporate considerable amounts of a polar solvent. Values for the c.m.c. of surfactants depend on the surfactant and solvent in question and are temperature dependent. For ionic surfactants, the c.m.c. may be as high as 0.3 M[9] while lipids may show values as low as 10^{-10} M. In an homologous series the rate of change of the c.m.c. has been found to decrease between about the C16 to C18 member, and above the C18 member it tends to remain approximately constant. This fact arises because of the coiling of the long hydrocarbon chains.

[8] A mer is a single molecular unit.

[9] M stands for molar, a chemical unit of concentration. For a chemical species, it is simply the ratio of the mass of the species per litre divided by the molar mass. For example, a 0.1 M solution of NaOH contains 4g of NaOH per litre of solution.

As the concentration of surfactant increases light scattering evidence has shown that micelles can deviate from spherical to become either prolate (rod-like) or oblate (disc-like) spheroids.

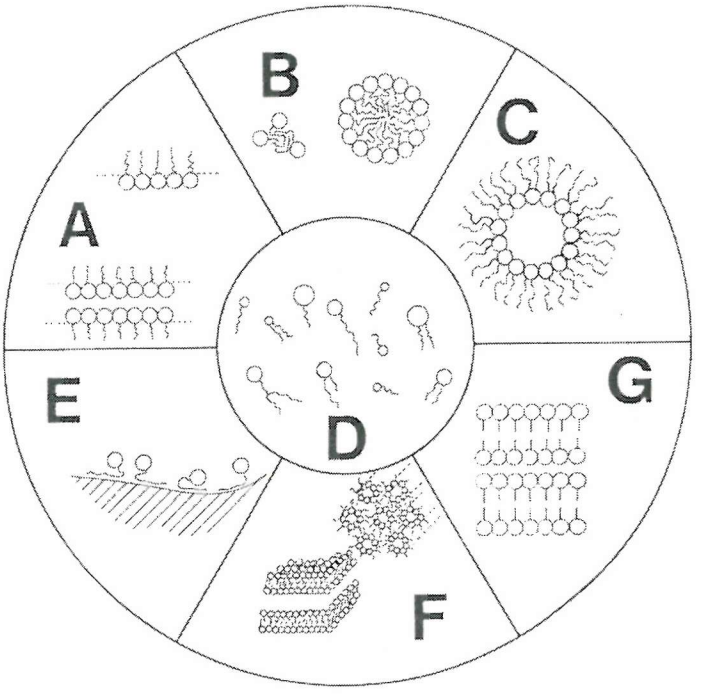

Figure 10.1 Schematic diagram to represent the polymorphism of amphiphiles (adapted from Mittal and Murkerjee, 1977; and Bansal and Shah, 1977).

Monomers (D), present for example in dilute solutions, may undergo aggregation and micellization (B).
In mixed liquid systems containing both polar and non-polar components, a liquid-liquid interface may give rise to a microemulsion (C) or alternatively, especially if surfactant concentrations are small, to a planar interface (A).
When interfaces (A) at liquid-air boundaries occur, stable structures such as soap films may arise.
On non-polar solids and to proteins and polymers, adsorption can occur (E). If surfactant is present at sufficient concentration, lyotropic liquid crystals (mesophases) form (F).
Although many surfactants are liquids under ambient conditions, many also form crystalline solids (G), while others are gels (G).

At higher concentrations, increased interactions between individual micelles may result in the formation of lyotropic[10] liquid crystalline phases. However, it should be noted that the ability

[10] Lyo- basically means loose or dispersed, lyotropic can be taken to mean a dispersed form.

of an amphiphile to show micellization ultimately depends on the balance of the hydrophilic and hydrophobic forces present in the system.

10.7.5 The Hydrophobic Effect

Water is the only chemical compound that occurs naturally in all three physical states, and although a seemingly simple compound consisting of an oxygen atom linked between two hydrogen atoms, it shows many physically and chemically unique properties. Indeed, life as we know it could not exist in its absence for in providing the 'reaction' medium in which life originated, its properties became a necessary requirement in the many biochemical and physiological processes that evolved. Consequently, because water is so universal, understanding its properties and behaviour is of considerable importance and much research has been devoted to it (Eisenburg and Kauzmann, 1969).

Most of water's properties and behaviour can be best understood from a description at the molecular level and by considering the intermolecular forces present. A water molecule by virtue of the electronegativity of the oxygen atom is polar, and because the oxygen atom contains two lone pairs of electrons, the two covalent hydrogen-oxygen bonds are angled 104.5^0 apart, slightly less than the tetrahedral angle of 109.4^0. This arrangement along with the relatively small size of the atoms provides each water molecule with the possibility of forming four hydrogen bonds, two in which it acts as a hydrogen donor and two in which it acts as an acceptor. Consequently, ordinary ice adopts a tetrahedral crystal structure, with a distance of about 2.76 Å between neighbouring oxygen atoms, and this relatively open structure accounts for the low density of ice, lower than that of liquid water, and its ability to form higher density structures at increased pressures.

Similarly, the ability of water molecules to form hydrogen bonds accounts for why it is the only simple hydride not gaseous at ordinary temperatures. Consequently, liquid water may be considered a very cohesive liquid in which the molecules, described as highly associated are isotropically arranged, and this simple description accounts for its anomalously high specific heat capacity; high surface tension; low standard molar entropy of formation; and its boiling point approximately 100^0 C higher than any other substance of comparable molecular mass. Somehow H_2O seems too simple a molecular formula for water in condensed phases, perhaps $(H_2O)n$ would be more appropriate to account for the highly hydrogen bonded structure of ice and the so called *flickering cluster* model of liquid water (Nemethy and Scheraga, 1962).

Ions have a strong affinity for water, owing to their electrostatic attraction to water dipoles. Similarly, moderately polar entities can also show strong affinity for water if present in

sufficient numbers and bonds between the polar solute and the water molecules may form, which in turn can give rise to less mobile, more ordered 'bound' water, thought to exist as clathrate (cage-like) type structures (Frank and Evans, 1945). Thus, ionic or polar substances easily solvate since the bonds that form more than compensate for the disruption or distortion of the so called *water structure*. In contrast, non-polar entities are not capable of bonding with the water molecules. Rather, they disrupt the water structure, increasing the order of the water around the solute (clathrate cage), which is an entropically expensive process and therefore their solvation is resisted. Thermodynamically then, it is a loss of entropy rather than bond energy that leads to an unfavourable free energy change for solvation (Tanford, 1980). Thus, non-polar molecules can be considered to be forced out of aqueous solution and this gives rise to what is known as the *hydrophobic effect.*

Since amphiphiles consist of both hydrophobic and hydrophilic parts, the extreme importance of the hydrophobic effect at once becomes recognised because the behaviour and properties of the solute will ultimately depend on how the different hydrophilic and hydrophobic parts respond to the solvent. An understanding of the hydrophobic effect therefore provides a more meaningful description of the solubilisation, surface tension, aggregation, micellization and liquid crystal formation properties of amphiphilic materials.

10.7.6 Phase Equilibria - The Phase Rule

Any understanding of phase behaviour requires knowledge of the phase rule (Smith and Van Ness, 1987), which conveniently summarises the general conditions of equilibrium in a simple form. However, before stating the rule it is first desirable to define the terms involved:

1. *A phase* is defined as any homogeneous and physically distinct part of a system which is separated from other parts of the system by definite bounding surfaces (see Chapter 3).
2. The *number of components* in any system is the smallest number of independent chemicals by means of which the composition of every possible phase can be expressed.
3. The *number of degrees of freedom* of a system is the number of variable factors, such as temperature, pressure and concentration, which need to be fixed in order that the conditions of a system at equilibrium may be completely defined.

The phase rule states that, provided the equilibrium between the phases is not influenced by gravity, electrical or magnetic forces, or by surface action, but only by the temperature, pressure and concentration, the number of degrees of freedom (F) of the system is related to the number of components (C) and phases (P) at equilibrium by the equation:

$$F = C - P + 2 \qquad (10.10)$$

10.7.6.1 Single Component System

The simplest application of the phase rule is to a one-component system. In this case, C = 1, therefore the sum of the number of phases (P) and the number of degrees of freedom (F) should always be equal to 3, if the system is in equilibrium. To illustrate the conditions of equilibrium between various phases in any system, phase diagrams are used. The phase diagram for water, a one-component system, is shown in Figure 10.2. Each distinct region represented in this system consists of one phase only, i.e. solid, liquid or vapour. In order to specify any point in a single phase (P - 1), both the temperature and pressure are required since, temperature or pressure alone is insufficient to specify precisely any point in a particular region. A single phase thus has two degrees of freedom (F = 2) and is bivariant; consequently, F + P = 3, as predicted by the phase rule. However, when two phases are in equilibrium, the conditions must correspond to a point on one of the lines OA, OB or OC, and it is then unnecessary to state both the temperature and the pressure since from one fixed variable the other is automatically determined from the appropriate curve. Two phases in equilibrium in a one component system is thus univariant (F = 1); and again the phase rule is seen to apply.

At the triple point O, three phases (P = 3) coexist in equilibrium and the system is said to be invariant because now there are no degrees of freedom (F = 0). The fact that the three given phases are in equilibrium means that the system must be at the triple point, and it is unnecessary to prescribe either the temperature or the pressure.

It is possible to obtain super-cooled phases, for example, the dashed curve OA' in Figure 10.2 represents the variation with temperature of the vapour pressure of the super-cooled liquid. The liquid-vapour system along OA' is said to be in a condition of metastable equilibrium because although the system is at a definite equilibrium it is, nevertheless, not the most stable equilibrium for a given temperature.

10.7.6.2 Two Component System

A system consisting of a mixture of two volatile liquids is an example of a two-component system (C = 2). In such systems the phase rule requires that F + P = 4. A single phase (P = 1) will then have three degrees of freedom and temperature, pressure and the concentration of one component (c_1) will be necessary to fully specify the phase. The concentration of the second component is given by (100 - c_1) percent of the first component. When a system consists of two similar, non-interacting liquids such as benzene and toluene, which are soluble in one another in all proportions and at all temperatures no distinction can, or need be drawn between the solvent and the solute. Such systems are described as ideal in that both constituents obey Raoult's law[11] over the whole range of concentrations and at all temperatures.

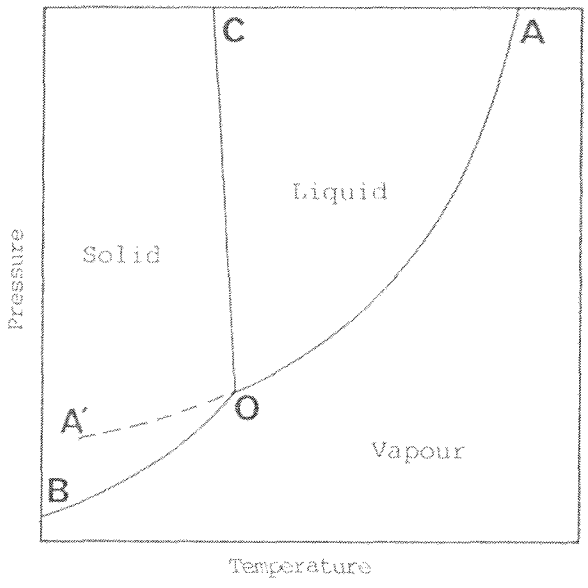

Figure 10.2 The phase diagram for water

In non-ideal mixtures of miscible liquids, the molecules of the two liquids differ in character from each other. Molecular forces acting between the dissimilar molecules will interfere with the forces acting between like molecules, and since these forces differ for the two components, such systems will show positive or negative deviations from Raoult's law.

[11] Dissolving a substance in a solvent lowers the vapor pressure of the solvent. Raoult's law states that for an ideal solution at a given temperature, the relative lowering of the vapour pressure is proportional to the mole fraction of the solute.

Negative deviations from ideality occur where the molecules of the two components attract one another strongly. In this case, there will be a reduced tendency of the molecules to vaporise, which in turn may lead to the system exhibiting a boiling point maximum. Positive deviations occur for liquid mixtures where one or both components have a stronger attraction towards like molecules than to the molecules of the other component. Such a mixture has an increased tendency to vaporise, than either of the pure components, a phenomenon which is especially important for distillation. Where the dissimilarity between molecules is not large, the positive deviations from ideal behaviour are small. On the other hand, if one component is slightly polar while the other is highly polar or, more particularly, if the mixture consists of a polar and a non-polar compound, for example, an alcohol and a hydrocarbon, considerable positive deviations may occur. Such large deviations may result in the liquids becoming only partially miscible, for example, between the two liquids, analine and hexane. Each liquid acts as a solvent for the other until each component can no longer dissolve further additions, then two coexisting, saturated liquid layers, called conjugate solutions form, which are in equilibrium with each other. The phase diagram for this type of equilibrium at constant pressure is shown in Figure 10.3.

The tie line l_1, l_2 at temperature t, so called because it connects (or ties together) phases in equilibrium, gives the composition of the two conjugate solutions; l_1, with composition x_a, is the solution richer in analine, and l_2 with composition x_b is the solution richer in hexane. The relative number of moles of l_1 to l_2 at composition x will be in the ratio of the linear distances xl_2 to xl_1.

Since the solubility of each liquid in each other increases with increasing temperature, the compositions of the conjugate solutions become closer on raising the temperature. At the temperature tc, known as the critical solution temperature or (upper) consolute temperature, the two liquids, which had previously been partially miscible, are now identical in composition. They have become completely miscible in all proportions, and only one phase then exists.

In some systems, two partially miscible liquids become completely miscible below a certain temperature so that there is a lower consolute temperature. Such systems e.g. water and ether, probably always have an upper consolute temperature, although in some cases it may not be accessible experimentally if it is above the temperature at which either of the liquids vaporises. There are thus two temperature limits outside of which the liquids are completely miscible and between which they are partially miscible. The increased solubility as the temperature is lowered is undoubtedly due to increased interactions between the two components in the liquid state. A system that then shows positive deviations from ideal at one temperature tends to exhibit less positive or even negative deviations as the temperature is lowered.

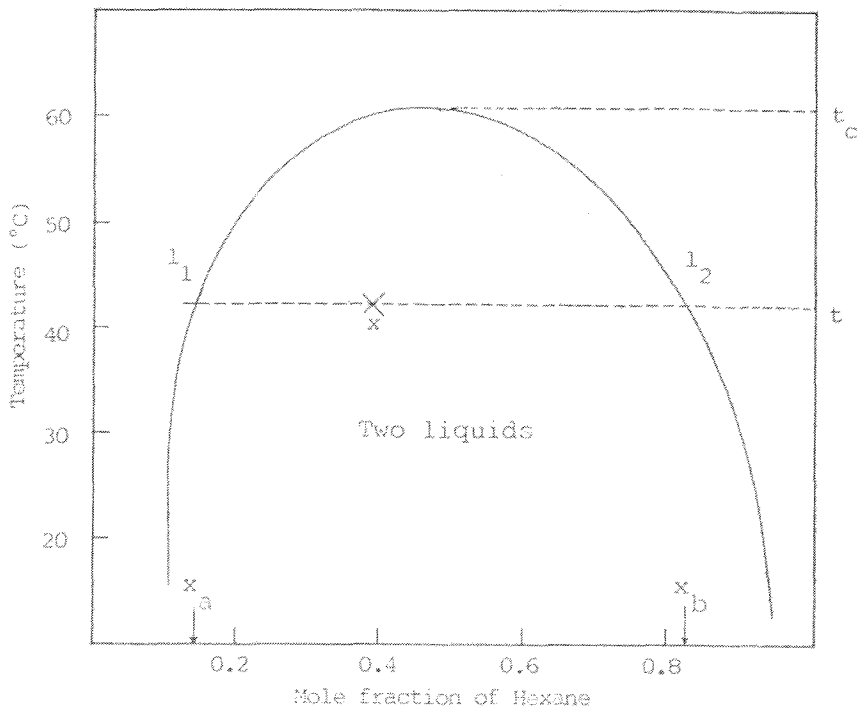

Figure 10.3 Phase diagram for the analine/hexane system.

Although systems with a lower consolute temperature will, in principle, also exhibit an upper consolute temperature, the reverse is not necessarily the case. Sometimes this is because the temperature may be below that at which the liquids solidify.

10.7.6.3 Three-component systems

For systems of three components (most important for understanding the behaviour of emulsions) with C = 3, the phase rule F + P = 5 applies, indicating that the maximum number of degrees of freedom is four. Thus, temperature, pressure and the concentrations of two components may be independently variable. The concentration of the third component is implicit from the known concentrations of the other two.

By considering a three-component system as a condensed system (constant pressure), this effectively reduces the number of degrees of freedom to three. Therefore, to represent the compositions at equilibrium, and at different temperatures, a three-dimensional model is necessary. Hence, phase diagrams of three-component condensed systems are represented by triangular diagrams (see Figure 10.4) at a constant temperature, the corners of the triangle representing the pure components.

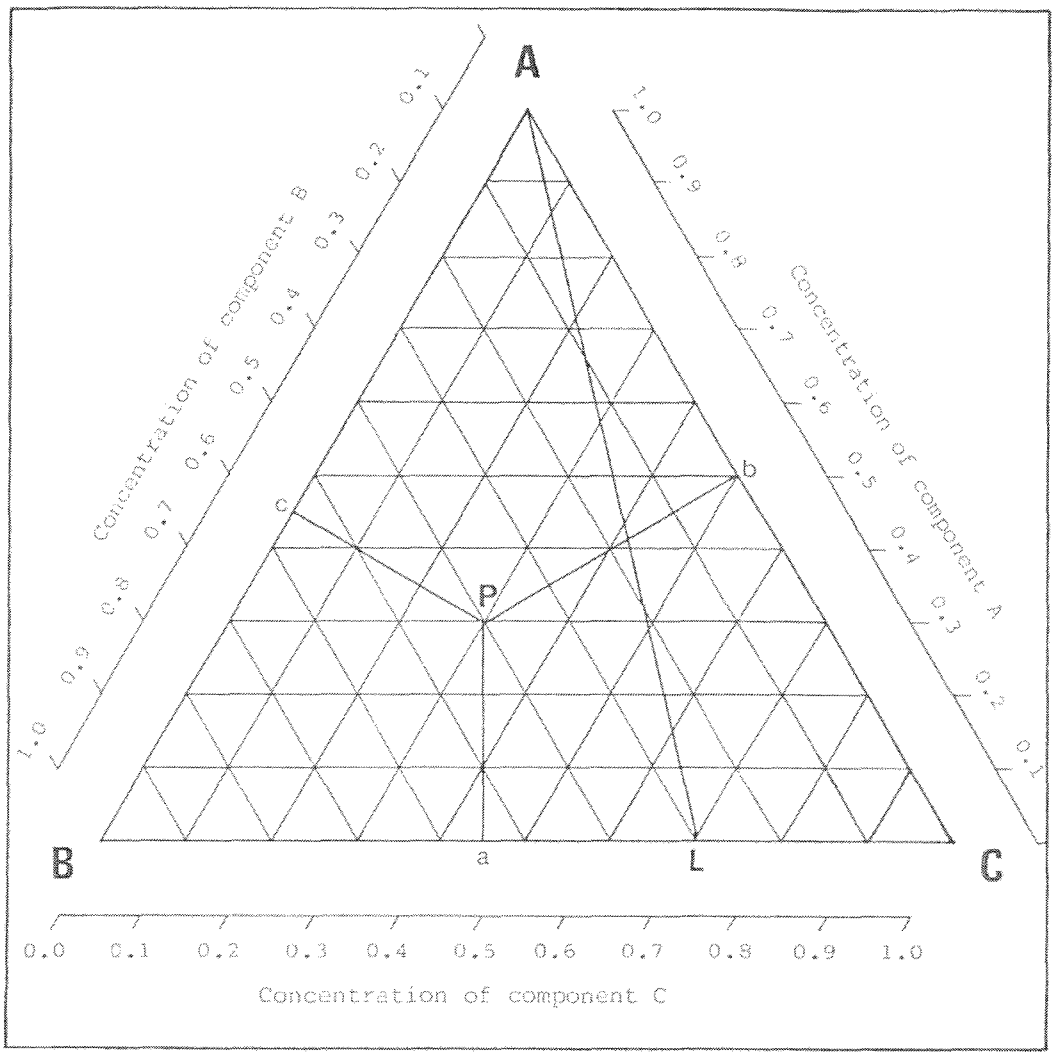

Figure 10.4 Principle of the triangular phase diagram

The ternary phase diagram utilises the property that the sum of the distances from any point within an equilateral triangle drawn perpendicular to the three sides is always equal to the height of the triangle. By taking this length as unity, and expressing the amounts of the three components of a given system as a fraction of the whole, it is then possible to represent the composition of any system by a point within the triangle. For example, the composition of point P is seen to be 0.3 A, 0.4 B and 0.3 C mole fraction or weight fraction.

Any point situated on one of the sides represents two components only, lacking the component at the corner not joined by the side passing through the point, e.g. point L would correspond to the composition 30% B : 70% G. Additions of the third component, A in this case, to the mixture at L will correspond to a point on the line AL, connecting to the A corner of the phase diagram.

The phase rule indicates that the maximum number of phases that can coexist in equilibrium (excluding the vapour) at any arbitrary fixed pressure (F = 1) is four.

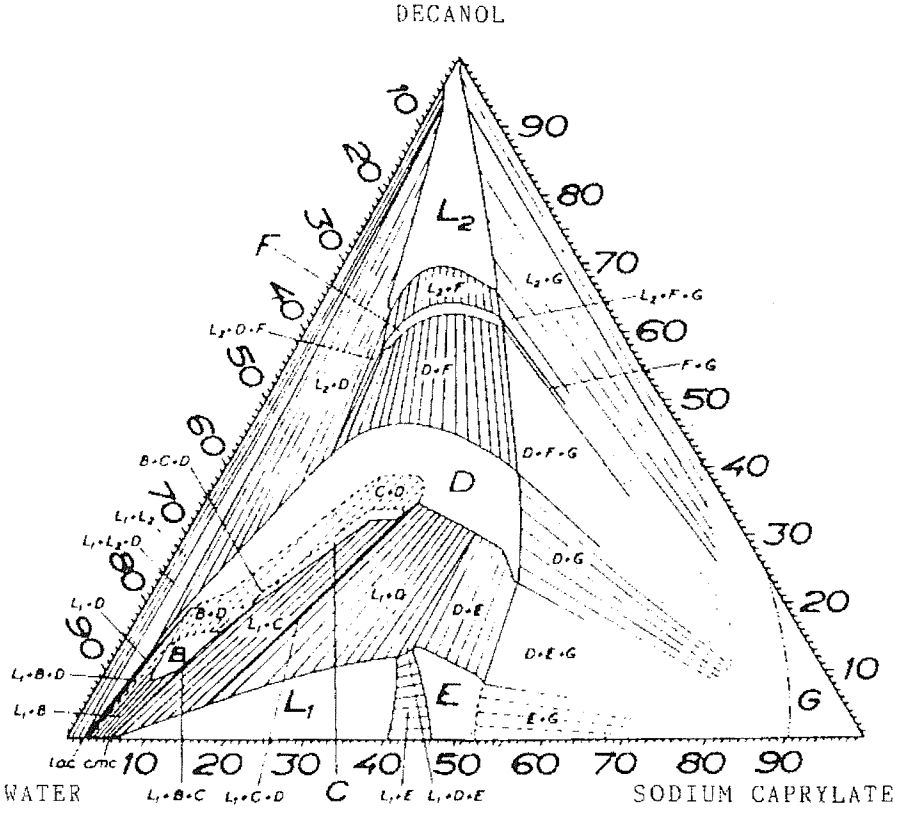

L_1	Region with homogeneous, isotropic aqueous solution.
L_2	Region with homogeneous, isotropic decanolic solution.
B, C, D, E, F	Regions with homogeneous mesomorphous phases.
E	Region with homogeneous mesophase with two-dimensional, hexagonal structure; amphiphilic cylinders; 'normal' structure.
F	Region with homogeneous mesophase with two-dimensional, hexagonal structure; amphiphilic cylinders; 'reversed' structure.
D	Region with homogeneous mesophase with lamellar structure; one-dimensional swelling.
C	Region with homogeneous mesophase with lamellar structure; two-dimensional swelling.
B	Region with homogeneous mesophase with lamellar structure; one-dimensional swelling.
G	Region with solid substances.

L_1+L_2, L_2+D, L_2+F, L_2+G, $F+G$, $D+G$, $E+G$, L_1+E, L_1+D, L_1+C, L_1+B, $D+F$, $D+E$, $C+D$, $B+D$, Two-phase zones.

L_1+L_2+D, L_2+D+F, L_2+F+G, $D+F+G$, $D+E+G$, L_1+D+E, L_1+C+D, L_1+B+C, L_1+B+D, $B+C+D$, Three-phase triangles.

Figure 10.5 Phase diagram for the three-component system sodium caprylate-n-decanol-water at 20^0 C. Concentrations expressed as percentage by weight. (After Mandell and Ekwall, 1968).

Consequently, considerable complexity can arise in condensed systems of three phases, for in addition to the vapour, which is neglected, there may be one, two or three liquid phases and three solid phases, apart from the possibility of solid compounds formed by combination of two or more of the components.

The phase diagram shown in Figure 10.5 is of a typical microemulsion system. Like the micellar phases, which occur in binary surfactant-solvent systems, microemulsions are stable isotropic solutions. However, unlike the micellar solutions, microemulsions typically consist of surfactant, oil and water, and also frequently present is a co-surfactant such as an alcohol or salt, which can partition along with the surfactant at the interface, between the aqueous and hydrocarbon regions.

It is difficult to see on this diagram, but the key area to focus on is alongside the left-hand side of the triangle, where the concentration of sodium caprylate is low. The phase diagram indicates that this region is filled with either an aqueous (water continuous emulsion) or a decanolic solution (oil continuous emulsion). Inversion will occur somewhere within this area as the relative concentrations of the water and decanol are varied.

10.8 Interfacial activity of dispersed solids

Emulsions may be stabilised by finely divided solids (see Figure 10.6). The hydrophobic effect (Section 10.7.5) is also a satisfactory way to explain this behaviour, which is important for the stabilisation of crude oil/water emulsions.

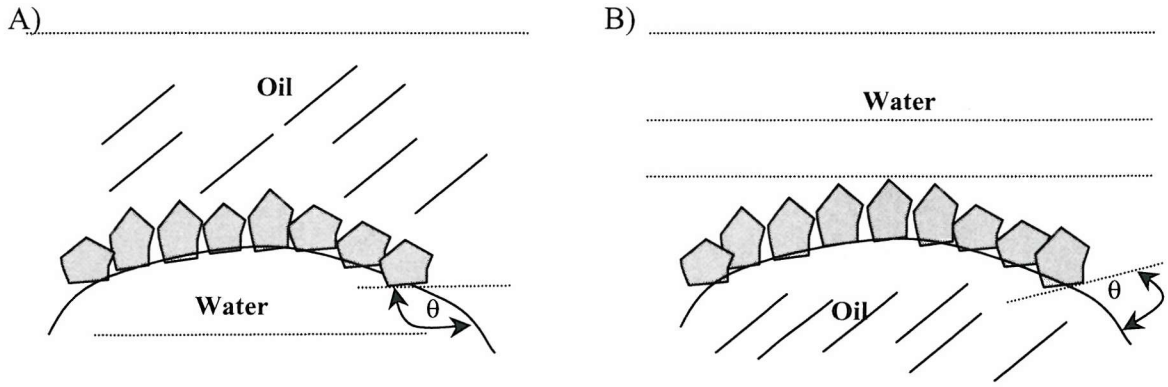

Figure 10.6 Stabilisation of emulsions by finely divided solids. A) Preferential wetting by water leading to o/w emulsions. B) Preferential wetting by oil leading to w/o emulsions.

For example, certain types of clay are preferentially wetted by water and these tend to give o/w type emulsions. Carbon black, which is preferentially oil wetted, tends to give w/o emulsions.

10.9 Gibbs - Marangoni Surface Elasticity Effect and Surface Rheology

Surface elasticity is a phenomenon caused by non-uniformity of surface or interfacial tension and can only arise in solutions in which solute molecules are subject to adsorption. It occurs when a fresh surface is created or an existing surface is enlarged, due to the dynamic lag in the adsorption process that supplies solute to the surface. As surface area is increased, the surface tension value rises to that of the pure solvent, since the surface excess of solute is reduced. Conversely, if surface area is reduced, the surface tension is reduced below the equilibrium value, since time is required for solute to desorb from the surface and diffuse into the bulk solution. Such differences between static and dynamic surface or interfacial tension are termed the Marangoni effect.

The Gibbs' effect (Sherman, 1968) gives rise to a second contribution to surface elasticity in a liquid lamella (such as the thin film of liquid between two colliding droplets of another, immiscible, liquid). It arises because a lamella of solution becomes depleted of solute as it thins down, causing interfacial tension to increase.

A thinning lamella of solution will tend to have uniform thickness due to the Marangoni and Gibbs effects. This is because interfacial tension is increased, at any point where the lamella is thinned down by external forces, which opposes the thinning process. The gradient of interfacial tension causes not only the interfacial monolayer to be moved but also the underlying liquid, by viscous effects. Ewers and Sutherland (1952) termed this tendency to heal points of potential rupture, surface transport.

A high surface viscosity will retard bulk liquid flow close to the surface and consequently, the drainage rate of the film close to the interface between phases is inhibited. This increases the stability of the emulsion. These effects are important for the design of chemical additives for destabilising w/o emulsions (Shah, 1970) J. Colloid Interface Sci., 37, 744).

10.10 Electrolytic activity and the electric double layer

Electrolytes, in low concentrations, are able to stabilise w/o emulsions (Cheesman and King, 1940). Emulsions can also be stabilised by electrical effects, brought about by the repulsion of dispersed phase droplets carrying charges of the same polarity. Alexander and Johnson (1949) postulated that particles in colloidal systems acquire charge by ionisation, adsorption

or frictional contact. The difference between the first two mechanisms is unclear in the case of emulsions. The polarity and magnitude of droplet charge is likely to depend on the type of emulsifying agent present. With regard to frictional charging, an empirical rule due to Coehn (1898) states that a substance having a high dielectric constant acquires positive charge when contacting a substance of lower dielectric constant. The oil droplets in an o/w emulsion, therefore, should be negatively charged whereas water droplets in a w/o emulsion should be positively charged.

According to Gouy (1910) - Chapman (1913) theory, the preferential adsorption of potential-determining ions, at the surface of a droplet, gives rise to an electric double layer. The inner layer comprises the preferentially adsorbed ions whereas the diffuse outer layer consists of counter ions, which are prevented from neutralising the droplet by random thermal motion. The double layer is characterised by the Debye parameter K and defined below.

$$K = \left[\frac{2ne^2v^2}{\varepsilon kT} \right]^{\frac{1}{2}} \tag{10.11}$$

n is the number density of counter ions in bulk solution, e is the electronic charge, v is the valency of the counter ions, ε is the permittivity of solution, k is Boltzmann's constant and T is absolute temperature.

The inverse K^{-1} of the parameter K is called the double layer "thickness" and is inversely proportional to the square root of the number density of counter ions in bulk solution. In water-continuous emulsions, where n is large, the double layer thickness is small, typically 10^{-3} - 10^{-2} μm (Becher, 1977).

Consequently, a flocculating water droplet has to overcome substantially the entire potential barrier in order to coalesce. Therefore, preferentially adsorbed charge, on dispersed phase droplets, provides a strong stabilising influence in O/W emulsions. In oil-continuous emulsions, however, n is relatively small and so the double layer thickness is significantly larger, being typically several micrometers (Becher, 1977). This is equivalent to the droplet separation in a moderately concentrated emulsion. In consequence, the potential barrier is much reduced and the stabilising influence of the adsorbed charge is much less in w/o emulsions.

10.11 Emulsion rheology

When discussing emulsion rheology in the context of emulsion stability, care should be exercised. Workers in the field of crude oil emulsions discuss rheology in two contexts, one pertaining to the bulk rheology of the emulsion and the other to the interfacial rheology. The bulk rheology, dominated by the continuous phase viscosity, in a flowing or static emulsion can be viewed as a dynamic factor influencing emulsion stability. It is a key parameter governing the stresses on the dispersed phase droplets (which can lead to droplet break-up) and the frequency of collisions between the dispersed phase droplets (which can lead to coalescence) (Williams et al, 1995).

Water-in-crude oil emulsions can be stable over a period of years, the stability being partly due to bulk viscosity but even where the continuous phase has a low viscosity, stable emulsions are found. In such cases, the stability is primarily the result of interfacial factors (as discussed previously) and these can neatly be combined into the interfacial viscosity (Cairns et al). Thus, the influence of interfacial tension, the electric double layer and the presence of colloidal particles on the stability of an emulsion can be interpreted through the influence each has on the interfacial viscosity (see for example Mohammed et al, 1993). A high interfacial viscosity reduces the rate of the oil film drainage between approaching water droplets and contributes to the resistance to deformation of these droplets and also the critical film thickness at which the droplets finally merge (see for example Lobo et al 1993). The dilational viscosity is also important where the interfacial layer is not rigid (Taylor, 1988).

Any model to predict the probability of disperse phase equilibrium droplet size in a given flow field (in the absence or presence of an electric field), requires knowledge of the bulk and interfacial viscosity. Although the development of such a model is beyond the scope of this thesis, the following is worth recording as it helps clarify understanding of the results presented in Chapter 12.

10.11.1 Emulsion bulk rheology

Emulsions exhibit four different types of basic flow behaviour, namely Newtonian, plastic, pseudo-plastic and dilatant (Shaw, 1975). Flow behaviour can also depend on the time of application of the shearing forces. An emulsion that exhibits decreasing viscosity with time is called thixotropic whilst one that exhibits an increase in viscosity with time is called rheopectic. Dilatant and rheopectic behaviour is not commonly exhibited by emulsions (Belcher, 1977).

Sherman (1955) listed the factors which affect the emulsion rheology and these are as follows:

- Viscosity of the continuous phase (η_c)
- Volume fraction of the dispersed phase (ϕ)
- Viscosity of the dispersed phase (η_d)
- Type of emulsifying agent and presence of interfacial film
- Dispersed phase size distribution
- Electroviscous effects, arising from the resistance to shear of the electric double layer.

Many expressions have been proposed as models for the viscosity of an emulsion that have terms for many of the above factors (see for example Williams, 1989 pp 46-48). Einstein's classical expression is the most simple and is applicable to low volume fraction ($\phi < 0.02$) where there is a no-slip condition at each dispersed phase boundary with the continuous phase, a non-deformable droplet assumption and no double layer effects.

$$\eta = \eta_c \left(1 + 2.5\phi\right) \tag{10.12}$$

For dispersions of non-rigid spheres, as found in most emulsions, the flow lines may be partially transmitted through the dispersed phase droplets and the constant in Einstein's equation becomes less than the 2.5 figure shown.
Extension of the equation to cover higher volume fractions has been attempted by many workers, the best known being that due to Guth and Simha (1935).

$$\eta = \eta_c \left(1 + 2.5\phi + b\phi^2 + ...\right) \tag{10.13}$$

With practical values of b lying in the range 5 to 8.
Expressions that involve the dispersed phase viscosity are few and are only important where dilation (or circulatory flow) of the dispersed phase in present. An expression due to Taylor (1932) is shown in equation (10.14) and is a special extension to Einstein's equation and applies in cases where the boundary is not rigid (Nawab and Mason,1958).

$$\eta = \eta_c \left\{ 1 + 2.5\phi \left[\frac{\eta_d + 0.4\eta_c}{\eta_d + \eta_c} \right] \right\} \tag{10.14}$$

As in Einstein's equation, Taylor's requires that the dispersed phase droplets remain spherical under shear and is valid for low volume fraction. Thus, practically, it is useful for dilute emulsions ($\phi < 0.02$) and small dispersed phase particle size.

The state of dispersion of the dispersed phase can be important, as Sherman pointed out. It is known that homogenization of a coarse emulsion can lead to an increase in its bulk viscosity (Sherman, 1955) and this is probably due to an increased interaction between the dispersed phase droplets which are more numerous and smaller in size (consider the similarity to increased vapor pressure above a highly curved surface (section 10.4). Higher adsorption of charged species or greater packing of amphiphilic molecules at the interface can stabilise the emulsion, stability being increased with increased emulsion viscosity.

An expression, shown below and due to Raja Gopal (1960) contains a term in r_m, the mean droplet radius, as well as a term, S_c, giving an indication of the slippage between the dispersed and continuous phases.

$$\eta = \eta_c \left\{ 1 + \frac{2.5\phi}{(\eta_d + \eta_c)} \left[\eta_d + \frac{2}{5}\eta_c + \frac{2\,\eta_c\,\eta_d}{S_c} \left(\frac{1}{r_m} \right) \right] \right\} \qquad (10.15)$$

CHAPTER 11

INVESTIGATION INTO DISPERSED PHASE COALESCENCE IN A FLOWING WATER-IN-OIL EMULSION UNDER AN APPLIED AC ELECTROSTATIC FIELD

11.1 Experimental Apparatus and Techniques

11.1.1 Overview of the emulsion flow system, and measurement and analysis of coalescence

As outlined in Chapter 9, the investigations presented here were designed to build upon the knowledge accumulated over many years of work in the departments of Electrical Engineering and Mechanical Engineering. Specifically, the task was to examine the dispersed phase size distribution in a variety of emulsions (which were designed to model saline- or water-in-crude oil emulsions) undergoing electrical treatment in a rapidly flowing channel. From knowledge of the emulsion parameters, the flow patterns and the applied field, information pertinent to the design of rapid compact water separation devices could be gained. Larger droplet sizes imply a less stable emulsion and one ripe for rapid phase separation. The kinetics of phase separation in a settling tank, or indeed the practicality of phase separation in a cyclonic device, are both functions of stable droplet size.

The experimental rig used was that described by Williams et al (1995), which was designed and built during work commencing in 1992 by Williams, Bailey and Thew (Williams et al, 1992). The duct within which the electrocoalescence of this study was effected, was of rectangular cross-section, the internal flow channel having cross-sectional dimensions of 20 *mm* in height by 100 *mm* in width. The treatment duct comprised of seven independently electrically activated modules, each of 500 *mm* length (the maximum treatment length being therefore 3500 *mm*). An eighth identically dimensioned module at the downstream end had no electrodes and served doubly as a sampling duct, with three isokinetic sampling pipes, and an

area within which visual phenomena related to the flow properties of the emulsion were observed within the same flow environment as the rest of the duct. The electrodes in the seven treatment modules were positioned on the top and bottom of the duct, and insulated from the flow by 5 *mm* of clear acrylic material, the gap between the electrodes thus being 30 *mm*. For safety, further insulation covered the non-flow gap area of the electrodes on the sides, top and bottom of the coalescer.

The seven electrode pairs could be earthed or energized independently. This enabled studies on the effect of residence time in an electric field on droplet growth to be carried out by selectively energizing electrode pairs. The supply for the applied voltage was a mains transformer operating at a sinusoidal frequency of 50 Hz. The output voltage was controlled by a variac connected in series with the mains supply. The maximum output of the supply was -15 kV to +15kV peak-peak, although at a total peak potential difference across the duct of in excess of 20 kV, shorting across insulating nylon bolts or dielectric breakdown of the insulating acrylic sometimes occurred, especially during studies using saline as the dispersed phase. Chapter 12 sets out electrical considerations for a flowing water-in-oil compact electrocoalescer and shows in all probability that stray current leakage occurred routinely but not enough to effect the actual electric field across the emulsion due to the capability of the power supply to cope with the total current drawn.

The duct was originally conceived to handle maximum flow rates of up to 60 $l\ min^{-1}$ (Williams et al 1995) but, for the purposes of this study, alterations were made to extend that upper limit to 100 $l\ min^{-1}$. The activity to upgrade the rig included reinforcing it with mild steel clamps, the use of silicon gaskets between modules in place of previous rubber gaskets and the general refreshing of nylon bolts and other fatigued elements. The main emulsion pump was upgraded from a 2-stage centrifugal unit to a 4-stage unit (originally a Grundfos CR 2-130 was used, its replacement was a Grundfos CR 4-120). To meet the requirement to test coalescence rates at different temperatures, a thermostatically controlled water bath was installed. Thermostatically heated water was pumped through a copper coil immersed in the emulsion reservoir tank and experiments commenced when the emulsion reached equilibrium temperature. Experiments were conducted at 25^0 C and 50^0 C on model emulsions (to be described shortly) to assess the effect of temperature on coalescence. Temperature affects both the system's stability and its flow parameters, especially viscosity (see section 10.11). Other key factors investigated were dispersed phase conductivity, water cut and applied electrostatic field.

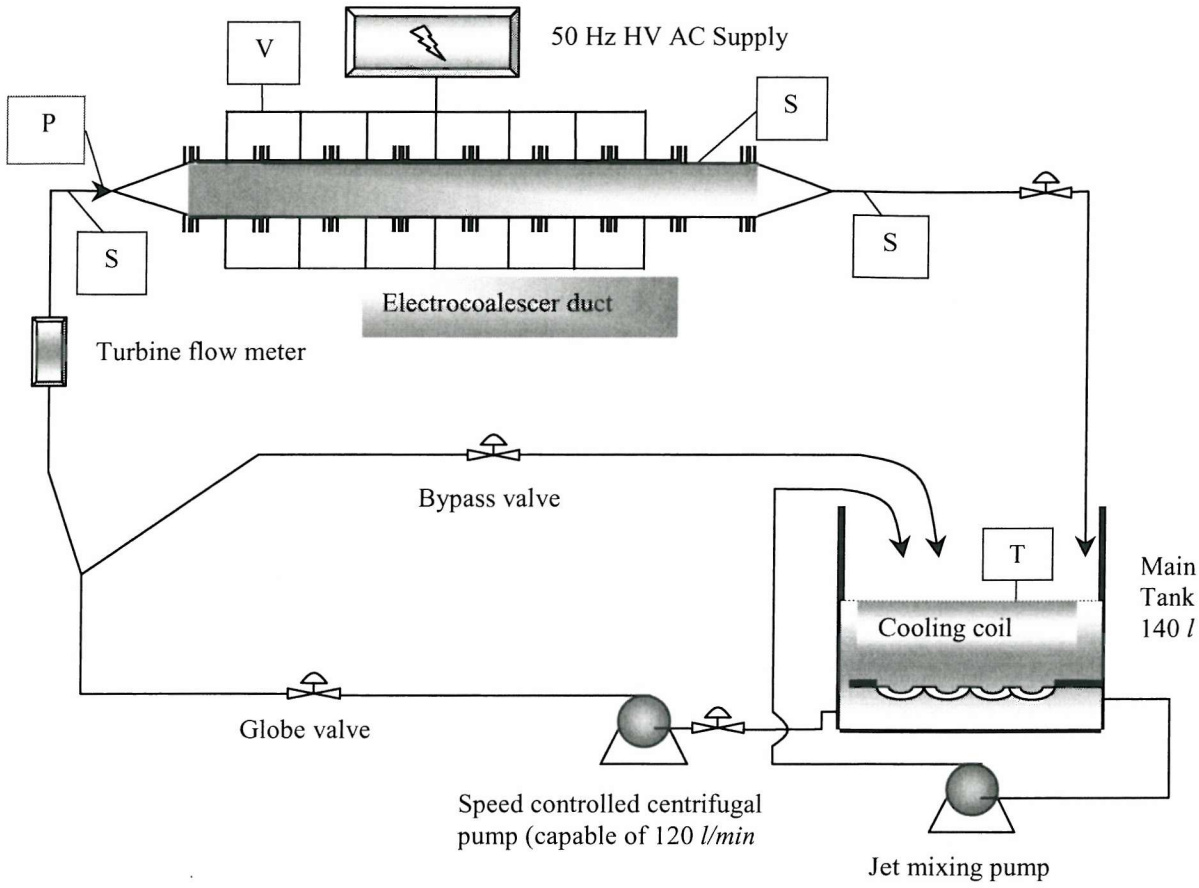

Figure 11.1 Schematic of electrocoalescer duct with recirculating emulsion flow system.

Key: S = Isokinetic sample position; P = Pressure gauge; T = Thermometer; V = RMS Voltmeter.

11.1.2 Schematic of the Compact Electrocoalescence Device

Figure 11.1 shows a schematic of the rectangular duct described above. The steel reservoir tank, of volume approximately 140 *l*, was coated with protective acrylic-based paint to prevent its corrosion and potential contamination of the emulsion.

Experiments were run with an approximate emulsion volume of between 50 to 80 *l*, dependent on the desired water-cut. The hold up around the pump circuit of pipe work and duct was estimated to be about 17 *l* and it was important to maintain sufficient head in the tank to prevent air entering the pump circuit.

To ensure that the emulsion entering the duct had constant water-cut (equivalent, of course to the planned overall water cur for the experiment), the reservoir tank (where free water drop out could on occasion occur) was agitated with either a separate jet-mixing pumping loop or via a return from the main pump. The main input energy into the emulsion before entry into the duct came from two sources. Passage through the centrifugal pump effectively mixed the two phases and a downstream globe valve could be set to vary the pressure drop across it so that, at the same effective flow rate, the emulsion could be made to experience different levels of shear across the valve. Thus, it was possible to control the initial inlet droplet size distribution of the dispersed phase. Davies (1984) discusses the outlet droplet sizes of emulsions undergoing high shear across globe valves and other turbulent energy dissipation devices.

11.1.3 Emulsion Sampling and Dispersed Phase Droplet size Measurement Procedures

The sampling technique and droplet sizing technique used in this work were similar to those developed by Williams et al (1992) and Sinker (1995). Basically, isokinetic samples of the emulsions at various points in the flow were taken, diluted in pure continuous phase and by the use of a specially designed cell, the dispersed phase droplet size distribution was measured using a Malvern 2600C Laser Particle and Droplet Sizer. The inlet or outlet sample port[12] to be used was firstly flushed by running emulsion through it for a few seconds during steady operation of the system. A clean 250 *ml* conical flask, with 100 *ml* of clean continuous phase oil (see section 11.2 for explanation of the model emulsion used in this study) was then used to collect approximately 1 *ml* of sample from the sample stream. The dilution factor of 100 to 1 was required to avoid the effects of multiple scattering of the laser beam during the size measuring procedure (Williams et al, 1992). At the sort of size distributions in question (1-500 μm) and with the type of flow cell used for measurement, a dispersed phase concentration of greater than about 0.25% can cause multiple scattering of the laser and give erroneous results. The dependency of the required dilution factor upon the dispersed phase concentration meant that the sample volume was varied in accordance with the total water cut in the emulsion under investigation.

The technique of taking correct sample volume at varying total emulsion flow rates was perfected through practice and verified by repeat measurements. On an individual basis, the

[12] For outlet sampling, it was found that samples taken from the exit pipe location provided much better representation of the flow than samples from module 8, hence this was used in the results presented here.

success of the method was evident immediately by the obscuration data output from the laser measurement device. Providing this parameter lay between 0.05 to 0.5, the sample was in a range for which the data could be accepted (Malvern Instruments Ltd., 1991).
Wayth (1999) gives further details of the Malvern instrument and expands upon the measurement routine employed in this study. Figure 11.2 shows a schematic of the fixture. The use of the peristaltic pump to draw the diluted sample through the flow cell is necessary to achieve as near constant residence time for each droplet size band as possible. This helps prevent biasing of the results toward smaller droplet sizes. Preparation of the fixture before sampling involved ensuring the flow cell was cleaned of internal surface contamination, correction of the laser system for background light scattering and ensuring a clean oil interface was above the flow cell window.

The various steps in the technique needed to be well practiced for the sake of accuracy and repeatability. Of particular concern was the need to prevent either droplet coalescence or indeed break-up during handling and measurement. The diluted sample was pored gently into the funnel from whence it flowed into the outlet pipe until it met the interface of clean oil. As soon as any entrained air bubbles had disappeared, the peristaltic pump (a Cole Palmer) was turned on and the Malvern set running.

Following the recommended practice of Williams et al (1992), the software was set to take a series of 10 measurements of 1500 sweeps each. The 10 measurements were then inspected for inconsistency (often either the first or last held spurious data due to starting the measurement routine too early or because the sample had flowed entirely past the measuring window), averaged and saved. The VMD was taken as the most representative statistic for data comparisons and analysis, although following the example of Karabelas (1978), the $D_{0.1}$ and $D_{0.9}$ were used as experimental values for the stable equilibrium minimum droplet size and maximum droplet size respectively.

11.2 Model Emulsion

Practicality and safety concerns dictate the need to use a model emulsion to simulate saline- or water-in-crude oil emulsions in most laboratory studies of this nature.
Williams et al (1992) had used tap water-in-kerosene as a model emulsion for early important studies but had to work under the strain of biological attack on the oil phase. Despite the use of a biocide, an alternate emulsion was sought and a system of tap water-in-gas oil (a

distillate) stabilised with a very small percentage of *Span 80* a sodium monoleate surfactant produced by ICI was hit upon (Williams et al, 1995, Urdahl et al, 1995).

It was expected that this study would continue to use this latter design but for some reason, attributable perhaps to variations between newer batches of gas oil to that in the studies referenced above (see Wayth, 1999, p90), problems were encountered. A cloudy aqueous phase resulted when the emulsion was resolved into its two major components indicating that an inverted w/o emulsion was partially formed (see Figure 10.7). Investigations were carried out to understand the root cause of the shift in behaviour but it became clear early on that a fresh emulsion design was needed.

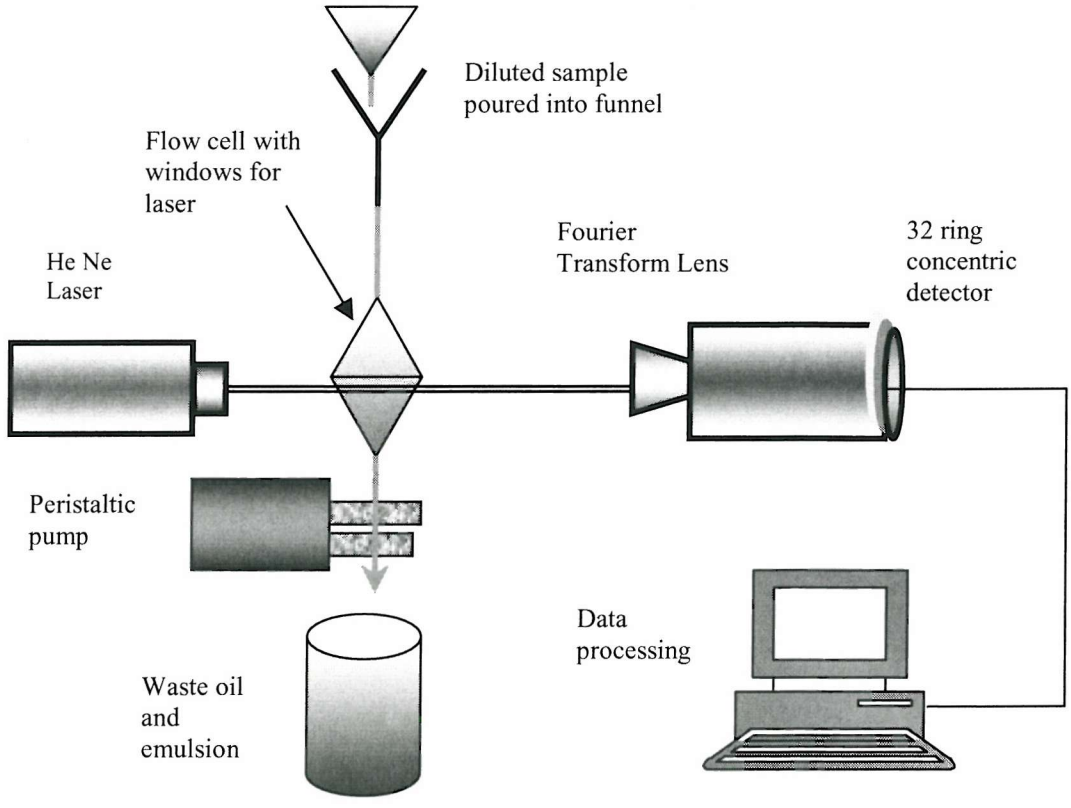

Figure 11.2 Malvern based dispersed phase droplet sizing schematic

After trials with mainly non-ionic surfactants, a nonylphenol non-ionic surfactant (from ICI's Synperonic range called Synperonic NP2 a clear viscous liquid) at a concentration of 2.5% by volume to the oil phase was selected. This system gave properties equivalent to a low to medium stability water-in-crude oil emulsion and its use was approved by sponsors, Statoil, for these experiments.

The criteria used to judge the emulsion quality and match it to a real oil system (Wayth, 1999, Chapter 5) were:

1. Stability across water cuts from 1% to inversion. This was judged by settling times either under gravity of under gravity and a resolving electrostatic field.
2. The interfacial tension between the phases. Water-in-crude oil systems tend not to vary beyond around 24-30 mNm^{-1}.
3. The viscosity of the emulsion and its trend against temperature.
4. The clarity and condition at the interface of the subsequently resolved phases.
5. The stability over time of the model emulsion.

The properties of the model emulsion used in this study are set out in Table 11.1 and compared against the properties of saline-in-crude oil emulsion from Statoil's Yme field[13] from the Norwegian sector of the North Sea (Block 9/2).
The data for the YME crude is reproduced, with the author's kind permission, from Wayth (1999).

Fluid system	**Mass Density** gcm^{-3}	**Viscosity** $mPa\ s$	**Surface Tension** mNm^{-1}	**Interfacial Tension*** mNm^{-1}
Pure Gas Oil	0.852	4.6	37	16
Gas Oil + 2.5% v/v NP2	0.855	4.9	38	14
Yme Gamma	0.818	8.6	37	25
Yme Gamma 60^0 C	0.802	3.2	35	24

Table 11.1 Measured Properties of the model emulsion system compared with Yme Gamma West Crude

* Against water

All measurements taken at 25^0 C. Viscosity measured at a shear rate of 73.4 s^{-1} using a Brookfield Cylinder Viscometer

[13] Statoil have experienced difficulties removing the highly saline (0.5-1.7 $mg\ l^{-1}$ produced water from the crude oil. Indeed, the exported oil has often fallen short of the design contaminant removal specification resulting in financial penalty (Wayth, 1999).

11.3 Experimental Results

The results presented here cover droplet growth in the duct of the dispersed phase of the model emulsion under the following matrix of parameters:

Parameter	Values tested
Temperature	25, 50 (^0C)
Water cut	1, 5, 15, 30 (%)
Salinity	0 (tap water) and salinity of 4, 8 and 12 (%)[14]
Flow rate in duct	20, 40, 60, 80, 100 ($l\ min^{-1}$)
Applied voltage	0, 7.5, 12.5, 17.5 ($kV\ pk\text{-}pk$)

11.3.1 Effect on dispersed phase exit VMD of flow rate and electrostatic field at 1% water cut

Shown here are results obtained at an emulsion temperature of $25^0\ C$ at water cut of 1%. Conditions across the inlet valve were such as to produce both high and low shear and hence the influence of inlet droplet size distribution could be investigated. The total flow rate of the emulsion through the duct was varied from 20 to 100 $l\ min^{-1}$ in a series of runs and the applied voltage varied from 0 to 17.5 kV at each flow rate. Figure 11.3 shows the results at all applied voltages whilst, for clarity, figure 11.4 only shows results at 12.5 kV, the trend being similar at the other voltages.

As stated above Figure 11.4 shows the effect that inlet droplet size has on the outlet droplet size across the flow rates studied. Data are shown for no applied voltage and for the case of 12.5 kV applied voltage. As can be seen, within the overall accuracy of the technique, what emerged, surprisingly, was that the final outlet VMD had no strong dependency on the inlet droplet size distribution.

Figure 11.5 shows the results for the outlet VMD of the emulsion at temperature of 50^0 C. Increase in temperature, as noted earlier, lowers the stability of the emulsion by decreasing the continuous phase viscosity. The viscosity change will alter the bulk flow properties also, as expressed by Reynolds number. Thus at the same flow rate, the Reynolds number will be

[14] Artificially made up from pure salts mixed in the ratio of a typical formation water at dissolved into the emulsion at the approximate concentration of the Yme field.

lower and hence delay the onset of turbulence and the degree of laminar or turbulent mixing will decrease, along with the energy required to maintain the flow.

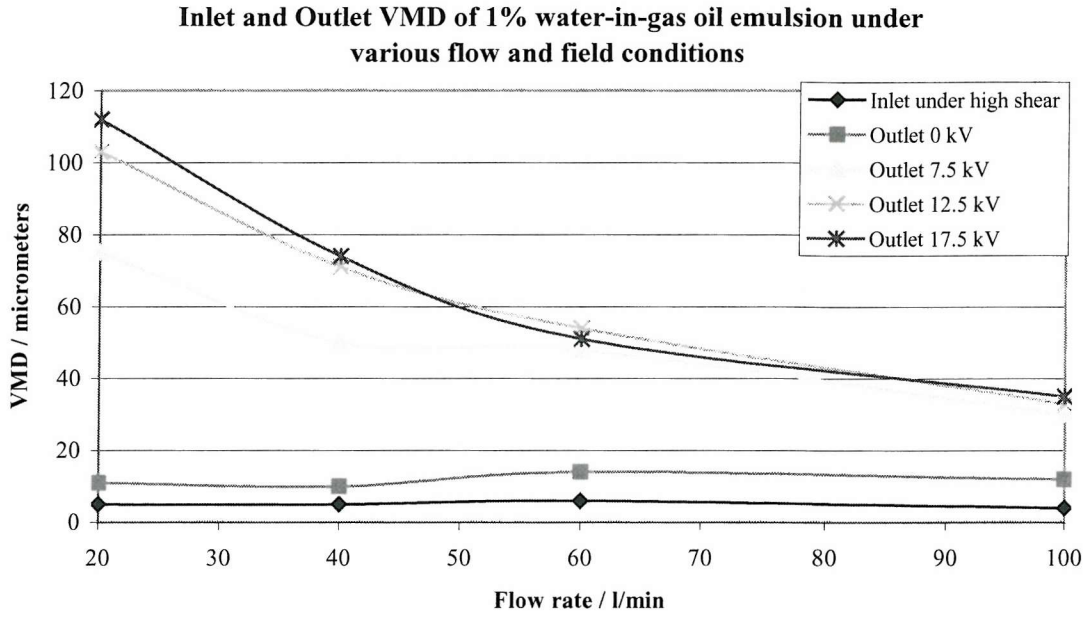

Figure 11.3 Results at 1% water cut, 25 ^{0} *C*

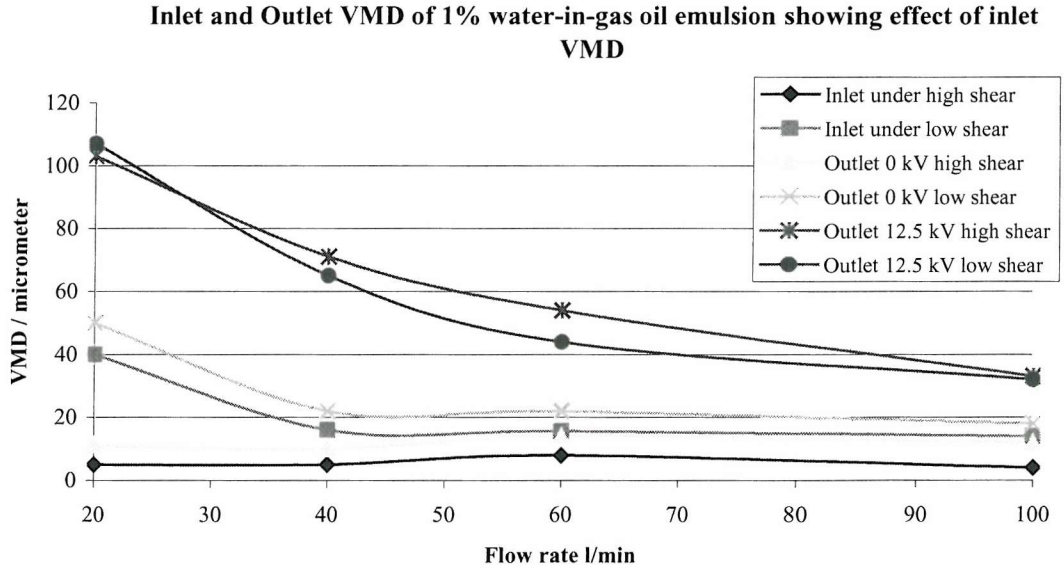

Figure 11.4 Results at 1% water cut, 25 ^{0} *C* showing negligible effect on outlet VMD in this emulsion system on inlet VMD at levels investigated.

Figure 11.6 shows a direct comparison between the outlet droplet sizes at the two temperatures at no applied voltage and a voltage of 12.5 kV. As can be seen, no significant difference is noted apart from slightly larger outlet VMD with no applied field.

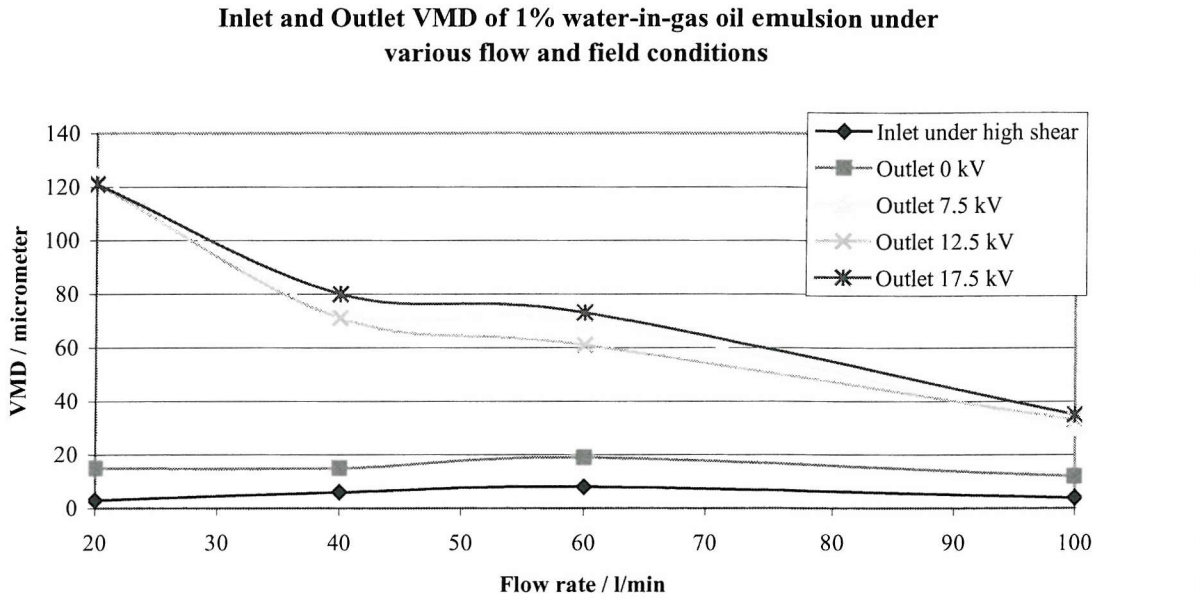

Figure 11.5 Results at 1% water cut, 50 ^{0} C

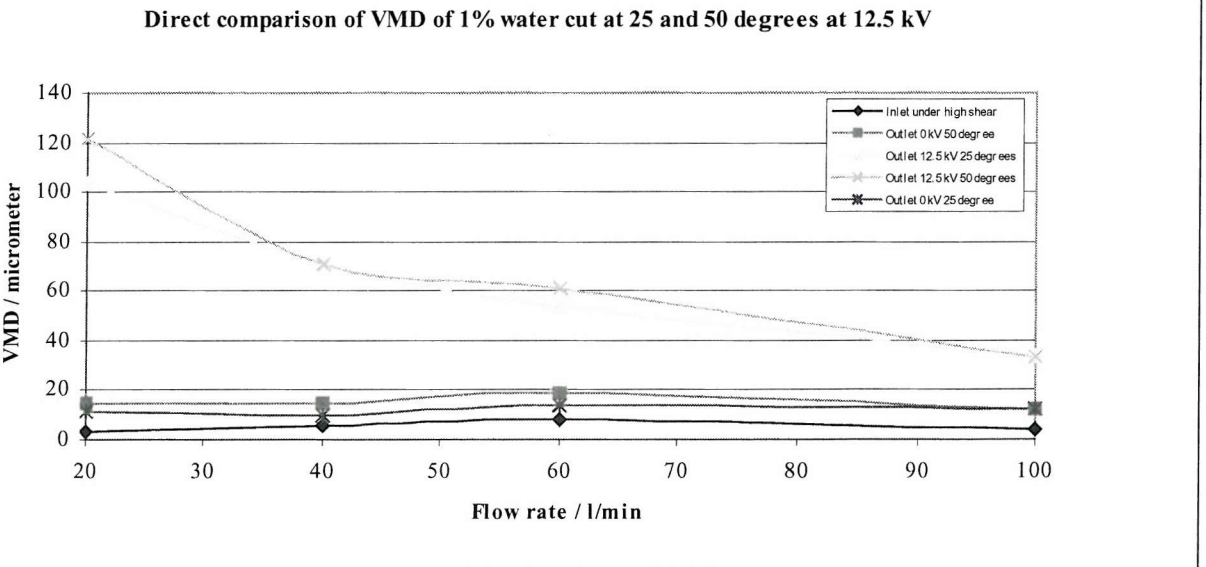

Figure 11.6 Results at 1% water cut, 25 and 50 ^{0} C with zero and 12.5 kV.

11.3.2 Effect on dispersed phase exit VMD of flow rate and electrostatic field at 5% water cut

Figure 11.7 shows the effects of flow rate and applied voltages on the exit VMD of the model emulsion at 5% water cut. The trend is similar to that observed in Figure 11.3 with the VMD at the three applied voltages being quite consistent at each of the higher flow rates examined, with only the VMD at low flow rates showing what could be called an electric field dependency.

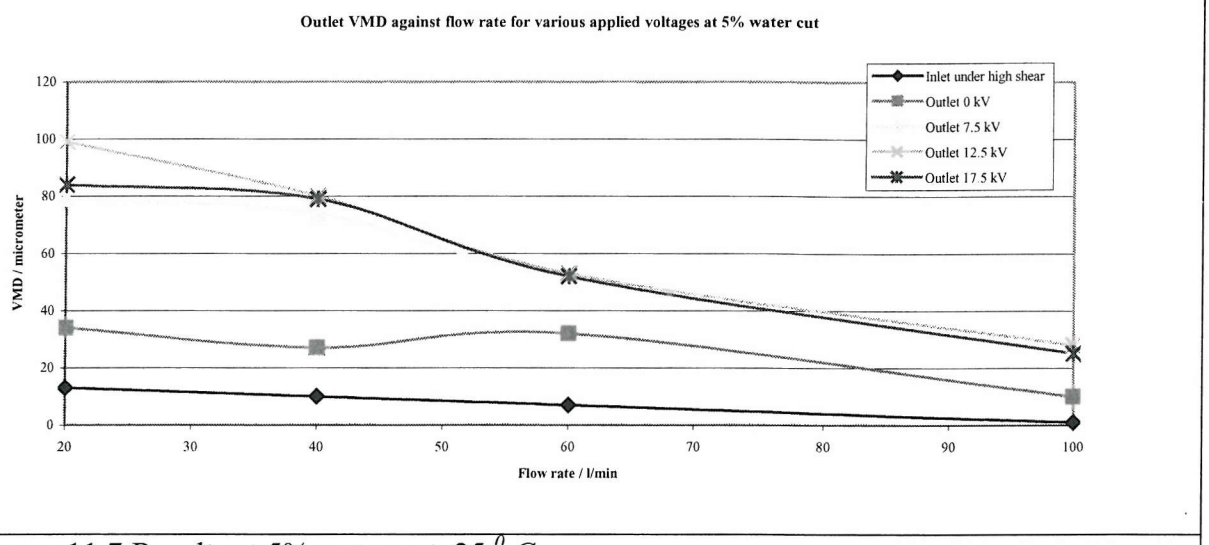

Figure 11.7 Results at 5% water cut, 25 ^{0} C

A direct comparison between the findings at 1% and 5% water cut at zero applied voltage and 12.5 kV is shown in Figure 11.8. Once again, as with temperature, it is immediately evident that the VMD shows little dependency on water cut at any of the flow rates and applied fields investigated. With no field applied, the outlet VMD at the higher water cut does show a dependency upon water cut up to 60 $l\ min^{-1}$ but at 100 $l\ min^{-1}$ it is seen that the outlet VMDs are equal.

Further analysis on the results presented to this point can be developed by reference to theories developed by Williams et al (1995) and Wayth (1999) as well as from other sources, most of which are referenced within the above works. It is beyond the scope of this thesis to develop such analysis.

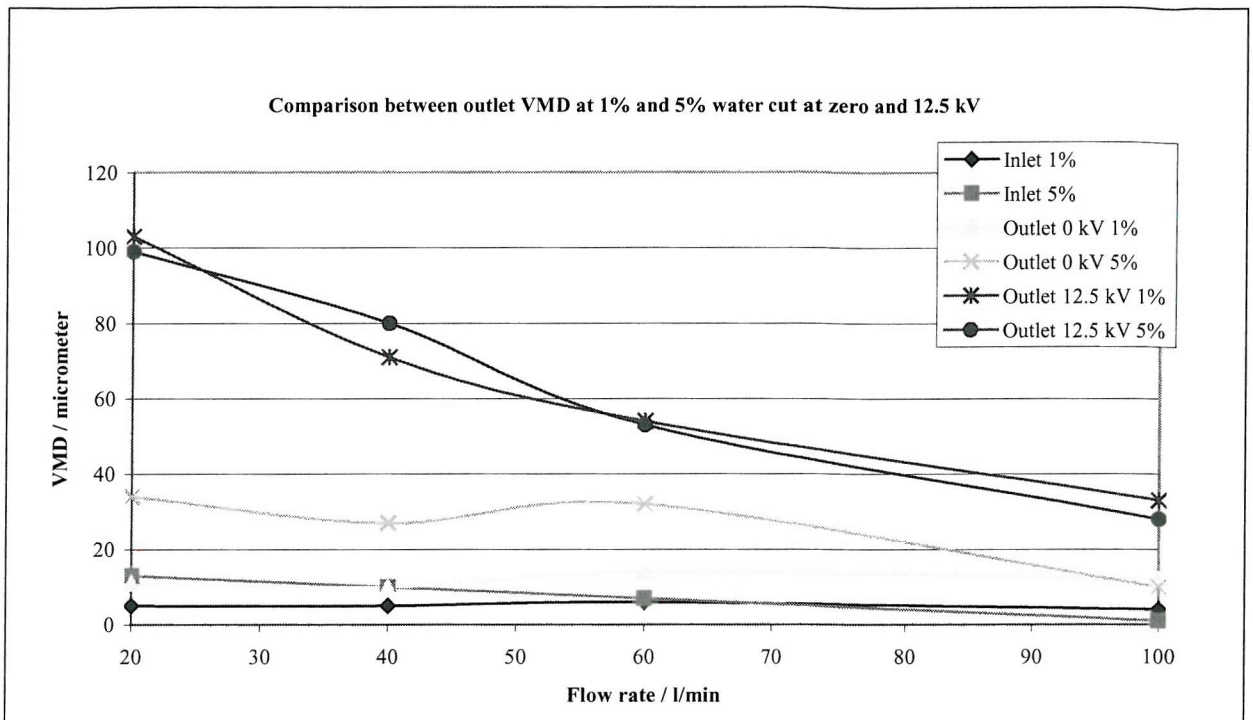

Figure 11.8 Comparison of results at 1% and 5% water cut, 25 ^{0} *C* and 12.5 *kV*.

11.3.3 Effect of dispersed phase salinity

It was felt important to assess the performance of the electrocoalescer on an emulsion with dispersed phase highly conductive and representative of produced water which is saline in nature. The conductivity of the emulsion will increase with increased dispersed phase conductivity but only marginally at low frequency of operation. Deviations to this rule are usually explained by the presence of polar groups within the oil phase, partial solubility of the dispersed phase in the oil and even partial migration of salt ions into the oil phase (Sowa et al, 1995).

To simulate saline, the following salts were made up in the ratios shown and dissolved into the dispersed phase.

For expediency, outlet droplet sizes were measured at flow rates of 40 and 100 $l\ min^{-1}$ at zero and 12.5 *kV* only. Most noticeable, is the effect that salt had on the outlet VMD at the 40 $l\ min^{-1}$ flow rate with no applied voltage. This is assumed here to be due to the increased density of the dispersed phase, as well as perhaps destabilisation of the emulsion. The growth with applied potential seems robust against changes in salinity, within the level of confidence achieved with these techniques. This is an encouraging result.

Salt	4 % w/w	8 % w/w	12 % w/w
$CaCl_2 + 2\ H_2O$	9.07	18.14	27.21
$MgCl_2 + 6\ H_2O$	1.79	3.58	5.37
$BaCl_2 + 2\ H_2O$	2.065	4.13	6.20
$SrCl_2 + 6\ H_2O$	1.32	2.64	3.96
KCl	1.51	3.01	4.52
NaCl	50.62	101.24	151.86
$NaHCO_3$	0.415	0.83	1.25

Table 11.2 Synthetic formation water in grammes per litre at investigated salinity levels

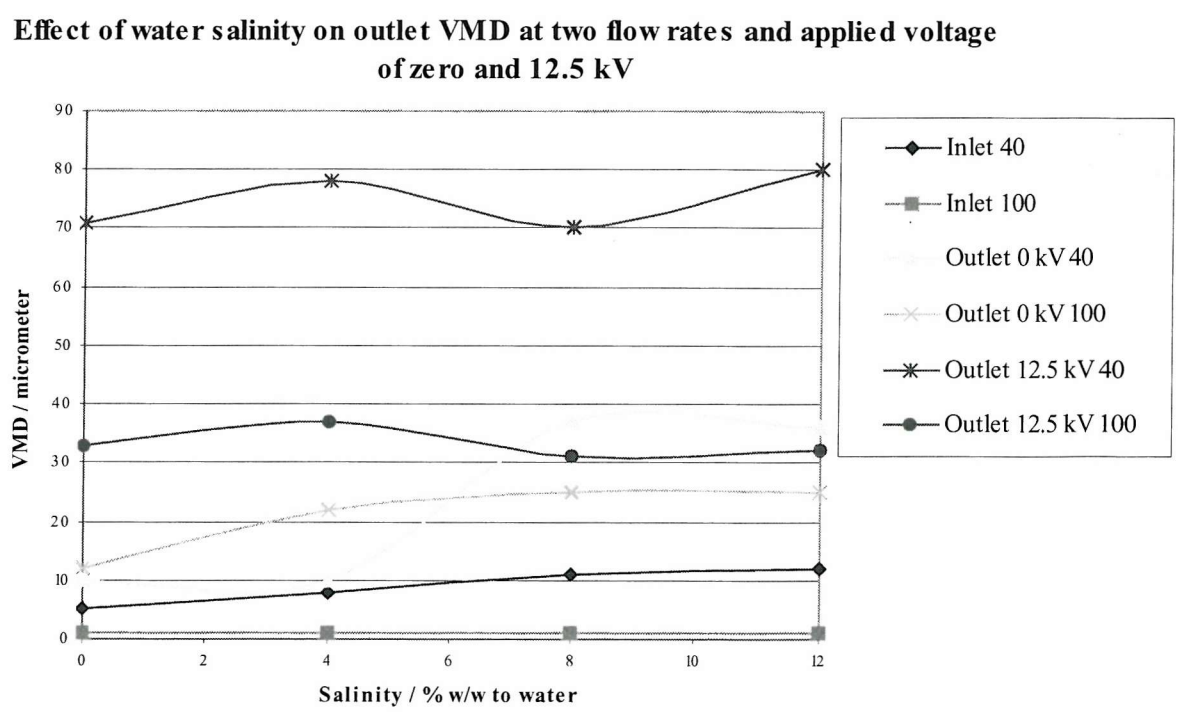

Figure 11.9 Effect of dispersed phase salinity on outlet VMD.

11.3.4 Effect on dispersed phase of flow rate and electrostatic field at higher water cut

At the higher dispersed phase concentrations investigated (15% and 30%), quantitative evaluation of the coalescer duct proved difficult. With applied voltage of even 7.5 kV, a layer of free water built up along the bottom of the duct and was especially noticeable at the lower flow rates. The power of the device to rapidly break the emulsion was therefore evident as without an applied field virtually no drop-out was noted.

CHAPTER 12

ELECTRICAL AND ELECTROSTATIC CONSIDERATIONS FOR A FLOWING WATER-IN-OIL COMPACT ELECTROCOALESCER.

Summary

The AC electrical characteristics of an insulated electrode and flowing emulsion system have been analysed. The key equations are detailed here along with the important assumptions in their derivation. The approach taken is similar to that of Williams (1989). Here, an attempt is made to not over complicate the analysis and to highlight the essential physical facts, which govern the overall behaviour, and to present the findings with some graphical interpretations.

12.1 Electrical Properties of a W/0 Emulsion

The application of an electric field to a dispersion or emulsion within an electrocoalescer having insulated electrodes is a difficult situation to analyse. Fortunately, it is possible to consider the dispersion independently of the electrocoalescer and power supply. This is because a dispersion of water in oil has a natural frequency that is generally greater than that of the combined system of dispersion, electrocoalescer and power supply.

To account for dielectric dispersion due to interfacial polarization in an ac field (so-called Maxwell-Wagner dispersion (Jones, 1979)) the need arises to introduce a complex form of the dielectric constant:

$$\kappa = \kappa' - j\kappa'' \tag{12.1}$$

Or

$$\kappa = \kappa' - j\frac{\sigma}{\varepsilon_0\,\omega} \tag{12.2}$$

Where κ is the absolute complex permittivity of the emulsion, κ' is the real part of κ and represents the pure capacitive element, κ'' is the dissipative element, ω is the angular frequency of the applied voltage, σ is the real conductivity of the emulsion and ε_0 is the permittivity of free space.

A capacitor filled with an emulsion of complex conductivity κ has a real capacitance κ' times greater than would have a capacitor with the same electrodes in a vacuum. The emulsion filled capacitor would also have a power dissipation per unit volume at each point when, resulting from an applied voltage, an electric field of frequency ω and RMS value E *V/m* exists at that point. This power dissipation is given by the expression:

$$W = \omega E^2 \kappa'' \tag{12.3}$$

Although κ' is frequency dependent, Hanai (1967) has shown that for operation at low frequency (less than the natural electrical dispersion frequency of the emulsion) a simple expression for κ' can be used:

$$\frac{\kappa_e'}{\kappa_o'} = \frac{1}{(1-\phi)^3} \tag{12.4}$$

and a similar expression for the emulsion conductivity also exists:

$$\frac{\varepsilon_e}{\varepsilon_o} = \frac{1}{(1-\phi)^3} \tag{12.5}$$

Where κ_e' is the permittivity of the emulsion, κ_o' is the permittivity of the pure oil phase, σ_e is the conductivity of the emulsion, σ_o is the conductivity of the pure oil phase and ϕ is the volume ratio of water in the emulsion (hold-up)

To use the above expressions in a practical sense, two points must be taken into account. One is that the pure conductivity and permittivity values for the oil phase should not in fact be used but rather the experimentally determined values for the oil after it has been in contact with water. Partial solution of water in the oil will have an appreciable effect on the oil's apparent electric properties; once determined, these values can be used to determine how the emulsion's electrical properties vary with water hold-up.

The second is that, in the derivation of the above, a number of assumptions are made. The chief assumptions are that the electrical conductivity and permittivity of the dispersed water phase are very much greater than those of the continuous oil phase. This is true for the system described in section 11.2 where the following values hold:

Fluid	σ / Sm^{-1}	κ'_r
Gas Oil after contact with water	1×10^{-9}	2.3
Distilled Water[15]	5×10^{-4}	80

Table 12.1 Conductivity and permittivity of emulsion phases

The above expressions are independent of the dispersed phase size spectrum which, in fact, may not be the case (Williams, 1989) but in the interests of clarity and absence of a more suitable model, this factor will be ignored.

12.2 Bulked electrical model of the system

In Figure 12.1, R represents the internal resistance of the power supply, V_s being the supply voltage. Subscript p refers to the perspex insulation and $\boldsymbol{E}_p$ and $\boldsymbol{E}_e$ are the instantaneous field strengths in the perspex and emulsion respectively. It can be shown that the insulators can be lumped together with thickness d_p (where d_p represents the combined or total perspex thickness) as $\boldsymbol{E}_p$ is equal in each layer of the insulation.

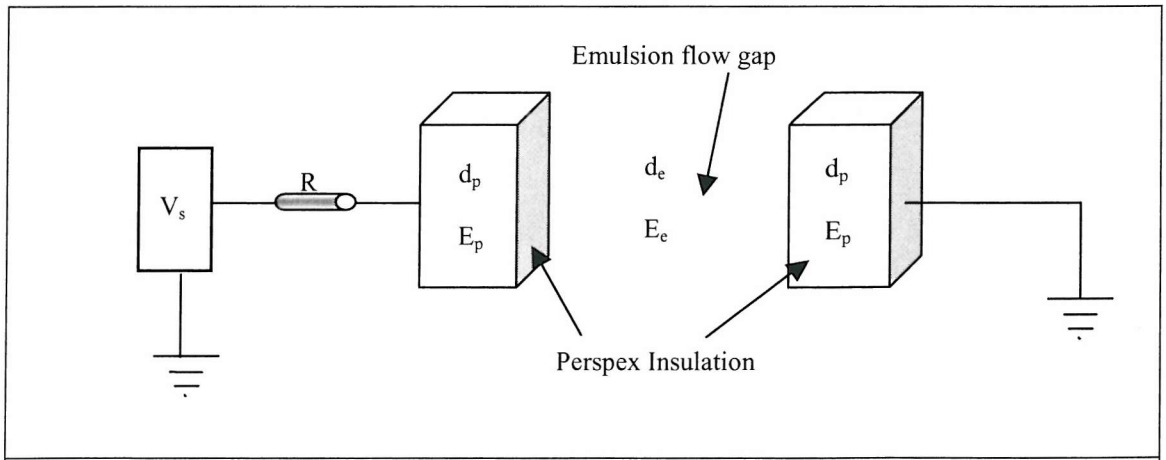

Figure 12.1 Schematic of coalescer module showing main electrical elements

[15] Distilled water; with salt present, the conductivity of the dispersed phase will increase by up to 3 orders of magnitude.

Thus the potential can be expressed as:

$$V = d_p E_p + d_e E_e \tag{12.6}$$

Since the field is uniform and using Gauss's Law and the equation for charge continuity:

$$\left(\kappa_e' d_p + \kappa_p' d_e\right)\frac{dE_e}{dt} + \left(\sigma_e d_p + \sigma_p d_e\right)E_e = \sigma_p V + \kappa_p' \frac{dV}{dt} \tag{12.7}$$

Equation (12.7) is a first order differential equation if V is a known function of time. The natural frequency of the *system* may be determined from the coefficients of the homogeneous form of (12.7):

$$\omega_s = \frac{\sigma_p d_e + \sigma_e d_p}{\kappa_p' d_e + \kappa_e' d_p} \tag{12.8}$$

This can be related to more familiar frequency or time characteristics such as the RC time constant from consideration of the physical resistances and capacitances of the module:

$$R_p = \frac{d_p A}{\sigma_p} \quad ; \quad R_e = \frac{d_e A}{\sigma_e} \tag{12.9}$$

$$C_p = \frac{\kappa'_p A}{d_p} \quad ; \quad C_e = \frac{\kappa'_e A}{d_e} \tag{12.10}$$

Where A is the electrode area.

As the resistances and capacitances are in series:

$$R_s = R_p + R_e \quad ; \quad \frac{1}{C_s} = \frac{1}{C_p} + \frac{1}{C_e} \tag{12.11}$$

and with $\frac{1}{\tau_s} = \frac{1}{R_s C_s} = \omega_s$ we have:

$$\omega_s = \frac{\frac{1}{R_p} + \frac{1}{R_s}}{C_p + C_s} \tag{12.12}$$

Returning to (12.7), V and V_s, are related by:

$$V_s - V = iR \tag{12.13}$$

The expression for i is:

$$i = A\sigma_p E_p + A\kappa'_p \frac{dE_p}{dt} = A(\sigma_p E_p + \kappa'_p \frac{dE_p}{dt}) = A(\sigma_e E_e + \kappa'_e \frac{dE_e}{dt}) \tag{12.14}$$

Thus:

$$V_s - V = AR(\sigma_e E_e + \kappa'_e \frac{dE_e}{dt}) \tag{12.15}$$

Eliminating V from (12.7) using (12.15) gives:

$$\frac{d^2 E_e}{dt^2} + L\frac{dE_e}{dt} + ME_e = \frac{\sigma_p V_s}{\kappa'_p \kappa' AR} + \frac{1}{\kappa'_e AR}\frac{dV_s}{dt} \tag{12.16}$$

Where:

$$L = \frac{\kappa'_p d_e + \kappa_e d_p + AR(\kappa'_p \sigma_e + \kappa'_e \sigma_p)}{\kappa'_p \kappa'_e AR} \approx \frac{\kappa'_p d_e + \kappa'_e d_p}{\kappa'_p \kappa'_e AR} \tag{12.17}$$

and

$$M = \frac{\sigma_p d_e + \sigma_e d_p + \sigma_e \sigma_p AR}{\kappa'_e \kappa'_p AR} \approx \frac{\sigma'_e dp}{\kappa'_e \kappa'_p AR} \tag{12.18}$$

12.3 AC Excitation

If we excite the system with a potential waveform of the type:

$$V_s - V_o \cos \omega t \tag{12.19}$$

where V_0 is the maximum amplitude delivered by the supply and ω is the phase angular frequency in radians per second, we can find a steady state solution of (12.16) by the usual methods of second order ordinary differential equations by trying as a solution:

$$E_e = B\cos\lambda\cos\omega t - B\sin\lambda\sin\omega t \tag{12.20}$$

or

$$E_e = G\cos\omega t + H\sin\omega t \tag{12.21}$$

$$E_e = B\cos(\omega t + \lambda) \tag{12.22}$$

We can immediately see from (12.20) to (12.22) that the electric field *in the emulsion* has a phase angle of $\lambda = \arctan\left(\frac{H}{G}\right)$ and an amplitude B where:

$$B(\omega) = \frac{V_0}{\kappa_e \kappa_p RA}\left[\frac{\sigma_p^2 + \kappa'_p\omega^2}{(M-\omega^2)^2 + L^2\omega^2}\right] \tag{12.23}$$

And λ is the phase angle between the applied voltage and the electric field in the emulsion.

At low frequencies B(ω) has a low value. As frequency increases B(ω) rises to a maximum then decays to zero. At dc excitation:

$$B(0) = \frac{V_0\sigma_p}{\kappa'_p\,\kappa'_e RAM} = \frac{V_o\sigma_p}{\sigma_p d_e + \sigma_e d_p + \sigma_e\sigma_p\, AR} \approx \frac{\sigma_p V_o}{\sigma_e d_p} \tag{12.24}$$

This low value is due to interfacial polarization, and as can be seen is highly dependent on the resistance per unit area of the perspex insulation. The reason for low amplitude at high frequency however is due to the inability of the power supply to switch electric energy (and therefore deliver current) at high frequency, due to its intrinsic resistance.

For an *ideal* power supply, where R =0:

$$B(\omega) = \frac{V_0\kappa'_p}{\kappa_p d_e + \kappa'_e d_p}\left[\frac{\omega_p^2 + \omega^2}{\omega_s^{\,2} + \omega^2}\right]^{\frac{1}{2}} \tag{12.25}$$

here $\omega = \frac{\sigma}{\kappa'_p}$, is the natural frequency of the perspex insulator. As ω increases

$$B(\infty) = \frac{V_0 \kappa'_p}{\kappa_p d_e + \kappa'_e d_p} \tag{12.26}$$

For the real case, it can be shown that the electric field magnitude in the emulsion occurs at a supply frequency given by:

$$\omega_m \approx M^{\frac{1}{2}} \tag{12.27}$$

and that this magnitude corresponds favourably with (12.26).

12.4 Current and Power Requirements

From equations (12.13) and (12.14):

$$i \approx A\left(\sigma_e E_e + \kappa_e \frac{dE_e}{dt}\right) = \frac{V_s - V}{R} \tag{12.28}$$

and from equation (12.22):

$$E_e = B\cos(\omega t + \lambda) \tag{12.29}$$

The current can be expressed as:

$$i = AB\left[\sigma_e \cos(\omega t + \lambda) - \kappa'_e \omega \sin(\omega t + \lambda)\right] \tag{12.30}$$

The above equation can be conveniently modified to a single cosinusoidal component with an additional phase angle given by $\lambda = \arctan\left(\frac{\kappa'_e \omega}{\sigma_e}\right)$

$$i = AB\left[(\sigma^2{}_e + \kappa'^2_e \omega^2)^{\frac{1}{2}} \cos(\omega t + \lambda + \psi)\right] \tag{12.31}$$

The phase angle ψ is the angle between the electric field $\boldsymbol{E}_e$ and the current $\boldsymbol{i}$. $\lambda + \psi$ is the phase angle between the applied voltage and the current.

It can be assumed, for low frequency, R = zero and use made of equation (12.31) to determine $\boldsymbol{i}$ in this case. This value for the current can then be used to estimate W, the power dissipated in the coalescer with $V = V\cos(\omega t)$ exciting the electrodes.

In equation (12.31), B and λ are functions of R but returning to (12.21) to obtain an expression for G and H as R goes to zero:

$$G = \frac{V_0(\sigma_p X + \kappa'_p Y\omega^2)}{X^2 + Y^2\omega^2} \tag{12.32}$$

$$H = \frac{V_0\omega(\sigma_p Y - \kappa'_p X)}{X^2 + Y^2\omega^2} \tag{12.33}$$

Where

$$X = \sigma_p d_e + \sigma_e d_p \quad ; \quad Y = \kappa'_p d_e + \kappa'_e d_p \tag{12.34}$$

and

$$\lambda = \arctan\left(-\frac{H}{G}\right) \tag{12.35}$$

The RMS power is given by:

$$W = \frac{\omega}{2\pi}\int_0^{\frac{2\pi}{\omega}} iV\,dt \tag{12.36}$$

Which is, in this case:

$$W = \frac{\omega}{2\pi}\int_0^{\frac{2\pi}{\omega}} ABV_0\,(\sigma_e^2 + \kappa'^2_e\omega^2)^{\frac{1}{2}}\cos(\omega t)\cos(\omega t + \lambda + \psi)\,dt \tag{12.37}$$

$$W = \frac{ABV_0}{2}(\sigma_e^2 + \kappa'^2_e\omega^2)^{\frac{1}{2}}\cos(\lambda + \psi) = \frac{1}{2}V_0\,i_{\max}\cos(\lambda + \psi) \tag{12.38}$$

From (12.38), $\cos(\lambda + \psi)$ is the power factor for the system.

Now,

$$W = \frac{AV_0}{2}(\sigma_e^2\kappa'^2_e\omega^2)^{\frac{1}{2}}(G\cos\psi + H\sin\psi) \tag{12.39}$$

but $\tan\psi = \kappa'_e\omega / \varepsilon_e$ hence:

$$W = \frac{AV_0}{2}(G\sigma_e + H\kappa'_e\omega) \tag{12.40}$$

With G and H given by equations (12.32) to (12.34), we have finally after algebraic manipulation (where the internal resistance of the power supply is neglected, practically valid for lower frequency as the system current is mainly a displacement current rather that a conduction current):

$$W = \frac{AV_0^2}{2}\left[\frac{d_p\sigma_p(\sigma_e^2+\kappa'^2_e\omega^2)+d_e\sigma_e(\sigma_p^2+\kappa'^2_p\omega^2)}{(\sigma_p d_e+\sigma_e d_p)^2+(\kappa'_p d_e+\kappa'_e d_p)^2\omega^2}\right] \tag{12.41}$$

If we assume that the perspex is a perfect insulator, then $\sigma_p = 0$ and with ω_s from equation (12.8) we have:

$$W_{pi} = \frac{AV_0^2}{2(\omega_s^2+\omega^2)}\left[\frac{\omega^2 d_e\sigma_e\kappa'^2_p}{\kappa'_p d_e+\kappa'_e d_p}\right] \tag{12.42}$$

The power dissipated per unit volume of the emulsion is then:

$$W_{pi} = \frac{W_{pi}}{Ad_e} = \frac{V_0^2\sigma_e}{2}\left[\frac{\omega^2}{\omega_s^2+\omega^2}\right]\left[\frac{\kappa'^2_p}{\kappa'_p d_e+\kappa'_e d_p}\right] \tag{12.43}$$

It is informative to compare the case where there is no insulation on the electrodes with the above result. If we return to equation (12.41) and let $\sigma_p = \sigma_e$ *and* $\kappa'_p = \kappa'_e$ then:

$$W_u = \frac{AV_0^2\sigma_e}{2(d_p+d_e)} \tag{12.44}$$

The power dissipated per unit volume in the uninsulated case is then:

$$W'_u = \frac{W_u}{A(d_e+d_p)} = \frac{V_0^2\sigma_e}{2(d_e+d_p)} \tag{12.45}$$

The ratio of insulated power consumption to uninsulated power consumption is then:

$$W_r = \left[\frac{\omega^2}{\omega_s^2+\omega^2}\right]\left[\frac{\kappa'_p(d_p+d_e)}{\kappa_e' d_p+\kappa'_p d_e}\right]^2 \tag{12.46}$$

It is a good approximation to assume that the dielectric constant of the insulation is very similar to that of the emulsion, in which case:

$$W_r = \frac{\omega^2}{\omega_s^2 + \omega^2} = \frac{1}{1 + \left(\frac{\omega_s}{\omega}\right)^2} \tag{12.47}$$

Operation of the coalescer at or above its natural frequency is necessary to establish a strong electric field in the emulsion. Therefore, from equation (12.47) it is evident that approximately a halving of the power consumption is brought about by insulating the electrodes. As the operational frequency is increased however, the power consumption increases towards that of the uninsulated coalescer.

12.5 Current and Power Requirements in the Experimental Rig

In this section the actual values for current and power requirements to operate a module of the experimental rig will be calculated based on the results and analysis of the previous section. The electrostatic field enhancing coalescence will also be examined. To analyse the effects of varying the values of some of the key parameters governing the electrical and electrostatic behaviour of the electrocoalescer, graphs will be presented outlining the response to such changes.

12.5.1 Applied Voltage and Resulting Field

As previously stated, the properties of the oil and water are:

Fluid	σ / Sm^{-1}	κ'_r
Gas Oil after contact with water	1×10^{-9}	2.3
Distilled Water	5×10^{-4}	80

The conductivity value for the oil has been measured after equilibration with water and with 2.5% by volume surfactant dissolved in it. This value approaches a worse case scenario in that the conductivity of, for example, a crude oil is not expected to be greatly in excess of this

value (Sowa et al, 1994). The value for the conductivity of the water is not critical and in fact is likely to be a couple of orders of magnitude in excess of this value. Here, use is made of the conductivity value for a sample of singly distilled water but the presence of any inorganic salts in the emulsion will enhance the conductivity of the aqueous dispersed phase resulting in a very conducting (in electrostatic terms) dispersed phase. It has also been assumed that the presence of up to 5 % by volume of the oil phase of non-ionic surfactant NP2 will not effect the validity of equations (12.4) and (12.5).

The system comprising electrocoalescer with insulated electrodes, water-in-oil emulsion and power supply is shown schematically in Figure 12.1. The insulating perspex is 5 *mm* thick on each electrode. Thus, in the lumped electrical model d_p = 10 *mm*. The length and breadth of the insulated electrodes are 50 *cm* and 10 *cm* respectively, giving an area, A, of 0.05 m^2. The emulsion treatment depth, d_e, is 20 *mm* . It is, of course, assumed that the velocity of the emulsion through the duct will have no influence on its electrical properties so long as the velocity is great enough to prevent free water layer evolution.

As dispersed phase concentration increases, the conductivity and permittivity of the emulsion increases approximately in accordance with equations (12.4) and (12.5). This will result in the need to increase the applied voltage to maintain a constant peak electric field across the emulsion as water cut increases.

Figure 12.2 Peak Amplitude of Electric Field in the Flowing Emulsion versus Water-cut

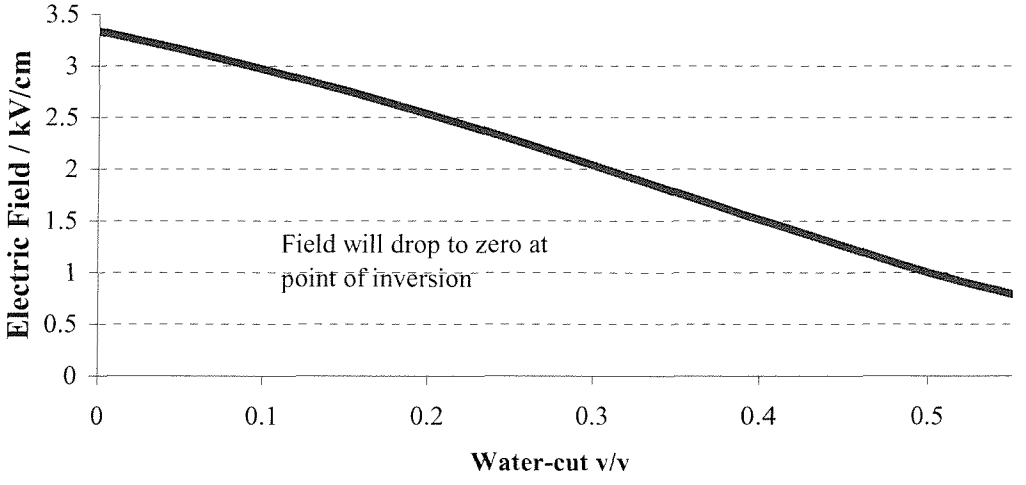

Figure 12.2 showing how the electric field across the emulsion reduces with increased dispersed phase concentration.

The conditions modelled are for an applied voltage of 10 kV peak-to-peak at 50 Hz across the emulsion having properties as shown in Table 12.1.

The inter-relation between water cut, Reynold's number and E_e is not fully understood and it is more tractable to think of operating at a constant applied voltage. Figure 12.2 shows the fall-off in peak electric field as water cut increases. Applied voltage is modelled at 10 kV, 50 Hz.

12.6 Operating Frequency

The natural frequency of the system, ω_s, from equation (12.8) is a very important factor as it indicates a value of frequency above which it is necessary to operate the supply voltage to produce a strong electric field in the emulsion. Operation below ω_s allows interfacial polarisation to occur at the insulation/emulsion interface, setting up charges that oppose the applied field. However, even at relatively low frequencies (10's of Hz) an excellent response is achieved and saturation of the field strength occurs very quickly. Thus, there is no apparent advantage in increasing the frequency of applied voltage beyond say 50 Hz.

The value of field depends on the system parameters σ_e, σ_p, κ'_e, κ'_p, electrode area A, and on the applied voltage magnitude and frequency, $V = V_0 \cos \omega t$ and internal resistance, R. Usually, the internal resistance of a step-up transformer is low and would represent a small drop in potential, $V_s - V$. If, for safety purposes, a current-limiting resistor may be connected in series with the power supply. Equations (12.31) and (12.23) can be used to determine what the maximum potential drop would be:

$$V_s - V = \Delta V = AB(\omega)(\sigma_e^2 + \kappa_e'^2 \omega^2)^{\frac{1}{2}} \tag{12.48}$$

$$= \frac{V_0}{\kappa'_d \kappa'_e}\left[\frac{\sigma_p^2 + \kappa'^2_p \omega^2}{(M-\omega)^2 + L^2\omega^2}\right]^{\frac{1}{2}} (\sigma_e^2 + \kappa'^2_e \omega^2)^{\frac{1}{2}} \tag{12.49}$$

$$\approx \frac{\omega}{L} V_0 \tag{12.50}$$

The choice of resistor will be such that the current delivered by the supply should be limited to non-lethal values. The experimental rig has completely insulated electrodes so the possibility of an operator touching a live electrode is zero hence no resistor was used in the system. To analyse the effect of inserting one (equivalently analysing the situation where the internal resistance of the supply is high) a value for R of 10 $M\Omega$ is inserted in equation (12.17) then equation (12.50) gives a reasonable estimate of the voltage dropped across the

resistor as a function of operating frequency. It is clear that the potential dropped across the resistor increases linearly with frequency and even at low frequencies represents a significant potential drop compared with the supply voltage.

Significant resistance in the circuit also affects the electric field in the emulsion as frequency increases. The field first increases as interfacial effects reduce then reaches a maximum (at a frequency of approximately $M^{0.5}$) then decreases due to potential dropped across the resistance for the value of R given above of 10 $M\Omega$.
A 10 $M\Omega$ resistor was in fact connected in series with the power supply to a single module and the potential dropped across it used to determine the current flowing to the module (see section 12.8).

12.7 Current and Power Dissipation

By fixing f = 50 Hz, we can determine the current and power dissipated in the system at various water cuts using equations (12.31) to (12.35), with B from equation (12.25).

12.7.1 Current

From equation (12.31) and using V_0 = *10 kV* at *50 Hz*, it can be shown that relatively low values of current are needed to set up the fields plotted in Figure 12.3. This means a small compact power supply or transformer can be used. It is interesting to note that the current is limited to a maximum of just less than 0.35 mA once inversion of the emulsion occurs and its conductivity increases. The insulation thus effectively protects the power supply from short-circuiting as its presence turns the module into a purely capacitive load once inversion has occurred and ω_s increases to a value greatly in excess of the supply frequency of 50 Hz.

12.7.2 Power

The power dissipated in the emulsion increases to a maximum as water cut increases, then decreases and effectively makes a step-change to zero once inversion occurs. The presence of a maximum has been proven by expressing σ_e and $\kappa_e^{'}$ as functions of ϕ in equation (12.41) then differentiating with respect to ϕ and setting equal to zero. A clear maximum is apparent for continuous phase conductivities up to approximately 1.5 x 10^{-8} Sm^{-1} with the locus of the maximum shifting towards lower water cuts as conductivity increases.

The power dissipation is expressed in terms of watts per cubic metre of emulsion. At a water cut of 15 %, a power dissipation of approximately 85 Wm^{-3} occurs. Thus, to treat 1000 bbl using the system described in Chapter 12, approximately 0.027 *kWhr* of energy is required (i.e. one would need to run 46.3 rigs of this configuration with all 7 modules active at a flow rate of 60 $l\ min^{-1}$ each). This compares favourably to the energy requirements of a standard electrocoalescer, which when treating distillates (low conductivity) consumes 0.2 kWhr/1000 *bbls* (Waterman, 1965).

From further analysis of equation (12.41) to (12.43) the maximum continuous phase conductivity for which the present system can still be used to enhance coalescence appears to be about 1 x 10^{-7} Sm^{-1}. Operation at higher frequencies could extend this range, however.

12.8 Confirmation of Theory by Experimental Measurement

To confirm some of the values quoted above, direct measurements of the both capacitance of a single module and the current flowing to it were made.

12.8.1 Capacitance

The capacitance of module seven was measured using a modified Wheatstone bridge. Initially it was hoped that changes in capacitance could be linked quantitatively to a layer of free water which appears in the duct under certain operating conditions but it was discovered that the changes were insensitive to water layer thickness. Values of capacitance for the module containing a flowing emulsion of water cut 15% were in the range 150-180 *pF*. Using equations (12.9) and (12.10) and electrostatic theory, the capacitance of the module is 54.5 pF at the same water cut. The factor of three or so difference between the measured and the actual values is felt to be due to stray cable capacitances and to coupling between module 7 and module 6 and other fringe effects.

12.8.2 Current

At a water cut of 15 %, a current of approximately 0.12 *mA* RMS is calculated with a supply voltage of 7.07 kV RMS (10 kV peak-to-peak). Measurement of the current flowing to one plate of module 7 was carried out by measuring the potential difference across a 10 *MΩ*

(±5%) resistor in series with the supply. The second plate was earthed. At a supply voltage of 10 *kV* peak-to-peak, a number of values were measured for the potential difference across the resistor. Interestingly, it was discovered that the potential difference (and so the current) depended on the flow rate of the emulsion and the number of modules that were 'on' in addition to module 7. This indicates that the dispersed state of the emulsion is the key to determining the frequency of the system and thus the current it will draw from the supply. Obviously, the electrical properties of the emulsion having evolved a free water layer are more complicated to predict than Hanai's theory for a well-behaved emulsion.

The current with one electrode only energised (the seventh) was found to vary between 0.34 *mA* at 20 $l\ min^{-1}$ to 0.53 *mA* at 40 $l\ min^{-1}$. The current rose slightly to 0.54 *mA* at 60 $l\ min^{-1}$. The degree of emulsion resolution into two separate phases depends on the number of electrodes energised and this would appear to be the reason why the current decreases with the number of active modules. The effect was found to saturate after 5 active modules in this case.

The measured current is in excess of the expected current by a factor of 2-3. Reasons why this is so could centre on stray leakage current down bolt-holes or current lost due to corona discharges. These factors should be independent of the degree of separation of the emulsion and should be constant for a particular applied voltage. To explain variations due to flow rate and exposure time to the field, a more in depth model of the electrical behaviour of the emulsion/two phase dispersion is required.

12.9 Conclusions on Electrical Behaviour of Flowing Emulsion

A model of the electrical and electrostatic behaviour of an insulated electrode compact electrocoalescer has been developed. The theory has been used to generate predictions on how the electric field, current and power dissipation alter as some of the key operating parameters such as applied voltage (frequency and amplitude) and water hold up in the emulsion are varied.

Measurements were made of the capacitance and the current delivered to a single module and were found to lie within experimental limits of those expected.

For its part, the emulsion's electrical properties have been modelled using Hanai's theory, which is deemed adequate so long as phase separation does not occur. Where complete inversion of the emulsion occurs, the current delivered by the supply will be limited to a value dependent upon the properties of the insulation and the power dissipation will effectively drop to zero. The electrical energy requirements to treat an emulsion with continuous phase conductivity of $1x10^{-9}$ Sm^{-1} and having a water cut of 15% using our system is estimated to be 0.027 *kWhr/1000 bbls*.

An operational frequency of 50 Hz produces an excellent field magnitude in the continuous phase of the emulsion and for the continuous phase conductivity expected of crude oil. For this reason and due to the enormously practical reason of using mains frequency, 50 Hz is put forward as being the ideal frequency for compact electrocoalescence devices of this sort.

Overall Conclusions to Thesis

This thesis essentially records three theoretical and experimental studies into the behaviour of dispersed systems in intense electrostatic fields. It is broken into 4 parts.

Part I lays down theoretical basics in the areas of electrostatics and dispersed systems and defines many of the fundamental physical concepts dealt with in the latter parts.

Part II spans Chapters 3-6 and details the author's work on developing a novel approach to electrostatically charge powder for use in powder coating applications. The chief conclusions from the author's work are:

1. Induction charging is not widely used in electrophotography but instances of its successful deployment are known (Chapter 5).
2. Much lower electric fields can be used to inductively charge particles to levels necessary for manipulation in powder spraying (Equation (5.6))
3. Many commonly used powders can be modified so they are suitable for induction charging. Modification methods used in this study involved addition of a surface active agent to either the surface of the internal part of the powder particulate (Chapter 5, Tables 5.2 and 5.3)
4. Devices can be designed which inductively charge and spray powders in a manner analogous with tribo and corona charging guns. The novelty of this approached resulted in a patent being granted of which the author is named as a co-inventor (Chapter 5, Section 5.6).
5. Knowledge of how to modify resins and polymers so their charge relaxation time can be optimised is a very advanced science and opens the way for widespread adaptation of induction charging in powder coating (Chapter 6).
6. The advantages of induction charging over tribo or corona charging are that, in principal, devices using this method may be operated at lower voltages than corona devices, no production of free ions occurs and the unpredictable nature of tribo charge exchange phenomena is eliminated. (Chapter 4, Section 4.5).
7. The chief challenge is that charge relaxation after deposition means relying on image charge adhesion before a permanent fix is achieved by curing is unlikely to succeed in practice. Ways around this are listed in Section 5.2.

Part III spans Chapters 7 and 8 and detail's the author's work on the electrostatic atomization of liquids into aerosols, also know as electrospraying. Chapter 7 is a literature search whilst

Chapter 8 contains a design methodology along with the author's experimental results. Focus is on the cone-jet mode of electrospraying. The chief conclusions from the author's work are:

8. Studies into electrostatic disruption of liquid/gas interfaces are numerous and some date back hundreds of years.
9. One of the most noteworthy early researchers was Zeleny who, in a series of experiments on various liquid/gas combinations, laid the framework for much that has been researched since.
10. Mathematical models to predict the onset of instability at a liquid/gas interface usually discuss the maximum surface charge density that an isolated liquid droplet can hold before disruption occurs. Lord Rayleigh's analysis is the most famous and leads to a formula for predicting the Rayleigh limiting charge (equation 7.2):

$$q_r = 8\pi\left(\varepsilon_0\ \gamma\ r^3\right)^{\frac{1}{2}}$$

11. Most modeling of the electrostatic stresses leading to disruption of menisci held at the end of cannulae adapts the Rayleigh limit to fit the particular geometry.
12. Using Taylor's analysis of a conical meniscus, typical field strengths at the liquid/gas interface needed to develop a cone-jet mode of electrostatic atomisation for water are 5 MVm^{-1}. Air ionisation often accompanies electrostatic atomisation events.
13. Deterministic and parametric analyses of atomisation abound and some of the more pertinent and insightful of these are reviewed in Chapter 7.
14. Production of monodisperse droplets occurs from the break-up of an electrically accelerated jet which extends from the apex of a conically-shaped meniscus. The conical shape is a resultant of the balance of the electrostatic, surface tension and hydrostatic forces acting on the liquid (Hayati *et al.,* 1989; Taylor, 1964).
15. Cone-jet formation is possible for liquids spanning an enormous range in electrical conductivity (Grace and Marijnissen, 1994).
16. The fastest growing disturbance on the jet, in the varicose mode, occurs at a wavelength which is relatively unaffected by the charge on the jet below a certain critical charge (Bailey, 1981; Melchor and Taylor, 1969; Mutoh *et al.,* 1979; Neukermans, 1973; Schneider *et al.,*1967; Taylor and Van Dyke, 1969) and may lead to uniformly sized drops. Above this level of charge break up is controlled by the growth of a laterally propagating wave which has the tendency to produce a polydispersed spray (Bailey, 1981; Taylor and Van Dyke, 1969) or alternatively the rim emission or multi-jet mode is onset whereby several spray sites are distributed at equal spacings around the rim of the cannula (Meesters, 1992). The rim mode is usually observed with liquids of low surface tension and at high field values, especially with low flow rates. The size distribution of the

droplets is a complex function of the liquid's physical and electrical properties and the system parameters.

17. The spray system can be characterised by considering three time constants, the charge relaxation time, the viscous relaxation time and the flow characteristic time. Different regimes of spraying can be understood by considering the ratio of these time constants.
18. The experimental spray behaviour of three systems showed good agreement to time constant based analysis.
19. Water-in-oil emulsions can be broken by the application of an intense electric field and this technique is widely used in the crude oil industry.
20. The challenges for the crude oil industry are to maximise utilisation of existing infrastructure, to design solutions that enable longer transport of well streams from the well to the production site or vessel, to be able to process and separate water at cooler temperatures, to implement more flexible process solutions to petroleum transport and handling (to react to changing oil/water conditions), to deploy lightweight process solutions to deal with the production and processing of higher water cuts in order to lower chemical use and to react positively to tighter environmental regulations.
21. Rapid throughput coalescence or emulsion breaking devices offer a key route to meeting these challenges and research on the theory and practical design of such devices has a long history at the University of Southampton, some of which is outlined in Chapter 9.
22. Water-in-oil emulsions are a incredibly complex systems and their physiochemical interfacial properties need to be understood before analysing their electrical responses to applied fields. Most analyses immediately focus on the amphiphilic nature of the system but sections 10.2 to 10.6 review the pure liquid properties as understanding of these is key to complete understanding of emulsions, especially their stability.
23. Stability of an oil-in-water emulsion usually relies on agents known as emulsifiers which can be surface-active agents (surfactants), naturally occurring materials with amphiphilic properties or finely divided solids with special surface properties intermediate between those of an oil and a water.
24. Aggregation and micellization is a way an emulsion system lowers it internal energy to achieve stability.
25. Work by the author on a model emulsion in a rapid-throughput flowing electrocoalescer helped extend the knowledge base which eventually lead to the granting of a patent to a co-worker and allied researchers (Chapter 11) and commercialisation of the device is going ahead.
26. A model of the electrical and electrostatic behaviour of an insulated electrode compact electrocoalescer has been developed. The theory has been used to generate predictions on how the electric field, current and power dissipation alter as some of the key operating

parameters such as applied voltage (frequency and amplitude) and water hold up in the emulsion are varied.

27. Measurements were made of the capacitance and the current delivered to a single module and were found to lie within experimental limits of those expected.
28. For its part, the emulsion's electrical properties have been modelled using Hanai's theory, which is deemed adequate so long as phase separation does not occur. Where complete inversion of the emulsion occurs, the current delivered by the supply will be limited to a value dependent upon the properties of the insulation and the power dissipation will effectively drop to zero. The electrical energy requirements to treat an emulsion with continuous phase conductivity of $1x10^{-9}$ Sm^{-1} and having a water cut of 15% using our system is estimated to be 0.027 *kWhr/1000 bbls*.
29. An operational frequency of 50 Hz produces an excellent field magnitude in the continuous phase of the emulsion and for the continuous phase conductivity expected of crude oil. For this reason and due to the enormously practical reason of using mains frequency, 50 Hz is put forward as being the ideal frequency for compact electrocoalescence devices of this sort.

References

Abbas, M.A. and Latham, J., (1967), " The instability of evaporating charged droplets", J Fluid Mech, **30,** p663.

Abraham and Becker Ref needed from University of Southampton

Alexander, A.E. and Johnson, P., (1949), Colloid Sci., Oxford University Press)

Allan, R. S. and Mason, S. G., (1962), "Particle motions in sheared suspensions XIV. Coalescence of liquid drops in electric and shear fields", Journal of Colloid Science, **7**, 338-408.

Alston, L.L., (1968), "High Voltage Technology". Oxford University Press.

Anderson, J H, Bugner, D E, De Mejo, L P, Sutton, R C and Wilson, J C, (1989), US Patent 4,837,392.

Anderson, J. H. and Bugner, D E, 1989, USP 4,837,391.

Anderson, J. H., (1997b), "Surface State Models of Tribocharging of Insulators of Office Imaging", Recent Progress in Toner Technologies, IS&T, 146-148.

Anderson, J.H., (1997a), "A Comparison of Experimental Data and Model Predictions for Tribocharging of Two-Component Electrophotographic Developers", Recent Progress in Toner Technologies, IS&T, 189-194.

Anestos, T.C., Sickles, J.E., and Tepper, R.M., (1977), "Charge-to-Mass Distributions in Electrostatic Sprays", IEEE Trans Ind Appl, **1A-13,** pl68.

Asimov, I., (1984), "Asimov's New Guide to Science", Penguin Books.

ASTM Standard, (1979), "Paint-Tests for Formulated Products and Applied Coatings" Annual Book of ASTM Standards, Part 27, American Society for Testing and Materials, Philadelphia, Pa.

Ataman, S and Hanson, D.N., (1969), "Measurement of Charged Drops", I and E.C. Fundamentals, **8** , No. 4.

Bailey, A. G. (1988) *Electrostatic Spraying of Liquids.* Research Studies Press.

Bailey, A. G. and Balachandran W. (1981) The disruption of electrically charged jets of viscous liquid. *J. Electrostatics* **10**, 99-105.

Bailey, A. G. and Balachandran, W., (1981), "The Disruption of Electrically Charged Jets of Viscous Liquid', J Electrostatics, **10**, pp 99-105.

Bailey, A. G., (1988), "Electrostatic Spraying of Liquids", Research Studies Press.

Bailey, A. G., (1998), "The science and technology of electrostatic powder spraying, transport and coating", J of Electrostatics, **45**, 85-120.

Bailey, A.G. and Borzabadi, E., (1978), "Natural Periodic Electrostatic Spraying of Liquids", IEEE Trans Ind Appl, **1A-14,** p l62.

Balachandran, W. (1985), "Electrostatic Charging of Solid Particles and Liquid Droplets". IEE Colloquium on ions in the atmosphere.

Bartok, W. and Mason, S. G., (1958), "Particle motions in sheared suspensions VIII. Singlets and doublets of fluid spheres", Journal of Colloid Science, **14**, 13-26.

Bassett, A. B., (1894), Am J Math, **16**, p 95.

Bassett, J.D., Corbett, R.P., and Cross, J., (1975), "The self limiting of electrostatic powder coatings", Inst. Phys. Conf. No. 27, 221-227.

Bauch, H., (1992), Proc. Amer. Chem. Soc., **67**, 344-347.

Becher, P., (1977), Emulsions: theory and Practice, 2nd Edn., Krieger, New York

Blythe, A. R., (1979), "Electrical Properties of Polymers", Cambridge Solid State Science Series, Cambridge University Press.

Borzabadi, E. and Bailey, A. G., (1978), "The Profiles of Axially Symmetric Electrified Pendent Drops", J Electrostatics, **5,** pp 369-380.

Bose, G. M., (1670?), "Reserches sur la cause et sur la veritable theorie de l'electricite", Wittenberg.

Bright A.W., Martin B., and Corbett R.P., (1970), IEE Conf. Publ. No. 61, 111.

Cadle, R.D., (1965), "Particle Size, Theory and Industrial Applications", Reinhold Publishing Corporation, New York.

Cairns, C. J. R., Grist, D. M. and Neustadter, E. L. "The Effect of Crude Oil-Water Interfacial Properties on Water-Crude Oil Emulsion Stability", In Water-Crude Oil Interface Properties and Emulsions, details needed.

Calero, J. F., (1986), "The electrohydrodynamics of a conducting liquid meniscus", Master's Thesis, Univ of Illinois, Urbana, Illinois, Dept Elec Eng.

Chapman (1913), D. Phil Mag. **25**, 475.

Cheesman and King, (1940) Trans. Faraday Society, **36**, 1241.

Cho, A.Y.H., (1964). "Contact Charging of Micron-sized Particles in Intense Electric Fields". Journal of Applied Phys, 35,9, pp 2561-2564.

Chung, M. , Cutler, P.H., Feuchtwang, T.E., Miskowsky, N.M. and Sujatha, N, (1987), Scanning Electron Microscopy, **IV,** pl547.

Clampitt et al, (1974), European Propulsion Conf, Hinterzanten, pp 118-121.

Clampitt, R. and Jefferies, D.K., (1972), "Electric Propulsion and Applications", CNES, Toulouse.

Cloupeau, M. and Brunet-Foch, B., (1989), "Electrostatic Spraying of Liquids in Cone Jet Mode", J Electrostatics, **22,** ppl35-150.

Cloupeau, M. and Prunet-Foch, B. (1994) Electrohydrodynamic spraying functioning modes: a critical review, J. Aerosol Sci. **25,** 1021-1036.

Cloupeau, M. and Prunet-Foch, B., (1989), "Electrostatic spraying of liquids in cone jet mode". J. Electrostatics **22,** 135.

Coehn, A., (1898), Ann Physik, Vol. 66, 217

Cross J., and Cetronia A., (1977), "Frictional Charging and Powder Coating", Trans. Institute of Metal Finishing, **55**, 174-176.

Cross, J., (1987), "Electrostatics: principles, problems and applications", IOP Publishing.

Davies, D.K. (1969), J. Phys. D Applied Physics, **2**, 1533.

Davies, D.K. (1970), *details needed, ref lost!*

Davies, J. T., (1984), "Drop size of emulsions related to turbulent energy dissipation rates", Chem. Eng. Sci., **40**, 5, 839.

Davies, J.T. and Rideal, E.K., (1963), "Interfacial Phenomena". Academic Press, New York and London.

Davis, H. T., (1994), "Factors determining emulsion type: hydrophile - lipophile balance and beyond", Colloids and Surfaces A: Physiochemical and Engineering Aspects, **91**, 9-24.

DeShon, W.E. and Carson, R.S., (1968), "Electrical Field Investigations and a Model for Electrical Liquid Spraying", J Coll Int Sci, **28,** 1.

Diaz, A., (1989), "Ionomers as charge additives", 5th International Congress on Non-Impact Printing Technologies, San Diego, Ca, USA.

Diaz, A., Fenzel-Alexander, D., and Wollmann, D., (1981), "Effect of ionomer ion aggregation on contact charging", J. Polym. Sci., Part B: Polym. Phys., **29**.

Drozin, V.G., (1955), "The Electrical Dispersion of Liquids as Aerosols", J Coll Sci, **10**, pp 158 -164.

Duffin, W.J., (1980), "Electricity and Magnetism, 3rd ed" - McGraw-Hill Book Company, London.

Dunn, P.F. and Snarski, S.R., (1991), "Velocity Component and Diameter Distribution Characteristics of Droplets within Two Interacting Electrohydrodynamic Sprays", Phys Fluids, **A3** No. 3, p492.

Dunn, P.F. and Snarski, S.R., (1992), " Droplet Diameter Flux and Total Current Measurement in an Electrohydrodynamic Spray", J Appl Phys, **71 ,** No. 1.

Eyring, C. F., McKeown, S. and Millikan, R. A., (1928), "Field Currents from Points", Phys Rev, **31,** pp 900-909.

Fernandez de la Mora (1992), "The Effect of Charge Emission from Electrified Liquid Cones", J. Fluid Mech., 243, pp 561-574.

Fernandez de la Mora, J. (1992) The effect of charge emission from electrified liquid cones. J. Fluid Mech. **243,** 561.

Fernandez de la Mora, Navascues, J., Fernandez, F. and Rosell-Llompart (1990) Generation of monodisperse aerosols in electrosprays. J. Aerosol Sci. **21**, Suppl. 1, s673.

Frohlich, H., (1958), "Theory of Dielectrics", Oxford Clarendon Press, p33 &c.
GB Patent 2021794A

Goldman and Goldman, (1975), Gaseous Electronic *details needed from Southampton Library.*

Gomez and Tang, (1990) "Characterisation of Liquid Fuel Electrostatic Sprays", Western States Section, The Combustion Institute 1990 Fall Meeting, La Jolla, California, USA.

Gomez, A. (1993) The electrospray: fundamentals and applications, Invited Paper, Proc. 3rd World Conf. on Experimental Heat Trans., Fluid Mechs. and Thermodynamics. Honolulu, Hawaii.

Gomez, A. and Tang, K., (1991), "Atomization and Dispersion of Quasi-Monodisperse Electrostatic Sprays of Heptane", ICLASS-91 Gaithersburg, MD, USA.

Gouy, G. J., (1910), J. Phys Radium, **9**, 457.

Grace, J. M. and Dunn, P., (1992), "Speed measurements in the developing region of an electrohydrodynamic spray using laser diagnostics", Experiments in Fluids, **12** , pp 261-269.

Grace, J. M. and Marijnissen J. C. M., (1994), A review of liquid atomization by electrical means. J. Aerosol. Sci., **26**,1005-1036.

Grace, L.M. and Dunn, P.F., (1992) , "Enhanced Droplet Mixing in an Electrohydrodynamic Spray", ILASS-Americas 92, 51 Annual Conference on Liquid Atomization and Spray Systems, May 18-20, San Ramon, California.

Grady, P.L. and Hersh, S.P., (1975), "The effect of antistatic additives on the charge-transport properties of nylon fibres", Static Electrification.

Gramme, P. E., (1993), Keynote Address in Developments in Production Separation Systems, London, 4/5 March, Published by IBC Technical Services

Gremmer, E., (1955), German Pat 983,019 (to Knapsack-Gridsham, AG)
Gremmer, E., (1958), US Pat 2,844,489 (to Knapsack-Gridsham, AG)

Hamamoto, N. and Nakajima, Y., (1992), "Experimental discussion on maximum charge density of fine particles sustainable in normal atmosphere", Journal of Electrostatics, **28**, 161-173.

Hardy, G.F., (1974), "Role of Critical Coating Thickness in Electrostatic Powder Deposition", Journal of Paint Technology, **46**, 599, pp73-82.

Harper, W.R, (1967), "Contact and Frictional Electrification", Oxford University Press
Harpur, I.G., Wayth, N. J., Bailey, A.G., Thew, M. T., Williams, T. J., and Urdahl, O., (1997), "Destabilization of Water-In-Oil Emulsions Under the Influence of an A.C. Electric Field: Experimental Assessment of Performance", Journal of Electrostatics, **40 & 41**, pp. 135-140.

Harpur, I. G., Bailey, A. G. and Hashish, A. H., (1996), "A design method for the electrostatic atomization of liquid aerosols", J. Aerosol Sci., **27**, 7, 987-996.

Hashish, A., Bailey, A. G and Harpur, I.G., (1995), "Determination of the production rate, size and charge of electrostatically atomized aerosol droplets", Int. Conf. on Electrostatics 1995, York, UK.

Hashish, A., Bailey, A. G. and Williams, T. J. (1994) "Modelling the effect of electrostatic charge on selective deposition of pulsed aerosols in the human lung." Phys. Med. Biol. **39,** 2247.

Hayati, I., Bailey, A. I. and Tadros, T. F. (1989) Investigations into the mechanisms of electrohydrodynamic spraying of liquids. Part I. J. Colloid. Interface Sci**. 117**, 205.

Hayati, I., Bailey, A. I. and Tadros, T. F. (1989) Investigations into the mechanisms of electrohydrodynamic spraying of liquids. Part II. J. Colloid. Interface Sci. **117**, 218.

Hendricks, C. D. and Schneider, J. M., "Stability of a Conducting droplet under the Influence of Surface Tension and Electrostatic Forces", pp450-453.

Hendricks, C. D., (1962), "Charged Droplet Experiments", J Coll Sci, **17**, pp249-259.

Hinds, W.C., (1982), "Aerosol Technology". John Wiley and Sons, New York.
Horning, D. W. and Hendricks, C. D., (1979), "Study of an Electrically Driven Jet", J. Appl. Phys., **50,** pp 2614-2617.

Hu, D. and Makin, B., (1991), "Investigation of the characteristics of a non-conducting liquid spraying process using a finite element method to map liquid profiles", Inst Phys Conf Ser, No 118, Paper at Electrostatics '91 Oxford.

Huberman, M.N., (1970), "Measurement of the Energy Dissipated in the Electrostatic Spraying Process", J Appl Phys, **41** , No. 2, pp578-584.

Hughes, J. F., (1982), "Future trends in Powder." Finishing, Wheatland .Journals Ltd. Nov issue, 17-21.

Hughes, J.F., (1984), "Powder optimization - an alternative approach?" Finishing, Wheatland Journals Ltd, Nov issue, 20-21.

Hughes, J.F., (1985), "Electrostatic Charging of Solid Particles". Phys Bull, **36**, 8, pp339-341.

Hughes, J. F., (1990), "Measurement techniques and future Trends in Powder Coating", Second World Congress on Particle Technology, Part iv.

Joffre, G. H. and Cloupeau, (1986), "Characteristic Forms of Electrified Menisci Emitting Charges", **J** Electrostatics, **18,** ppl47-161.

Joffre, G., Brunet-Foch, Berthomme and Cloupeau, (1982), "Deformation of Liquid Menisci under the Action of an Electric Field", J Electrostatics, **13,** ppl5l-165.

Jones, A. R. and Thong, K. C., (1971), "The Production of Charged Monodispersed Fuel Droplets by Electrical Dispersion", J Phys D: Appl Phys, **4,** pp 1159-1166.

Kamiyama, M., Maeda, M., Totsuka, H., and Hamanaka, T., (1997), "Properties of Polymerized Toners", Recent Progress in Toner Technologies, IS&T, 387-392.

Kelly, A. J.,(1976), "Electrostatic Spray Theory", J Appl Phys.

Kelly, A. J., (1976), "Metallic Spray Theory", J Appl Phys, **47**, No. 12.

Kelly, A. J., (1984), "Low Charge Density Electrostatic Atomization", IEEE Trans Ind Appl, **IA-20**, pp 267-273.

Kim, K. and Turnbull, R.J., (1976), "Generation of Charged Droplets of Insulating Liquids by Electrostatic Spraying", J Appi Phys , **47,** p1964.

Kingham, D. R. and Bell, A. E, (1984), J de Physique, Proc 3rd Intl. Field Emission Symp, Paris, **45,** Suppl. No. 12, C9.

Kjellander, R. and Florin, E., (1981), J. Chem. Soc,. Faraday Trans. **1**, 77, 2053-2077.

Kleber, W., (1993), "Electrostatic Powder Gun Design", J of Electrostatics, 30, 393.

Kozhenkov and Fuks, (1976), "Electrodydrodynamic Atomization Of Liquids", Russian Chem Revs, **45,** No. 12, pp 1 179-84.

Kreyszig, E., (1972). "Advanced Engineering Mathematics, 3rd ed". John Wiley and sons, Inc, New York.

Krohn (1961), in "Progress in Aeronautics and Rocketry", edited by D.B. Langmuir et al, Academic Press New York, Vol 5, p73.

Krohn, V.E., (1974), J Appl Phys, **45,** ppl 144-1146.

Lebedev, N.N. and Skal'skaya, I.P., (1962). "Force acting on a conducting sphere in the field of a parallel plate condenser". Sov Phys-Tech Phys, 2, pp 268-270.

Lefebvre, A.H., (1989). "Atomization and Sprays". Hemisphere Publishing Corporation, New York.

Lehr, W. and Hiller, W., (1993), "Electrostatic Atomization of Liquid Hydrocarbons", J Electrostatics, **30**, 433.

Ling, T. F., Lee, H. K. and Shah, D. O., (1987?), Surfactants in Enhanced Oil Recovery", Industrial Applications of Surfactants, details needed.

Lobo, L., Ivanov, I. And Wasan, D., (1993), "Dispersion Coalescence: Kinetic Stability of Creamed Dispersions", AIChE Journal, **39**, 2, 322-334.

Loeb (1965), *details needed from Southampton library*

Loken, K., Vangen, G. and Nordstad, K., (1996), "Field Test of Separator Internals for Oil Production", Third Intl. Conf. On Current Developments in Production Separation Systems, Aberdeen, April 23 and 24.

Macholdt, H. and Sieber, A. (1988) "Triboelectric charging properties of organic colour pigments". Journal of Imaging Technology 14, pp 89-93.

Macky, W.A., (1930), Proc. Camb. Philosophical Society, **26,** No. 421.

Mahoney, J., Yahiku, Daley, Moore and Perell, (1969) "Electrohydrodynamic Ion Source", J Appl Phys, **40**, No. 13.

Marsh, J. F. and Nunn, A., (1988), " The Control of Electrostatic Atomization Using a Closed-Loop System", J. Electrostatics, **20**, pp3l3-318.

Mayer B., and Kordes D., (1977), Farb & Lacke, **83**, p997.

Meesters, G. M. H. (1992) Mechanisms of droplet formation. Ph.D. thesis, Delft University Press.

Meesters, G. M. H., Vercoulen, P. H. W., Marijnissen, J. C. M. and Scariett, B. (1992) Generation of micron-sized droplets from the Taylor cone. *J. Aerosol Sci.* **23,** 37-49.

Melcher and Warren, (1971), "Electrohydrodynainics of a Current Carrying Semi-Insulating Jet", J Fluid Mech, **47,** pl27.

Melcher, J. R. and Taylor, G. 1. (1969) Electrohydrodynamics: a review of the role of interfacial shear stress. Ann.Rev. Fluid Mech. **1**, III.

Melcher, J.R. and Taylor, G.I., (1969), "Electrohydrodynamics: a review of the role of interfacial shear stress", Annual review of fluid mechanics, **1**, pp I 1 1-46.

Miksis, M.J., (1981), "Shape of a Drop in an Electric Field", Phys Fluids, **24,** No. 11.

Moore D., (1993), Finishers' Management, April issue, 22.

Moses D.L., (1993), Powder Coating, Nov issue, 41.

Moyle, B.D. and Hughes, (1983), J.F., Electrostatics, Oxford.

Moyle, B.D. and Hughes, J.F, (1984), IEEE Trans. Ind. Appl., **1A-20**, 6.

Muralidhar, R. and Ramkrishna, D., (1986), "Analysis of Droplet Coalescence in Turbulent Liquid - Liquid Dispersions", Ind. Eng. Chem. Fundam., **25**, 554-560.

Muto, K., Fushimi, H., Kotsugai, A.,Watanabe, Y. and Harpur, I. G., US5418103 (1995) "Toner for developing latent electrostatic images".

Mutoh, M. , Kaieda, S. and Kamimura, M., (1979), "Convergence and disintegration of liquid jets induced by electrostatic fields", J Appl Phys, **50,** pp3l74-3179.

Mutoh, M., Kaieda, S. and Kamimufa, M., (1979), Convergence and disintegration of liquid jets induced by electrostatic fields. *J. Appl. Phys.* **50,** 3174.

Nawab, M. A. and Mason, S. G., (1958), Trans. Faraday Soc. **54**, 1712.

Neeson, P. G., Jennings, B. R. and Tiddy, G. J. T., (1983), Chem. Phys. Lett., **95**, 6, 533-535.

Netzel, D. A., Hoch, G. and Marx, T. I., (1964), "Adsorption studies of surfactants at the liquid-vapour interface: Apparatus and method for rapidly determining the dynamic surface tension", J Coll Sci, **19**, pp 774-785.

Neubauer, R.L. and Vonnegut, B., (1953), J Coll Sci, **8,** 551.

Neukermans, A., (1973), "Stability Criteria of an Electrified Liquid Jet", J Appl. Phys, pp 4769-4770.

Pfeifer, R. J. (1973) Reply to comments by S. A. Ryce on "Charge-to-mass relationships for electrohydrodynamic sprayed liquid droplets". Phys. Fluids, **16,** 454.

Nix, J.R. (1967), Ann Phys, **41,** No. 52.

Nolan, J. J. (1926), Proc Royal Irish Academy, **37**, p28.

Ogata S., Ishikawa M., and Murakami T., (1981), "Velocity measurements of electrostatically sprayed droplets by means of two laser pulses of different wavelength", J Electrostatics, **9,** pp 223-234.

Ott, L.M. and Mizes, H.A. " Atomic force microscopy adhesion measurements of surface modified toners for xerographic applications". Colloids and Surfaces, A: Physiochemical and Engineering Aspects 87, pp245-256.

Panofsky, W. K. H. and Phillips, M, (1978), "Classical Electricity and Magnetism", 2nd. Ed., Addison-Wesley, Publishing Co.

Panton, R. L., (1996), "Incompressible Flow", 2nd Ed., John Wiley and Sons.

Pauthemier, (1932), J. Phys. Radium, Ser 7, 590.

Peek, F., (1929), "Dielectric phenomena in high-voltage engineering". McGraw-Hill, NY.

Pfeifer, R.J. and Hendricks, C.D., (1967), "Charge-to-Mass Relationships for Electrohydrodynamic Sprayed Liquid Droplets", Phys Fluids, **10** , No. 10, p2l49.

Pfeifer, R.J., (1973), 'Reply to comments by S.A. Ryce on 'Charge-to-Mass Relationships for Electrohydrodynamic Sprayed Liquid Droplets" ", Phys Fluids, **16**, No. 3, pp454-455.

Plastics World, (1980), **38**, 35

Powder Coating Handbook, (1994), The Powder Coating Institute, VA, USA, 224.

Pryde, J. A., (1966), "The Liquid State", Hutchinson University Library.

RAPRA, (1993), "Polymers for Electrostatic Environments", RAPRA Technology Limited, UK.

Rayleigh, (1878), "On the Instability of Jets", Proc Lond Math Soc, **10**, pp4-13.

Rayleigh, (1882), "On the Equilibrium of Liquid Conducting Masses Charged with Electricity", Phil Mag, **34**, p481.

Robinson, K.S., Turnbull, R.J. and Kim, K., (1980), "Electrostatic Spraying of Liquid Insulators", IEEE Trans Ind Appl , **1A-16,** No. 2.

Rosenkilde, C. E., (1969), Proc Royal Soc, **A312**, p473.

Rulison, A. J. and Flagan, R. C., (1992), Synthesis of sub-micron ceramic powders by electrospray pyrolysis, *A.A.A.R. llth Annual Meeting,* San Francisco, CA.

Rumpf, H., (1990), "Particle Technology". Chapman and Hall, London.

Ryce, S.A., (1964), J. Coll Sci, **69,** pp490-492.

Saffman, P. G. and Turner, J. S., (1956), "On the collision of drops in turbulent clouds", J. Fluid Mech., **1**, 16-30.

Sample, S.B. and Bollini, R., (1972), "Production of Liquid Aerosols by Harmonic Electrical Spraying", Coll Int Sci, **41**, No. 2, ppl85-193.

Sample, S.B., Bollini, R. and Hendricks, C.D., (1970), "Quiescent distortion and resonant oscillations of a liquid drop in an electric field", Int J Engng Sci, **8,** pp 97-109.

Sato, M, (1984), "The production of essentially uniform-sized liquid droplets in gaseous or immiscible liquid media under applied a.c. potential', J Electrostatics, **15,** pp 237-247.

Sato, M, (1991), "Formation of uniformly sized liquid droplets using spinning disk under applied electrostatic fields", IEEE Trans Ind Appl, **27**, No. 2.

Sato, M., (1980), "Cloudy bubble formation in a strong non-uniform electric field", J Electrostatics, **8,** pp 285-287.

Schneider, J. M., Lindblad, N. R., Hendricks, C. D. and Crowley, J. M. (1967) Stability of an electrified liquid jet. *J. Appl. Phys.* **38,** 2599.

Schneider, J.M., Lindblad, N.R., Hendricks, C.R. and Crowley, J.M., (1967), J Appl Phys, **38,** p2599.

Schneider, J.M., Lindblad, N.R., Hendricks, C.R. and Crowley, J.M, (1967), "Stability of an Electrified Liquid Jet", J Appl Phys, **44**, No. 6, pp 2599-2605.

Seanor, D. A., (1965), "Charge Transfer in Polymers", Adv. Polymer Sci., **4**, pp.317-352.

Shah, J., (1970) J. Colloid Interface Sci., 37, 744.

Sherman, P., (1968), "Emulsion Science". Academic Press, London and New York.

Singh, S., (1981), "Charging Characteristics of some powders used in Electrostatic Coating", IEEE Trans IAS, **IA-17**, 1

Smith, D. P. H, (1986), "The Electrohydrodynamic Atomization of Liquids", IEEE Trans Ind Appl, **IA-22,** No. 3. 527.

Smith, J.M., and Van Ness, H. C., (1987), "Introduction to Chemical Engineering Thermodynamics", McGraw Hill.

Snarski and Dunn, (1991), Exp. Fluids, 11 , p268.

Snarski, S.R. and Dunn, P.F., (1991), "Experiments characterizing the interaction between two sprays of electrically charged liquid droplets', Experiments in Fluids, **11**, 268-278.

Solymar, L., and Walsh, D., (1987), "Lectures on the electrical properties of materials", Oxford Science Publications.

Sowa, J. M., Sheng, P., Zhou, M. Y., Chen, T., Serres, A. J. and Sieben, M. C., (1994), "Electrical Properties of Bitumen Emulsions", Fuel, **74**, 8, 1176-1179.

Tang, K. and Gomez, A., (1994), "On the structure of an electrostatic spray of monodisperse droplets" Phys. Fluids **6,** 2317.

Taylor, G. I., (1964), "Disintegration of water droplets in an electric field", Proc Roy Soc Lond, **A280,** pp 383-397.

Taylor, G. I. and Van Dyke, M.D., (1969), "Electrically Driven Jets", Proc Roy Soc Lond, **A313,** pp453-475.

Taylor, S. E., (1987), "Investigations into the Electrical and Coalescence Behaviour of Water-in-Crude Oil Emulsions in High Voltage Gradients", Colloids and Surfaces, **29**, 29-51.

Thong and Weinberg, (1971), "Electrical Control of the Combustion of Solid and Liquid Particle Suspensions", Proc Roy Soc Lond, **A324 ,** p2Ol.

Turnbull, R.J., (1989), "Self-Acceleration of a Charged Jet", IEEE Trans Ind Appl, **25**, No. 4.

Turnbull, R.J., (1992), "On the Instability of an Electrostatically Sprayed Liquid Jet", IEEE Trans Ind Appl, **28,** No. 6.

UK Patent 1,527,291, (1976), Hitachi Metals Ltd, Tokyo, Japan.

UK Patent 1,539,080, (1976), Hitachi Metals Ltd, Tokyo, Japan.

UK Patent, 2,021,794 A&B, (1979), Hitachi Metals Ltd, Tokyo, Japan.

Urbanski, J., (1977), "Handbook of analysis of synthetic polymers and plastics", Ellis Horwood.

Urdahl, O., Williams, T. J.,Bailey, A. G. and Thew, M. T., (1995), "Electrostatic Destabilisation of Water-in-Oil Emulsions under Conditions of Turbulent Flow", Chem. Eng. Res. Des., **74**, A2, 158-165.

US Patent 4,121,931, (1976), 3M, Minnesota, USA.

US PATENT 5034463, (1991), "Conductive polymer compositions"

US PATENT 5217649, (1993), "Electrically conductive blends of intrinsically conductive polymers and thermoplastic polymers containing sulfonamide plasticizer and acidic surfactant"

US PATENT 5290483, (1994), "Electrically conductive blends of intrinsically conductive polymers and thermoplastic polymers and a process for their preparation"

US PATENT 5290483, (2000), "Solvent spinning of fibers containing an intrinsically conductive polymer"

US PATENT 5532025, (1996), "Corrosion inhibiting compositions"

US Patent 5595689, (1997), "Highly conductive polymer blends with intrinsically conductive polymers"

US PATENT 5691062, (1997), "Molecularly bonded inherently conductive polymers on substrates and shaped articles thereof"

US PATENT 5720903, (1998), "Dispersible intrinsically conductive polymer and process for its manufacture"

US PATENT 5846606, (1998), "Process for the production of metallized materials"

US PATENT 5849415, (1998), "Molecularly bonded inherently conductive polymers on substrates and shaped articles thereof"

US PATENT 5871671, (1999), "Intrinsically conductive polymer/plasticizer blends with enhanced conductivity"

US PATENT 5908898, (1999), "Intrinsically conductive polymer blends having a low percolation threshold"

US PATENT 5911930, (1999), "Solvent spinning of fibers containing an intrinsically conductive polymer"

US PATENT 6004418, (1999), "Method of joining a cover material to a substrate utilizing electrically conductive bonding"

US PATENT 6015613, (2000), "Corrosion inhibiting multilayer coating"

US PATENT 6020275, (2000), "Bonded composite open mesh structural textiles"

US PATENT 6056479, (2000), "Bonded composite open mesh structural textiles"

US PATENT 6060116, (2000), "Polyaniline in the form of an easily dispersible powder and its use in corrosion protection and electrostatic dissipation"

US PATENT 6099756, (2000), "Vibrational methods of deaggregation of electrically conductive polymers and precursors thereof"

US PATENT 6117554, (2000), "Modulated molecularly bonded inherently conductive polymers on substrates with conjugated multiple lamellae and shaped articles thereof"

US4384078, (1983), "Antistatic resin composition"

US4545926, (1985), "Conductive polymer compositions and devices"

US4803096, (1989), "Electrically conductive textile materials and method for making same"

US4859727, (1989), "Antistatic thermoplastic resin composition"

US4909959, (1990), "Conductive polymers derived from 3-alkylthiophenes, a process for manufacturing them and electroconductive devices containing them" internal addition"

Vereshchagin, I. P et al, (1986), "Investigation of the process of induction charging of particles", Power Engng, **24**, l, pp 115-122.

Vonnegut, B. and Neubauer, R. L., (1952), "Production of Monodisperse Liquid Particles by Electrical Atomization", J Coll Sci, **7** , pp6l6-622.

Vonnegut, B. and Neubauer, R. L., (1952), Production of monodisperse liquid particles by electrical atomization. *J. Colloid Sci.* **7**, 616.

Watanabe, M., and Nagase, H., (1989), US Patent 4,883,735.

Wayth, N. J. (1989), "The development of a rapid through-flow compact electrostatic coalescer for dewatering of crude oil", PhD Thesis, Depts. of Mechanical and Electrical Engineering, University of Southampton, UK.

Wayth, N. J., Williams, T. J., Bailey, A. G., Thew, M. T. and Urdahl, O, (1999), "The Influence of Flow Regime on Electrostatic Destabilisation of Water-in-Oil Emulsions: A Theoretical and Experimental Assessment", Electrostatics 11th International Conference.

Weckstrom, K. and Zulauf, M., (1985) J. Chem. Soc., Farday Trans, **1**, 81, 2947-2958.

Williams, B. E., Harpur, I. G., Hearn, G. and Hughes, J. F., US5518546, (1996), "Apparatus for coating substrates with inductively charged resinous powder particles".

Williams T. J., (1989), PhD Thesis, Dept. Electrical Engineering, University of Southampton, UK.

Williams, T. J., Bailey, A. G. and Thew M. T., (1991), "Rapid Throughflow Electrostatic-Centrifugal De-Watering of Crude Oil" Treatment of Water Offshore -Phase I - Project 2, University of Southampton Report.

Williams, T. J., Bailey, A. G. and Thew M. T., (1992), "Rapid Throughflow Electrostatic-Centrifugal De-Watering of Crude Oil" Treatment of Water Offshore -Phase II - Project 2, University of Southampton Report.

Williams, T. J., Bailey, A. G. and Thew M. T., (1994), "Rapid Throughflow Electrostatic-Centrifugal De-Watering of Crude Oil" Statoil Report, University of Southampton.

Williams, T. J., Bailey, A. G. and Thew M. T., (1995), "The electrostatic destabilization of water-in-oil emulsions in turbulent flow", Electrostatics 9th International Conference, York, 2-5 April.

Wilson, C. T. R. and Taylor, G. I., (1925), Proc Camb Phil Soc, **22**, 78.

Wright, G. S., Krein and Chato, (1989) "Factors Affecting Electrical Manipulation of Menisci", Conf Rec IEEE IAS Annual Meeting, San Diego, CA, USA, pp2066-72, Vol 2.

Zeleny, J., (1914), Proc. Camb. Philosophical Society (from The Physical Review N.S. 2, p69).

Zeleny, J. (1917), "Instability of Electrified Liquid Surfaces", The Physical Review, 2' Series, **X**, No 1.

Zeleny, J., (1935), "The Role of Surface Instability in Electrical Discharges from Drops of Alcohol and Water in Air at Atmospheric Pressure", J Franklin Institute, **219,** No.6.

Zomeran, A.A., van Kelder, E. M., Marijnissen, J. C. M. and Schoonman, J., (1994), The production of thin films of LiMn3O, by electrospraying. *J. Aerosol. Sci.* **25,** 1229-1235.

APPENDIX ONE

ABSTRACTS FROM AUTHOR'S PUBLICATIONS

I

IAN G. HARPUR, ADRIAN G. BAILEY AND ADEL H. HASHISH

A DESIGN METHOD FOR THE ELECTROSTATIC ATOMIZATION OF LIQUID AEROSOLS

Journal of Aerosol Science, Vol 27, No. 7, pp 987-996, 1996

Abstract – A design method based on analysing and matching the physical time constants of the electrostatic atomization process in the cone-jet mode is presented. An algorithm is developed whereby the liquid properties are used as a basis for recommending a capillary diameter and a liquid flow rate such that a stable spray will result once appropriate electric field conditions are established. The algorithm also predicts the droplet diameter about which the aerosol is distributed. Experimental results are presented which confirm he design methodology.

II

ADEL H. HASHISH, ADRIAN G. BAILEY AND IAN G. HARPUR

DETERMINATIONS OF THE PRODUCTION RATE, SIZE AND CHARGE OF ELECTROSTATICALLY ATOMIZED AEROSOL DROPLETS

Inst. Phys. Conf. Ser. No 143.
Paper presented at the 9th Int. Conf. on Electrostatics, York, 2-5 April 1995

Abstract – A method of determining the production rate, average particle size and mean charge of electrostatically atomized aerosol droplets is described. The method is based on detecting current pulses which accompany droplet emission from a capillary tip. A good agreement of drop size is obtained with laser diffraction size measurement and a predictive atomization algorithm.

III

IAN G. HARPUR, NICHOLAS J. WAYTH, ADRIAN G. BAILEY, MARTIN T. THEW AND OLAV URDAHL

DESTABILISATION OF WATER-IN-OIL EMULSIONS UNDER THE INFLUENCE OF AN A.C. ELECTRIC FILED: EXPERIMENTAL ASSESSMENT OF PERFORMANCE

Journal of Electrostatics 40&41 (1997) 135-140

Abstract – The destabilisation of water-in-oil emulsions is an important industrial process and is often the rate-determining step in the dewatering and desalting of crude oils. In this study, the influence of a 50 Hz sinusoidal electric field on flowing water-in-oil emulsions is reported. A horizontal rectangular duct was used, with emulsion flowing through at flow rates up to 100 litre min^{-1}, giving Reynolds number in the range 1000 to 12000. Electrocoalescer performance was assessed by measuring water droplet growth, using a specially developed technique with a laser diffraction particle sizer. Under conditions of high water-cut, electrocoalescence can be so efficient that free-water drop-out may occur, even in conditions of turbulent flow. This can lead to the formation of a layer of water co-flowing with the depleted emulsion in the duct. Study of the electrocoalescer under these conditions has been carried out by image analysis using a Hamamatsu Image Processor.

IV

BARBARA E. WILLIAMS, IAN G. HARPUR, GRAHAM HEARN AND JOHN K. HUGHES
ASSIGNEE: ENEXUS CORPORATION, GREENWICH, CONN.

APPARATUS FOR COATING SUBSTRATES WITH INDUCTIVELY CHARGED RESINOUS POWDER PARTICLES

United States Patent No. 5,518,546, May 21, 1996

Abstract – An apparatus for improving the electrostatic charge developed on a resin powder composition for electrostatic coating of solid objects and the method of application thereof. The apparatus comprises a device for charging the powder by electrical induction/conduction such that the powder particles have a resistivity of from 10^9 to about 10^{13} ohm.meters at 20 percent relative humidity and spraying the charged particles onto a grounded solid object to which it adheres prior to thermal fusing to produce a permanent finish.

V

KENKICHI MUTO, HIROYUKI FUSHIMI, AKIHIRO KOTSUGAI, YOICHIRO WATANABE AND IAN G. HARPUR
ASSIGNEE: RICOH COMPANY, LTD., TOKYO, JAPAN

TONER FOR DEVELOPING LATENT ELECTROSTATIC IMAGES

United States Patent No. 5,418,103, May 23, 1995

Abstract – A toner prepared by allowing finely-divided particles of a vinyl resin having an alkali-reactive group to react with a fluorine-containing quaternary ammonium salt to obtain surface-modified finely-divided particles; mixing the surface-modified finely-divided particles and core particles composed of a resin and a coloring agent; and filming the above core particles with the finely-divided particles of the surface-modified vinyl resin with application of mechanical energy thereto.